Lalit Batra

PhD Thesis.pdf

Bennett University

Document Details

Submission ID
trn:oid:::29034:141996562

Submission Date
Jun 7, 2026, 3:22 PM GMT+5:30

Download Date
Jun 7, 2026, 3:27 PM GMT+5:30

File Name
Thesis combine (CH1-CH7).pdf

File Size
25.3 MB

261 Pages

43,299 Words

226,710 Characters

5% Overall Similarity

The combined total of all matches, including overlapping sources, for each database.

Filtered from the Report

- Bibliography
- Quoted Text
- Cited Text
- Small Matches (less than 10 words)

Match Groups

139 Not Cited or Quoted 5%
Matches with neither in-text citation nor quotation marks

0 Missing Quotations 0%
Matches that are still very similar to source material

0 Missing Citation 0%
Matches that have quotation marks, but no in-text citation

0 Cited and Quoted 0%
Matches with in-text citation present, but no quotation marks

Top Sources

4% Internet sources
3% Publications
2% Submitted works (Student Papers)

Integrity Flags

0 Integrity Flags for Review

No suspicious text manipulations found.

Our system's algorithms look deeply at a document for any inconsistencies that would set it apart from a normal submission. If we notice something strange, we flag it for you to review.

A Flag is not necessarily an indicator of a problem. However, we'd recommend you focus your attention there for further review.

Match Groups

139 Not Cited or Quoted 5%
Matches with neither in-text citation nor quotation marks

0 Missing Quotations 0%
Matches that are still very similar to source material

0 Missing Citation 0%
Matches that have quotation marks, but no in-text citation

0 Cited and Quoted 0%
Matches with in-text citation present, but no quotation marks

Top Sources

4% Internet sources
3% Publications
2% Submitted works (Student Papers)

Top Sources

The sources with the highest number of matches within the submission. Overlapping sources will not be displayed.

1	Internet	studylib.net <1%
2	Internet	www.researchgate.net <1%
3	Internet	morth.nic.in <1%
4	Internet	www.intmaritimeengineering.org <1%
5	Internet	dspace.dtu.ac.in:8080 <1%
6	Internet	ttu-ir.tdl.org <1%
7	Internet	www.diva-portal.org <1%
8	Publication	Bouazara, M.. "An optimization method designed to improve 3-D vehicle comfort ... <1%
9	Internet	spectrum.library.concordia.ca <1%
10	Internet	ndl.ethernet.edu.et <1%

11	Publication	Borutzky. "Bond Graph Based Physical Systems Modelling", Bond Graph Methodo... <1%
12	Publication	Ajit G. Mohite, Anirban C. Mitra. "Development of Linear and Non-linear Vehicle S... <1%
13	Publication	D. Hrovat. "Optimal active suspension structures for quarter-car vehicle models",... <1%
14	Internet	radar.brookes.ac.uk <1%
15	Submitted works	VIT University on 2016-10-21 <1%
16	Publication	Sushila Rani. "Parametric Evaluation and Dynamic Analysis of Turbine Blades–Da... <1%
17	Internet	www.rroij.com <1%
18	Internet	scholar.archive.org <1%
19	Internet	es.scribd.com <1%
20	Publication	Gerger, Ozan. "Design, Control and Optimization of Vehicle Suspensions with Iner... <1%
21	Publication	Martin Rosenberger, Manfred Pl&#65533;chl, Klaus Six, Johannes Edelmann. "The Dynam... <1%
22	Internet	serialsjournals.com <1%
23	Publication	Raj Desai, Anirban Guha, Pasumarthy Seshu. "An appropriate biomechanical mod... <1%
24	Publication	Zorica Srdjevic, Livija Cveticanin. "Identifying nonlinear biomechanical models by ... <1%

25 Publication
A. C. Mitra, M. V. Patil, N. Banerjee. "Optimization of Vehicle Suspension Paramet... <1%

26 Publication
Tufan Dogruer, Nusret Tan. "Design of PI Controller using Optimization Method i... <1%

27 Publication
S.K. Agrawal, K. Vishal. "Existence of Chaos, dynamical behaviour with fractional ... <1%

28 Publication
Srivastava, M., S.K. Agrawal, K. Vishal, and S. Das. "Chaos control of fractional ord... <1%

29 Publication
Hakan Yazici, Mert Sever. "Output derivative feedback vibration control of an inte... <1%

30 Internet
www.ijsrd.com <1%

31 Internet
www.iosrjen.org <1%

32 Publication
M. Ramalingam, Raju Patel, M. Arul Thirumurugan, D. Davidson Jebaseelan, C. Jeb... <1%

33 Submitted works
Modern Education Society's College of Engineering, Pune on 2020-06-27 <1%

34 Submitted works
Monash University on 2025-09-28 <1%

35 Publication
Saayan Banerjee, V. Balamurugan, R. Krishnakumar. "Ride Comfort Analysis of M... <1%

36 Submitted works
Universiti Teknikal Malaysia Melaka on 2016-08-24 <1%

37 Internet
link.springer.com <1%

38 Publication
Hao Kuang, Yi Qiu, Chi Liu, Xu Zheng. "A nonlinear biodynamic model of seated h... <1%

39 Publication

Jianfeng Wu, Lijun Zhang, Dejian Meng. "Ride Comfort Analysis of Seated Occupa... <1%

40 Submitted works

Loughborough University on 2026-04-13 <1%

41 Submitted works

The Hong Kong Polytechnic University on 2014-09-10 <1%

42 Internet

icas.org <1%

43 Internet

www.mdpi.com <1%

44 Publication

M Ramsbottom, D. A. Crolla, A. R. Plummer. "Robust adaptive control of an active ... <1%

45 Publication

Mohamed Essam Shalabi, Ahmed M. R. Fath Elbab, Haitham El-Hussieny, A. A. Abo... <1%

46 Submitted works

Sri Balaji University, Pune on 2024-08-23 <1%

47 Submitted works

University of Birmingham on 2009-04-29 <1%

48 Submitted works

University of Bristol on 2025-04-30 <1%

49 Publication

Vedant Mehta, Yash Gandhi, Mayuri Patel, Bhargav Gadhvi, Anil Markana, Jay J. V... <1%

50 Publication

Yutan Li, Chengjun Wang, Chuanjin Zhang. "Optimization of the suspension syste... <1%

51 Internet

coek.info <1%

52 Internet

idr.nitk.ac.in <1%

53 Internet
iosrjournals.org <1%

54 Internet
www.hindawi.com <1%

55 Internet
www.uobabylon.edu.iq <1%

56 Publication
"Advances in Italian Mechanism Science", Springer Science and Business Media L... <1%

57 Publication
A. Larsen, G. L. Larose, F. M. Livesey. "Wind Engineering into the 21st Century - Pr... <1%

58 Submitted works
De Montfort University on 2021-05-06 <1%

59 Publication
Krishna N. Dewangan, Arman Shahmir, Subhash Rakheja, Pierre Marcotte. "Vertic... <1%

60 Submitted works
Monash University on 2018-08-24 <1%

61 Submitted works
National Institute Of Technology, Tiruchirappalli on 2021-05-31 <1%

62 Publication
Shriram S. Sonawane, Parag P. Thakur, Manjakuppam Malika. "Nanofluids for Effi... <1%

63 Submitted works
Taylor's Education Group on 2016-11-23 <1%

64 Submitted works
University College London on 2021-09-13 <1%

65 Submitted works
University of Central England in Birmingham on 2020-09-30 <1%

66 Submitted works
University of Leeds on 2023-05-04 <1%

67 Submitted works

University of Sheffield on 2015-08-29 <1%

68 Submitted works

University of Southampton on 2022-09-22 <1%

69 Publication

Zongfa Zhang, Xinbiao Xiao, Hanwen Xu, Xuesong Jin. "Analysis of human body vi... <1%

70 Internet

eprints.soton.ac.uk <1%

71 Internet

pepite-depot.univ-lille.fr <1%

72 Internet

tudr.thapar.edu:8080 <1%

CHAPTER 1

INTRODUCTION

1.1 Background and Motivation

Road transport is the most widely used transportation mode in most developed and developing countries and Road transport is the most preferred mode of transportation for its convenience. With the growing number of car owners, providing safe, comfortable and reliable transportation has become a major focus of automotive engineers, road transport authorities and public health agencies. An important factor affecting ride comfort is the ability of the suspension system to decouple road vibrations from the occupants. Vehicle suspension system has to isolate the input disturbances from any road roughness, bumps, potholes, undulations and other discontinuities.

Ride comfort is affected by irregularities in road conditions, particularly in countries with rapid urbanization, traffic congestion and severe climatic conditions. Even high quality roads are subject to deterioration caused by traffic loads, environmental factors and construction faults. This results in dynamic forces which are transmitted to the human body through the vehicle. This requires robust modeling of vehicle–road–human dynamics to assess and improve ride comfort.

Transport is a vital component of economic development, enabling travel, trade and communication. But the rapid increase in the number of vehicles has led to issues such as increasing accidents, passenger discomfort and vibration-induced health issues. Comfort and safety is as important as efficiency and performance in vehicle design. Suspension systems are vital in ensuring ride comfort by absorbing vibrations. The interaction between the vehicle, road and human body forms a complex dynamic system, requiring advanced modeling techniques.

In the design of vehicles, performance and efficiency are no longer the only considerations; comfort and safety are also paramount. The suspension system of a vehicle plays a major role in ride comfort, buffering passengers against the effects of road disturbance. The integration of vehicle dynamics, road dynamics and human bio-dynamics creates an intricate coupled system, which needs to be studied using advanced modeling approaches. Transportation is a critical sector for economic growth, facilitating movement of people, goods and services.

All kinds of vehicle environments expose the human body to vibrations like on-road vehicle transport in the car, buses, off-road transport in the tractors, mining machines, rail transport in trains, monorails and marine transport in ships and boats. In each of these environments the human body receives vibrations through the contact area and it causes discomfort and some health problems.

Suspension system is considered very important as far as vehicle safety and comfort of the driver. Main function of suspension system is to carry vehicle structure and riders weight and also to absorb vibration during bump or uneven road conditions. The Suspension system in real has some non-linear characteristics in springs and dampers. So considering those non linear parameters may give some chaotic response which leads research to more realistic. As various researchers introduces controller to improve ride comfort. A better control strategy is very much required in order to reduce settling time and to reduce presence of chaos if any in vehicle system.

The importance of improving vehicles dynamic properties is constantly growing in automobile sector. Various areas like active safety and driver environment are dependent on enhanced dynamic behaviour. Vehicle dynamic response can have multiple meanings and is often split into two: Handling and Ride, which may be defined as:

Ride: Vibrations in vehicle in response to road irregularities.
Vibration comfort: low frequency vibrations (0-20Hz)
Harshness: high frequency vibrations (>20Hz)

Handling: Response of vehicle towards input from driver

Fig 1.1 shows how vibration propagate from wheel to human head just after hitting road obstacles and it is clear that each and every part in car may affect transmission of vibration. Further cushioning in seat plays a major role in mitigating the vibration received from vehicle body (chassis). Despite careful consideration of road irregularities

there exist trade off between responses, thus become a major challenging job for engineers to design effective suspension.

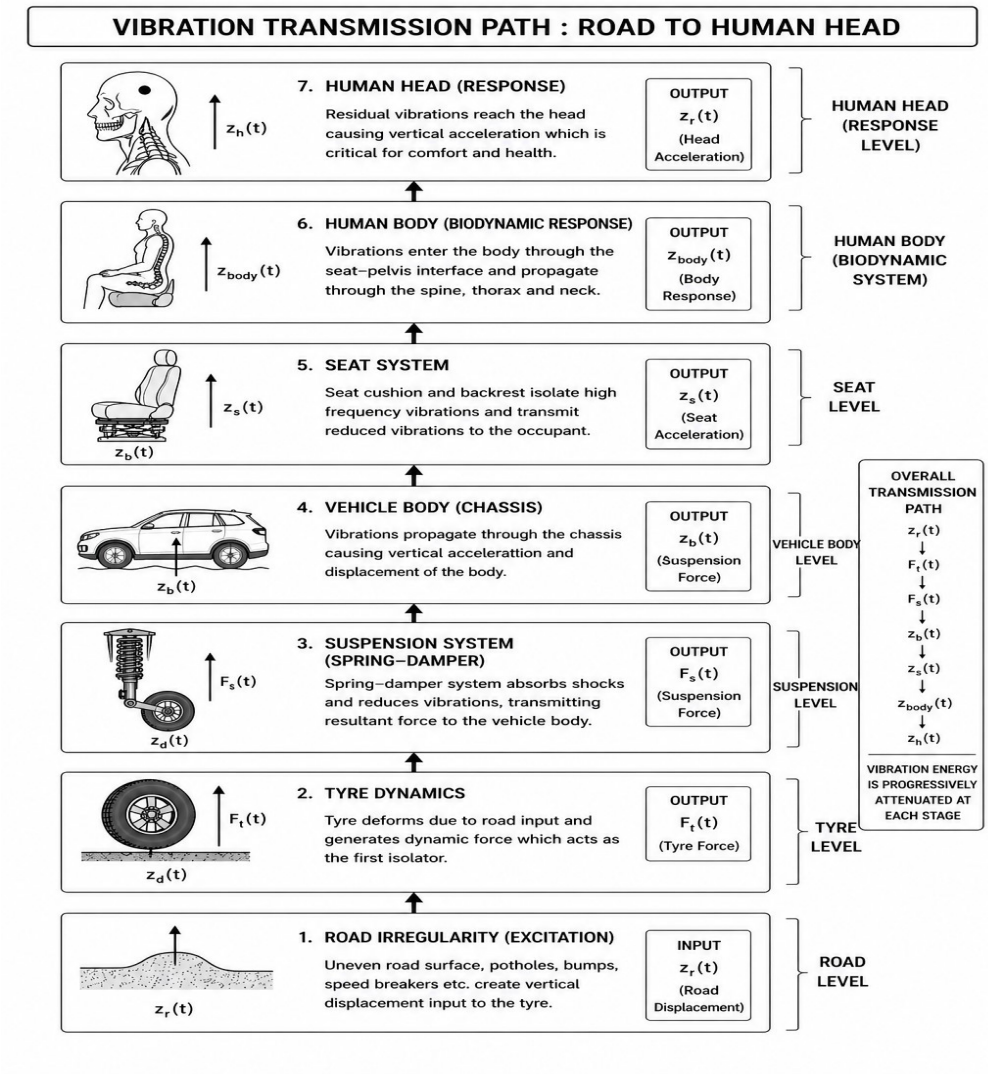


Figure 1.1 Vibration transmission structure during transportation

1.2 Road Accident Causes

Traffic accidents are leading causes of death in the surrounding world and mostly affect individuals aged 15 to 49. In 2023, 1.73 lakh people in India died and 4.63

lakh were injured in road accidents. Given that there are numerous factors that interact to bring about traffic accidents, multifaceted measures are needed to reduce the proportion of accidents and deaths. Thus, integrating the active involvement of all stakeholders in the country, the Ministry of Road Transport and Highways has begun a proactive policy towards road safety.

Table 1.1 Total number of Accidents, Fatalities and Persons Injured during 2019 to 2023 *(Ministry of Road and Highway Transport Rsearch Wing, 2023)*

Year	Accidents	% change over previous period	Fatalities	% change over previous period	Person Injuries	% change over previous period
2019	4,56,959	-2..9	1,58,984	0.9	4,49,360	-3.3
2020	3,72,181	-18.6	1,38,383	-13	3,46,747	-22.8
2021	4,12,432	-10.8	1,53,972	11.3	3,84,448	10.9
2022	4,61,312	11.9	1,68,491	9.4	4,43,366	15.3
2023	4,80,583	4.2	1,72,890	2.6	4,62,825	4.4

A decline in accidents and fatalities in the country was unprecedented in 2020 (Table 1.1). This is primarily due to the sudden outbreak of the Covid-19 pandemic and the lockdown imposed by the state especially in March and April of 2020. The confinement procedures were then slowly decontaminated and eliminated. Until 2019, the parameters of accidents exhibited the same trend, but the COVID-19 pandemic led to a significant decrease in 2020. Table 1.1 demonstrates that the levels

of main accident indicators were higher in 2023 compared to 2022. In Fig 1.2, the total amount of traffic accidents, fatalities, and injuries between 2019 and 2023 are illustrated.

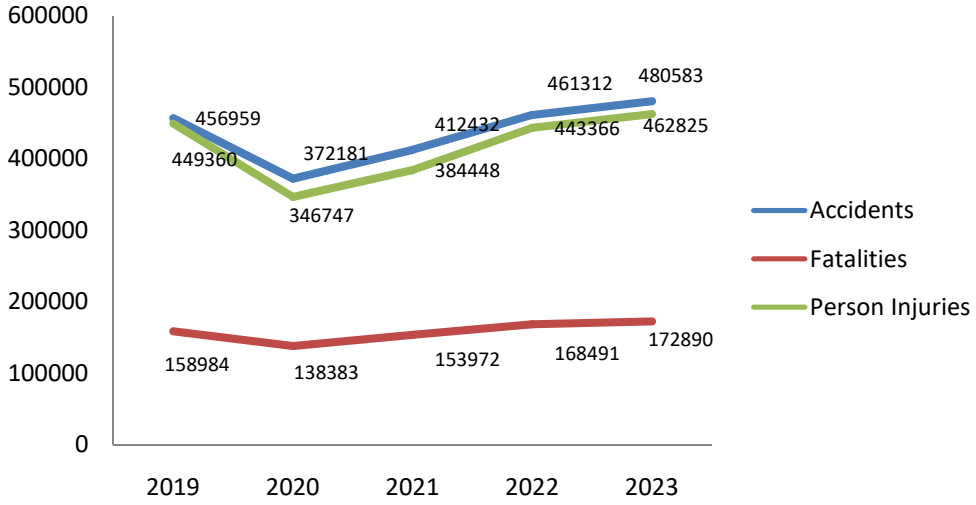


Figure 1.2 Trend in accidents, Fatalities and Person Injured (2019-2023)

During the year 2023, a total of 4,80,583 accidents were noted, of which 1,60,509 (33.4%) were fatal accidents, 2,92,424 (60.8%) were injury (minor and grievous) causing accidents. Among injury causing accidents, 1,58,576 (33.0%) were grievous and 1,33,848 (27.9%) were minor injury causing accidents (Fig 1.3). As compared to the 2022, there is increase in total number of fatal accidents. non-injury accidents and grievous injury accidents in 2023 (Table 1.2). Fig 1.3 depicts that the accidents of fatal and grievous injuries together accounted for over 66% of total accidents during 2023.

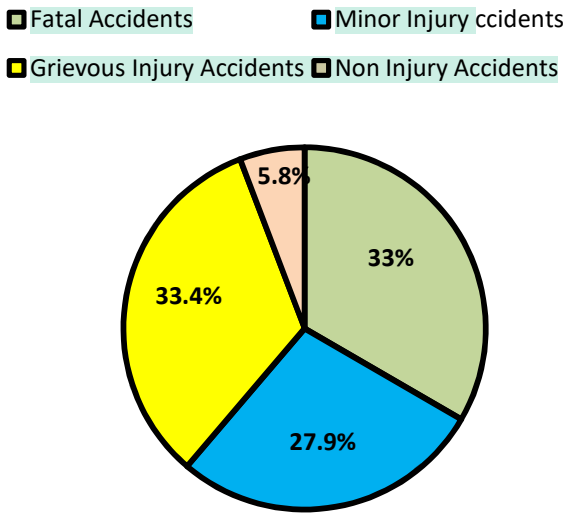


Figure 1.3 Types of road accidents in 2023 (in percentage)

Road accidents are caused by a combination of human, vehicle, and road factors. Driver fatigue, distraction, and over-speeding are major contributors. However, vibration-induced discomfort also reduces driver alertness and increases reaction time. Vehicle-related factors include poor suspension performance, brake failure, and tire issues. Road-related causes such as potholes, uneven surfaces, and non-standard speed breakers significantly affect vehicle stability. Thus, ride comfort is directly linked to road safety and accident prevention.

1.3 Health and Safety Concerns Due to Road-Induced Vibrations

Vehicle occupants are continuously exposed to whole-body vibration (WBV) during travel. Studies conducted under ISO 2631 highlight that displacement and acceleration

levels in the frequency range of 1–20 Hz have pronounced effects on the spine, pelvis, cervical region, and internal organs. Prolonged exposure to vibration is associated with:

- Lower-back pain
- Lumbar spine degeneration
- Disc herniation
- Muscular fatigue and discomfort
- Reduced cognitive performance while driving
- Increased fatigue-related road accidents
- Chronic musculoskeletal disorders

For professional drivers (truck, bus, taxi, construction vehicles), long-term exposure to road-induced WBV is classified as a serious occupational hazard. The transmissibility of vibration is affected not only by the road quality but also by the suspension characteristics, seat and posture of the driver, biodynamic response of the human body.

Therefore, worldwide regulatory authorities promote better road quality and vibration standards. But in many developing countries, there are notable departures from these standards; therefore, there is a need for improved suspension design and vibration reduction.

1.4 Impact of Faulty Road Surfaces

Improperly maintained or poorly constructed road surfaces generate irregular excitation inputs such as:

- Increased vertical and pitch acceleration of the vehicle
- Reduced tire contact force,
- Damage to suspension elements,
- Degradation of ride comfort,
- Higher transmissibility of vibration to passengers Fatigue and discomfort especially in long-haul travel.

These challenges create a strong motivation to study vehicle response under standardized random road profiles such as ISO 8608 Class A–D roads.

1.5 Traffic Calming Devices (TCDs) and Their Implications

Traffic calming elements are used to control traffic speed along roads and highways. These include speed bumps and speed tables. In India, the Indian Roads Congress (IRC) provides guidance for the geometric design in IRC:99-1988. However, these are often not implemented according to the design recommendations due to poor supervision, speedy constructions, or improper materials. Poorly designed bumps exhibit:

- Excessive height
- Sharp slopes
- Incorrect length-to-height ratio
- Inconsistent geometry

These irregularities create transient high-intensity shocks when vehicles pass over them, leading to:

- Severe vertical acceleration (jerk)

- Loss of control at moderate speeds
- High impact on suspension mountings
- Increased injury risk to passengers
- Spine compression and discomfort
- Reduced lifespan of vehicle components

Understanding the dynamic response of both the vehicle and the human body under these transient excitations is essential to ensure safety.

1.6 Ride Comfort and Evaluation Methods

Ride comfort is the measure of the vehicle's vibration isolation capacity. It can be divided into primary (low-frequency) and secondary (high-frequency) ride comfort. The ideal suspension system is a compromise between ride comfort and handling. An stiff suspension results in better handling but poor comfort, and a soft suspension results in better comfort but poor handling.

Assessing ride comfort is a multifaceted task that involves measuring the vibrations experienced by a human body, and analyzing their physiological impact. The test methods of ride comfort include objective, subjective and simulation. Because human sensitivity to vibration depends on frequency, amplitude and duration, both objective indices and subjective opinions are used. ISO 2631 is a well-known international standard for the evaluation of whole-body vibration. Objective indices include RMS acceleration, frequency-weighted acceleration (ISO 2631) and power spectral density. Subjective methods involve passenger feedback. Simulation-based

evaluation using multi-DOF models enables accurate prediction of vibration behavior under different road conditions.

1.6.1 Objective Evaluation Methods

Objective methods rely on measurable physical parameters, primarily acceleration, to quantify ride comfort. Several indices have been developed to characterize vibration severity:

1.6.1.1 Weighted root mean square (rms) Acceleration

The Root Mean Square (RMS) acceleration is very commonly used ride comfort indicator which represents the average of energy content of vibration signal for a given time period and here by represented as:

$$a_{RMS} = \sqrt{\frac{1}{T}\int_0^T a^2(t)dt} \qquad (1.1)$$

Where a(t)= Instantaneous acceleration and T= Time duration

RMS acceleration provides a measure of steady and continuous vibrations. However, it may not effectively capture transient shock caused by speed breaker or potholes.

1.6.1.2 Frequency-Weighted RMS Acceleration

Since human body is sensitive to different frequency rages, the RMS values are modified using frequency weighting factor which is represented by w*(f) (Eq. 1.2).*

$$a_w = \sqrt{\frac{1}{T}\int_0^T [w(f).a(t)]^2 dt} \quad (1.2)$$

This method provides human discomfort levels. As per ISO 2631 standards, human body is very sensitive in the frequencies range of 4-8 Hz.

1.6.1.3 Vibration Dose Value (VDV)

This method usually evaluate transient and shock types vibrations which counts cumulative effect of vibrations over time period thus provides better peak accelerations which make it suitable method to analyze vibrations caused due to different traffic calming devices such as speed breaker or potholes.

$$VDV = \left(\int_0^T a^4(t)dt\right)^{1/4} \quad (1.3)$$

1.6.1.4 Maximum transient vibration value (MTVV)

This weighted rms value does not include transient vibration and sporadic shocks. The running rms assessment approach is used for this. For this purpose, the running RMS assessment approach is used with a short integration time constant. The running RMS acceleration is calculated using the Eq 1.4 as in ISO 2631-1.

$$a_w = \sqrt{\frac{1}{T}\int_{(t_0-T}^{t_0} [a_w(t)]^2 dt} \quad (1.4)$$

Where, a_w is the frequency weighted acceleration, T is the integration time and t_0 is the time of observation. MTVV is selected as the maximum value out of these running rms

accelerations. Eq. 1.5 illustrates this. This will indicate the amount of vibration during strong shocks.

$$MTVV = max[a_w(t_0)] \quad (1.5)$$

1.6.1.5 Crest Factor

Crest factor is ratio of peak acceleration to RMS acceleration and is used to determine whether the vibration signal contains significant peak. RMS based evaluation is considered when crest factor is less than 9 whereas VDV is used for accurate assessment if crest factor exceeds 9

$$Crest\ Factor = \frac{a_{peak}}{a_{RMS}} \quad (1.6)$$

1.6.1.6 Power Spectral Density (PSD)

The Power Spectral Density (PSD) method is used to study the distribution of vibration energy over a range of frequencies. It is commonly used to detect peaks which may fall in the frequency range of the human body, and may cause resonance. PSD is commonly applied in the field of vehicle dynamics to examine the impact of road roughness on vehicle comfort.

1.6.2 Bio-dynamic Responses

1.6.2.1 Mechanical Impedance (DPMI)

The mechanical impedance is defined by ISO/DIS 5982 (2001) as a ratio of the periodic excitation force at frequency (*f*) to the consequent vibration velocity. Equation 1.7

provides a numerical expression for this ratio. It is also known as DPMI and indicates force required to cause specific response in the system.

$$Z(f) = \frac{\mathrm{F}(f)}{\mathrm{v}(f)} \tag{1.7}$$

1.6.2.2 Apparent Mass (APMS)

Apparent mass (also known as effective mass) defined as ratio of excitation force to resulting acceleration at frequency (*f*) measured at same point and in same direction. It is calculated using Eq. 1.8 as given below.

$$APMS(f) = \frac{F(f)}{a(f)} \tag{1.8}$$

The APMS gives information on the force applied to a body that results in the body accelerating in direct proportion to the mass of the body. The information is associated with the biodynamic response function of the body. An advantage of apparent mass is that it can be measured directly from the accelerometer and force transducer signals.

1.6.2.3 Seat to Heat Transmissibility (STHT)

The Seat-to-Head Transmissibility (STHT) is the ratio of the acceleration at the head to acceleration at the seat. It is a key measure of the performance of seats and suspensions.

$$STHT(f) = \frac{a_{head}(f)}{a_{seat}(f)} \tag{1.9}$$

STHT indicates the resonance effect in human body and widely used in bio-dynamics

1.6.3 Factors Affecting Ride Comfort

Ride comfort depends on multiple interacting factors including suspension parameters, tire characteristics, road roughness, human posture, and driving conditions. Vehicle speed, load distribution, and damping characteristics significantly influence vibration transmission.

A triad of road conditions, vehicle dynamics and human sensitivity to vibration dictate the ride comfort in a vehicle. The main excitation cause is the profile of the road, which contains anomalies like bumps, potholes, and roughness that create vibrations to be transmitted by the tires to the vehicle body. The suspension system is important in the control of these vibrations; the stiffness and damping properties of the suspension system will show the effectiveness of absorbing the disturbances. An overly hard suspension will pass more vibration to the occupants, whereas an overly soft suspension could result in excessive body movement and instability. Speed of the vehicle also has an effect on the comfort of the ride with speeds causing the excitation rate to rise thus the possibility of resonance when the natural frequency of the vehicle matches the natural frequency of the human body or when the natural frequency matches the vehicle natural frequency.

Also, the mass of the car can play a major role in the vibration behavior, with a larger sprung mass typically providing a better isolation, and the larger the un-sprung mass, the more vibrations caused by the road are transmitted. The properties of tires such as stiffness and pressure in case of inflation also play a role because tires form the

initial stage of vibration isolation. Another aspect is seat design, which acts as the direct interface between the car and the human body; appropriate cushioning and damping of the seat can go a long way to minimize vibrations to be conveyed to the human body. Moreover, vehicle body structural properties, including rigidity and modal behavior, may increase or reduce vibrations, as circumstances vary.

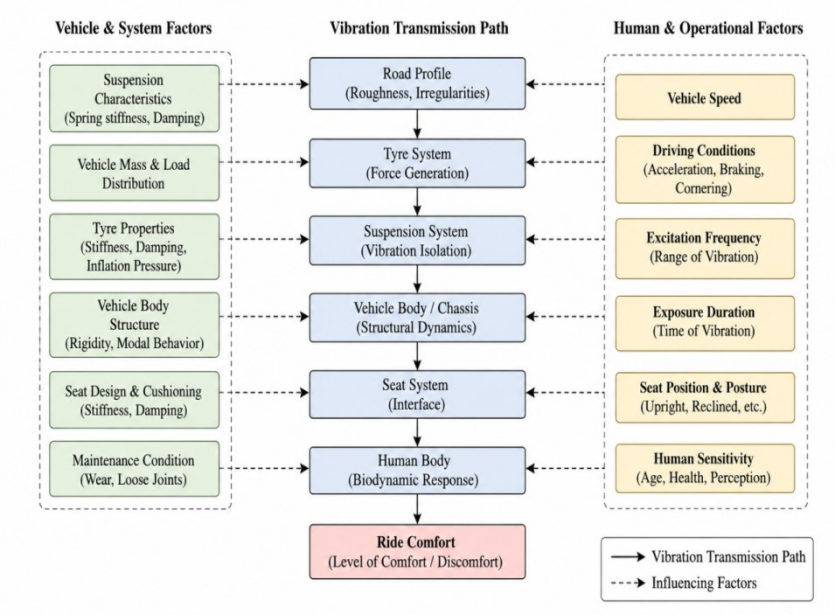


Figure 1.4 Structure diagram of factor affecting ride comfort in vehicle

A crucial element of ride comfort is human biodynamic response where various body parts are susceptible to various frequency ranges with the most discomfort normally experienced within the 4-8 Hz frequency range as a result of resonance. The acceleration, braking, and cornering driving conditions present some extra dynamic forces that affect the level of comfort. The length of exposure to vibration is also a factor, where long-term exposure may cause fatigue and discomfort, which is usually

assessed in terms of RMS acceleration and VDV according to ISO 2631 regulations. Ride comfort in general is a multi-disciplinary phenomenon that must rely on the interplay of road input, vehicle design and human perception and is extremely sensitive to optimization to ensure a balance between comfort and vehicle stability.

1.7 Vibration Frequency and Human Body Resonance

The human body is a complex mechanical system and not a rigid system but has elastic properties. The vibration frequency also influences the human body response to whole body vibrations besides its magnitude and duration. Human body responds differently to vibrations that are produced at various frequencies. The vertical vibrations of the body parts and the seat are quite similar at lower frequencies below 1 Hz due to relatively low relative motion. The higher the frequency, the higher is the motion of the body until the resonance frequency is reached. So, resonance frequency occurs when transmissibility becomes a maximum. At the resonant frequency, the body part will vibrate with a greater magnitude than the vibratory force provided. There may be an effect on the physiology of the human body, i.e. on muscular, respiratory and circulatory functions.

Magid and Coermann (1960) experimented on sitting human participants who were exposed to vibrations of different frequencies in increasing frequency to investigate physiological response of human body. These people are exposed to vibrations of 1-20 Hz. Participants will be requested to give their experiences and complaints on physical discomfort or reactions after the test. These reactions are summarized in Table 1.1.

In practice the human body does not experience pure and simple vibrations but a complex of waves of different frequencies, magnitudes and directions. The resonance occurs when there is coincidence in the frequency of the human body and the excitation frequency. The largest amount of vibration is transmitted to body parts that are resonant at the vibration frequency. The frequency of resonance of different parts of the body is different. These resonance frequencies of various parts of the human body are summarized in Table 1.2 under the different body postures *(Dupuis, H., & Zerlett, 2012)*. The resonance frequency of the same human body will differ according to the direction of vibration. The coordinate system of the same is as follows: X is the front side of the body, Y is the left side and Z is the upper side.

Table 1.2 Human body parts complaints in frequency range *(Kumbhar et al, 2012)*

Complaint	Vibration Frequency (Hz)
Headache	4-9
Speech disturbance	13-20
Jaw resonance	6-8
Throat disturbance	12-16
Respiration problem	4-8
Chest pain	5-7
Lower back pain	8-12
Abdominal pain	4-10
Constant desire for urination	10-18
Muscle pain	13-20

Table 1.3 Human body parts resonance frequency *(Kumbhar et al, 2012)*

Body Posture	Body Parts	Vibration Direction	Resonance Frequency (Hz)
Sitting	Trunk	Z	3-6
	Chest		4-6
	Spinal column		3-5
	Shoulder		2-6
	Stomach		4-5
	Eyes		20-25
Standing	Knee	X	1-3
	Shoulder		1-2
	Head		1-2
	Whole body	Z	4-7
Reclining	Foot	X	16 - 31
	Knee		4 - 8
	Abdomen		4 - 8
	Chest		6-12
	Skull		50-70
	Foot	Y	0.8-3
	Abdomen		0.8-4
	Head		0.6-4
	Foot	Z	1-3
	Abdomen		1.5-6
	Head		1-4

The *ISO 2631-1 (1997)* is now a guideline to the human tolerance to the whole body vibration. Exposure to high levels of vibration and shocks have been assessed using *ISO 2631-5 (2004). ISO 2631-4 (2001)* defines various methods of measuring periodic, random, and transient vibration. The motion sickness range is 0.1-0.5 Hz and the health, comfort, and perception range is 0.5-80 Hz.

1.8 Need for Modeling Human–Vehicle–Road Dynamics

Traditional suspension analysis often uses simplified vehicle models without considering the biodynamic response of the human body. However, the human body exhibits nonlinear and frequency-dependent behavior which must be included for realistic comfort assessment.

A 4-degree-of-freedom (4-DOF) biodynamic human model representing the head, upper torso, lower torso, and pelvis, when coupled with vehicle models, provides a more accurate representation of the vibration transmissibility path. This integration enables:

- Prediction of internal forces acting on body segments
- Understanding resonance phenomena
- Evaluation of comfort based on ISO 2631 indices
- Design of suspension control strategies to minimize human exposure

Advanced modeling techniques such as bond graph modeling provide modular, energy-based representation of the suspension system and controllers, making them suitable for coupled multi-domain dynamic systems.

1.8.1 Types and Characteristics of Biodynamic Models

Biodynamic models of seated human occupants exposed to vibration are typically characterized by two main functions *(Abbas et al., 2010)*:

1. **"To-the-body" response function:** This describes the force-motion relationship at the point of vibration entry, such as the human-seat interface. It is often expressed as the driving-point mechanical impedance or apparent mass.
2. **"Through-the-body" response function:** This characterizes the transmission of vibration to different body segments, commonly termed as seat-to-head transmissibility for seated occupants

Various biodynamic models have been developed, ranging from single-degree-of-freedom to multi-DOF models. These can be broadly categorized into:

- **Lumped-parameter models:** These are popular analytical methods for studying biodynamic responses of seated human subjects, though they are often limited to one-directional analysis, typically focusing on vertical vibration.
- **Multi-body models:** These models represent the human body as a system of interconnected rigid or flexible segments. For instance, a 15-DOF multi-body dynamic model can depict segments like shanks with feet, thighs, pelvis, torso with arms, and the head, considering contact between the occupant and the seat, backrest, headrest, and vehicle floor. Similarly, a 20-DOF biomechanical model has been proposed that includes a backrest to analyze cross-coupled segmental transmissibility, addressing issues like lumbar pain caused by force transmitted from the backrest *(Guruguntla, V., & Lal, 2023)*.

- **Distributed (finite element) models:** These models treat complex body structures, such as the spine, as layered rigid and deformable elements to capture more detailed biomechanical responses.

1.8.2 Application in Vehicle Ride Comfort Analysis

Vehicle-human dynamic models are used to study ride comfort. This includes coupling a human model (e.g., a 15-DOF multi-body model) with a vehicle model (e.g., a half-car model) to examine the vibration response of different parts of the human body during driving. These models facilitate a more detailed evaluation of the effects of low-frequency vibration, arising from road roughness and transmitted through the tires, suspension and seats, on human comfort and health.

1.8.3 Challenges and Advancements in Biodynamic Modeling

Unlike traditional vehicle models that consider components as rigid bodies, biodynamic models emphasize the human body as a biological system with non-linear characteristics. For instance, the apparent mass of a seated human body subjected to vertical vibration is non-linear, with resonance frequency dropping with increased vibration level. This requires sophisticated models that can account for such non-linear biodynamic responses, including the effect of elements such as legs, thighs, pelvis, torso, head and viscera *(Kuang et al, 2023)*.

Also, the effects of vibration frequency, magnitude, direction and duration, and subject-specific factors such as posture, age, gender and anthropometry on the human

response, are critical for predicting ride comfort. The goal is to create biomechanical models capable of assessing vibration transmissibility and dynamic response, especially to vertical vibration, since this is a major driver for driver exposure.

To conclude, biodynamic models are critical for predicting human response to vehicle vibration, and subsequently designing suspension systems that offer improved ride comfort, while also reducing the risks of health problems and improving safety. Such models go beyond simplistic models to provide a more realistic description of the vehicle-occupant system.

1.9 International Standards ISO 2631:1

ISO 2631-1 was developed by the international standard organization (ISO). This standard provides the general data necessary to evaluate the human body exposure to whole body vibrations. This includes numerous methods of measuring and assessing vibration, including rms acceleration, VDV value, and MMTV value. Moreover, this standard defines several frequency weighting variables which are useful in calculations related to motion sickness, comfort, health, and perception.

This section describes these ISO 2631-1 frequency weighting factors. The human body has a different sensitivity according to frequency. Frequency weighting factors explain this change of sensitivity with frequency. As a result, frequency weighting factors compensate and normalize the human susceptibility and sensitivity at different frequencies.

Table 1.3 summarized the frequency weighting factors of the frequency within the one-third octave band. The one-third octave band frequency range (between 0.1 and 400 Hz) offers standard frequency weighting factors. Since frequency below 0.1 Hz is not significant in the calculation of the weighted acceleration, the weighting factors of frequency are not calculated below 0.1 Hz. Another focus of this standard is the possible tolerance of these weighing factors.

The main and additional frequency weighting factors are outlined in Table 1.3. Vibration frequency content defines the effect of vibration on perception, comfort, health and motion sickness. Different frequency weighting factors are offered depending on the vibration axes and the purpose, e.g. motion sickness and comfort. Table 1.3 shows that there are six criteria of weighting in motion sickness, comfort, perception, and health. These are of two kinds:

(a) Principal weighting factor

W_k – For vibration in Z direction

W_d – For vibration in X and Y direction

W_f – For motion sickness

(b) Additional weighting factor

W_k - For vibration at seat and back interface

W_d – For rotational vibration

W_f – For head vibration

1.10 Bond Graph Modeling

In physical system when interconnected, it is energy which play important role and the connection points of a bond graph node that enable the energy exchange with other nodes across a power bond are called power ports. Power ports may be viewed as places where energy can enter or leave a subsystem. Each energy port is represented by a bond which is associated with two factors of power, i.e., Effort and Flow.

$$\text{Power} = \text{Effort}(e) \times \text{Flow}(f)$$

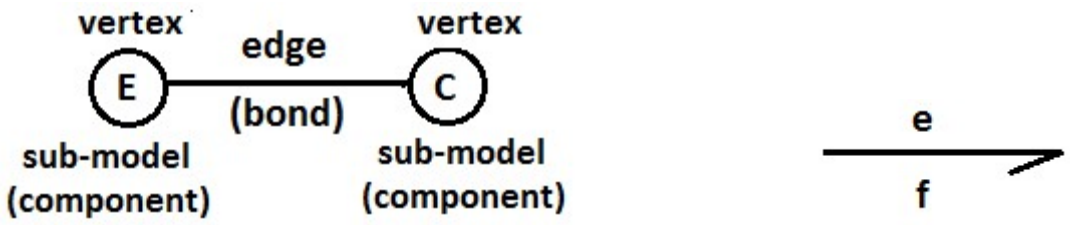


Fig. 1.5 Bond Representation

An energy flow between two power ports also involves a transfer of information. one needs to recognize only four groups of basic symbols,

(1) 3 basic one port passive elements inertance (I), capacitance (C), and resistance (R);

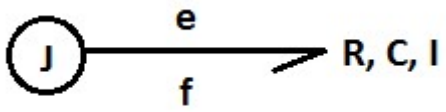


Fig. 1.6 Passive element port

(2) 2 basic active elements source of effort (SE), and source of flow (SF);



Fig. 1.7 Source Representation

(3) 2 basic two-port elements transformer (TF) and gyrator (GY);



Fig. 1.8 Two-port element representation

(4) 2 basic junctions i.e., common effort junction (0), and common flow junction (1).

The basic variables are effort (e), flow (f), time integral of effort (P) and the time integral of flow (Q). The bond graph modeling can able to describe the systems with diverse energy in a unified manner. Bond graph technique offers flexibility in modeling and formulation of system equations. A very large system may also be modeled in a modular form by creating subsystem models and then joining them together at their interaction port to create an integrated system model. Bond graph equations normally use generalized displacement and generalized moment as state variables. The bond graph modeling, their simulation and animation are performed using SYMBOLS Sonata® (*Mukherjee and Samantaray,* 2006), a bond graph modeling software.

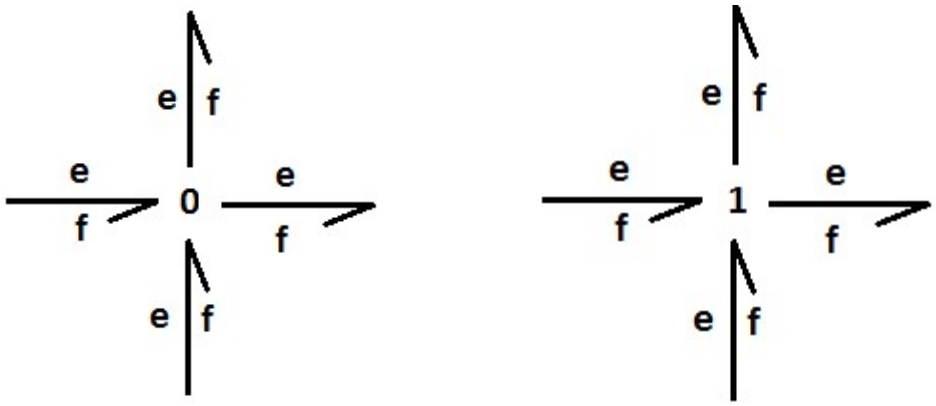


Fig. 1.9 Junction representation

10 The advantages offered by bond graph modeling are as follows:

- It is a unique language for all physical domains,
- It clearly shows the cause and effect relations in the model,
- It allows further possible development and evolution of the model, it is also a tool for analyzing the system's structural properties

turnitin Page 36 of 269 - Integrity Submission Submission ID trn:oid:::29034:141996562

CHAPTER 2

Literature Review

In this Chapter, we discuss our extensive literature review on Vehicle Suspension Modeling, Biodynamic Human Response to Vehicle Motion and Advanced Control Strategies for Enhancing Ride Comfort. We present an evaluation of the shortcomings of traditional models and emphasize the need for an Integrated Human-Vehicle Analysis Framework. The Research Gaps have been methodically identified which has led to the definition of well-defined Objectives for our Study. Each Objective has been linked to the Gaps and their Relevance to Real-World Applications. Our Research Direction is justified at the end of this Chapter and describes the Methodology adopted to meet the Stated Objectives of our Research. The Chapter also outlines the steps involved in the Modeling, Simulation, Control, Validation and Optimization Processes. In addition, the Tools, Approaches and Experimental Setup used for Verification are discussed in detail. The Chapter also includes a Diagrammatic Representation of the Research Flow

illustrating the Interactions between the Different Phases of Work. The Chapters will follow from this Literature Review Chapter.

2.1 Literature Review

Many researchers employed different controller and further optimization techniques to improve Ride Comfort (RC). Literature review is carried out on various published papers around the globe related to simulation of vehicle suspension by different approach and by using different controllers with optimized parameters. Major works have been captured to identify the research gap.

2.1.1 Literature Review Based on bio dynamic model

In literature, several mathematical models have been developed to study the biodynamic reaction of the seated human body. Biodynamic models are as old as the 1900's *(Hamilton, 1918).* There have been numerous models developed since then. The models can be divided into three types: Multi-body models, Finite element models and Lumped parameter models *(Kumbhar et al, 2012).* There are many models placed in the literature which represent each of these types of models.

The human body is a multi-part structure composed of physically distinct parts including head, neck, torso, legs and hands. According to lumped parameter model, the human body is considered a system of masses at concentrated locations, each mass representing a body part, and linked to other masses by springs and dampers. It, therefore, consists of dampers, springs and lumped masses. It is the most frequently used

analytical method for analyzing the seated body's reaction. This is a simple analysis technique and easy to check the results. It has several drawbacks however, as it is a 1-D vibration analysis.

Nigam and Malik (1987) have identified the critical steps for developing a lumped parameter model. As human body is build up of various body parts, the LP model breaks these parts of the body into various divisions of mass. These masses are connected with springs and dampers to represent the flexibility between body parts. After that mass and stiffness values of segments are determined and grouped together at various locations connected by springs and damper, springs and dampers' stiffness values are then evaluated. The lumped parameter models are classified based on the number of degrees of freedom (DOF) they have.

(Coermann (1962) presented the simplest model to predict vibration response considering human body as a single mass and represented it as 1-DOF (Fig. 2.1) although this model was able to capture body parts responses efficiently. *Wei and Griffin (1998)* presented whole body as two parts where seat with neglected mass is considered in rigid contact with leg and buttocks as shown in Fig 1.2.

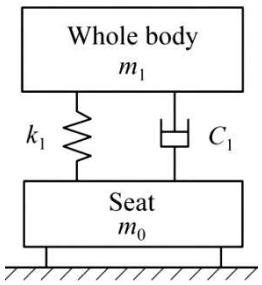


Figure 2.1 1-DOF Coremann Model

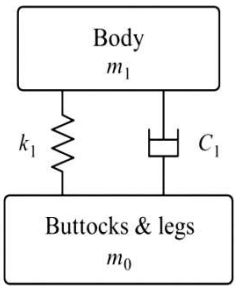


Figure 2.2 1-DOF Wei and Griffin Model

A nonlinear 2-DOF model with a total mass of 79.83 kg was proposed by *(Muksian and Nash, 1976)* and is shown in Figure 2.3. In this model, there are three mass segments: head, body and pelvis. Each of the spring and damper (except for the body, used to connect to the body and pelvis) is linear. There are both linear and nonlinear components to the damper that joins the body and pelvis. The physical characteristics of the pelvis are incorporated into the spring/damper between the pelvis and the seat, so the pelvis is firmly joined to the seat.

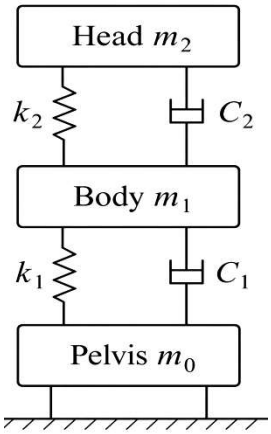


Figure 2.3 2-DOF Muskian and Nash model

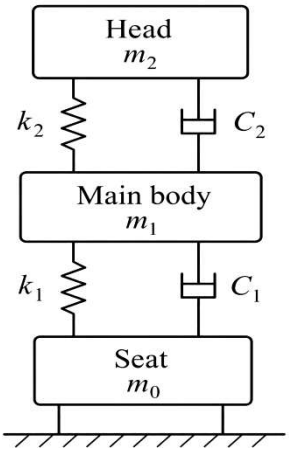


Figure 2.4 2-DOF Allen model

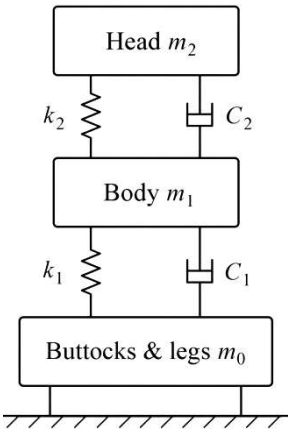


Figure 2.5 2-DOF Wei and Griffin model

Allen (1978) presented a linear 2-DOF model having a total mass of 56.8kg consisting head and body, which are seated on the seat as seen in Figure 2.4. *Wei and Griffin (1998)* extended their 1-DOF model to 2-DOF, with an assumption that the model was linear. This model's overall mass is subdivided into three separate mass components as shown in the model in Figure 2.5. These three components are the buttocks and legs, body and head. Similar to their 1-DOF model, the seat's mass is disregarded while the buttocks and legs' masses are in strict touch with it.

Lewis and Griffin (2002) used Wei & Griffin's 1 and 2-DOF models to test seats with five foam cushions. For testing these seats anthrop dynamic dummies with an appropriate apparent mass were developed. The measured cushion transmissibility's for both the 2-DOF model and 1-DOF model showed that there was a larger difference in this frequency range between 2-4 Hz. This suggests that in order to obtain more accurate results, more degrees of freedom must be increased.

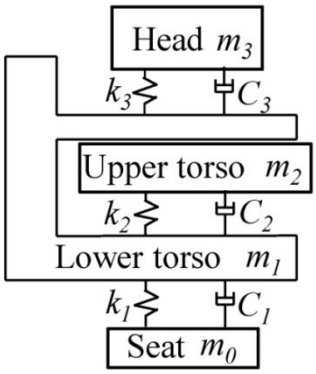


Figure 2.6 3-DOF Suggs linear model

A linear 3-DOF model (Fig 2.6) with a total mass of 56.8 kg was reported by *(Suggs et al, 1969)*, the model has four different mass elements: head, upper torso, lower torso, and seat. The upper and lower torso are coupled with a spring and damper with stiffness and damping coefficient set to infinity and linear springs and dampers are used in throughout the rest of the structure.

Wan and Schimmels (1995) have introduced a linear 4 DOF model with total mass 60.67 kg as shown in figure 2.7. This model has 4 separate parts of the body - the head, upper torso, viscera and the lower torso which is securely fastened to the seat.

Boileau and Rakheja (1998) have presented a 4-DOF linear model with a total mass of 55.2 kg. The four mass segments of this model, namely the head, upper torso with chest, lower torso and thigh and pelvis on the seat are shown in Figure 2.8. The four sets of linear springs and dampers (ki & Ci) connect these segments together.

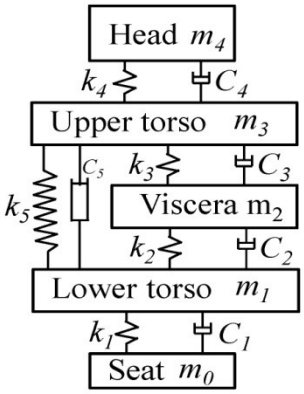


Figure 2.7 4-DOF Wan and Schimmel model

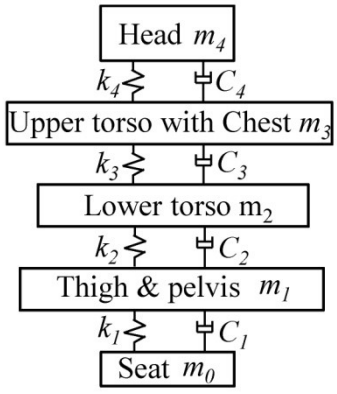


Figure 2.8 4-DOF Boileau and Rakheja model

Liu et al, (1998) provided a four-DOF nonlinear model including a total mass of 55.2 kg. Four mass elements, each representing the head, upper torso, viscera, and pelvis inter-connected through nonlinear springs and dampers as depicted in Fig. 2.9. The upper abdomen and internal organs are not attached but it is suspended from them. Thus, the gravitational effect is taken into account in this model.

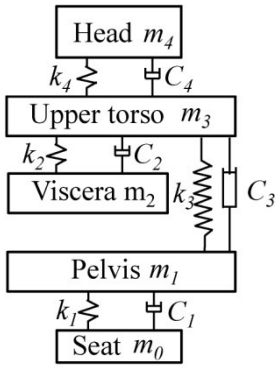


Figure 2.9 4-DOF Liu model

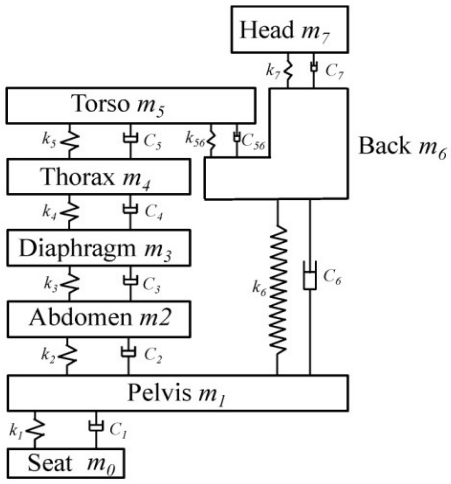


Figure 2.10 4-DOF Muskian and Nash model

Muksian and Nash (1974) developed a 7-DOF nonlinear model having a total of 7 elements of 80 kg of mass, as shown in Fig. 2.10. The head, back, torso, thorax, diaphragm, abdomen, and pelvis are represented by each element. With the exception of two sets of linear springs and dampers that connect the neck and back, are coupled by nonlinear spring and damper sets. The mass of the pelvis is securely connected to the seat. This model also incorporates new phenomena related to Coulomb damping forces (the friction between the torso and back, and related muscle forces during contractions

and diaphragm muscle forces) The vibrations of the whole body were studied in the vertical direction.

2.1.2 Literature review based on Computational Approach

Mohite et al. (2018) created Linear and Non-linear vehicle suspension Model and simulation was done analytically and with MATLAB/SIMULINK for Ride comfort (sprung mass displacement and acceleration) and observed that RMS acceleration for linear system is less than non-linear system where settling time for linear is more than non-linear system.

Mahala et al. (2009) developed 2-DOF, 4-DOF and 7-DOF mathematical model and further analyzed using simulink for pitch and roll modes of inputs and response of body displacement and acceleration was observed. It was concluded that 7-DOF model can simulate for pitch and roll accurately while 4-DOF is giving better result for pitch.

Talukdar et al, (2012) incorporated a flexible Ring Tire model into a 4-DOF half car model and effect of tire flexibility on vehicle ride is analyzed. Also a 2-DOF with chassis considered as an EULER BEAM on spring is analyzed and compare with rigid chassis and Simulation of MR damper using Bouc-Wen Model has been studied using PID controller and observed there was 50% reduction in acceleration and displacement settling time using PI controller with MR damper.

Jiang et al., (2008) investigated on chaotic response of a non-linear 2-DOF ground vehicle by giving pyramidal wave disturbance at wheel. Phase diagrams and Poincare

maps are used to confirm the chaotic motion once the bifurcation phenomenon has been identified. The bifurcation diagram indicates that the frequency may have an impact on the chaotic response.

Jin et al. (2016) studied how Ride comfort of vehicles driven by in-wheel motors affected, for the purpose 11-DOF vehicle ride comfort model studied with MATLAB/Simulink and the result obtained shows that ride comfort become poor with increasing un-sprung mass and for improving comfort semi active air suspension PID control system was proposed.

Banerjee et al. (2016) developed a 17-DOF full tracked vehicle with trailing arm hydro gas suspension and non-linear coupled governing differential equation of motion was derived for sprung mass and 14 un-sprung masses with actual trailing arm kinematics and inertia coupling effects. Results were obtained in matlab and validated using developed ADAMS multi-dynamic model and it was observed that higher suspension charging pressures enhance vibration transmissibility to the vehicle.

Tejas et al. (2016) studied a 2-DOF half car model using state space formulation and Matlab/Simulink and further observed that change of mass on rear wheel has more effect on vehicle vibration than on front wheel. Also it was observed that with the increase of sprung mass, settling and rise time increases whereas peak time and peak magnitude point decreases.

Ikenaga et al. (2000) proposed an active suspension control approach combining a filtered feedback control scheme and an "input decoupling transformation"(IDT) for a

full-vehicle suspension system in order to reduce heave, pitch and roll accelerations and improve ride quality of the vehicle. It was demonstrated that active filtering of spring and damping coefficients through inner control loops (ride controller) and skyhook damping of heave, pitch, and roll velocities through outer control loops (attitude controller) could reduce motions of the sprung mass above and below the wheel frequency. Simulations were used to show how well the active suspension control worked.

Sathishkumar et al. (2007) discussed state space mathematical model for 2-DOF quarter car model and further simulated under Matlab and Simulink environment. Further Passive, semi-active and active suspension systems connected in a single loop and tested under step and single bump input and found active suspension better efficient than passive and semi-active.

Modi et al. (2016) have done analysis of road handling and ride performance was done for 2 DOF quarter car model by Matlab simulink and state space formulation and it was observed that peak for sprung mass displacement is reduced and for un-sprung mass increased for different combination of sprung and un-sprung mass.

2.1.3 Literature review based on Controllers

Sever et al. (2017) used L2 gain state derivative feedback controller for active suspension with 5-DOF driver quarter model with integrated drive seat by using ISO 02631 random road disturbance for A, B, C and D class with different speed. Further

performance of l2 gain controller and conventional feedback controller were compared and found L2 gain controller improve ride comfort better than state feedback controller.

Mouleeswaran et al. (2012) designed PID controller for active suspension system of 2-DOF quarter car model and determined the gain, reset rate and derivative time of PID controller by following Ziegler Nicholas tuning rule. Bumpy road, pothole and random road inputs were used for simulation and found ride comfort can be improved with less rattle space.

Heidari et al. (2013) carried out analysis on quarter car suspension system model for the design of PID controller and found the gain parameter of controller by using Back Propagation Neural Network (BPN) and found BPN is most accurate, quickly and low cost method as compared to classical methods. The result shows best regression value (0.9999) with newelm function and found it (newelm) more accurate than newff and newcf.

Ahmed et al. (2013) scanned road profile in front of vehicle using lidar sensors further signal were analyzed using FFT and proposed a preview controller, a control signal is generated based on Model Predictive Control (MPC) which is further calculated offline using half car model and system performance is compared with passive suspension, skyhook approach, adaptive robust controller and an optimal preview controller thus found better ride comfort.

Sinha et al. (2017) designed PI, PID, and H infinity Controllers and employed for controlling a suspension system of a quarter Car model using Matlab/Simulink and

compared the response of above mentioned controllers. Overshoot and settling time for open loop, PI and PID was recorded 0.08, 0.0058, 0.0039 and 35second, 6 second and 2second respectively. A separate analysis of H infinity control method is also been carried out which also improves the ride quality, vehicle stability and handling . It was observed that active suspension can not only improve the effects of increased un-sprung mass of the vehicles but also present better performance of the stability of the system.

Shah et al. (2016) reviewed different controllers and highlights developments of fractional PID controllers including their design and tuning, as well as explores their various versions and Software tools associated to the design of fractional PID controllers and it was suggested that Caputo definition is more relevant in the case of engineering applications as compared to other definitions and found many researcher using order of differentiation and integration in the range of 0 to 2 as initially it was 0 to 1.

Li and Wei, (2009) established stochastic road model by filtering white noise, and then the precise stationary response of the vehicle is deduced using the stochastic averaging method and the optimal feedback control law is determined based on the theory as mentioned earlier and further velocity feedback control and the unknown control gains are determined by minimizing the modal performance indices.

Dabiri et al. (2018) studied variable fractional order PID (VFPID) controller and further optimization was done using particle swarm optimization technique and results were compared with PID and FPID (fractional order PID) and found VFPID more flexible.

Dogruer et al. (2018) designed PI controller for stabling system using Stability boundary locus method (SBL) and further controller parameter (gain) which stable the system are optimized by using Integral Performance Criteria optimization. Simulation was carried out for closed loop control system using fractional order transfer function. A comparison of control parameter from optimized result and Ziegler Nicholas was done and found better optimized result. Best settling time was achieved using IAE criterion, while the less % overshoot was achieved using ITAE criterion.

Rao, (2014) Analyzed performance of a quarter car semi-active suspension system using PID controller under MATLAB Simulink Model. Two types of road input were used as input and result shows (Table 2.1) reduction in wheel and body displacement and acceleration by using PID controller.

Table 2.1 Response comparison of Passive and semi-active quarter car

	Settling Time(Sec)		
	Passive	**Semi-active**	**Improvement**
Body Acceleration	300	50	83 %
Wheel Deflection	250	60	76 %
Wheel Position	255	65	74.5 %
Suspension Deflection	300	85	71.66 %
Body Position	300	75	75%

Singh et al. (2017) Evaluated ride comfort of semi-active quarter car system with 3-DOF. Displacement of suspension system was analyzed under PID, Fuzzy logic and Hybrid Fuzzy PID controller. Results demonstrated that the semi-active suspension system having HFPIDCR in combination with magneto-rheological shock absorber

exhibits best performance in controlling the acceleration and displacement response of passenger seat as shown in Table 2.1.

Mehta et al. (2016) used Teacher-Learning based Optimization (TLBO) for improving Ride Comfort by using optimized spring stiffness. Further a novel approach was used to control damping coefficient, an active suspension parameter, using PID controller for better performance. Acceleration of sprung mass and Rattle space (Relative displacement) of semi active and passive quarter car suspension were compared.

Zheng et al. (2018) proposed tuning method by an improved frequency domain method to design FPID controller. A proportional relation was built between integral and derivative control while order of integral and derivative order are set equal and found this new designed FPID gives better result.

Cokmez et al. (2018) found stability regions based on specified gain and phase margins for a PI controller to control integrating processes with time delay have been obtained and depending on the values of the order λ, and phase and gain margins, different stability regions have been obtained. Two stability boundaries have been used to obtain stability regions; RRB (Real Root Boundary) and CRB (Complex Root Boundary). Result shows that the integral integer order $\lambda<1$ gives larger stability region.

Gandhi et al. (2017) used 4 DOF half car active suspension system to design PID, Linear Quadric Regulator (LQR), Fuzzy and adaptive neuro fuzzy Inference System (ANFIS) controller using Matlab/Simulink and response of controller was analyzed

using ISO-8608 road profile and found ANFIS based controller perform better as compared to others in terms of Settling time and amplitude as shown in Table 2.2.

Table 2.2 Response comparison of Passive, LQR, FUZZY and ANFIS controller

Control System	Peak Overshoot (metres)				Settling Time (seconds)	Max. Front Control Force (N)
	1st Peak		2nd Peak			
	Value	Time	Value	Time		
Passive	0.460	0.683	0.425	1.59	>20	-
LQR	0.468	0.683	0.276	1.55	10	1054
Fuzzy	0.417	0.683	0.228	1.56	9	771
PID	0.373	0.683	0.078	1.54	4.6	1463
ANFIS	0.369	0.675	0.061	1.54	4	1367

Ashish et al. (2012) created 7-DOF road truck model using bond graph further dynamic behavior has been presented under various vehicle speed and found vertical force is higher at 60 km/hr and lower at 80 km/hr. Simulation results shows reduction in vibration with proportional control.

Gupta et al. (2016) established 11DOF full truck model using bond graph approach and analyzed dynamic behavior under various speed and bum conditions and found vertical deflection comparatively less for first bump condition and cab acceleration also found within range for first bum condition.

Frih et al. (2017) created quarter, half and full car model using bond graph approach and analyzed vertical displacement and suspension velocity. Further concluded that the Bond graph as effective tool for ride comfort analysis.

Tiwari et al. (2014) created 2DOF quarter car model with or without PID controller using bond graph and simulated under various operating speed the fourth order runge-kutta method. Result shows active suspension better than passive suspension system.

Agrawal et al. (2013) proposed a modified adaptive synchronization method for fractional order chaotic systems and developed identification parameters law based on Lyapunov direct stability theory in such a way the components of the error systems and parameter estimation error systems decay towards zero as time becomes large.

Agrawal et al. (2012) studied dynamical behavior of coupled chaotic systems of fractional order and employed powerful active control method which provides a simple way to synchronize a pair of chaotic systems. Further it was observed that the synchronization time varying not only depends on derivative order but also on chaotic behavior of the system.

Agrawal et al. (2017) investigated local stability, stability of the equilibrium points using the fractional Routh–Hurwitz criterion and sufficient conditions for control of the fractional- order Duffing Van-der Pol system by linear feedback control and studied dynamical behavior and existence of chaos in model. Simulation demonstrates that the feedback control is better and easy to implement for controlling the fractional order chaotic systems.

28

2.1.4 Literature review based on Optimization

Schiehlen et al. (2015) analyzed driving comfort with two criteria-

Criterion 1: the vertical body acceleration characterizing the driving comfort $a_A = \ddot{z}_A$ has to be minimal and Criterion 2: the dynamical wheel load affecting the driving safety has to be minimal. A multi criteria approach was taken for studying damping value required for drive safety as well as drive comfort and further conflict diagram of vehicle suspension for variable damping was studied.

Mitra et al, (2015) implemented response surface methodology (RSM) for the purpose of finding optimal setting that assure optimal ride comfort (RC) of vehicle with respect to suspension spring stiffness (Ks), damping coefficient (Cs) and sprung mass (ms). The model is fitted with significant term of coefficient of determination R2 is equal to 99.74 %. Result show that minimum value of RC is achieved by considering Ks, Cs low and m_s high.

Bouazara et al. (2001) analyzed effects of vibrations on the comfort and road holding capability of road vehicles as observed by varying different parameters such as spring constant, road disturbances , and the seat position. A 3-D vehicle model with 8-DOF active and semi-active suspension system on road prove to be beneficial for comfort without compromising road holding (RH). An objective function was taken for different performance criterion which allows to feed in an optimization algorithm sequential unconstrained minimization technique (SUMT) in order to obtain optimal suspension parameters. It was analyzed and concluded that the active and semi-active suspensions

enhance comfort by 30% to 50% as compared with the passive model and on an average there was 30% improvement for driver and sprung mass bounce and 50% for roll acceleration.

Chi et al. (2008) presented a comparative study of three optimization algorithms, namely Genetic Algorithms (GA), Pattern Search Algorithm (PSA) and Sequential Quadratic Program (SQP) for the design optimization of vehicle suspensions based on a quarter-vehicle model. To implement the design optimization, five parameters M_s, M_{us}, K, C, K_t respectively are selected as the design variables using three design criteria, vertical vehicle body acceleration, rattle space, and the dynamic tire load. It was analyzed that the global search algorithm (GA) and the direct search algorithm (PSA) are more reliable than the gradient based local search algorithm (SQP).

Hrovat (1990) explored connections between optimal 1-DOF and 2-DOF models and maximum possible ride and handling improvements for 2-DOF systems obtained in the limiting case of singular control with zero penalty on un-sprung actuator force and concluded that absolutely optimal structure turns out to be yet another special 1-DOF system, which in practice could be approached with the help of active dynamic absorbers.

Likaj et al. (2014) used two optimization algorithm Sequential Quadratic Program (SQP) and Genetic Algorithms (GA) for a five chosen design parameters with ride comfort, suspension travel and road holding as a goal function. Fuzzy Logic Control (FLC) is

considered to control active suspension for the optimal parameters derived by GA's, and found decrease in sprung mass acceleration by optimizing design parameter.

Mitra et al. (2016) done analysis on quarter car model it was observed that work that the RC cannot be successfully optimized by controlling only spring stiffness, damping coefficient, and the sprung mass and concluded that the steering geometry angles, camber and toe with the tire pressure, significantly affect the ride behavior of a vehicle along with the primary suspension parameters.

Mahmoodi-Kaleibar et al., (2013) optimized geometric parameters of suspension system using genetic algorithm (GA) in a way that RC, RH and stability of vehicle can be improved and the simulation results indicate that the camber angle variations decrease by the optimized suspension system, resulting in improved handling and ride comfort characteristics.

Fernandes, (2017) found optimum values of suspension and steering parameters to give the best ride comfort using an validated ADAMS model which has the capability of altering seven different influential parameters namely sprung mass, un-sprung mass, spring stiffness, damping coefficient, tire stiffness, camber and toe. The Design of Experiment approach was implemented in order to obtain optimal values for each parameter.

Table 2.3 Literature Summary

A. Literature review based on Computational Techniques				
Author	**Vehicle Model**	**Investigating Parameter**	**Methodology**	**Outcome response**
Mohite et al. (2018)	2-DOF Quarter Car	Ride Comfort (RC)	Mathematical Modeling, MATLAB, SIMULINK	RMS acceleration of linear system is smaller than the non-linear system
Mahala et al. (2009)	2-DOF Quarter Car, 4-DOF Half Car. 7-DOF Full Car	Ride Comfort (RC) and Body displacement	Mathematical Model, SIMULINK	7-DOF model can simulate for pitch and roll accurately while 4-DOF is giving better result for pitch
Talukdar et al. (2012)	2-DOF Quarter Car 2-DOF Half Car 4-DOF Full Car	Ride Comfort (RC) and Settling time of acceleration	Mathematical Modeling, State Space formulation, MATLAB	Reduction in 50% settling time in acceleration and displacement response using PI controller with MR damper.

Jiang et al. (2008)	2-DOF Quarter Car	Chaotic response, Poincare maps and phase diagrams, Neimark-Sarker bifurcation	Mathematical Modeling, Quarter car model, MATLAB	There exist chaotic in non linear vehicle system and the chaotic response could be sensitive to the frequency as shown in bifurcation diagram.
Jin et al. (2016)	11-DOF Full Car	Ride Comfort (RC)	Mathematical Modeling, SIMULINK	Ride comfort become poor with increasing un-sprung mass and proposed semi active air suspension PID controller for improving ride comfort.
Banerjee et al. (2016)	17-DOF Full Car	Ride Comfort (RC)	Mathematical Modeling, MSC-ADAMS	Increase in transmissibility due to higher suspension charging pressures
Tejas et al. (2016)	3-DOF Half Car	Sprung mass deflection, settling time, rise time, peak time.	Mathematical Modeling, State Space formulation, SIMULINK	Effect of changing rear wheel mass has more effect on vehicle vibration than on changing

				front wheel mass.
Ikenaga et al. (2000)	7-DOF Full Car	Ride comfort (RC), Pitch accelerations and Roll accelerations	Mathematical Modeling, State Space formulation, MATLAB	There achieves reduction in motion of the sprung mass above and below the wheel frequency using active filtering of spring and damping coefficients through inner control loops (ride controller) plus skyhook damping of heave, pitch and roll velocities through outer control loops (attitude controller).
S.kumar et al. (2007)	2-DOF Quarter Car	Sprung and Un-sprung mass displacement, Suspension deflection	Mathematical Modeling, State Space formulation, SIMULINK	Active suspension achieves reduction in peak amplitude and settling time in

				comparison to semi-active and passive suspension.
Tejas et al. (2016)	2-DOF Quarter Car	Ride Comfort (RC), Road Holding (RH)	Mathematical Modeling, MATLAB, SIMULINK	Reduction in peak displacement for sprung mass and for un-sprung mass increasing for different combination of sprung and un-sprung mass.
B. Literature review based on Controllers				
Author	**Vehicle Model**	**Investigating Parameter**	**Methodology**	**Outcome response**
Sever et al. (2017)	5-DOF Quarter Car	Cabin floor acceleration, Human body acceleration	Mathematical model, L2 gain state derivative feedback controller	Performance of l2 gain controller and conventional feedback controller were compared and found L2 gain controller improve ride comfort better than state feedback controller.

29

Mouleeswaran et al. (2012)	2-DOF Quarter Car	Car body displacement and acceleration, suspension travel, tire deflection and Gain (Kp, Ti & Td) of PID controller	PID Controller, Mathematical Modeling, SIMULINK	Ride comfort can be improved with less rattle space
Heidari et al. (2013)	2-DOF Quarter Car	Gain parameter (Kp, Ki & Kd), Body displacement and acceleration	Mathematical Modeling, Controller, Artificial Neural Network, BPN	Found BPN as low cost, high speed and more accurate as compared to other classical methods in the designing of PID controller.
Ahmed et al. (2013)	2-DOF Half Car	Chasis displacement and acceleration, pitch angle	Mathematical Modeling, Model predictive Control (MPC)	System performance of passive suspension, skyhook approach, adaptive robust controller and an optimal preview controller are compared

				and found better ride comfort.
Sinha et al. (2015)	2-DOF Quarter Car	Overshoot and settling time, Ride comfort, Road holding and Vehicle stability	PI, PID & H infinity Controller, Mathematical Modeling, SIMULINK	Active suspension can not only improve the effects of increased un-sprung mass of the vehicles but also present better performance of the stability of the system.
Shah et al. (2016)	Review paper			
Xueping et al. (2019)	2-DOF Quarter Car	Sprung mass displacement, velocity and acceleration	Controller, Mathematical Modeling, Optimization using Stochastic Averaging Method	Controller gains are calculated by minimizing the modal performance indices.
Dabiri et al. (2018)	1-DOF Quarter Car	Settling time, Tracking error (ITSE)	PID, FPID & VFPID Controller, particle swarm optimization (PSO)	Found VFPID more flexible as compare to FPID and PID

Dogruer et al. (2018)	Fractional order system, Unit Step Response	Controller gain, Settling time, Overshoot	Stability boundary locus method (SBL), optimization of gain parameter using IPC, Ziegler Nicholas, SIMULINK	Controller gain from optimization results found better than Ziegler Nicholas. Also best settling time achieved with the IAE criterion while the smallest % overshoot value was achieved with the ITAE criterion.
Dhananjay et al. (2014)	2-DOF Quarter Car	Ride comfort (RC), Suspension deflection,	State space formulation, PID controller, SIMULINK	Reduction in wheel and body displacement and acceleration by using PID controller.
Singh et al. (2017)	3-DOF Quarter Car	Ride comfort (RC), Suspension displacement,	Mathematical modeling, State Space formulation, PID, Hybrid Fuzzy PID & HFPIDCR controllers	HFPIDCR in combination with magneto-rheological shock absorber provide best performance in controlling the passenger seat acceleration and displacement

				response compared to PID, HFPID
Mehta et al. [22]	2-DOF Quarter Car (Passive & Semi-Active)	Ride comfort (RC), Rattle space, Spring stiffness, damping coefficient	Optimization (TLBO), PID controller	Improved ride comfort achieved by using variable damping constant.
Zheng et al. (2018)	Unit Step response	Motor speed, Controller gain	Improved frequency domain design, FPID Controller	Proposed tuning method by an improved frequency domain method for designing FPID gives better control
Cokmez et al. (2018)	Fractional order system	Stability region, specific gain, phase margin, integral order	Fractional-PI/PID Controllers	Integral integer order $\lambda<1$ gives larger stability region.
Gandhi et al. (2017)	4-DOF Half Car	Peak overshoot, Settling time and Amplitude.	Mathematical modeling, State Space formulation, MATLAB SIMULINK, PID, LQR, FUZZY and ANFIS Controllers	ANFIS based controller perform better as compared to others in terms of Settling time and amplitude.
Gupta et al. (2012)	6-DOF Full truck	Suspension displacement, Vertical force	Bond Graph modeling, Proportional controller	Vibration reduced using proportional controller hence validating simulation

				using bond graph.
Gupta et al. (2016)	11-DOF Full truck	Suspension deflection, Cabin acceleration	Bond Graph modeling under different vehicle speed	Suspension deflection and cabin acceleration simulated under various speed and bumps and found optimized bump size for better ride comfort.
Abderrahim et al. (2017)	Quarter Car, Half Car, Full Car	Vertical force, Relative suspension velocity	Mathematical modeling, Bond Graph modeling	Proposed Bond graph simulation as an effective tool for ride comfort analysis.
Tiwari et al. (2014)	Quarter Car	Ride comfort, Road holding,	Bond Graph modeling, PID controller	For better handling performance minimum wheel deflection and for better ride comfort minimum vertical car body velocity have been achieved in terms of low overshoot and settling time

22

Agarwal et al. (2013)	Chaotic Model	Variation of synchronization time w.r.t different fractional order derivative	Modification of adaptive control method	Modification of adaptive control method with unknown parameters for fractional order derivatives of the existing adaptive control method to reduce time of synchronization
Agarwal et al. (2012)	Different Chaotic Model	Analysis of synchronization time w.r.t different fractional order derivative between different chaotic system	Active Control Method	Reduce standard error between two fractional order chaotic system during synchronization using Active control method with respect to different order of derivative.
Agarwal et al. (2017)	Non Linear dynamical model	Stability analysis, chaotic behavior & its control and synchronization	Routh-Hurwitz criteria, LFC, Lyapunov Exponent (LLE), modification in adaptive function projective method	Analyzed presence of chaotic behavior and controlled its chaoticity by finding conditions for control of the fractional-order Duffing - Van der Pol

27

				system using linear feedback control.

C. Literature review based on Optimization

Author	Vehicle Model	Investigating Parameter	Methodology	Outcome response
Schiehlen et al. (2015)	2-DOF Quarter Car	Damping Coefficient	Mathematical Modeling, Multi-criteria Optimization, Pareto-optimal points	Optimized damping coefficient for best ride comfort and road safety found
Mitra et al. (2015)	2-DOF Quarter Car	Optimal Ride Comfort, Ks, Cs, Ms	Mathematical Modeling, SIMULINK, Optimization using Response Surface Methodology(RSM)	Minimum value of RC is achieved by considering Ks, Cs low and m_s high.
Bouazara et al. (2001)	8-DOF Full Car	Ride Comfort (RC),Road Holding (RH)	Mathematical Modeling, Sequential unconstrained minimization technique (SUMT), MATLAB	Active and semi-active suspensions enhance the ride comfort by 30% to 50% as compared with the passive model. Around 30% vertical driver acceleration, 30% bounce acceleration of the sprung mass and 50% roll acceleration improved

Zhongzhe et al. (2008)	2-DOF Quarter Car	Vertical vehicle body acceleration, Rattle space, and Dynamic tire load	Stochastic road modeling, Genetic Algorithm (GA), Sequential Quadratic Program (SQP), Direct Search Algorithm	Genetic algorithm (GA) and the direct search algorithm (PSA) are proven more reliable than the gradient based local search algorithm (SQP).
Hrovat et al. (1990)	1-DOF and 2-DOF Quarter Car	Ride Comfort (RC), Road Holding (RH)	Mathematical modeling, Linear Quadric Gaussian (LQG),	Performance of an active suspension can be improved by attaching the passive dynamic absorber to the un-sprung mass. The Dynamic absorber(DA) performance can be further improved by reducing the un-sprung mass and/or increasing the DA mass
Likaj et al. (2014)	2-DOF Quarter Car	Ride comfort, Suspension travel and Road holding	Mathematical Modeling, MATLAB, Stochastic Road Modeling, Genetic Algorithm (GA) and Sequential Quadratic Program (SQP), Fuzzy Logic Controller (FLC)	Found decrease in sprung mass acceleration by optimizing design parameter.
Mitra et al. (2016)	2-DOF Quarter	Ride Comfort (RC)	Lab View, Regression analysis, Design of Experiment,	Optimized ride comfort considering spring stiffness, damping coefficient,

	Car		ANOVA, Response Optimization	the sprung mass, steering geometry angles with the tire pressure which significantly affect the ride behavior.
Kaleibar et al. (2013)	DW link suspension	Ride Comfort (RC), Road Holding (RH) and Vehicle stability	Genetic Algorithm (GA), ADAMS	Camber angle variations decreased by optimizing suspension system this resulting in better ride comfort and handling
Fernandes et al. (2017)	Front wheel (L & R) ADAM Model	Ride Comfort (RC)	MSC-ADAMS, Design of Experiment, Minitab for regression model, ANOVA, Response Optimization	Using factorial method with 7 input parameters obtained optimal RC

2.2 Research Gaps

There is no doubt that substantial research is going in the field of automobile suspension. However, some issues are there, which have been less explored or not consider by researchers. One may summaries the research gaps:

- Modeling and simulation of full car model considering driver comfort as well as passenger comfort.

- Vehicle are required to simulate under various profile bump like (hump, flat top and circular) so that designed vehicle can meet all unfavorable conditions.
- More effective controllers are required like Fractional-PI (FOPI) and Fractional-PID (FOPID) than simple PID to bring vehicle into stable condition or to increase Road handling and Ride comfort.
- Effect of un-sprung mass on Road handling and Ride comfort can be research area.
- Limited research investigates full-car models with human biodynamics for IRC-standardized bump responses.
- Few studies compare PID vs. FOPID control when applied to human-coupled vehicle models
- Optimization of suspension parameters using RSM for human–vehicle coupled systems is lacking.
- Analysis on Ride Comfort can be done by considering non-linearity in vehicle suspension (like varying stiffness and damping coefficient)
- A higher degree DOF driver model with full car body can be used to study physiological effects of vibration on human body.

2.3 Problem Statement

Vehicle occupants are exposed to harmful vibrations due to poor road conditions, improperly designed traffic calming devices, and suboptimal suspension configurations. These vibrations adversely impact comfort, safety, and long-term health. Existing vehicle suspension systems and analytical models often fail to accurately predict vibration transmission to the human body across diverse road excitations. There is a need for comprehensive modeling of vehicle–human interaction under both deterministic and random road inputs and for designing optimized suspension systems capable of improving occupant comfort.

2.4 Research Objectives

Although a lot of research has been conducted on the assessment of ride comfort and on vehicle suspension systems, there are still some problems that should be solved. Previous studies have focused mainly on either ride comfort or handling performance alone, and little effort has been made to minimize them both together under various road and loading conditions. Additional studies are also required to understand the influence of passenger postures, suspension parameter changes and dynamic response during operation on passenger comfort.

Following a thorough analysis of the literature, the following goals have been established for the study:

1. To analyze dynamic behavior of a higher DOF driver and vehicle model for different profile bumps to study physiological effects of vibration on human body.

2. To develop a novel Bond-Graph based PID Controller and evaluating effectiveness in improving ride comfort by minimizing human body accelerations.

3. To model a full-car (11-DOF) vehicle coupled with a 4-DOF biodynamic human model and analyze its behavior when subjected to IRC:99–1988 standard bump inputs.

4. To perform suspension parameter optimization using Response Surface Methodology (RSM) for the quarter-car–human coupled model to achieve minimum occupant acceleration.

2.5 Research Methodology

2.5.1 Overview

This study uses a systematic approach for studying the four key objectives through a methodology that includes Analytical Modeling; Simulation; Control; Experimental Validation; Optimization to obtain an overall comprehensive understanding of vehicle – human coupled dynamics and optimize ride comfort.

There are four primary stages or phases within the overall study framework, which can be seen within the Methodology Framework diagram provided in Fig 2.3, with each phase representing one of the objectives.

2.5.2 Phase I – Development and Analysis of Quarter-Car Coupled Human Model (Objective 1)

1. **Model Formulation:**

- A 3-DOF quarter-car model representing vehicle suspension and body dynamics is coupled with a 4-DOF biodynamic human model representing the head, upper torso, lower torso, and pelvis.
- The coupling is achieved through the interface of the seat cushion modeled as a spring–damper system.

2. **Road Excitation Inputs:**

- The coupled system is subjected to both deterministic and stochastic excitations:
  - **Deterministic:** Sinusoidal, trapezoidal, and square profiles.
  - **Stochastic:** ISO 8606 road classes A, B, C, and D.

- Bond Graph methodology is used for model implementation and numerical integration.

3. **Ride Comfort Evaluation:**

- The model's behavior is analyzed in terms of vibration transmission from vehicle to human body segments.

4. **Model Validation:**

- The quarter-car bond graph model is validated experimentally using a laboratory-scale test rig.

- The test rig comprises an electromechanical actuator, suspension assembly, and accelerometers to capture real-time body accelerations.
- Experimental results are compared with simulation outcomes to ensure model fidelity.

2.5.3 Phase II – Active Suspension Control Using Bond Graph PID and PSO-Optimized FOPID Controller (Objective 2)

1. **Bond Graph Representation:**

- The validated quarter-car–human coupled system is represented using bond graph modeling, facilitating an energy-based representation of dynamic interactions.
- System equations are derived in state-space form.

2. **Controller Design:**

- A novel bond graph PID controller model is developed for ride comfort improvement.
- A fractional-order PID (FOPID) controller is subsequently implemented, where the fractional orders (λ, μ) and gain parameters (Kp, Ki, Kd) are tuned using Particle Swarm Optimization (PSO) algorithm.

3. **Performance Assessment:**

- The performance of each controller is evaluated under identical excitation conditions.
- Key parameters compared: ride comfort, body segment, seat and sprung mass acceleration and displacement,

- Bond graph PID model significantly reduced the vibration effect and further FOPID controller demonstrates superior vibration attenuation compared to the classical PID.

2.5.4 Phase III – Full-Car Model Analysis under Transient Bump (Objective 3)

1. **Model Expansion:**

- The vehicle model is extended to an 11-DOF full-car system, incorporating heave, pitch, roll, and un-sprung mass motions for all four wheels.
- The same 4-DOF biodynamic human model is integrated on the driver's seat.

2. **Road Input:**

- The transient excitation is defined using the **IRC 99:1988 bump** specification.
- Vehicle speed and bump dimensions are varied to simulate realistic driving scenarios.

3. **Simulation and Response Analysis:**

- The system responses (vehicle body, seat and human body segment behavior analyzed in terms of acceleration and displacement response, suspension stroke and dynamic load at varying speed) are analyzed.

2.5.5 Phase IV – Suspension Parameter Optimization using RSM (Objective 4)

1. **Selection of Design Parameters:**

   - Suspension parameters such as spring stiffness, damping coefficient, and tire stiffness are chosen as design variables.
   - The validated quarter-car coupled model is used for simulation-based optimization.

2. **Design of Experiments (DoE):**

   - A Central Composite Design (CCD) is employed to generate experimental runs.
   - The simulation results for each run are recorded for response variables such as ride comfort and road holding.

3. **Response Surface Development:**

   - Using RSM, polynomial regression models are developed to relate input parameters to response variables.
   - Statistical tools (ANOVA, regression coefficients) are used to assess model adequacy.

4. **Optimization:**

   - Multi-objective optimization is carried out to minimize vibration exposure and maximize ride comfort using desirability

2.6 Methodology Flow Diagram

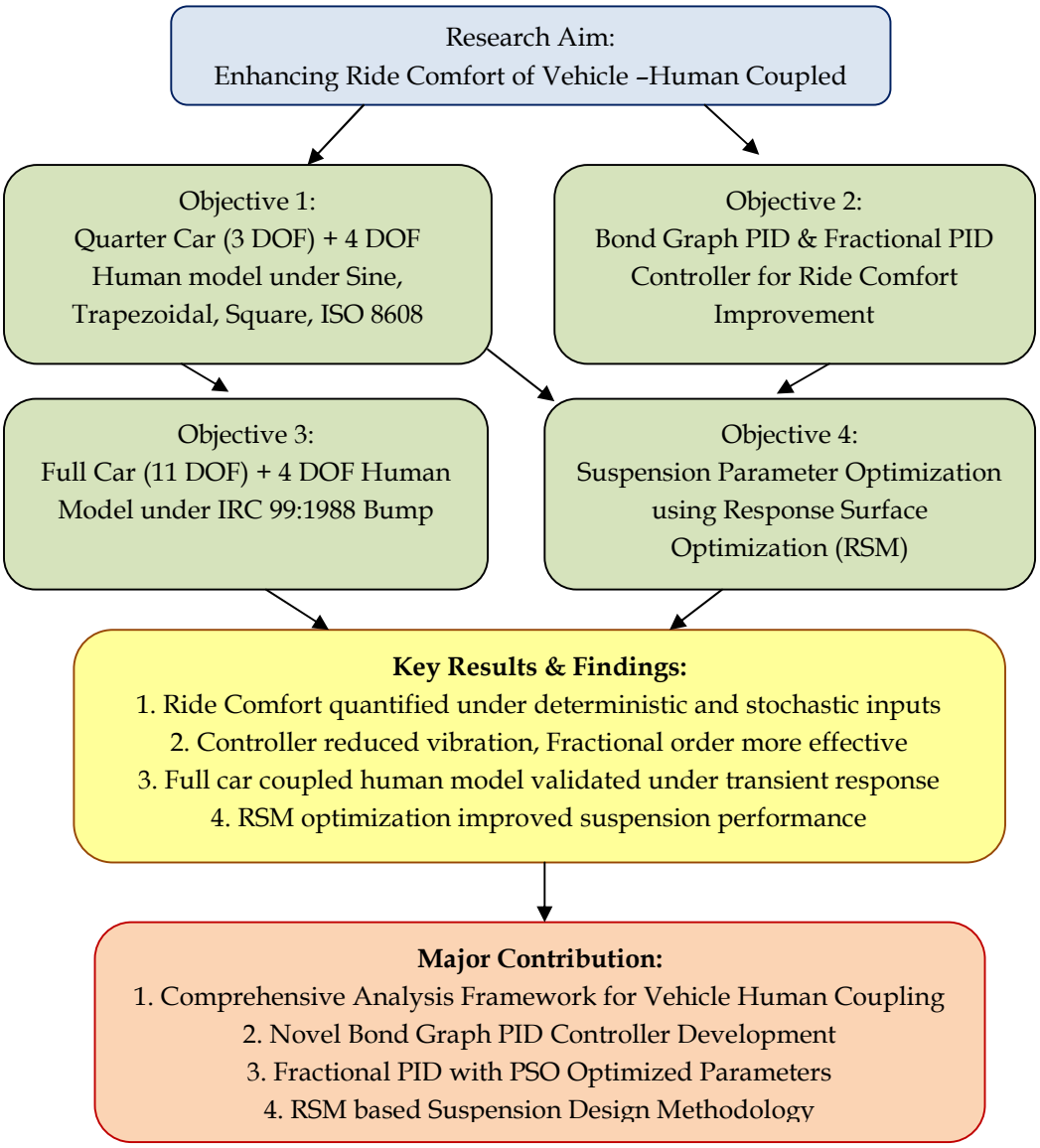


Fig 2.11 Research Methodology flow diagram

2.7 Summary

This methodology ensures:

i. Systematic linkage between modeling, control design, and experimental validation.
ii. Integration of deterministic, stochastic, and transient road excitations.
iii. Use of test rig experiments to validate numerical models.
iv. Incorporation of optimization and control to achieve the ultimate goal of enhanced ride comfort in vehicle–human coupled systems.

2.8 Contribution of the thesis

The following are major contribution of thesis:

i.) **Ride Comfort Evaluation** A detailed Ride Comfort Evaluation Framework using a quarter car and full car model were developed, along with a 4-DOF biodynamic human model. Various vibration transmission characteristics to the body segments (pelvis, torso, head) were examined, allowing detailed analyses of the vibration transmission characteristics and the comfort of the human occupants.

ii.) **Behavioral Analysis under Stochastic and Deterministic Road Conditions** The dynamic properties of the coupled vehicle–human system were investigated when excited by deterministic road inputs such as sine, trapezoidal and square road profiles as well as stochastic road inputs in the

form of ISO 8606 road classes A, B, C and D. The study demonstrated the effects of different road irregularities on the dynamics of vehicles and human vibrations response.

iii.) **Novel Control Strategy** In order to minimize the transmissibility of vibration and to enhance ride comfort, a novel Bond Graph based PID control model for the coupled vehicle–human system was developed and an optimized fractional-order PID controller was designed. These proposed control strategies showed substantial reduction in the body acceleration and improvement in vibration isolation performance with respect to passive suspension systems.

iv. **Suspension Optimization** The optimization of the suspension parameters of the quarter car coupled biodynamic human model, by applying Response Surface Methodology (RSM), was performed. The optimization process resulted in optimal relation between the various suspension stiffness and damping parameters that minimize the whole-body vibration and enhance ride comfort under different road surface conditions.

2.9 Outline of the thesis

The thesis consists of total seven chapters with *first chapter* is introduction to vehicle dynamics and ride comforts. It discussed the role of transportation and road conditions affecting human body health and safety. Further it will discuss impact of faulty roads and implications of different traffic calming devices to regulate vehicle speed. Thus the primary goal of this chapter

is to develop need for biodynamic modeling and simulation. The *second chapter* presents in depth review of existing literature related different biodynamic model, vehicle suspension modeling, advance control and optimization techniques for the enhancement of ride comfort. . It evaluated limitation of conventional models and thus enlighten need for integrated biodynamic human-vehicle analysis. The research gap are systematically identified and chapter concludes with chosen research direction justification with outlining overall methodology adopted to achieve research objectives

The *third chapter* presents the development and analysis of 3-DOF quarter car model coupled with 4-DOF biodynamic human model through bond graph modeling. Further the couple system subjected to different deterministic and stochastic road conditions thus evaluates time and frequency domain vibration responses. The *fourth chapter* focuses on design and implementation of novel bond graph based PID controller for enhancing ride comfort. The performance of fractional-order PID (FOPID) controller is further evaluated with optimally tuned parameters using particle swarm optimization (PSO) algorithm.

The *fifth chapter* extends the study to demonstrate the dynamic behaviour of the 4 DOF lumped human biomechanical model coupled with an 11 DOF full-car vehicle model under transient road excitation as defined by IRC 99:1988 bump standards using the Bond Graph simulation technique. The responses of human segment and vehicle are examined to assess ride comfort. The results provide a deeper insight into heave, pitch and roll dynamics affecting human comfort. Further the model is validated with archival literature. This chapter bridge the gap between analysis of idealized quarter car and realistic full car behaviour.

The *chapter six* deals with suspension parameter optimization of quarter car coupled with biodynamic human model using Response Surface Methodology (RSM). This study

focuses on developing a mathematical model to predict ride comfort and road holding using Central Composite Design (CCD). Multi-objective optimization is performed to achieve the optimal suspension parameter values for best combination of suspension performance and ride quality. The *chapter seven* concluded the thesis and presents future scope and social implication of present research

CHAPTER 3

Development and Analysis of Quarter-Car Coupled Human Model

3.1 Introduction

41

Ride comfort plays a vital role in the performance of vehicle handling and the safety of its occupants and is directly connected to the interaction between the vehicle suspension system, road excitation and the biodynamic response of the human body. The current research aims to enhance the ride comfort by developing sophisticated simulation, control and optimization approaches, which are based on modeling, analysis and control of vehicle-occupant systems. The study is based on a Bond Graph study of vehicle suspensions coupled with biodynamic human models to evaluate and improve suspension vibration performance in various road conditions observed in real-world applications.

The primary objective of vehicle systems is to attenuate vibrations and sudden impacts originating from road irregularities, thereby improving ride comfort and maintaining tire-to-road contact for optimal handling and stability *(Bouazara and Richard, 2001)* Achieving this balance necessitates sophisticated modeling and controlling techniques, given the intricate interplay of various parameters such as spring stiffness, damping coefficients, and geometric configurations *(Modibbo, Babangida and Szemes, 2025)*

Road surfaces are one of the key sources of vehicle suspension behavior, and there are different surface profiles (e.g., sinusoidal, random) that are used to assess ride comfort and handling characteristics *(Tran et al., 2024)*. For example, the ISO 8608 standard road profiles or stochastic processes are commonly used to create a variety of driving conditions for suspension systems to be evaluated in these challenging profiles. These profiles are frequently analyzed by a spectral analysis to identify the nature of the unevenness of the road surface, which is essential for designing suspension systems that will best reduce vibrations over a wide frequency range. Hence, to optimize the design of vehicle suspension systems, this knowledge of such diverse road inputs becomes crucial to balance the vehicle ride comfort and handling stability *(Iskandarani, 2022)*.

In general, road bumps and potholes are important issues to consider when assessing the performance of vehicle suspensions, considered both for stability and passenger comfort *(Abdelati et al., 2026)*. Furthermore, the dynamics of vehicles, including ride comfort and handling stability, have been examined in detail with the

help of multi-body simulation software, such as ADAMS, which has the advantage of parameterization to determine important vehicle parameters *(Yang et al., 2013)*. These models can then be used to conduct sensitivity analysis on suspension designs, to determine the impact of the different geometric parameters on various performance measures *(Freddi et al., 2025)*. Moreover, researchers have used Design of Experiments methodologies such as fractional factorial designs to systematically investigate the impact of suspension characteristics, such as tyre pressure, damping coefficient and stiffness on ride comfort, and have used quarter-car test rigs and data acquisition systems, such as NI LabVIEW® *(Mitra et al., 2015)*. This enables a thorough understanding of the interaction between suspension components and road irregularities and fine-tuning suspension parameters to ensure optimum vehicle dynamics and passenger experience *(Lee and Kang, 2024)*. These methodologies, when combined, provide a comprehensive approach to understanding the dynamic behavior of road disturbances, especially in terms of mass, damping, and stiffness, as they influence vehicle behavior during transients. In addition, the quantification of the impact of asymmetric damping on vehicle responses to transient excitations like bumps and potholes is also important for thorough suspension system analysis *(Ajayi et al., 2023)*

3.2 Modeling of 4-DOF lumped human biomechanical model coupled with an 3-DOF full-car vehicle

3.2.1 Physical Model

The 3-DOF quarter car model is connected to a 4-DOF biodynamic driver body model, as shown in **Figure 3.1**. Considering the human body as a combination of several lumped masses connected through springs, m_h, m_{ut}, m_{lt}, and m_p are the lumped masses of 'head', 'upper torso', 'lower torso' and 'pelvis', respectively, which receive the direct excitation from the seat. C_{ij} and K_{ij} are damping and stiffness between the two body sections (the subscripts i and j signify the first alphabet of the connected body parts).

K_{se} and C_{se} represent the stiffness and damping coefficients of seat suspension; Z_{se} is the excitation from the seat; Z_h, Z_{ut}, Z_{lt}, and Z_p indicate various mass displacements on 'head', 'upper torso', 'lower torso' and 'pelvis', respectively. Z represents the road input in the form of a sinusoidal profile bump. Cs and Ks represents the damping and stiffness coefficients of the car suspension. K_t represents the compressibility of the pneumatic tyre.

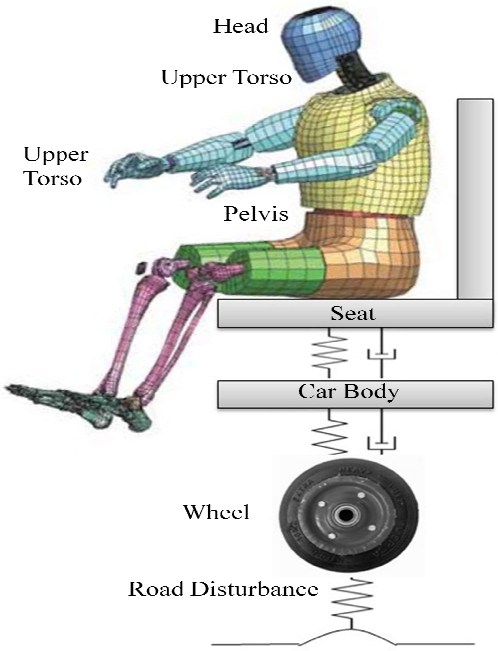


Figure 3.1: Schematic diagram of 4 DOF biodynamic lumped human model coupled with quarter car 3-DOF model

Fig 3.1 illustrates a quarter-car (7-DOF) physical model . The sprung mass alludes to the car body that is supported by springs, whereas the un-sprung mass corresponds to wheel assembly. The tire is modeled considering stiffness with negligible damping. Tires, passenger seats, and suspension are modeled using springs that are positioned parallel to the dampers.

3.2.2 Mathematical Model

A quarter car model (7-DOF) is considered for analysis. Fig 3.1 illustrates a quarter car (7-DOF) model consisting of passenger seats, a sprung mass, and un-sprung mass. The tire, with its neglected damping, is replaced by its equivalent stiffness. Linear springs

arranged parallel with dampers are used to model the suspension, tires, and passenger seat.

Z_b symbolize vertical displacements of the vehicle body and suspension connection points. Similarly, Z_{se} indicate the vertical displacements of the seat and car body connection points. Using Newton's second law of motion, the dynamic motion equations are obtained for the quarter car suspension, seats, and driver's body.

Human Model Equation

$$m_h\ddot{Z}_h = -C_{hu}(\dot{Z}_h - \dot{Z}_{ut}) - K_{hu}(Z_h - Z_{ut}) \tag{3.1}$$

$$\begin{aligned} m_{ut}\ddot{Z}_{ut} = {} & C_{hu}(\dot{Z}_h - \dot{Z}_{ut}) + K_{hu}(Z_h - Z_{ut}) - C_{ul}(\dot{Z}_{ut} - \dot{Z}_{lt}) - K_{ul}(Z_{ut} - Z_{lt}) \\ & - C_{up}(\dot{Z}_{ut} - \dot{Z}_p) - K_{up}(Z_{ut} - Z_p) \end{aligned} \tag{3.2}$$

$$m_{lt}\ddot{Z}_{lt} = C_{ul}(\dot{Z}_{ut} - \dot{Z}_{lt}) + K_{ul}(Z_{ut} - Z_{lt}) - C_{lp}(\dot{Z}_{lt} - \dot{Z}_p) - K_{lp}(Z_{lt} - Z_p) \tag{3.3}$$

$$\begin{aligned} m_p\ddot{Z}_p = {} & C_{lp}(\dot{Z}_{lt} - \dot{Z}_p) + K_{lp}(Z_{lt} - Z_p) + C_{up}(\dot{Z}_{ut} - \dot{Z}_p) + K_{up}(Z_{ut} - Z_p) \\ & - C_{pse}(\dot{Z}_p - \dot{Z}_{sefr}) + K_{pse}(Z_p - Z_{sefr}) \end{aligned} \tag{3.4}$$

Seat Equations

$$\begin{aligned} m_{se}\ddot{Z}_{se} = {} & +C_{pse}(\dot{Z}_p - \dot{Z}_{se}) + K_{pse}(Z_p - Z_{se}) - C_{se}(\dot{Z}_{se} - \dot{x}_{se}) \\ & - K_{se}(Z_{se} - Z_b) \end{aligned} \tag{3.5}$$

Vertical Motion of Car Body

$$m_b\ddot{Z}_b = -C_s(\dot{Z}_b - \dot{Z}_w) - K_s(Z_b - Z_w) + C_{se}(\dot{Z}_{se} - \dot{Z}_b) + K_{se}(Z_{se} - Z_b) \tag{3.6}$$

Four Wheel Equations

$$m_w\ddot{Z}_w = C_s(\dot{Z}_b - \dot{Z}_w) + K_s(Z_b - Z_w) - K_t(Z_w - Z) \tag{3.7}$$

3.2.3 Bond graph modeling

The car model has three interfaces. The first interface is defined between the car body and wheels motion; the second interface is between the car body and seats motion; and the third interface is between the seat and driver model. Fig 3.5 illustrates a 7- DOF quarter-car Bond Graph model comprising an integrated 3-DOF quarter-car system coupled with a 4-DOF biodynamic human model. For modeling and simulation, the software SYMBOLS 2000 *(Samantaray, 2015)* used in this work facilitates the creation of complete Bond Graph models.

The Bond Graph utilizes two junction elements: *1*-(common flow) and *0*-(common effort); three basic elements: *I*-(inertial), *C*-(compliant), and *R*-(resistive); two source elements: efforts *SE* (effort source) and *SF* (flow source); and two 2-port elements: *TF* (transformer) and *GY* (gyrator). All these elements are connected through lines called bonds, where energy exchange between elements in the Bond Graph occurs via these bonds in the form of power, i.e., effort and flow.

Starting with the human Bond Graph model, as illustrated in Fig 3.2, four I-elements are utilized at each 1-junction to represent the mass of different human body parts. A flow-activated (C-element) is attached to each 1-junction to capture the displacement and velocity of the human body parts. Stiffness and damping between each body part are introduced by attaching C and R elements between the 1-junctions. The acceleration of various body parts is captured by the I-elements. The Bond Graph model of the human body parts is further integrated with the seat Bond Graph model.

Furthermore, the interface between the car body (sprung-mass) and the wheel (un-sprung masses) is established by connecting the BG models of car and wheels at 0-junctions, with the introduction of C and R elements representing stiffness (K_s) and damping (C_s) of the wheel suspension. Tire stiffness (K_t) is incorporated using a C-element, while the damping of the tire neglected. However, it is represented in the wheel Bond Graph (BG) graph model illustrated in Fig 3.4.

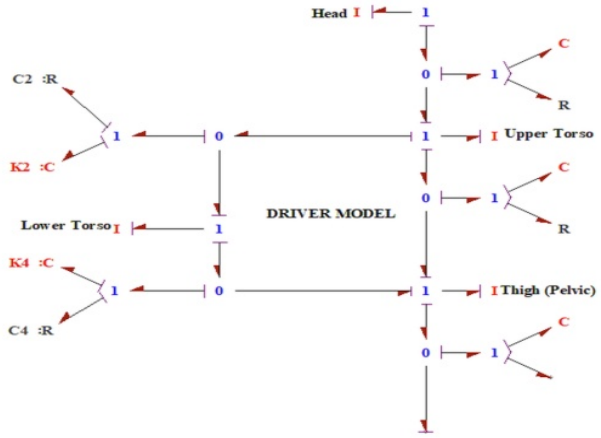


Figure 3.2: Bond Graph model of 4DOF bio-dynamics human

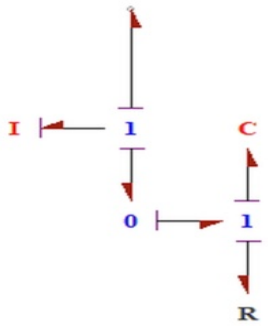


Figure 3.3 Seat BG model

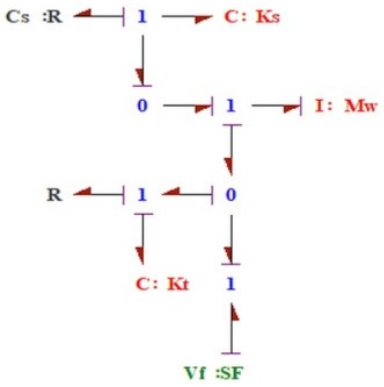


Figure 3.4 Wheel BG model

An interface between the car body and the seats is formed using C and R elements, which represent the stiffness and damping coefficients of the seat suspension system. Fig 3.3 illustrates a Bond Graph (BG) model of a seat. An activated C-element on the seat records the seat displacement. Finally, the BG model of the human is connected to the seat through C and R elements, representing the stiffness and damping parameters of the pelvis (thigh). Fig 3.5 presents the complete bond graph of the Bio-Dynamic Human Model coupled with the Quarter Car Model for simulation.

Figure 3.5 Integrated Bond Graph model of 7-DOF Quarter car model coupled with human bio-dynamic human

3.3 Road Excitation

Both deterministic and stochastic road profiles are used to evaluate the performance of quarter car model coupled with human bio-dynamic model. Three deterministic road profile sinusoidal, trapezoidal and square are used for simulation with height 0.1m and width 3.7 m is used for analysis, as illustrated in Fig 3.6. The road conditions, as a function of time, are expressed as follows

3.3.1 Sinusoidal road input

A sinusoidal road input is often used in vehicle ride dynamics to simulate a simple and continuous road disturbance. The sinusoidal bump is different from the square or step inputs in the way that it varies the displacement, causing gradual variation, which results in a more realistic set of excitation conditions for suspension and ride comfort analysis. The sinusoidal bump function displayed in the figure is given by:

$$\begin{cases} Z = \mathrm{h} * \sin\left(\frac{\pi . \mathrm{v}}{\mathrm{w}} * t\right) & for\ t < \frac{w}{v} \\ = 0 & for\ t > \frac{w}{v} \end{cases} \tag{3.8}$$

In the Bond Graph (BG), road input modeling is performed using the SF (source of flow) element. Thus, the flow to the wheel is determined by differentiating Z with respect to time.

SF to wheel is

$$\begin{cases} \dot{Z} = \frac{\mathrm{h.\pi.v}}{\mathrm{w}} * \cos\left(\frac{\pi.\mathrm{v}}{\mathrm{w}} * t\right) & for\ t < \frac{w}{v} \\ = 0 & for\ t > \frac{w}{v} \end{cases} \tag{3.9}$$

where, Z is vertical road displacement or sinusoidal bump input(m); h represents maximum height of sinusoidal bump; v is the vehicle velocity (m/s); w is width of bump(m); and t is time (s)

3.3.2 Trapezoidal road input

A road bump with a gradual rise, constant elevation and gradual fall is represented by the trapezoidal road input. This is similar to the type of excitation that is experienced by vehicles on the road in real-life road humps and speed breakers. A trapezoidal bump is mathematically represented as a piecewise function with 3 regions - ascending, constant and descending. The trapezoidal bump equation shown in the figure is given by:

$$\begin{cases} z = \frac{h}{t_1} * t & for\ t \le \frac{L_1}{v} \\ z = h & for\ \ \frac{L_1}{v} \le\ \ t \le \left(\frac{L_1}{v} + \frac{L_2}{v}\right) \\ z = h - \left(\frac{h}{t_1}\right) * \left(t - \frac{L_1}{v} - \frac{L_2}{v}\right) & for\ \left(\frac{L_1}{v} + \frac{L_2}{v}\right) \le\ \ t \le \left(2 * \frac{L_1}{v} + \frac{L_2}{v}\right) \end{cases} \tag{3.10}$$

where, where, Z is vertical road displacement or sinusoidal bump input(m); h represents maximum height of trapezoidal bump; L_1 represents horizontal length of ascending and descending slopes of bump (m); L_2 represents flat top length of trapezoidal bump (m); v

is the vehicle velocity (m/s); t_1 represents time required for the vehicle to travel the ascending portion of bump (s); and t is time.(s)

3.3.3 Square road input

The square road input is a road elevation step at which the vehicle wheel suddenly meets a bump of uniform height and then abruptly leaves the bump. This type of excitation is employed for the study of the transient response of vehicle suspension systems and biodynamic behavior of human under severe road disturbances. The bump function displayed in the figure is described by the following:

$$\{Z = \mathrm{h} \qquad for\ \ 0 < t < \frac{w}{v} \tag{3.11}$$

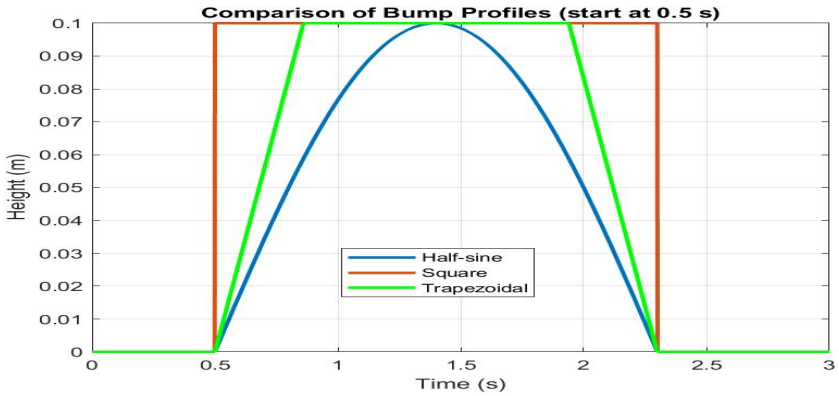


Figure 3.6 Various bump profiles used for simulations

3.3.4 ISO 8608 Random Road

In actual road conditions, vehicles are exposed more to random road profile as compared to deterministic road profiles. So using randomly generated profiles would be more appropriate in performance evaluation which in case of sine, trapezoidal and square

functions are limited. The random road profile can be represented in frequency domain using PSD function. The ISO 8608 standard *(ISO. Mechanical vibration - road surface profiles - reporting of measured data. Technical Report 8608, International Organization for Standardization, 1995)* defines road surface roughness in terms of its Power Spectral Density (PSD) of the vertical displacement as a function of spatial frequency (cycles per meter). The general PSD model according to ISO 8608 is:

$$G_q(n) = G_q(n_o)\left(\frac{n}{n_o}\right)^{-w} \tag{3.12}$$

Where "$G_q(n)$" is Power spectral density of road elevation (m³); "$G_q(n_0)$" is Reference PSD value at reference spatial frequency; *"n"* is Spatial frequency (cycles/m); "n_o" is Reference spatial frequency = 0.1 cycles/m and "*w*" is Slope of PSD (usually 2 for typical road surfaces.

As shown in shown in Fig 3.7 four random profiles A, B, C and D as per ISO road input are generated at 40 Km/h. The road profile category A is consider to be smooth and very good profile with maximum unevenness of 0.003 m in upward and -0.05m in downward direction at 40km/h. Similarly, road category C & D have maximum 0.042m, 0.055m and 0.403m in upward and -0.065m, -0.202m and 0.059m in downward direction at 40 Km/h. Among all road D profile is very poor condition where as road B and road C are good and in average category respectively.

Table 3.1 Random Road Roughness Classification

Road Class	$G_q(n_0)$ at n_0= 0.1 cycles/m	Description
A	16×10^{-6}	Very Good
B	64×10^{-6}	Good
C	256×10^{-6}	Average
D	1024×10^{-6}	Poor

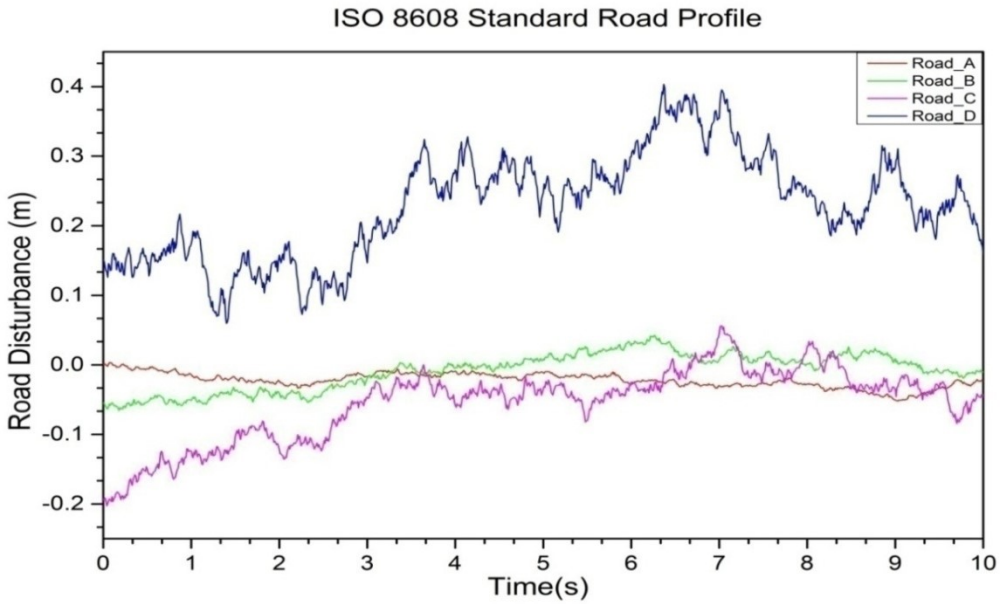


Figure 3.7 ISO 8601 road profile A, B, C & D at 40 Km/h

3.4 Simulation studies

The differential equations produced in the Bond Graph are solved using fifth-order Runge-Kutta method. The simulation is carried out for 5 seconds to obtain various dynamic responses. Simulation records are utilized, with errors in the order of 5.0 x 10^{-4}. The parameters used for the simulation are provided in **Table 3.1** *(Margolis and Shim, 2000; Abba et al., 2011)*

Table 3.2 Human and car model parameters for simulation

Vehicle parameter			
Symbol	Parameters	Value	Units
	Human model parameter by abbas		
m_h	Mass of head	4.17	kg
m_{ut}	Mass of upper torso	15	kg
M_{lt}	Mass of lower torso	5.5	kg
M_p	Mass of pelvis (thigh)	36	kg
C_{hu}	Damping between head & upper torso	310	N-s/m
K_{hu}	Stiffness between head & upper torso	166990	N/m
C_{ul}	Damping between upper torso & lower torso	200	N-s/m
K_{ul}	Stiffness between upper torso & lower torso	10000	N/m
C_{up}	Damping between upper torso & pelvis	909.1	N-s/m
K_{up}	Stiffness between upper torso & pelvis	144000	N/m
C_{lp}	Damping between lower torso & pelvis	330	N-s/m
K_{lp}	Stiffness between lower torso & pelvis	20000	N/m
C_{pse}	Damping between pelvis & seat	2475	N-s/m
K_{pse}	Stiffness between pelvis & seat	49340	N/m
	Seat parameter		
C_{se}	Damping coefficient of passenger seat	150	N-s/m
K_{se}	Stiffness coefficient of passenger seat	15000	N/m
m_{se}	Mass of four passenger seat	35	kg
	Wheel and suspension parameter		
m_w	Mass of wheel	35	kg
C_s	Damping coefficient of suspension	980	N-s/m
K_s	Stiffness coefficient of front left and right suspension	16000	N/m
K_t	Stiffness coefficient of four tyres	160000	N/m
	Car body frame parameter		
m_b	Mass of vehicle body	250	kg

3.5 Results and discussion

Various dynamic responses in the time and frequency domain have been captured in simulations with drivers and vehicle parameters as presented in **Table 3.2** for conditions where the vehicle was moving at 40 km/h over different deterministic and stochastic obstacles (bumps). The simulation results have been categorized in two parts,. In first parts both time and frequency domian reponses of vehicle and human body parts in terms of accleration is discussed when subjected to various deterministic road excitations. The secondd part presents time and frquency domain responses when subjected to stochastic road excitation (ISO 8608).

3.5.1 Time and Frequency Domain Responses under various deterministic road excitation

Acceleration response of quarter car vehicle coupled with human bio dynamic model both in time and frquency domain when subjected to deterministic profile bump is presented in this section. Three deterministic profile bump conditions namely sinusoidal, sqaure and trapezoidal are used for simulation. The result were obtained in terms of human body parts acceleration, seat acceleration and sprung mass (body) acceleration, both in time and frequency domain.

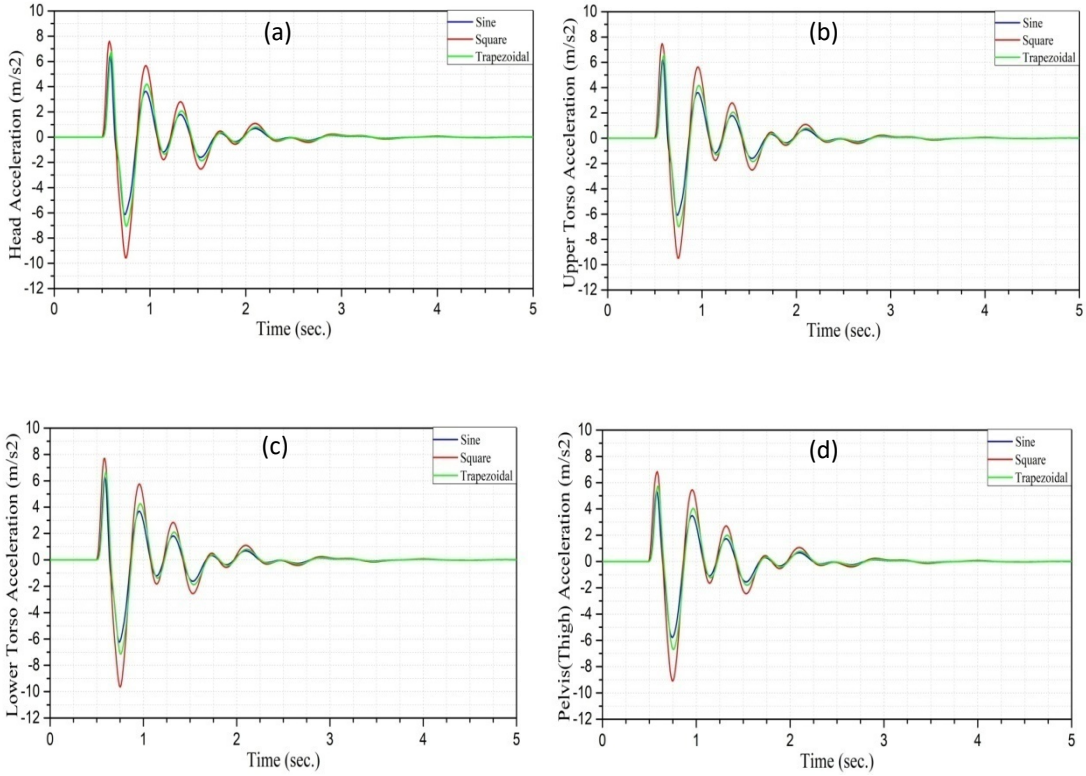


Figure 3.8 Time domain Acceleration responses of human body parts in different profile bump conditions at 40 km/h (a) Head (b) Upper Torso (c) Lower Torso (d) Pelvis (thigh)

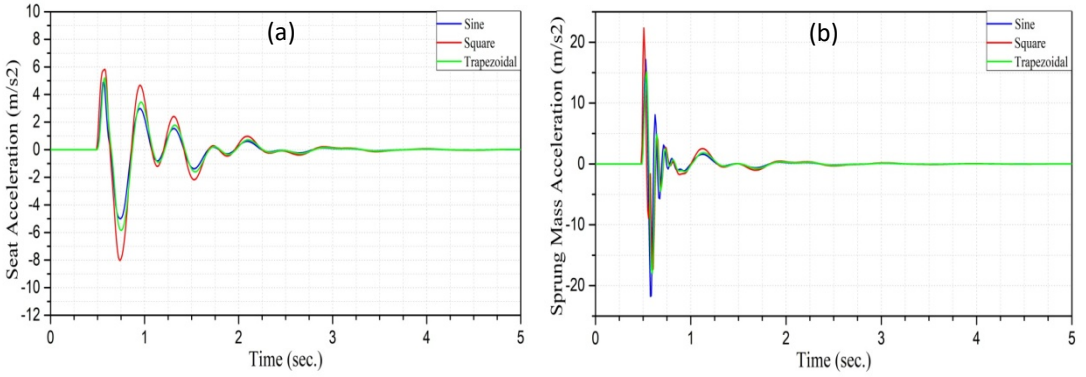


Figure 3.9 Time domain Acceleration responses in different profile bump condition at 40 km/h (a) Seat (b) Sprung Mass

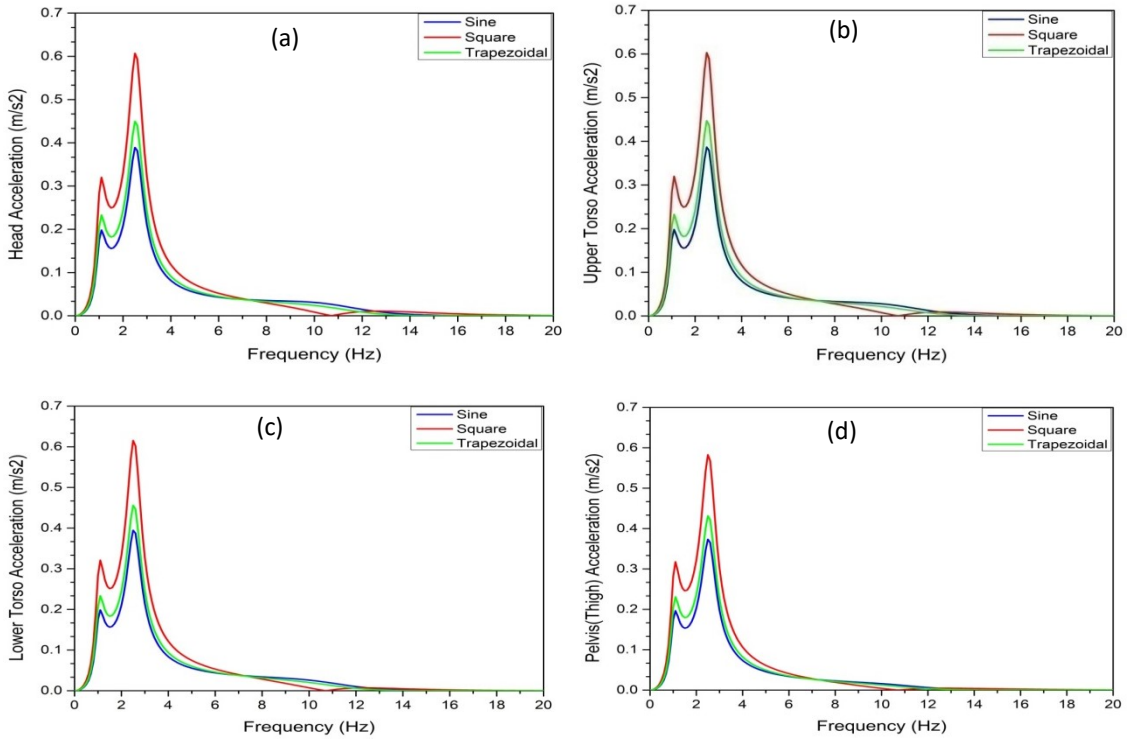


Figure 3.10 Frequency domain Acceleration responses in different profile bump condition at 40 km/h (a) Head (b) Upper Torso (c) Lower Torso (d) Pelvis (thigh)

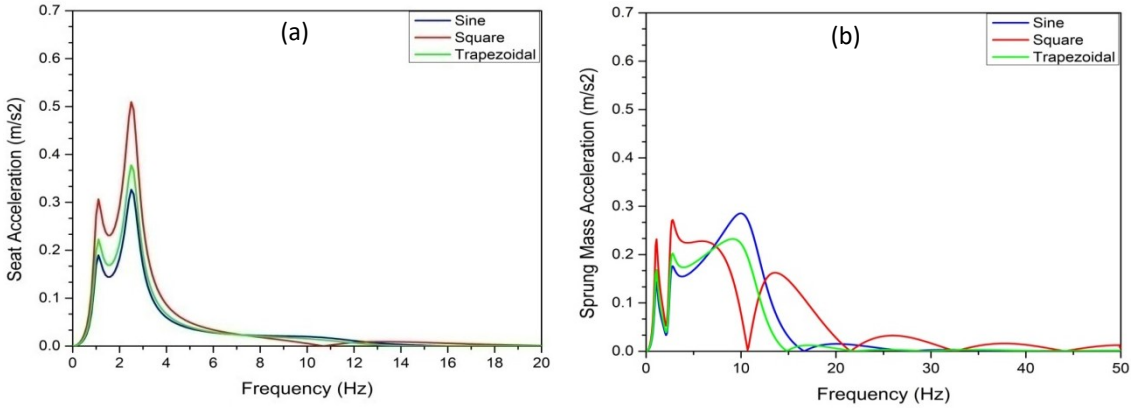


Figure 3.11 Frequency domain Acceleration responses in different profile bump condition at 40 km/h (a) Seat (b) Sprung Mass

Fig 3.8(a)-(d) illustrate the vertical acceleration of body parts ('head', 'upper torso', 'lower torso', and 'pelvis'). The acceleration of body parts is an indicator of comfort level. The peak accelerations of all body parts are observed to be nearly identical for the corresponding bump and all body segments experience sharp acceleration within this first second of excitation. Further it is observed that square bump input produces the highest peak in all body segments whic is due to abrupt discontinuities, while sine and trapezoidal input shows smooth transition. Oscillations gradually decay to approx. zero within 3 to 4 seconds, which confirms the damped biomechanical nature between human body parts. Decay trends generally indicates the dissipation of enery through soft tissues, joints, and interaction between seat and vehicle body. As shown in figure 3.8(a), Head shows largest amplitude and thus indicating sensitivity to vibration tranmitted from lower body parts. Further it is observed that magnitude of acceleration decreases from pelvis to head through lower and upper torso, thogh amplification due to resonance makes head more sensitive to vibration tranmitted.

Fig 3.9(a) illustrates seat and sprung mass acceleration in time domain and shows clear transient peaks immediately after excitation. The square bump generates the largest acceleration peak in seat with +5.8 m/s^2 in up and -8m/s^2 in down side due to its abrupt profile. Sine and trapezoidal bumps result in smoother acceleration comparitively with lower peak magnitudes. It is evident from Fig 3.9(b) that sprung mass (vehicle body) experience much higher acceleration amplitude in caomparison to the seat**.** The square excitation again induces the largest overshoot, whereas on the other side sinusoidal

results in gradual oscillations. There is clear visibilty of damping but oscillation persist slightly longer at the seat.

The acceleration of human body parts and vehicle in frequency domain are presented in Fig 3.10-3.11. It is observed from figure 3.10 there exist strong peanks in the 1-5 Hz range across all body segments and this coincides with human body‘s natural resonance frequencies (ISO 2631 comfort guidelines confirms human sensitivity between 4-8 Hz). The square input causes the hinghest amplitude spectral peaks, hence confirming the stronger excitaton of resonant modes. The sinusoidal input showing more controlled frequency excitation and has narrow peaks, whereas trapezoidal lies in-between noticeable smoother frequency content. It is evident from Fig 3.10, the head and upper torso experiencing relatively higher spectral peaks compared to pelvis, thus indicating amplification of transmitted vibrations as they travels upward the body segments. The pelvis act as the primary input point through which energy tranmits upward but damoing reduces contribution of higher frequency.

Fig 3.11(a)-(b) displays the acceleration response of seat and sprung mass (vehicle body) in frequency domain. It is shown that for all three bumps strong peaks occurs in the 1-5 Hz range, aligning with human sensitivity to vibration (ISO 2631). The square bump produces the highest spectral energy while sinusoidal and trapezoidal are lower and significant. Beyond 8-10 Hz, the response dimnishes hence showing effective damping at higher frequencies. Sprung mass acceleration shows broader peaks across lower to mid frequencies (5-20 Hz) as shown in Fig 3.11(b). The sinusoidal bump excites resonance near 10-15 Hz more strongly where square bump spreads energy

across multiple band due to its harmonic nature. The trapezoidal bump excites intermediate frequencies with lower energy as compared to square bump.

3.5.2 Time and Frequency Response under random road excitation

This section presents the acceleration response of quarter car vehicle coupled with human bio dynamic model both in time and frquency domain when subjected to stochastic road inputs (ISO 8608) where four random profile road conditions A, B, C and D are used. The result were obtained in terms of human body parts acceleration, seat acceleration and sprung mass (body) acceleration, both in time and frequency domain.

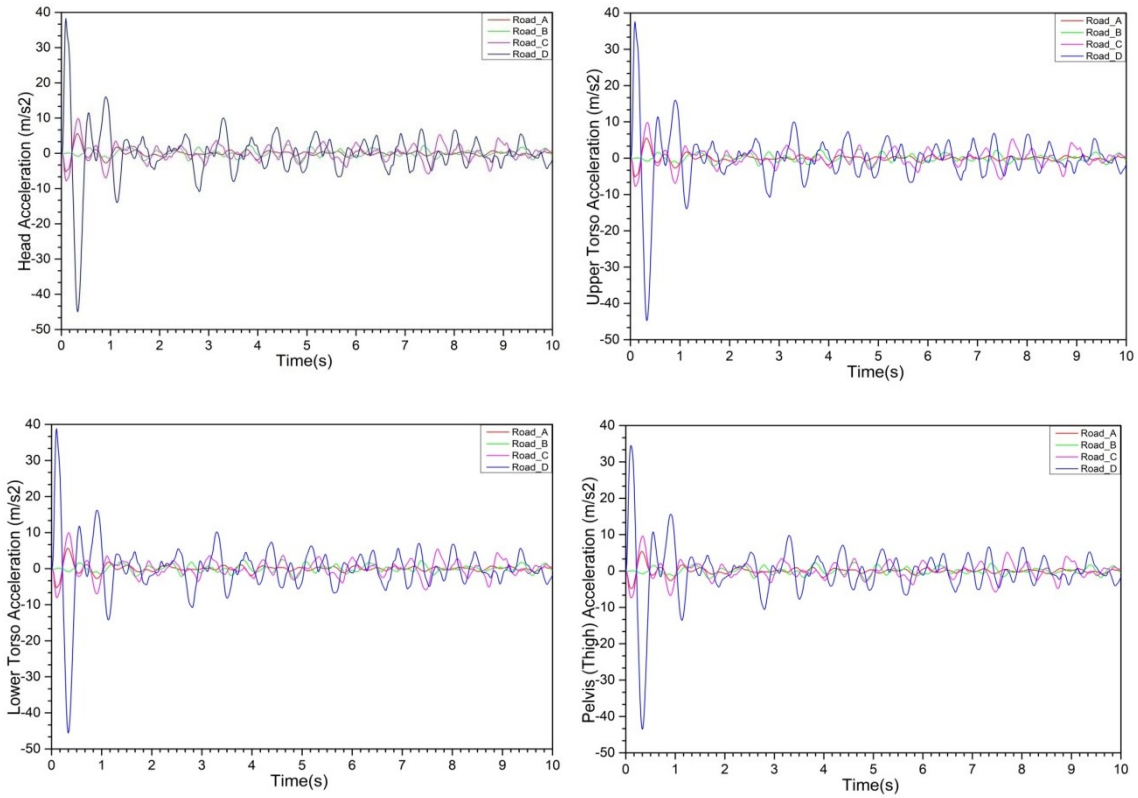


Figure 3.12 Time domain Acceleration responses of human body parts in random profile bump (ISO 8608) conditions at 40 km/h (a) Head (b) Upper Torso (c) Lower Torso (d) Pelvis (thigh)

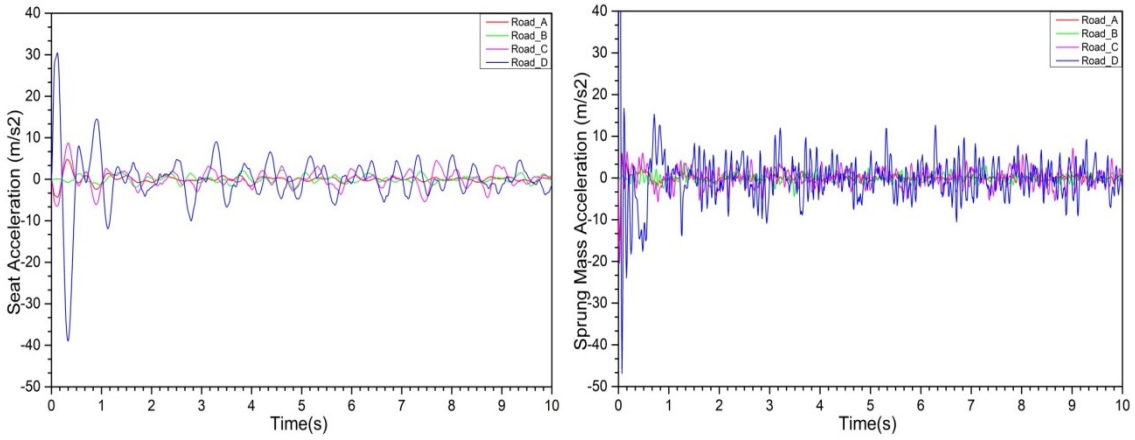


Figure 3.13 Time domain Acceleration responses of human body parts in random profile bump (ISO 8608) conditions at 40 km/h (a) Seat (b) Sprung Mass

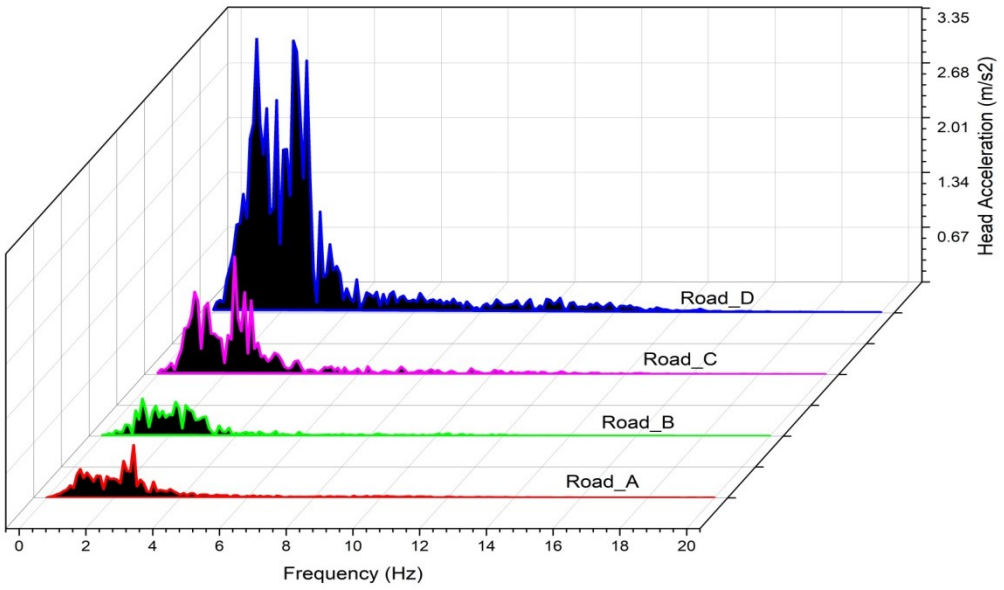


Figure 3.14(a) Frequency domain Acceleration responses of head in random profile bump (ISO 8608) conditions at 40 km/h

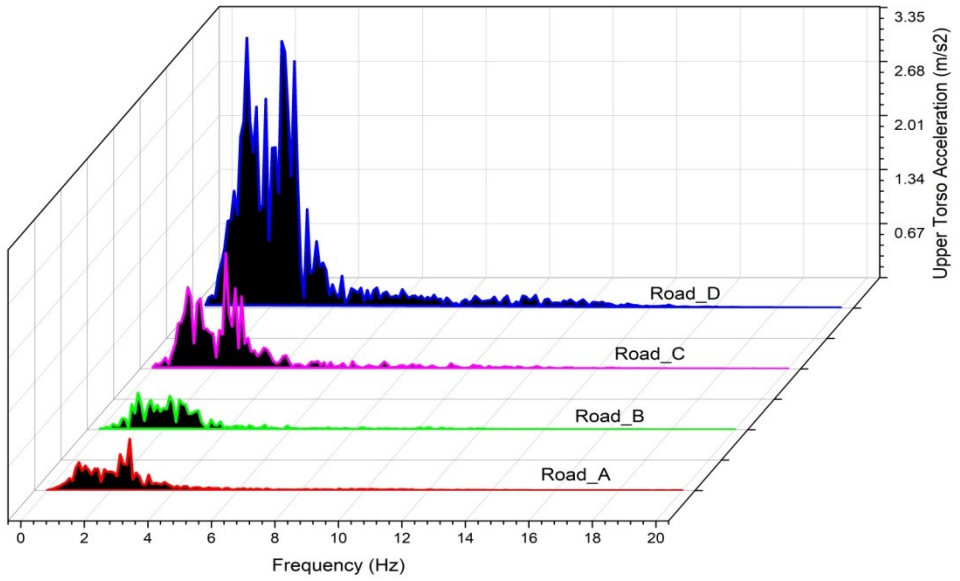


Figure 3.14(b) Frequency domain Acceleration responses of upper torso in random profile bump (ISO 8608) conditions at 40 km/h

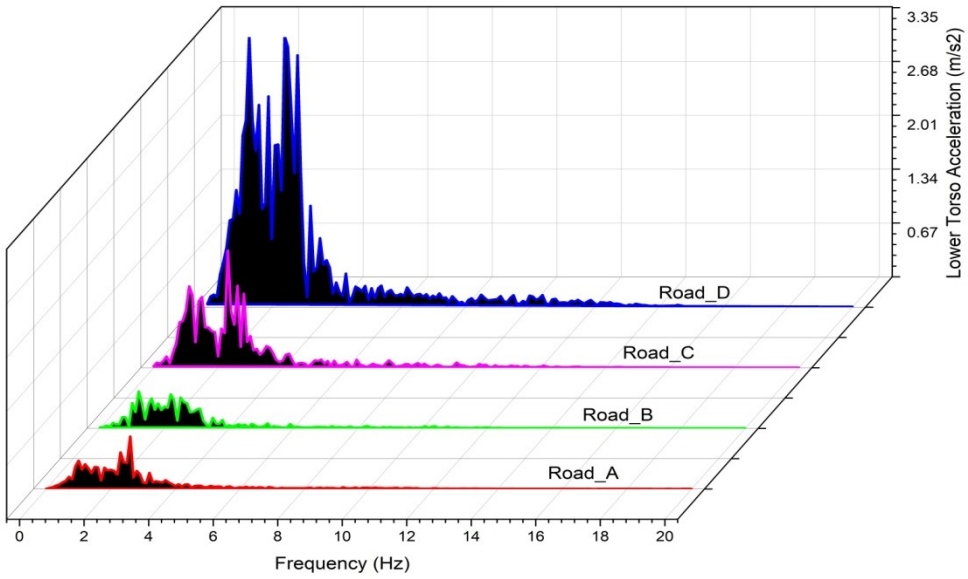


Figure 3.14(c) Frequency domain Acceleration responses of lower torso in random profile bump (ISO 8608) conditions at 40 km/h

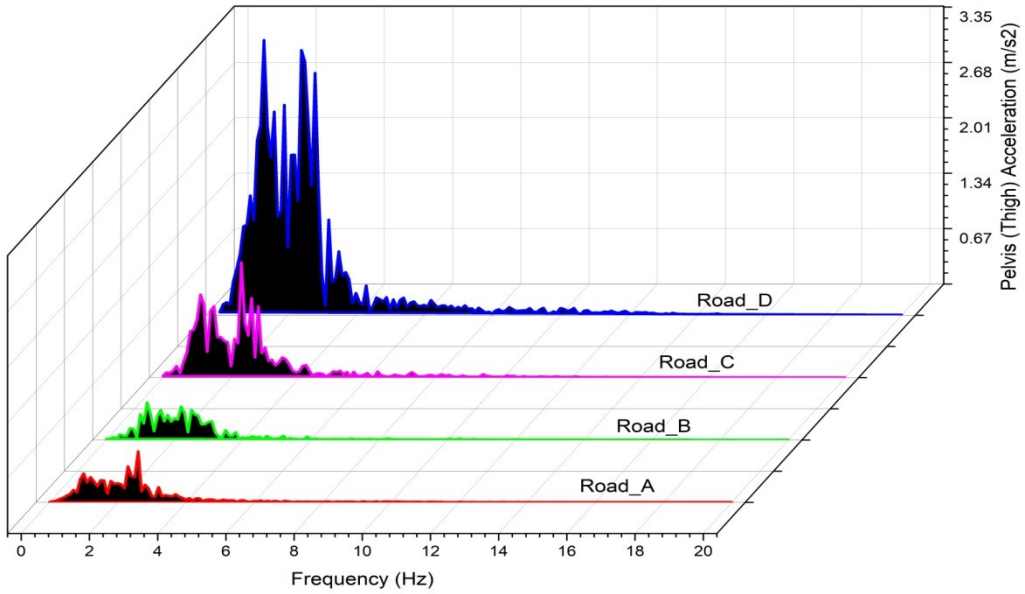


Figure 3.14(d) Frequency domain Acceleration responses of pelvis(thigh) in random profile bump (ISO 8608) conditions at 40 km/h

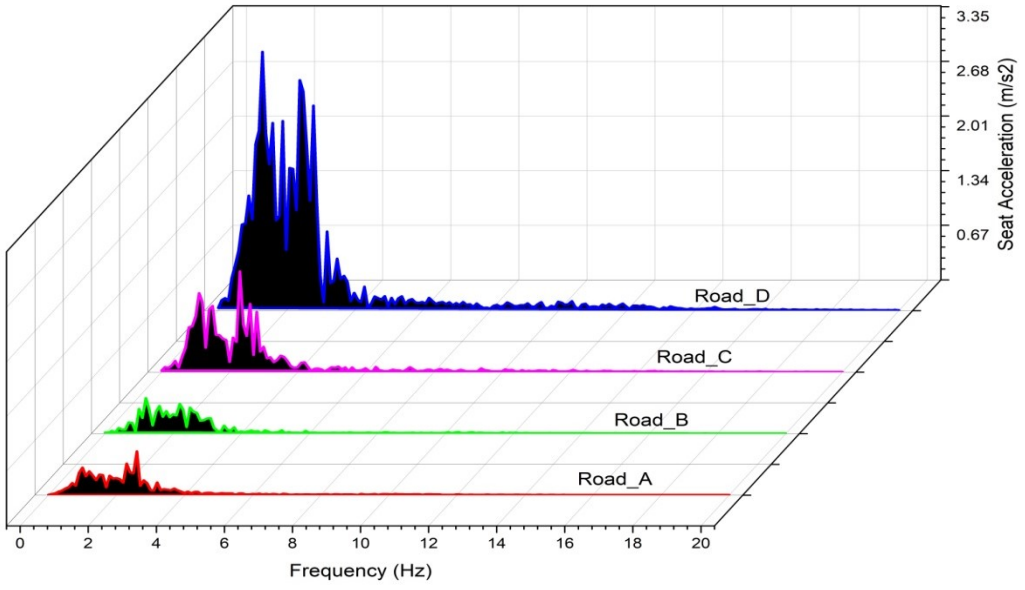


Figure 3.15 Frequency domain Acceleration responses of seat in random profile bump (ISO 8608) conditions at 40 km/h

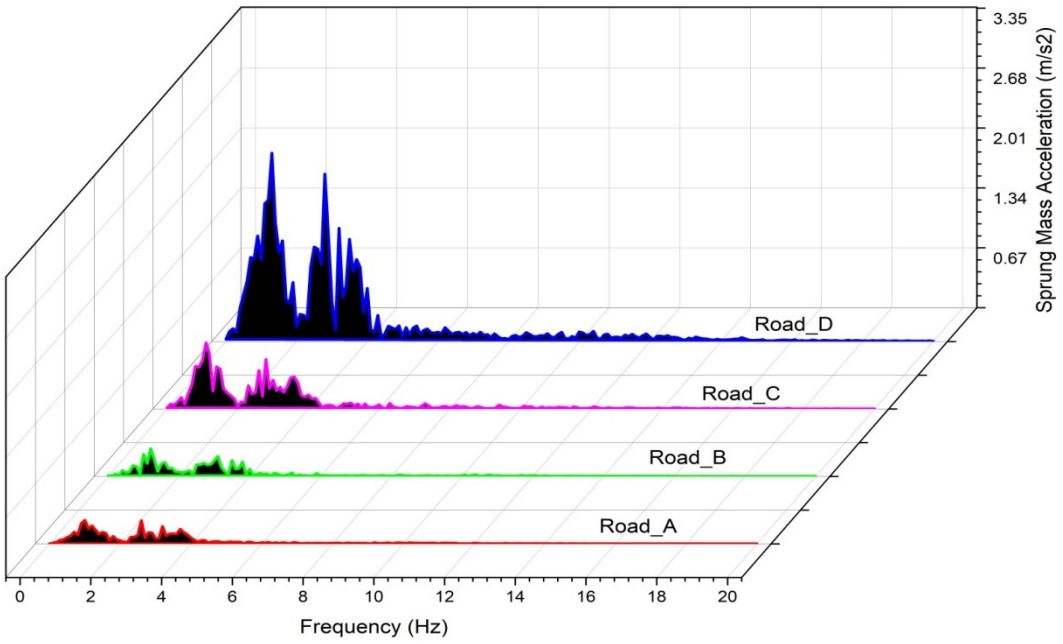


Figure 3.16 Frequency domain Acceleration responses of sprung mass (body) in random profile bump (ISO 8608) conditions at 40 km/h

Fig 3.12(a)-(d) displays the vertical acceleration of body parts ('head', 'upper torso', 'lower torso', and 'pelvis') in time domain. The acceleration of body parts is an indicator of comfort level. As shown in Fig 3.12(a), the head acceration shows the strong transient peak at the begining of each road excitation and then gradually decys. Highest acceleration amplitude caused by Road D which is upto ±40 m/s^2, while road A and B causes much smaller oscillations. The head is experiencing resonance excitation with Road D exciting it most strongly. It is also evident from 3D FFT plot as shown in Fig 3.14(a), Road D exhibit dominant peaks in the range of 4-7 Hz, which coincides with the natural frequency of human body segment head-neck system and thus high time-domain peaks shows Road D as the most critical road which causing discomfort. In the similar

band, Road C also exhibiting noticeable peaks but comparatively lower than Road D. Relatively Roads A and B shows lower spectral amplitudes, thus indicating smoother vibrations with less resonance excitation. As observed from behaviour of head from all road, vibration enrgy is mostly concentarated below 10 Hz, which is consistent with ISO 2631 guidelines highlighted the band as most harmful for human exposure to vibrations. Fig 3.12(b)-(d) shows Road D producing the highest transient accelerations across upper torso, lower torso and pelvis(thigh), while Road A and B yields comparatively smoother responses. The frequency domain responses for upper torso, lower torso and pelvis(thigh) from Fig 3.14(b)-(d) shows the dominant peak in the range of 4-8 Hz band coinciding with human torso-pelvis resonance range. The sustained excitation in this band causes the discomfort, tolerance reduction, and musculoskeletal fatigue *(ISO 2631).* It is evident in case of Road C and D, representing exceeds these comfort thresholds, thus indicating their greater impact on ride quality and occupant's health.

Fig 3.13 shows the time domain responses of acceleration in seat and sprung mass in random road profile conditions. Road D shows the highest ransient accelerations whereas Road A and B yiels comparatively smoother responses. In the frequency domain responses as illustrated in Fig 3.15-3.16, significant peaks are observed in the range of 4-8 Hz which coincides with the human body's most sensitive vibration band.

3.6 Experimental Validation

The quarter-car suspension system using experimental data obtained from a physical vibration test rig. The validation establishes the accuracy and reliability of the simulation model for further controller development and optimization. RMS sprung mass acceleration, Peak acceleration and Natural frequency response parameters were used for comparing simulation results with the test rig measurements. Simulation and experimental tests were performed using identical input excitations. The validation steps includes time domain response comparison, frequency domain comparison, error signal analysis and statistical evaluation of correlation index, NRMSE (Normalized root mean square error) and MAPE (Mean absolute percentage error)



Figure 3.17 Quarter car test rig (DTU)

3.6.1 Correlation coefficient (r)

It indicates waveform similarity by measuring shape of both signals. Mathematically correlation coefficient is given by

$$R = \frac{\sum(x_i - \bar{x})(y_i - \bar{y})}{\sqrt{\sum(x_i - \bar{x})^2 \sum(y_i - \bar{y})^2}} \quad (3.13)$$

where R> 0.85 indicates very good validation.

3.6.2 Normalized Root Mean Square Error (NRMSE)

It generally quantifies the normalized deviation between two responses (data set) and NRMSE < 10-15% is acceptable and is mathematically calculated as

$$NRMSE = \frac{\sqrt{\frac{1}{N}\sum(x_i - \bar{x})^2}}{x_{max} - x_{min}} \quad (3.14)$$

3.6.3 Mean Absolute Percentage Error (MAPE)

It measures average percentage error and its value less tha 10% is considered good and is calculated as

$$NRMSE = \frac{1}{N}\sum \left|\frac{(x_i - \bar{x})}{x_i}\right| \times 100 \quad (3.16)$$

Results were taken from quarter car test rig and bond graph quarter car mode and are presented in Table 3.3. The developed Bond Graph model of the quarter-car system showed good agreement with the data obtained from the experimental test rig. There was a good correlation between the simulated and measured sprung mass acceleration value i.e r=0.9787, and NRMSE calculated 4.23% was less than 10 and MAPE vale is 5.31% The frequency domain comparisons also showed that model was a good representative of the dominant vibration modes. These results confirm that the Bond Graph model is a valid representation of the physical system, which can be used for developing sophisticated controllers and optimizing parameters.

Table 3.3 Quarter car Simulation and experiment result

Parameter	Simulation result	Experimental Result	%error
RMS sprung mass acceleration (m/s^2)	0.8962	0.8666	3.3%
Peak acceleration (m/s^2)	6.509	5.218	8.40%
Natural frequency (Hz)	1.89	2.15	13.75%

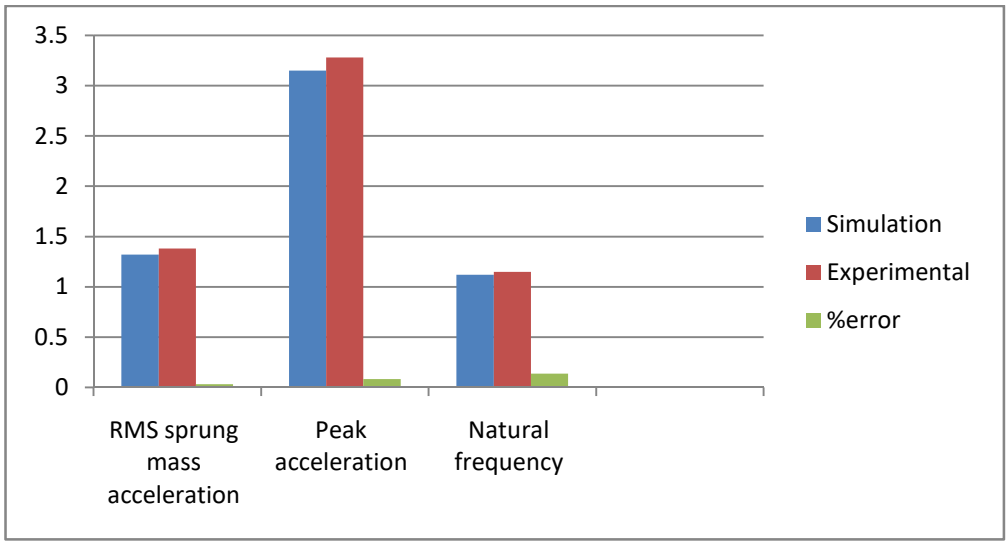


Figure 3.18 Comparison of Simulation and experimental responses

3.7 Conclusion

The dynamic model was constructed and simulated using bond graph technique. This study was developed through the development of a comprehensive coupled human-vehicle dynamic model to analyze human body behavior through computational bond graph modeling for a 3 DOF quarter car model combined with a (4-DOF) lumped human biodynamic model which represents the head, upper torso, lower torso and pelvis (thigh) when seated on a vehicle in a static posture with no backrest. A simulation is created by applying deterministic and random excitations to the model that represent the variability of road surfaces (ISO 8608) classified as A, B, C and D with sine, trapezoidal and square waveforms. This type of excitation allows for a wide range of variability in the road conditions from very smooth highways to very uneven terrain driving environments. Time and frequency domain biodynamic response values are measured for each part of the human body and the vehicle body in response to various road excitations. Results

demonstrate how the characteristics of the road surface affect the biodynamic response, providing important information regarding road roughness and its effect on human comfort.

Among all deterministic bumps (sinusoidal, square and trapezoidal), square excitation consistently causes worst response in terms of transmitted vibration across all body segments due to its abrupt discontinuity. In contrast, sinusoidal bump responses results in smoother and controlled response, while trapezoidal causes intermediate bahviour in terms of transmitted vibrations. These findings are confirming that sudden road irregularities cause worst loading conditions for occupant's comfort, further low frequency dominance peaks confirmed that in the range of 1-5 Hz there is human discomfort and risk of potential injury. Segment wise observations revealed that head experiencing the highest acceleration amplitude which thus indicating propagation of vibrations amplifies as it travels upward through human body parts. Although pelvis is primary contact interface between vehicle body and human body, resonance effect in the spinal and head-neck system significantly increases head sensitivity.

For stochastic ISO 8608 road profiles (Class A-D), Road D produced the highest acceleration level in both time and frequency domains. The peaks were observed in the range of 4-7 Hz which is closely matching with the natural frequencies of head –neck system. The Road C also showed significant vibrations levels, while Road A and D remained within acceptable comfort limits.

The next chapter will present the performance analysis of novel bond graph based PID controller for the quarter car model coupled with bio mechanical human model. Further a fractional-order PID (FOPID) controller developed to enhance ride comfort and to reduce human body segment vibration. The results from PID and FOPID were compared with passive system and thus demonstrating significant enhancement in vibration suppression and ride comfort.

CHAPTER 4

Active Suspension Control Using Bond Graph PID and PSO-Optimized FOPID Controller

In the last chapter, a complete mathematically-based study was carried out for the vibration performance of a quarter-car suspension system with a 4 degree of freedom biodynamic human model using a bond graph. Simulations were performed under deterministic and random road excitation conditions (sinusoidal, trapezoidal, square wave and ISO-8608 Class A-D). Through simulation, it has been shown that the passive suspension designs do not provide adequate vibration attenuation to the human body for all road conditions; specifically during harsher road conditions, this indicates the lack of control for the passive system.

As such, the current chapter will focus on Bond Graph modeling and implementation of PID controller in the active quarter-vehicle suspension system for the purpose of achieving better ride comfort. Bond graph is a better tool for modeling multi-domain energy systems with control hardware associated with it. SYMBOL SHAKTI

software is used to simulate the active vehicle suspension system, which is theoretically represented as a 4-DOF human Bio-dynamic model combined with a 3-DOF quarter automobile system. The suggested PID Controller's performance is contrasted with that of the passive model. To measure the effectiveness of the suggested PID controller suspension system, both time and frequency domain evaluations of systems performance criteria are conducted. Further the performance of fractional-order PID (FOPID) controller is evaluated with optimally tuned parameters using particle swarm optimization (PSO) algorithm.

The findings show that a significant improvement in ride comfort is offered by the suggested Bond graph PID controller model of the active vehicle suspension.

4.1 Introduction

Vehicle suspension isolates driver and occupants from the road irregularities to make the ride more comfortable. In other words we can say suspension system role is to provides better ride comfort and this purpose have gained more interest due to development of various control technologies which uses an active component which is controlled by microcontrollers and hence there achieves improvement in vehicle response.

Passive suspension systems have pre-determined spring stiffness and damper coefficients that can be determined by the engineer to meet the goals of the vehicle's design and for the expected operational environments. The engineer will select these values as they cannot be changed in operation; therefore, this method has little flexibility

to accommodate changing road excitation forces. In comparison, an active suspension system will replace the passive spring/damper assembly with a force generating device (actuator) that can add energy into the system and remove energy from the system. The energy added/removed by the force generating device is not directly dependent upon the relative motion or velocity of the two parts separated by the suspension.

Numerous model reduction techniques that can systematically reduce a model can be found in the appropriate modeling literature. Some are based on bond graphs and power flow diagrams. Basis for bond graphs is the power transfer between system components. Bond graph is a great tool for describing vehicle dynamics with related control systems because they provide a clear visual depiction of all different sorts of interacting energy domains and thus offer an accurate and clear representation of modeling for a variety of physical systems *(Gawthrop, 1995)*. Sensors, signal processing, and actuation are necessary for the controllers, and these components are incorporated and demonstrated using car models by Margolis et al. *(Margolis and Shim, 2001)*, a 4-DOF quarter car model was developed and response in terms of vibration transferred to occupant body parts (head & thorax) was captured using Simulink and Bond graph tool *(Mitra, A. C., & Benerjee, 2013)* Additionally, the 2-DOF quarter car vehicle system's passive, semi-active, and active performances were determined by *(Sathishkumar et al., 2007)* where as *Gupta et al, (2012)* used PI controller in Bond Graph and performs dynamic simulation of 6-DOF off road truck.

This experiment illustrates how heavy road vehicles respond dynamically to impediment. Bond graph modeling approach was used to build a computational model of

vehicle and analyze its dynamic behavior. This method was initially presented by Henry M. Paynter *(Paynter, 1961)*. Instead of simply one portion of the operator's body, such as their hand or foot, the vibrations force their entire body to tremble. When exposure time exceeds the acceptable standard established by ISO 2631-1 *(Standard, 1997)*, harmful consequences of whole-body vibration are felt. The experimental conditions and given results on the biodynamic responses of the standing and seated human body to whole-body vibration in various directions are thoroughly assessed by *(Rakheja et al., 2010)*

There were various attempts to improve passive suspension systems for automobiles for the purpose of lowering suspension stiffness and un-sprung mass and the ideal damping ratio for the optimal controllability. In order to find the vehicle suspension settings for the optimum human comfort, *Farid et al, (2011)* optimized a 4-DOF quarter vehicle suspension system paired with a sitting human. A simulation study was performed to show effectiveness of proportional-integral sliding mode controller *(Sam et al, 2004) (Kumar, J., & Bhushan, 2023)* Proposed a hybrid semi-active vibration isolator which combines a four-parametric viscoelastic model with a Bouc-Wen model, to realize the control of stiffness and damping simultaneously and improve the vibration management of vehicles. The PID parameters were optimized for integrated active suspension system's using a teacher learning-based optimization (TLBO) by *(Mehta et al., 2016)*

The active suspension system based with 7-DOF is the model suggested in this research. This modelling exercise's major objectives are to demonstrate how the bond

graph approach can be used to complex models and to highlight how easily plant and controller model fusion can be done using bond graph software. The bond graph model uses controller gains that were tuned using MATLAB/SIMULINK.

The Bond Graph PID controller is used for vehicle suspension system with the goal of lowering jerks and raising driver ride comfort. The controlled variable's value is established by this controller, which then computes the deviation between the actual and desired values and generates a control signal to reduce the difference to zero. The main objective of this work is to show how control system design can actually be based on such a basis.

4.2 Modeling and Implementation of Bond Graph PID Controller

4.2.1 PID Controller Structure

PID stands for proportional, integral and derivative. These controllers are designed to eliminate the need for continuous operator attention. In order to avoid the small variation of the output at the steady state, the PID controller is so designed that it reduces the errors by the derivative nature of the controller. A PID controller is depicted in Figure 4.1. Error is defined as the difference between set-point and measurement.

The PID controller output signal is represented by Eq 4.1 and the PID structure is shown

$$U(t) = K_p e(t) + K_I \int e(t)dt + K_D \frac{de(t)}{dt} \quad (4.1)$$

$U(t)$ = PID controller output signal

$e(t)$ = The error signal between desired set point and output signal

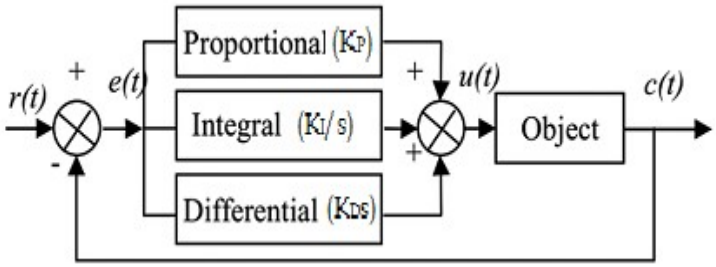


Fig. 4.1 PID controller structure *(Jin et al., 2016)*

4.2.2 Bond Graph PID controller modeling

Using same Bond Graph elements active quarter car model is formed. A flow triggered C-element link is attached to each 1-junction to record velocity and displacement of certain human body parts. Each body member's stiffness and damping are introduced by connecting C and R components at the 1-junction. Acceleration is captured on I-element. Finally bond graph model of human body parts is further attached with seat and wheel model.

Additionally, the bond graph model of the car body and wheels is attached at the 0-junction by incorporating C and R elements that reflect the stiffness (Ks) and damping (Cs) of the wheel suspension system. This creates the interface between the sprung mass (car body) and un-sprung mass (wheel). Tire damping is neglected and stiffness is introduced using C-element.

Fig 4.2 shows the Bond Graph PID controller designed for the purpose of controlling discomfort transferred to human body parts due to road irregularity in form

of acceleration and displacement. A PID controller is made up of the derivative (D), integral (I), and proportional (P) terms. The equation for the generalized PID controller is provided by

The output u(t) of a PID controller is, in theory, equal to the total of the three terms. While e(t)= r(t)-y(t) indicates the feedback error signal between the reference signal r(t) and the output y(t), K_P (Proportional constant), K_I (Integration constant), and K_D (Derivative constant). The controller's goal is to achieve predicted behavior for the model's output y(t) with respect to the set point r(t). Controller can be represented as bond graphs capsule and consequently constructed in the bond graph domain. The system's controller can measure any variable within the system, but it can only modify variables that relate to the system's physical sources. Stated differently, there are an endless number of virtual sensors but no virtual sources *(Gawthrop, 1995)*

As represented in Fig 4.2, Proportional, integral and derivative gains are introduced in model using transformer (TF). For the effective functioning of PID controller selection of gain parameter is one of the most challenging task here in this work tuning is done using Zeigler-Nichols method and parameter used in simulation are K_P=1200, KI=100 and K_D=4450.

Gyrators (GY) are used to convert effort into flow or vice-versa. The modulated flow provides the reference signal. It is then compared at the 0-junction with observed value and an error signal is generated, which is then sent as an input signal to different transformers where transformer gains are multiplied and summed at the 0-junction. The generated controlled signal used for required action.

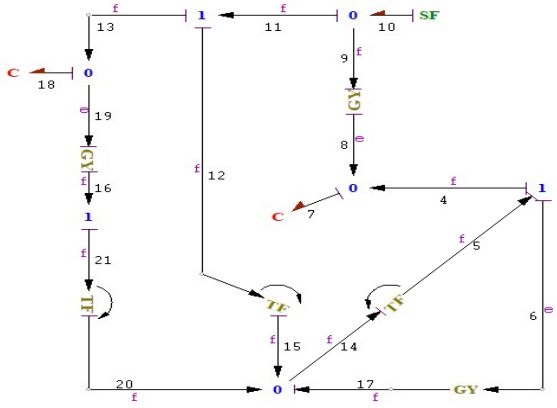


Figure 4.2 Bond Graph PID controller model

Transformer between flow 12 and 15 is modulated as K_p thus error signal multiplied to it. Further, Integral gain (K_I) is provided using transformer modulated gain between flow 21 and 20. The derivative gain (K_D) is provided between flow 14 and 5. As represented in the bond graph, the PID control system involves efforts and flows using activated bonds and controlled sources. In this case, the feedback signal is passed into the PID controller by the seat suspension mechanism and the resulting effort is used to compensate for the excess vibration. This happens when the controlled effort source influences the seat suspension mechanism.

The use of PID control greatly enhances the vibration isolation capability of the seat suspension system. Using appropriate settings for the controller gain will reduce the peak transmissibility near the resonance frequency, resulting in less seat acceleration and better ride quality. In addition, the controller ensures the stability of the system when subjected to different road excitations like sinusoidal, random, and bump excitation.

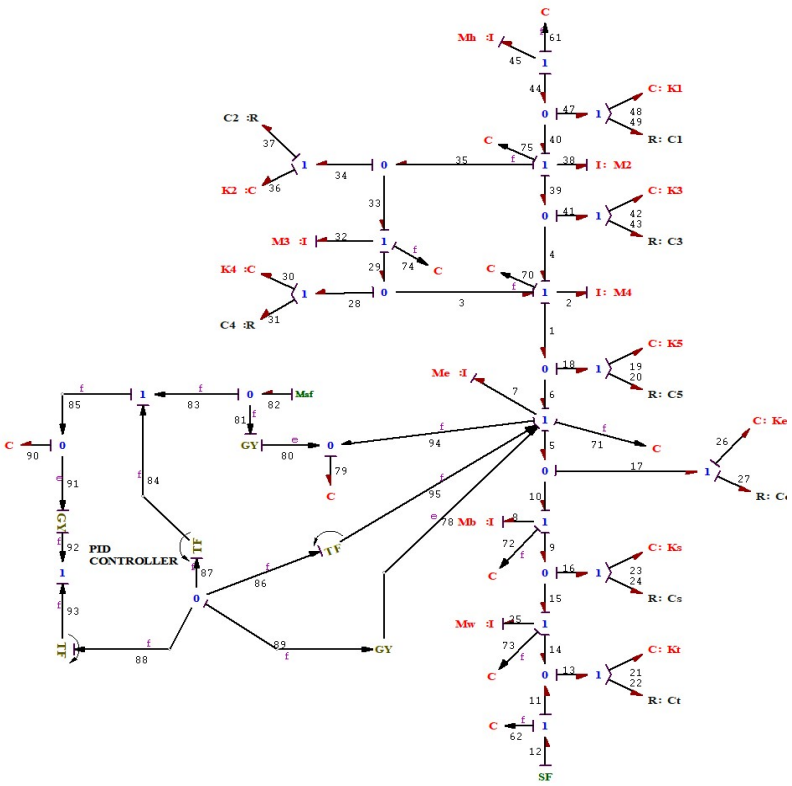


Figure 4.3 Integrated 7-DOF Active seat suspension quarter car Bond Graph model with PID controller

Moreover, the active control approach with PID control also allows for adaptive compensation of low frequency vibrations that have very high sensitivity in terms of human comfort and well-being. In terms of vibration damping performance, the seat suspension with active control performs significantly better than the passive suspension in the resonance range.

The bond graph formulation, thus proposed, is one of the methods to develop a comprehensive energy based modeling technique that helps in studying the interaction between the vehicle suspension, seat suspension, human body, and the control system.

The incorporation of the PID controller in the bond graph model makes possible the effective simulation of the overall coupled system dynamics.

As shown in Fig 4.3, the Bond Graph PID controller is implemented on 7 DOF quarter car model coupled with human bio-dynamic model, used in chapter 3 (Fig 3.5), for simulation purpose.

4.3 Road Excitation

A sinusoidal road profile bump of the same height (0.1 m) but varying widths 1 m is used for analysis, as illustrated in Fig 4.4. The road conditions, as a function of time, are expressed as follows

$$\begin{cases} Z = h * \sin\left(\frac{\pi . v}{w} * t\right) & for \ t < \frac{w}{v} \\ = 0 & for \ t > \frac{L}{v} \end{cases} \quad (4.1)$$

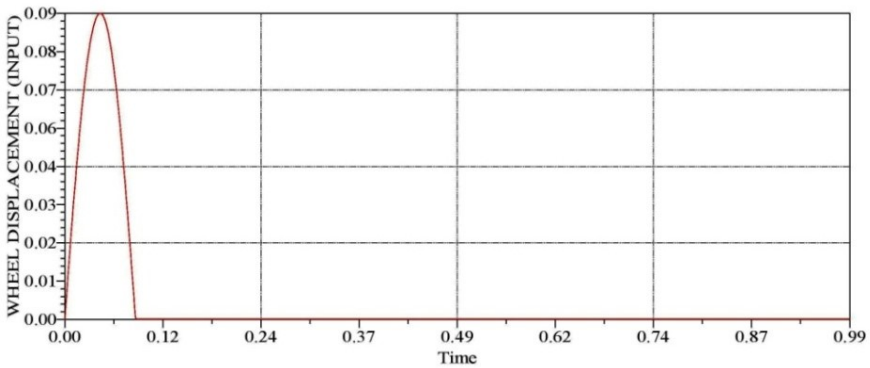


Figure 4.4 Sinusoidal road input

4.4 Simulation Studies

The differential equations of the bond graph are solved using a fifth-order Runge-Kutta method. Simulation is conducted for 10 seconds to obtain distinct dynamic reactions. The simulation employs 1024 data points with errors on the order of 5.0 x 10-4. Simulation parameters were taken from *(Farid, Salah and Abbas, 2011)* and are listed in Table.3.2

4.5 Results and Discussion

4.5.1 Time domain responses

Acceleration and displacements of body components, occupant seats, and sprung mass are among the time-domain responses investigated in this study when stimulated by artificially created sinusoidal inputs. Further Ride comfort was determined and compared the results of both passive and active (Bond Graph PID controller) model.

Fig.4.5-10 shows vertical acceleration and displacement of body parts as well as for passenger seat and sprung mass respectively. Peak accelerations and displacement of all body parts are observed nearly same. Acceleration in body parts measures the comfort level and it is observed in Fig 4.5(a)-(d) that body parts (head, upper torso, lower torso, pelvis) acceleration is decreased in term of peak acceleration and settling time. The maximum and minimum head acceleration (Fig 4.5(a)) for passive system is observed +5.2 m/s^2 and -4.5 m/s^2 respectively and it is evident that same are reduced to

+1.8 m/s^2 to -1 m/s^2, which is a significant reduction, hence ride comfort improved and similar reductions for upper torso, lower torso and pelvis (thigh) can be observed.

Fig.4.6-4.7 depicts the acceleration of seat and spring mass respectively and it is further visible that acceleration peak (maximum=+4.2 m/s^2 and minimum=– 3.8 m/s^2) in seat has been significantly reduced to 1.4m/s^2 and -0.9m/s^2 by applying BG PID controller and in case of sprung mass significant improve not observed due to fact that controlling force was provided to seat which affected human body resting on it.

Displacement in body parts measures the comfort level and it is observed in Fig 4.8(a)-(d) that body parts (head, upper torso, lower torso, pelvis) displacement is decreased in term of peak displacement and settling time. The maximum and minimum head displacement (Fig 4.5(a)) for passive system is observed +0.05m and -0.02m respectively and it is evident that same are reduced to +0.015m to +0.002m, which is a significant reduction, hence ride comfort improved and similar reductions for upper torso, lower torso and pelvis (thigh) can be observed.

Fig.4.9-4.10 depicts the displacement of seat and spring mass respectively and it is further depicted that displacement peak (max=+0.045m and min=-0.019m) in seat has been significantly reduced to 0.012m and +0.002 m by applying BG PID controller and in case of sprung mass significant improve not observed due to fact that controlling force was provided to seat which affected human body resting on it.

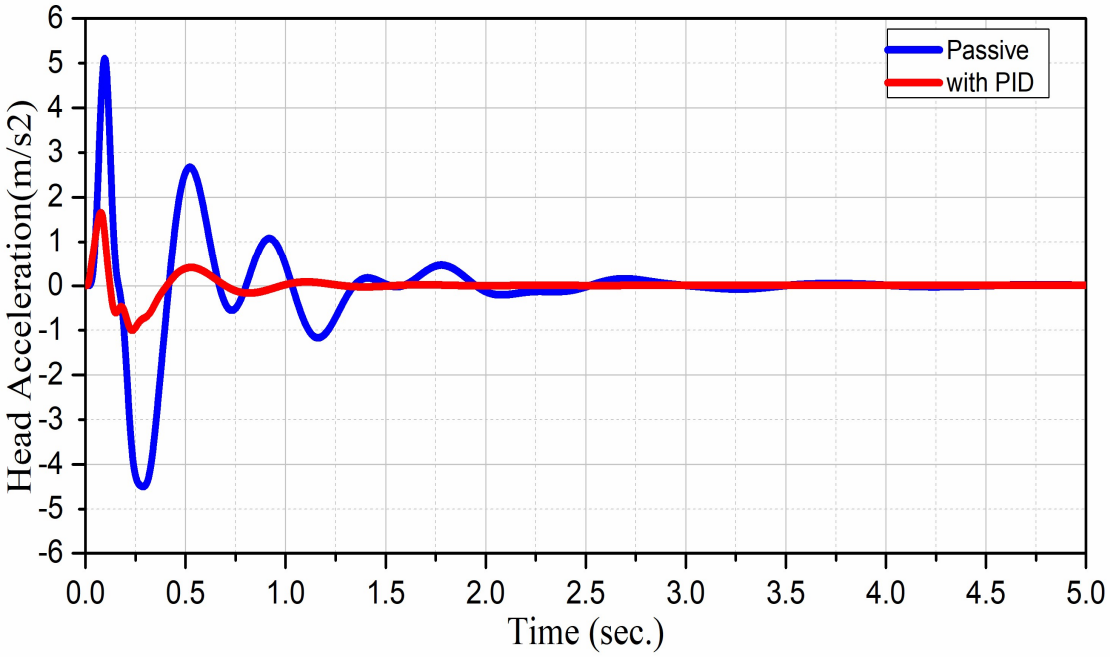


Figure 4.5(a) Head acceleration response (Time domain) comparison Passive vs Active (Bond Graph PID controller) at 40 Km/h

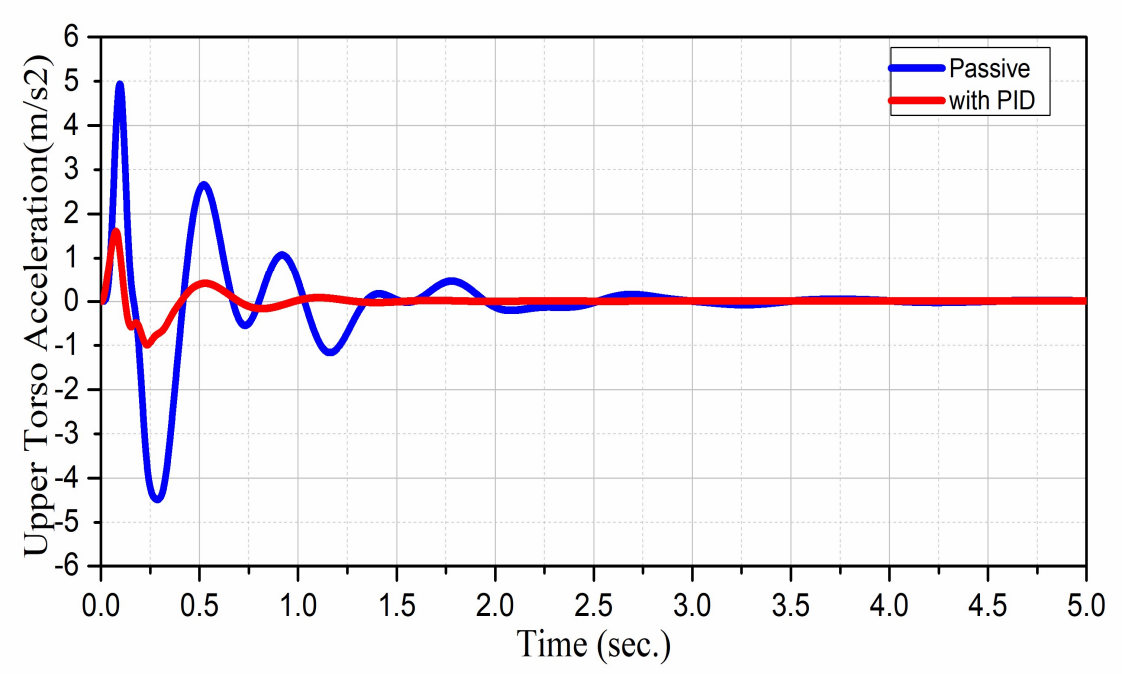


Figure 4.5(b) Upper Torso acceleration response (Time domain) comparison Passive vs Active (Bond Graph PID controller) at 40 Km/h

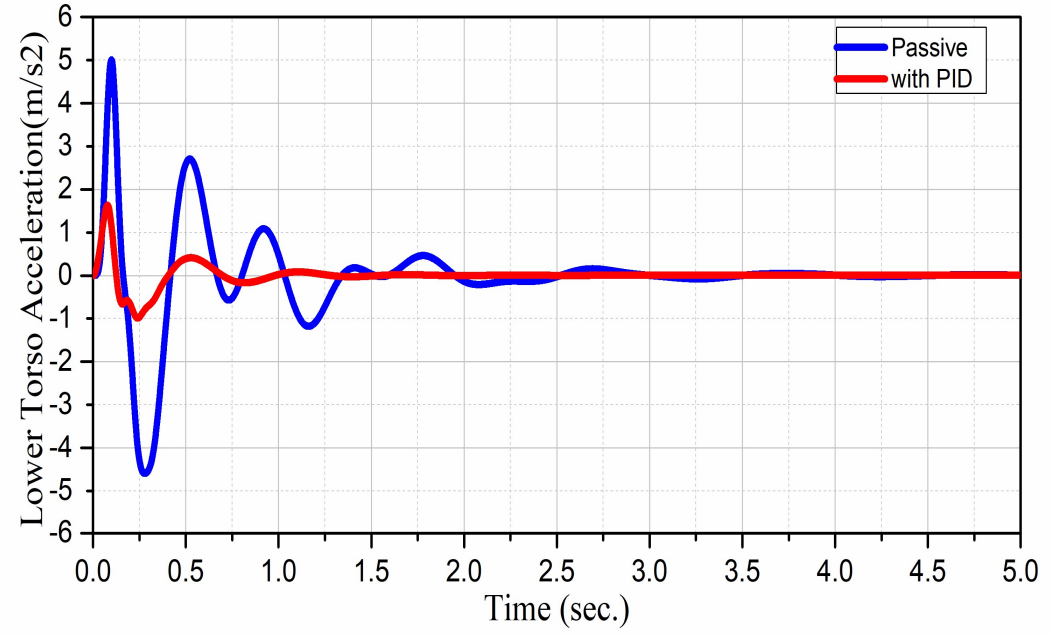


Figure 4.5(c) Lower Torso acceleration response (Time domain) comparison Passive vs Active (Bond Graph PID controller) at 40 Km/h

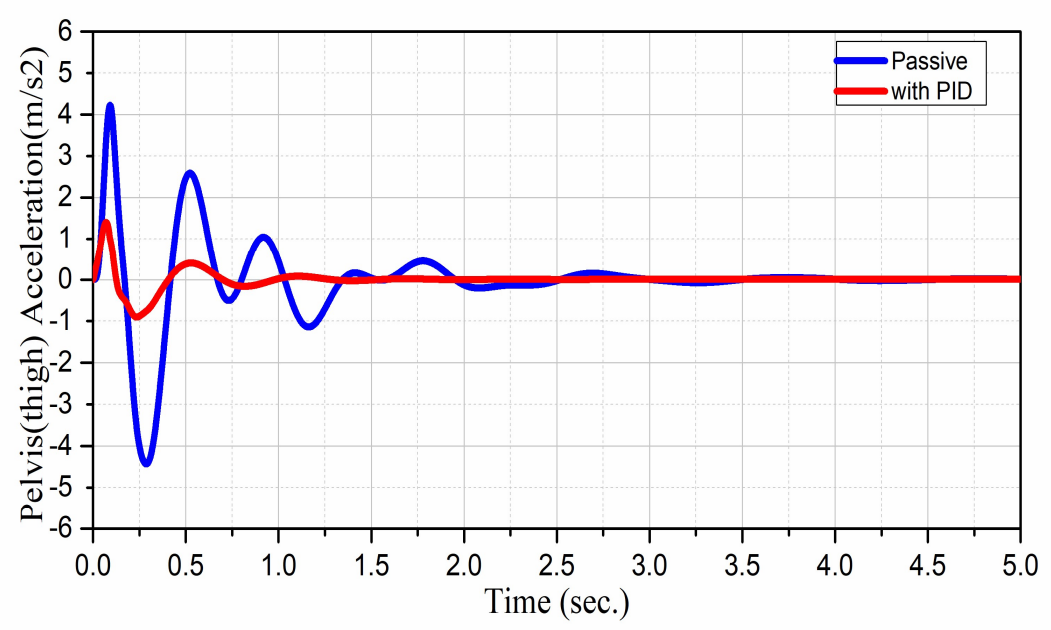


Figure 4.5(d) Pelvis (Thigh) acceleration response (Time domain) comparison Passive vs Active (Bond Graph PID controller) at 40 Km/h

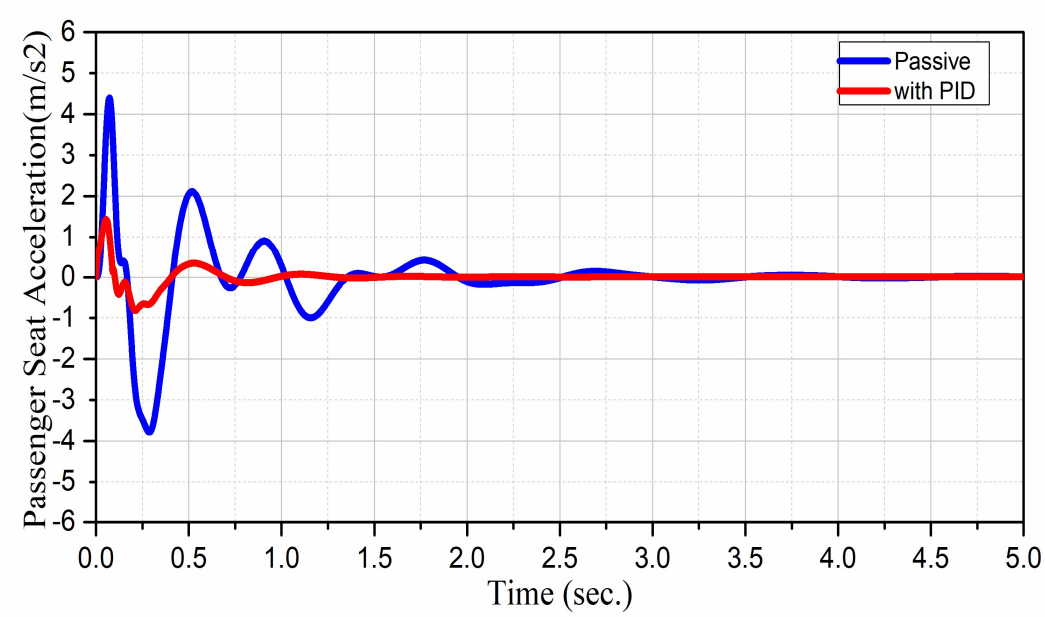


Figure 4.6 Seat acceleration response (Time domain) comparison Passive vs Active (Bond Graph PID controller) at 40 Km/h

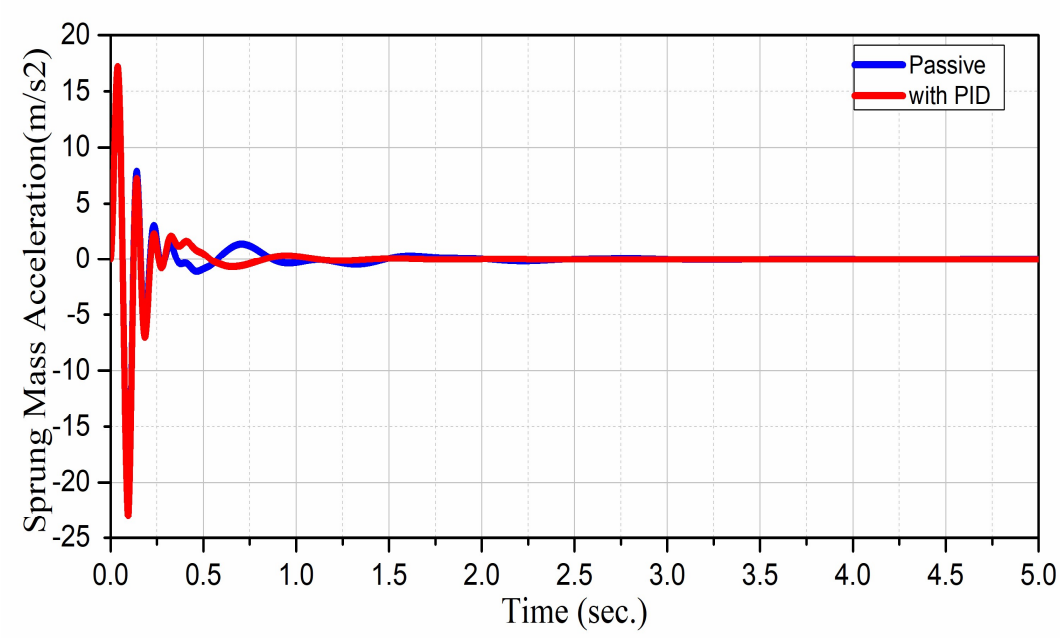


Figure 4.7 Sprung mass acceleration response (Time domain) comparison Passive vs Active (Bond Graph PID controller) at 40 Km/h

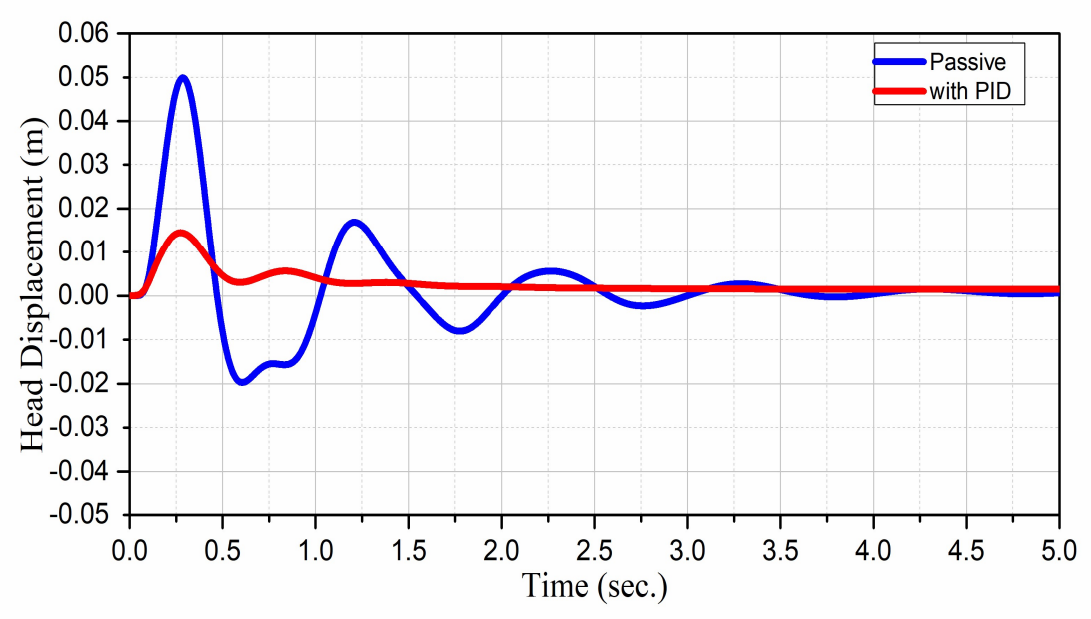


Figure 4.8(a) Head displacement response (Time domain) comparison Passive vs Active (Bond Graph PID controller) at 40 Km/h

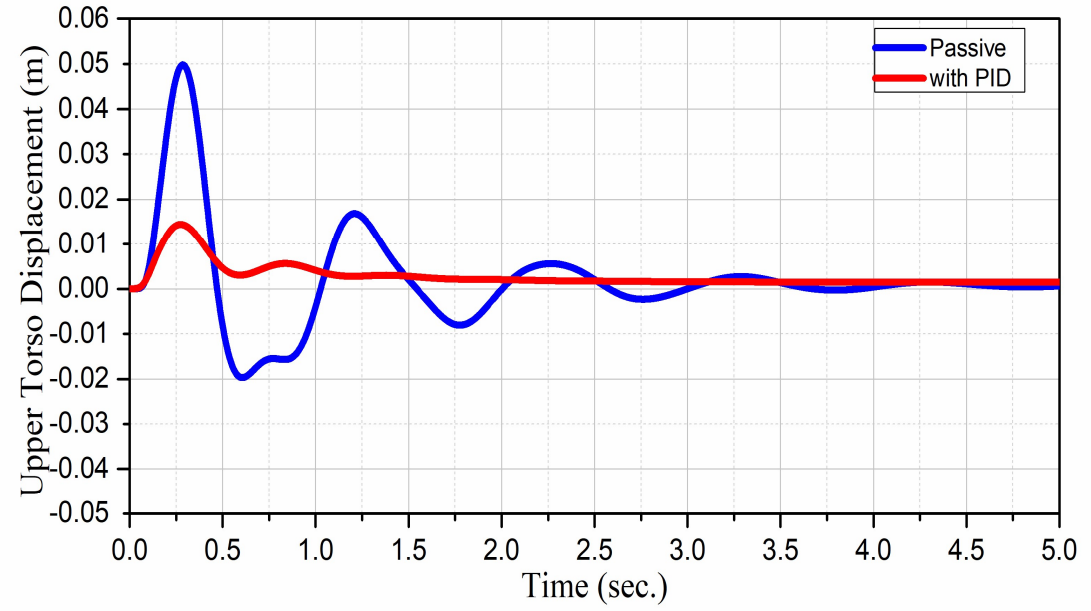


Figure 4.8(b) Upper Torso displacement response (Time domain) comparison Passive vs Active (Bond Graph PID controller) at 40 Km/h

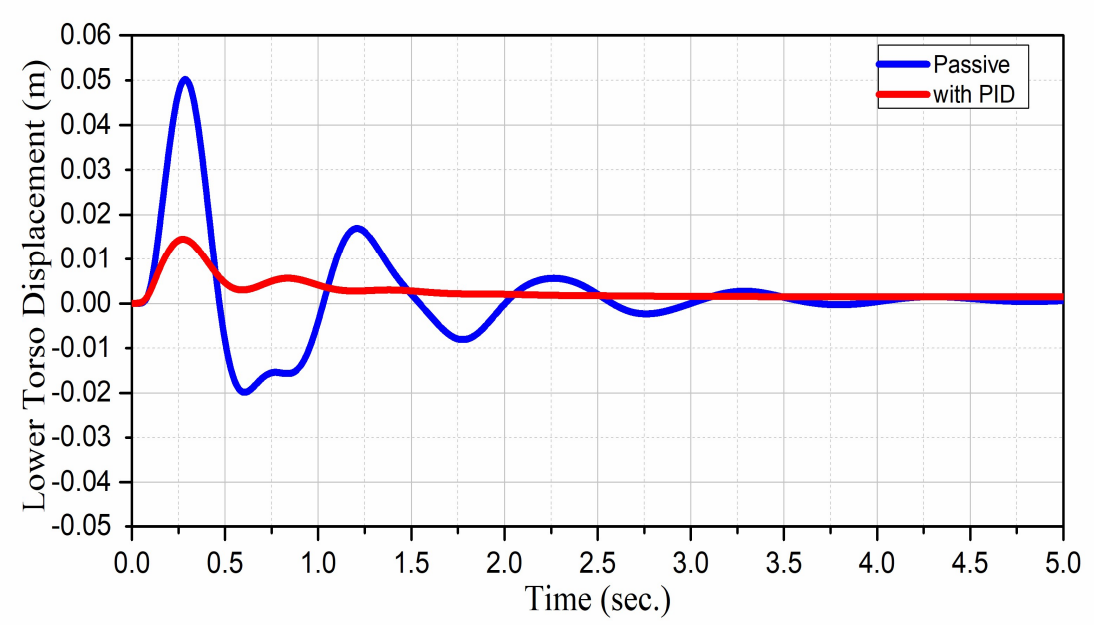


Figure 4.8(c) Lower Torso displacement response (Time domain) comparison Passive vs Active (Bond Graph PID controller) at 40 Km/h

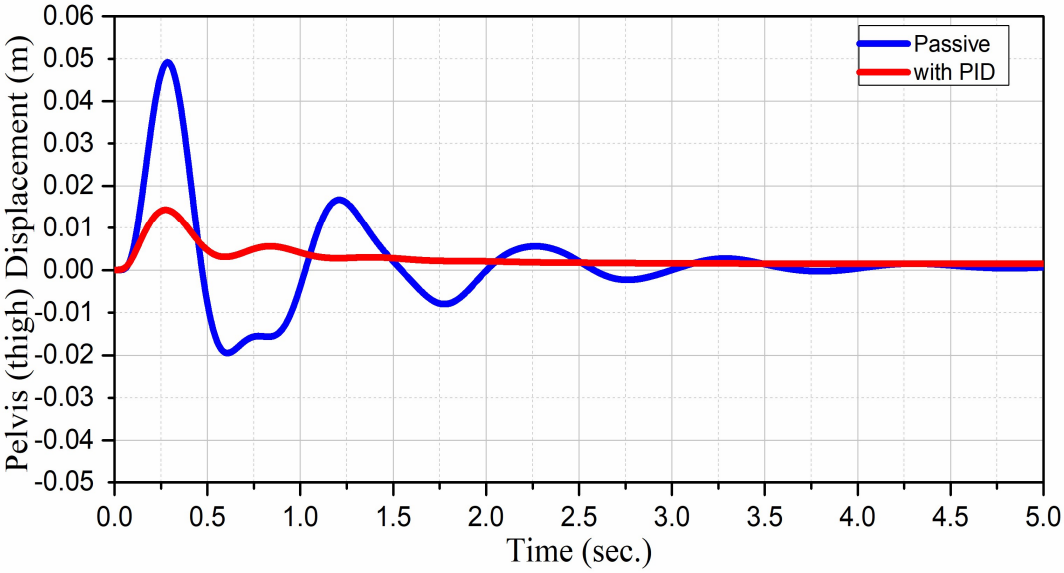


Figure 4.8(d) Pelvis (Thigh) displacement response (Time domain) comparison Passive vs Active (Bond Graph PID controller) at 40 Km/h

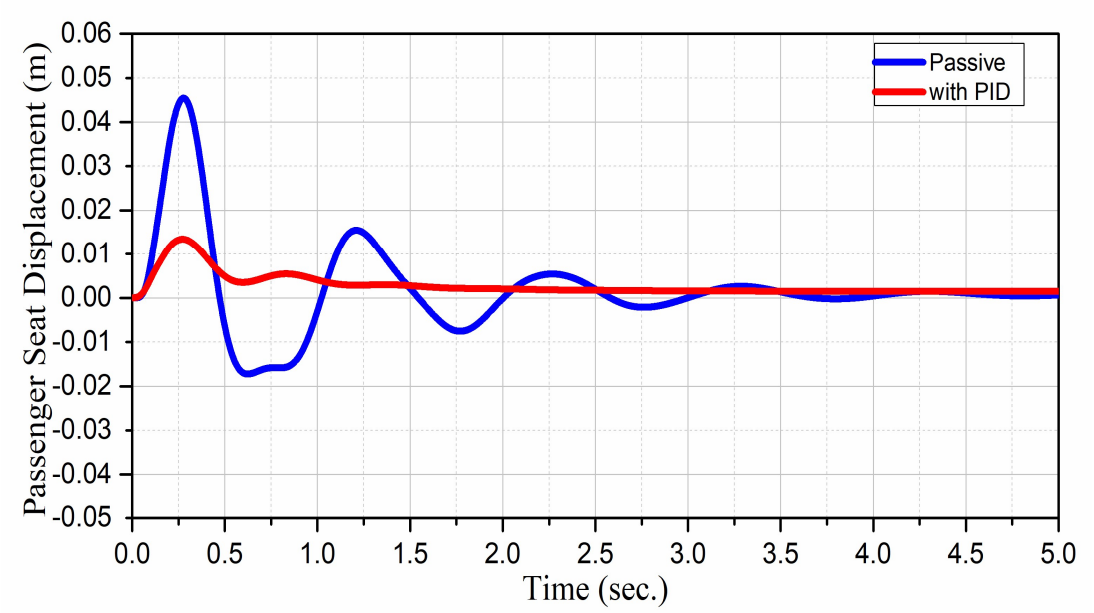


Figure 4.9 Seat displacement response (Time domain) comparison Passive vs Active (Bond Graph PID controller) at 40 Km/h

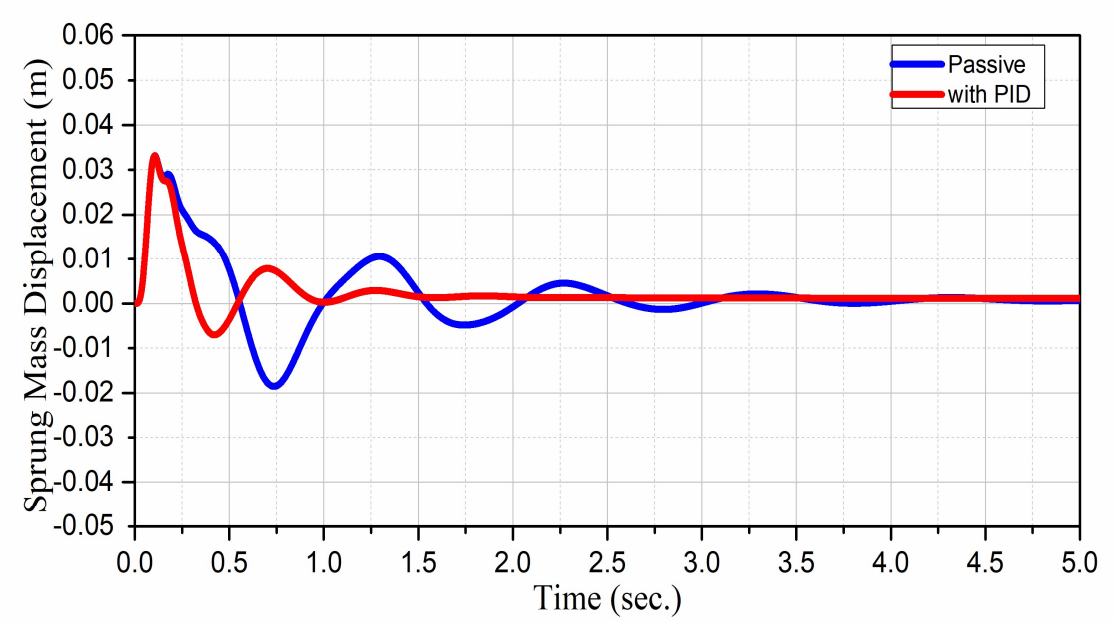


Figure 4.10 Sprung Mass displacement response (Time domain) comparison Passive vs Active (Bond Graph PID controller) at 40 Km/h

4.5.2 Frequency Domain Responses

The acceleration response characteristics of various human body segments for passive and PID controlled suspension systems are shown in Fig. 4.11(a)-(d). The head acceleration response from Fig 4.11(a) reveals a prominent peak at low frequency in the resonance region for the passive suspension system, which means there is significant transfer of vibrations to the head segment. For the passive suspension system, a high peak acceleration is seen around 1-3 Hz which corresponds to the resonance region of the system where a lot of vibration is being transmitted to the head segment. This high level of vibration can cause discomfort, fatigue and poor ride quality. The PID controller has a significant effect on the vibration isolation and, as a result, on the comfort of the passengers: The passive system (blue) shows a sharp peak near 1–2 Hz, with maximum head acceleration around 0.125 m/s^2. With PID control (red), the peak magnitude is drastically reduced to about 0.022 m/s^2. This means PID control effectively suppresses resonance, which is critical for ride comfort because low-frequency vibrations (around 1–2 Hz) correspond to the human body's most sensitive range.

The peak head acceleration is significantly reduced with the presence of the PID controller. The response characteristics of the controlled system are also smoother and the vibrations are also damped in the frequency range. Further, the passive curve has two visible peaks likely corresponding to vehicle body bounce and seat/head resonance. The PID-controlled system flattens these peaks, meaning it damps both modes effectively.

Likewise, the acceleration responses for the upper torso, lower torso and pelvis regions have significantly greater vibration amplitude for the passive suspension system, especially in the human resonance frequency range as depicted in Fig 4.11(b)-(d) respectively. This is because the body is very susceptible to whole-body vibration in these areas and extended exposure can lead to muscle strain, back pain, spinal pain, and fatigue. The vibration peaks are suppressed and the amount of acceleration transmitted to these body segments is considerably reduced by the PID-controlled suspension. Vibration reduction is confirmed by the decreased vibrations, which equates to improved dynamic stability and damping capability using the controller. In conclusion, the PID-controlled suspension system is found to perform better than the passive suspension system in terms of minimizing transmissibility of vibrations to the critical regions of the human body.

The vibration amplitude is clearly observed to be very low for all frequency ranges in the PID-controlled suspension system when compared with the passive suspension system from each of the above four acceleration response graphs. The greatest reduction is at the resonant frequencies to which the human body is most sensitive to vibration. It is thus concluded that the proposed PID controller is effective in alleviating the ride discomfort, minimizing vibration transmission to significant body locations and in enhancing the dynamic performance of the coupled vehicle–human system.

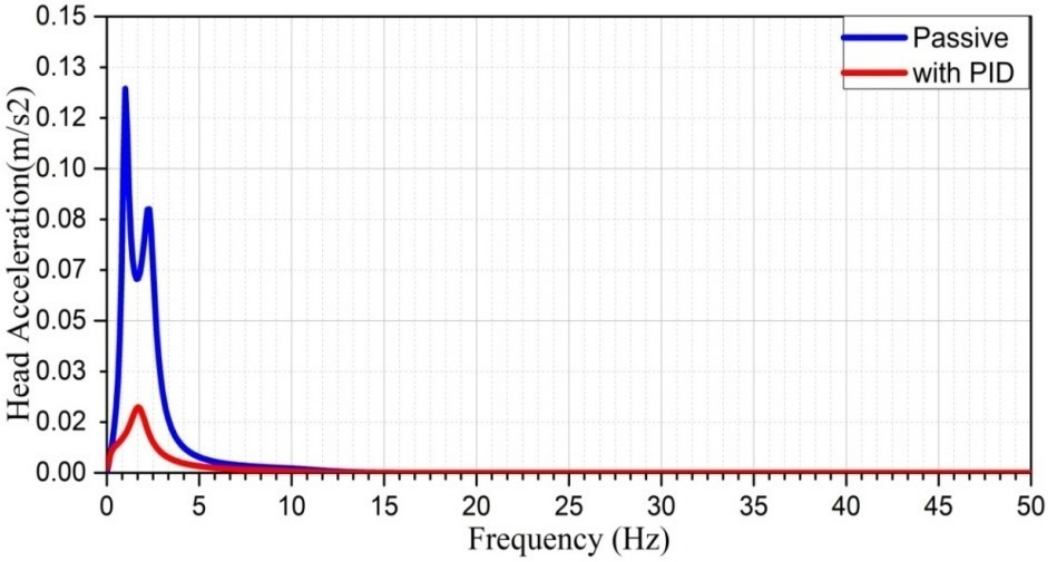


Figure 4.11(a) Head acceleration response (Frequency domain) comparison Passive vs Active (Bond Graph PID controller) at 40 Km/h

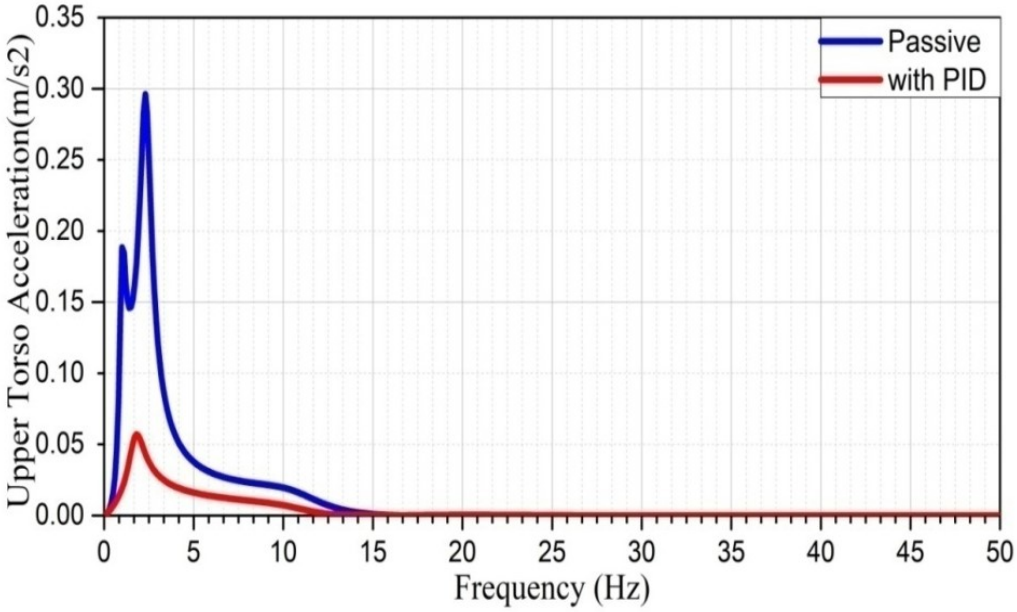


Figure 4.11(b) Upper Torso acceleration response (Frequency domain) comparison Passive vs Active (Bond Graph PID controller) at 40 Km/h

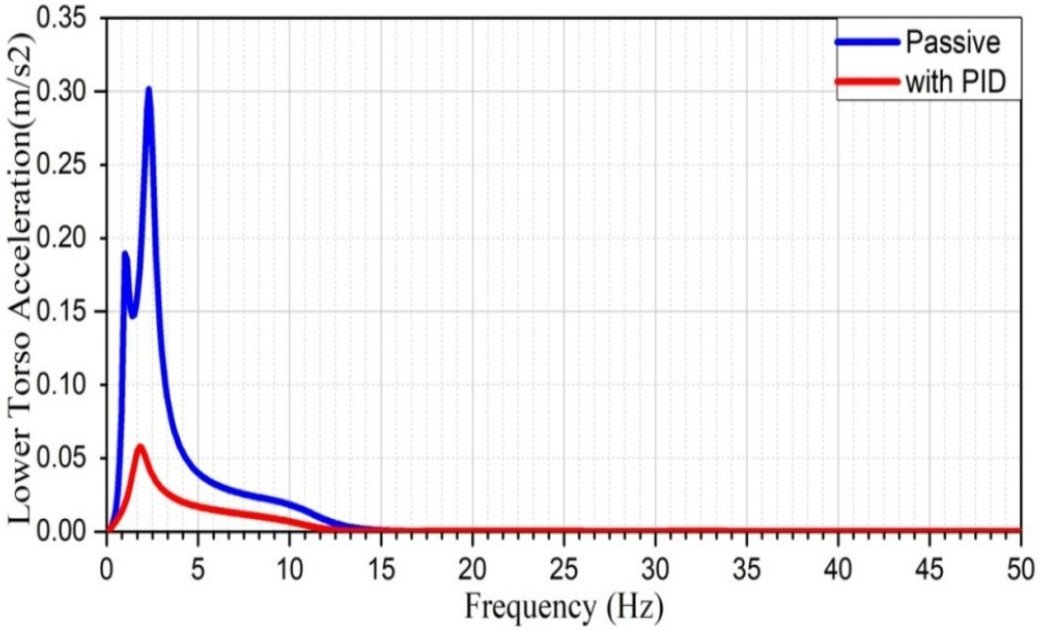


Figure 4.11(c) Lower Torso acceleration response (Frequency domain) comparison Passive vs Active (Bond Graph PID controller) at 40 Km/h

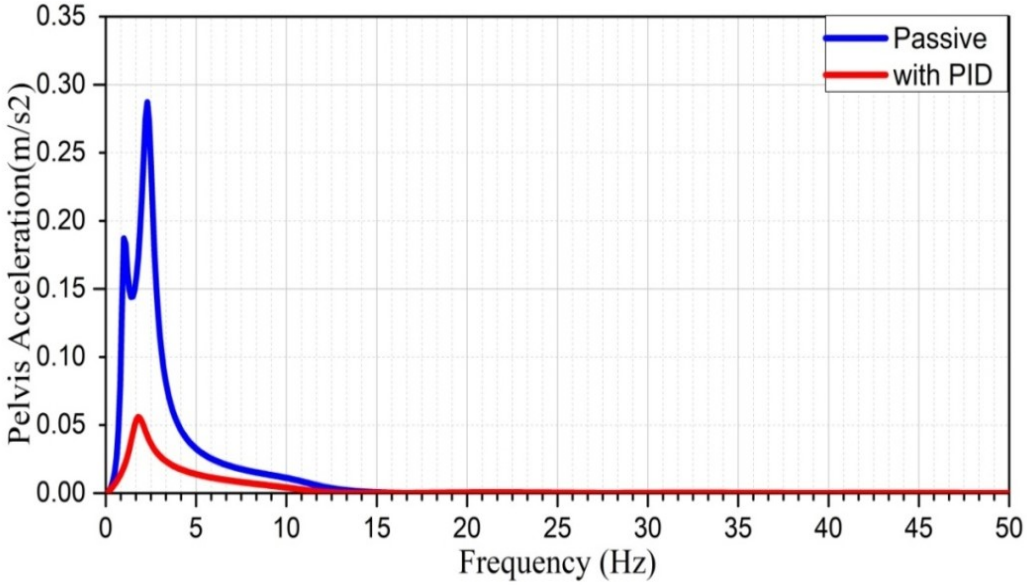


Figure 4.11(d) Upper Torso acceleration response (Frequency domain) comparison Passive vs Active (Bond Graph PID controller) at 40 Km/h

Table 4.1 Percentage improvement in RMS acceleration at 40 Km/h

	RMS Acceleration (m/s^2)					
	Head	**Upper Torso**	**Lower Torso**	**Pelvis**	**Seat**	**Sprung Mass**
Passive	0.711033	0.704951	0.717287	0.677774	0.593875	1.582208
Active (PID)	0.164251	0.161895	0.165359	0.151805	0.137434	1.593864
Percentage Improvement	**76.8997**	**77.03456**	**76.94654**	**77.60236**	**76.85806**	**-0.73667**

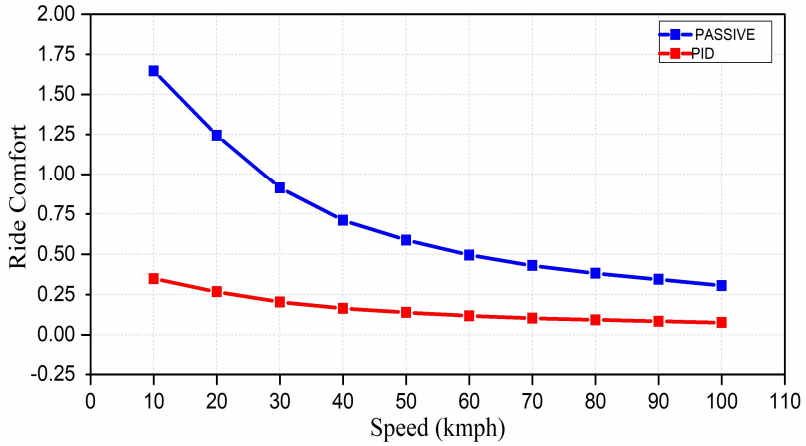


Figure 4.12 Ride Comfort response comparison Passive vs Active (Bond Graph PID controller) for various speed between 10 to 100 Km/h

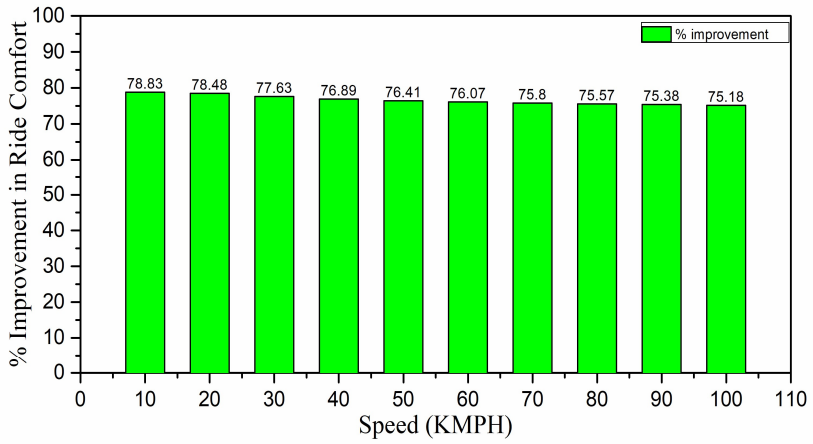


Figure 4.13 **%** Improvement in Ride Comfort for speed 10 to 100 Km/h using Bond Graph PID controller

Table 4.2 Percentage improvement in RMS displacement at 40 Km/h

	RMS Displacement (m)					
	Head	**Upper Torso**	**Lower Torso**	**Pelvis**	**Seat**	**Sprung Mass**
Passive	0.008013249	0.008001	0.008043	0.007934	0.007491	0.005657
Active (PID)	0.002892	0.002891	0.002896	0.002883	0.002833	0.00407
Percentage Improvemen	**63.90502**	**63.86835**	**63.99452**	**63.66343**	**62.17809**	**28.06441**

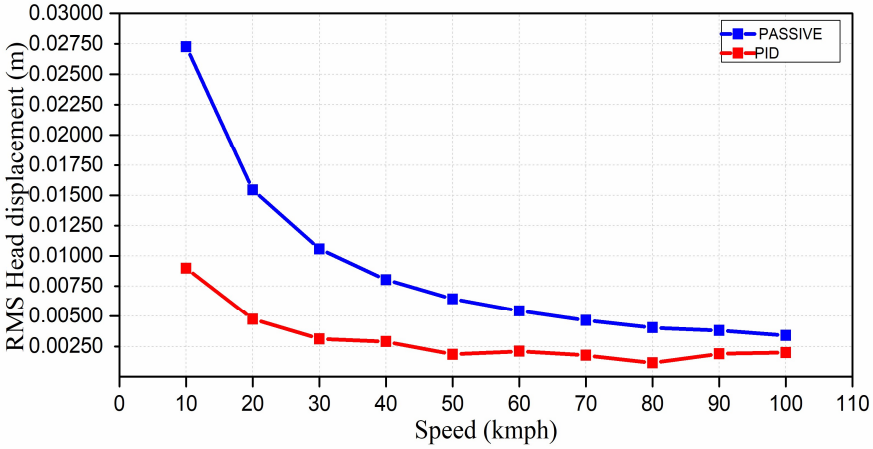


Figure 4.14 RMS head displacement response comparison passive vs active (Bond Graph PID controller) for various speed between 10 to 100 Km/h

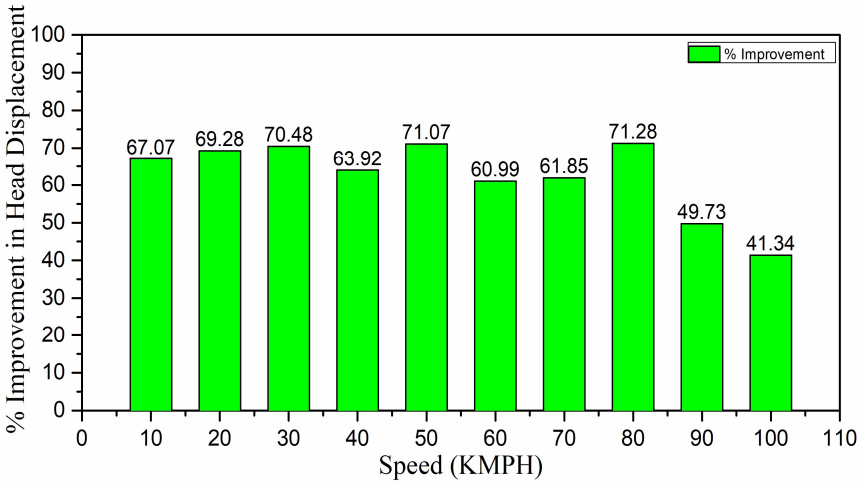


Figure 4.15 % Improvement in Head Displacement for speed 10 to 100 Km/h using Bond Graph PID controller

Body part acceleration and displacement, particularly of the head, is an essential concern for the occupants' health and safety (BS 6841-1987), since it is caused by force conveyed to the human body through seat contact as a reaction to disturbance from the road via the bump.

Figure 4.12 compares the RMS head acceleration (Ride Comfort) response of a passive and active system for a vehicle travelling over a bump at different speeds ranging 10-100 Km/h. The percentage improvement in Ride Comfort is shown in Fig 4.13. The results in Table 4.1 show that active (PID) suspension reduces the driver's vertical acceleration by 76.89% when compared to passive suspension for sinusoidal motion. Further there was reduction of 77.03%, 76.94%, 77.6% and 76.85% in acceleration in other body parts (upper torso, lower torso, pelvis) and seat respectively.

Figure 4.14 compares the RMS head displacement response of a passive and active system for a vehicle travelling over a bump at different speeds ranging 10-100 Km/h. The percentage improvement in RMS head displacement is shown in Fig 4.15. The results in Table 4.2 show that active (PID) suspension achieves reduction in RMS vertical displacement of body parts and seat by 63.90%, 63.86%, 63.99%, 63.66% and 62.17% respectively when compared to passive suspension for sinusoidal motion.

It is clear from the graph that Bond Graph PID model is successfully employed and achieves large improvement in Ride Comfort as well as reduction in head vertical displacement.

4.6 Particle Swarm Optimization (PSO) Based Optimization of a Fractional-Order PID (FOPID) Controller for Quarter Car coupled with 4 DOF human Biodynamic Model

4.6.1 Fractional-Order PID Controller and System Transfer Function

The traditional PID controller comprises three components: proportional, integral, and derivative. Its control law is expressed as follows:

$$U(t) = K_p e(t) + K_I \int e(t)dt + K_D \frac{de(t)}{dt} \tag{4.2}$$

The FOPID controller is an advanced form of the conventional PID controller, which can be integrated and differentiated any number of times in any order. The fraction calculus and other controllers have been discussed in *Appendix (B.1-B.4*) and the implementation of FOPID is shown in Fig 4.16. The time domain differential equation of the FOPID controller is as follows:

$$U(t) = K_p e(t) + \frac{K_I}{S^{\lambda}} e(t) + K_D S^{\mu} e(t) \tag{4.3}$$

where;

e(t) = error signal

K_p = Proportion gain

K_I = Integral gain

K_D = Derivative gain

λ = Fractional integral order

μ = Fractional derivative order

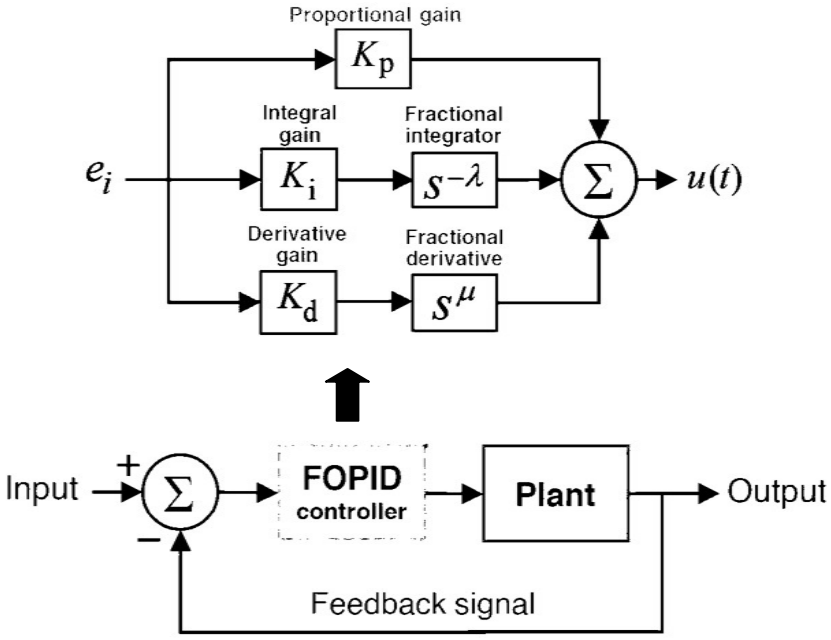


Figure 4.16 FOPID controller implementation

The FOPID controller has two extra tuning parameters (λ, μ} compared to the conventional PID controller, which offer flexibility and better control performance. The dynamic equation (Eq 3.1- Eq. 3.7) are used for derive the transfer function for the purpose of simulation. The state space equations are generated and represented in the form

$$\dot{Y(t)} = [A]y(t) + [B]u(t) \tag{4.3}$$

$$X(t) = [C]y(t) + [D] \tag{4.4}$$

The dimension of matrix depends upon

- No. of state variable (n)
- Number of input (m)
- Number of outputs (p)

where ;

Y = state vector $(n \times 1)$; $\dot{Y}$ = State derivative vector $(n \times 1)$

A = System matrix $(n \times n)$; B = Input matrix $(n \times m)$

U = Input vector $(m \times 1)$; C = Output matrix $(p \times n)$

D = Feed forward matrix $(p \times m)$; X = Output vector $(p \times 1)$

Let,

$Y_1 = x_1;$ $Y_2 = \dot{x_1};$ $Y_3 = x_2;$ $Y_4 = \dot{x_2};$ $Y_5 = x_3;$
$Y_6 = \dot{x_3};$ $Y_7 = x_4;$ $Y_8 = \dot{x_4};$ $Y_9 = x_{se};$ $Y_{10} = \dot{x_{se}};$
$Y_{11} = x_b;$ $Y_{12} = \dot{x_b};$ $Y_{13} = x_w;$ $Y_4 = \dot{x_w};$

which gives,

$\dot{x_1} = Y_2 = \dot{Y_1};$ $\dot{x_2} = Y_4 = \dot{Y_3}$ $\dot{x_3} = Y_6 = \dot{Y_5}$ $\dot{x_4} = Y_8 = \dot{Y_7};$

$\dot{x_{se}} = Y_{10} = \dot{Y_9};$ $\dot{x_b} = Y_{12} = \dot{Y_{11}};$ $\dot{x_w} = Y_{14} = \dot{Y_{13}};$

and

$\ddot{x_1} = \dot{Y_2};$ $\ddot{x_2} = \dot{Y_4};$ $\ddot{x_3} = \dot{Y_6};$ $\ddot{x_4} = \dot{Y_8};$ $\ddot{x_{se}} = \dot{Y_{10}};$ $\ddot{x_b} = \dot{Y_{12}};$ $\ddot{x_w} = \dot{Y_{14}};$

Using above relations in Eq (3.1)-(3.7)

$$\dot{Y_1} = Y_2 \tag{4.5}$$

$$\dot{Y_2} = \frac{1}{m_1}[-k_1 Y_1 - c_1 Y_2 + k_1 Y_3 + c_1 Y_4] \tag{4.6}$$

$$\dot{Y}_3 = Y_4 \tag{4.7}$$

$$\dot{Y}_4 = \frac{1}{m_2}[(k_1)Y_1 + (c_1)Y_2 + (-k_1 - k_2 - k_3)Y_3 + (-c_1 - c_2 - c_3)Y_4 + k_2(Y_5) + (c_2)Y_6 + (k_3)Y_7 + (c_3)Y_8] \tag{4.8}$$

$$\dot{Y}_5 = Y_6 \tag{4.9}$$

$$\dot{Y}_6 = \frac{1}{m_3}[(k_2)Y_3 + (c_2)Y_4 + (-k_2 - k_4)Y_5 + (-c_2 - c_4)Y_6 + (k_4)Y_7 + c_4(Y_8)] \tag{4.10}$$

$$\dot{Y}_7 = Y_8 \tag{4.11}$$

$$\dot{Y}_8 = \frac{1}{m_4}[(k_3)Y_3 + (c_3)Y_4 + (k_4)Y_5 + (c_4)Y_6 + (-k_2 - k_4 - k_5)Y_7 + (-c_3 - c_4 - c_5)Y_8 + (k_5)Y_9 + (c_5)Y_{10}] \tag{4.12}$$

$$\dot{Y}_9 = Y_{10} \tag{4.13}$$

$$\dot{Y}_{10} = \frac{1}{m_{se}}\left[\begin{matrix}(k_5)Y_7 + c_5(Y_8) + (-k_5 - k_{se})Y_9 + (-c_5 - c_{se})Y_{10} + (k_{se})Y_{11} + \\ (C_{se})Y_{12}\end{matrix}\right] \tag{4.14}$$

$$\dot{Y}_{11} = Y_{12} \tag{4.15}$$

$$\dot{Y}_{12} = \frac{1}{m_b}\left[\begin{matrix}(k_{se})Y_9 + (c_{se})Y_{10} + (-k_{se} - k_s)Y_{11} + (-c_{cse} - c_s)Y_{12} + k_5Y_{13} \\ +c_5Y_{14}\end{matrix}\right] \tag{4.16}$$

$$\dot{Y}_{13} = Y_{14} \tag{4.17}$$

$$\dot{Y}_{14} = \frac{1}{m_w}\left[\begin{matrix}(k_s)Y_{11} + (c_s)Y_{12} + (-\dot{k}_s - k_t)Y_{13} + (-c_s - c_t)Y_{14} + c_t\dot{r} \\ +k_t r\end{matrix}\right] \tag{4.18}$$

The state and output equations are represented as Eq 4.5-4.6

$$\begin{bmatrix} \dot{Y}_1 \\ \dot{Y}_2 \\ \dot{Y}_3 \\ \dot{Y}_4 \\ \dot{Y}_5 \\ \dot{Y}_6 \\ \dot{Y}_7 \\ \dot{Y}_8 \\ \dot{Y}_9 \\ \dot{Y}_{10} \\ \dot{Y}_{11} \\ \dot{Y}_{12} \\ \dot{Y}_{13} \\ \dot{Y}_{14} \end{bmatrix} = \begin{bmatrix} a1,1 & \cdots & a1,4 \\ a2,1 & \cdots & \vdots \\ \vdots & \cdots & \vdots \\ \vdots & \cdots & \vdots \\ \vdots & \cdots & \vdots \\ \vdots & \cdots & \vdots \\ \vdots & \cdots & \vdots \\ \vdots & \cdots & \vdots \\ \vdots & \cdots & \vdots \\ \vdots & \cdots & \vdots \\ \vdots & \cdots & \vdots \\ \vdots & \cdots & \vdots \\ \vdots & \cdots & \vdots \\ a14,1 & \cdots & a14,14 \end{bmatrix} \begin{bmatrix} Y_1 \\ Y_2 \\ Y_3 \\ Y_4 \\ Y_5 \\ Y_6 \\ Y_7 \\ Y_8 \\ Y_9 \\ Y_{10} \\ Y_{11} \\ Y_{12} \\ Y_{13} \\ Y_{14} \end{bmatrix} + \begin{bmatrix} 0 \\ 0 \\ 0 \\ 0 \\ 0 \\ 0 \\ 0 \\ 0 \\ 0 \\ 0 \\ 0 \\ 0 \\ 0 \\ \frac{K_t}{m_w} \end{bmatrix} r \qquad (4.19)$$

$$\begin{bmatrix} X_1 \\ X_2 \\ X_3 \\ X_4 \\ X_5 \\ X_6 \\ X_7 \\ X_8 \\ X_9 \\ X_{10} \\ X_{11} \\ X_{12} \\ X_{13} \\ X_{14} \end{bmatrix} = \begin{bmatrix} 1 & 0 & 0 & 0 & 0 & 0 & 0 & 0 & 0 & 0 & 0 & 0 & 0 & 0 \\ 0 & 1 & 0 & 0 & 0 & 0 & 0 & 0 & 0 & 0 & 0 & 0 & 0 & 0 \\ 0 & 0 & 1 & 0 & 0 & 0 & 0 & 0 & 0 & 0 & 0 & 0 & 0 & 0 \\ 0 & 0 & 0 & 1 & 0 & 0 & 0 & 0 & 0 & 0 & 0 & 0 & 0 & 0 \\ 0 & 0 & 0 & 0 & 1 & 0 & 0 & 0 & 0 & 0 & 0 & 0 & 0 & 0 \\ 0 & 0 & 0 & 0 & 0 & 1 & 0 & 0 & 0 & 0 & 0 & 0 & 0 & 0 \\ 0 & 0 & 0 & 0 & 0 & 0 & 1 & 0 & 0 & 0 & 0 & 0 & 0 & 0 \\ 0 & 0 & 0 & 0 & 0 & 0 & 0 & 1 & 0 & 0 & 0 & 0 & 0 & 0 \\ 0 & 0 & 0 & 0 & 0 & 0 & 0 & 0 & 1 & 0 & 0 & 0 & 0 & 0 \\ 0 & 0 & 0 & 0 & 0 & 0 & 0 & 0 & 0 & 1 & 0 & 0 & 0 & 0 \\ 0 & 0 & 0 & 0 & 0 & 0 & 0 & 0 & 0 & 0 & 1 & 0 & 0 & 0 \\ 0 & 0 & 0 & 0 & 0 & 0 & 0 & 0 & 0 & 0 & 0 & 1 & 0 & 0 \\ 0 & 0 & 0 & 0 & 0 & 0 & 0 & 0 & 0 & 0 & 0 & 0 & 1 & 0 \\ 0 & 0 & 0 & 0 & 0 & 0 & 0 & 0 & 0 & 0 & 0 & 0 & 0 & 0 \end{bmatrix} \begin{bmatrix} Y_1 \\ Y_2 \\ Y_3 \\ Y_4 \\ Y_5 \\ Y_6 \\ Y_7 \\ Y_8 \\ Y_9 \\ Y_{10} \\ Y_{11} \\ Y_{12} \\ Y_{13} \\ Y_{14} \end{bmatrix} + \begin{bmatrix} 0 \\ 0 \\ 0 \\ 0 \\ 0 \\ 0 \\ 0 \\ 0 \\ 0 \\ 0 \\ 0 \\ 0 \\ 0 \\ 0 \end{bmatrix}$$

(4.20)

The matrix vector of Eq 4.19 is given in *Appendix B.5*

[A]= [A_1; A_2; A_3; A_4; A_5; A_5; A_7; A_8; A_9; A_{10}; A_{11}; A_{12}; A_{13}; A_{14}];

[B]=[0; 0; 0; 0; 0; 0; 0; 0; 0; 0; 0; 0; 0; kt/mw;];

[C]=[1 0 0 0 0 0 0 0 0 0 0 0 0 0;

0 1 0 0 0 0 0 0 0 0 0 0 0 0;

0 0 1 0 0 0 0 0 0 0 0 0 0 0;

0 0 0 1 0 0 0 0 0 0 0 0 0 0;

0 0 0 0 1 0 0 0 0 0 0 0 0 0;

0 0 0 0 0 1 0 0 0 0 0 0 0 0;

0 0 0 0 0 0 1 0 0 0 0 0 0 0;

0 0 0 0 0 0 0 1 0 0 0 0 0 0;

0 0 0 0 0 0 0 0 1 0 0 0 0 0;

0 0 0 0 0 0 0 0 0 1 0 0 0 0;

0 0 0 0 0 0 0 0 0 0 1 0 0 0;

0 0 0 0 0 0 0 0 0 0 0 1 0 0;

0 0 0 0 0 0 0 0 0 0 0 0 1 0;

0 0 0 0 0 0 0 0 0 0 0 0 0 1;];

[D]=[0];

The variable used in equation are given below

m1=4.17; m2=15; m3=5.5; m4=36; mse=35; mb=250; mw=35; c1=310; c2=200; c3=909.1; c4=330; c5=2475; cse=150; cs=980; ct=0; k1=166990; k2=10000; k3=144000; k4=20000; k5=49340; kse=15000; ks=16000; kt=160000;

The transfer function is further derived from general formula

$$G(s) = C(sI - A)^{-1}B + D \tag{4.5}$$

The generalized transfer function of the coupled quarter-car and biodynamic human system is derived as:

$$TF = \frac{num(s)}{den(s)} \tag{4.6}$$

num(s)= (2.379e10*s^8 + 2.243e13*s^7 + 6.651e15*s^6 + 9.083e17*s^5 + 6.741e19*s^4 + 2.801e21*s^3 + 5.334e22*s^2+ 3.604e23*s - 4.803e09)

den(s)= (s^14 + 476*s^13 + 1.636e05*s^12 + 3.592e07*s^11 + 5.503e09*s^10 + 6.242e11*s^9 + 5.255e13*s^8+ 3.386e15*s^7 + 1.614e17*s^6 + 5.679e18*s^5 + 1.311e20*s^4 + 2.273e21*s^3 + 3.219e22*s^2 + 1.877e23*s + 1.551e24);

The final transfer function used for plant is

$$TF = \frac{\begin{array}{c}(2.379e10*s\text{^}8 + 2.243e1\ *s\text{^}7 + 6.651\ \ *s\text{^}6 + 9.083\ \ *s\text{^}5 + \\ 6.741e1\ *s^4 + 2.801e21*s^3 + \\ 5.334e22*s\text{^}2 + 3.604e\ \ *s - 4.803e09)\end{array}}{\begin{array}{c}(s\text{^}14 + 476*s\text{^}13 + 1.63\ \ \ *s\text{^}12 + 3.592e\ \ *s\text{^}11 + 5.503e\ \ *s\text{^}10 + \\ 6.242e11*s\text{^}9 + 5.255e13*s\text{^}8 + 3.386e\ \ *s\text{^}7 + 1.614e\ \ *s\text{^}6 + \\ 5.67\ \ \ *s\text{^}5 + 1.311\ \ \ *s\text{^}4 + 2.273e21*s\text{^}3 + 3.219e\ \ *s\text{^}2 + 1.877e\ \ *s + 1.551e\ \ );\end{array}} \tag{4.7}$$

Fig 4.18 shows the Simulink model of FOPID implementation with plant model where half sinusoidal bump given as input.

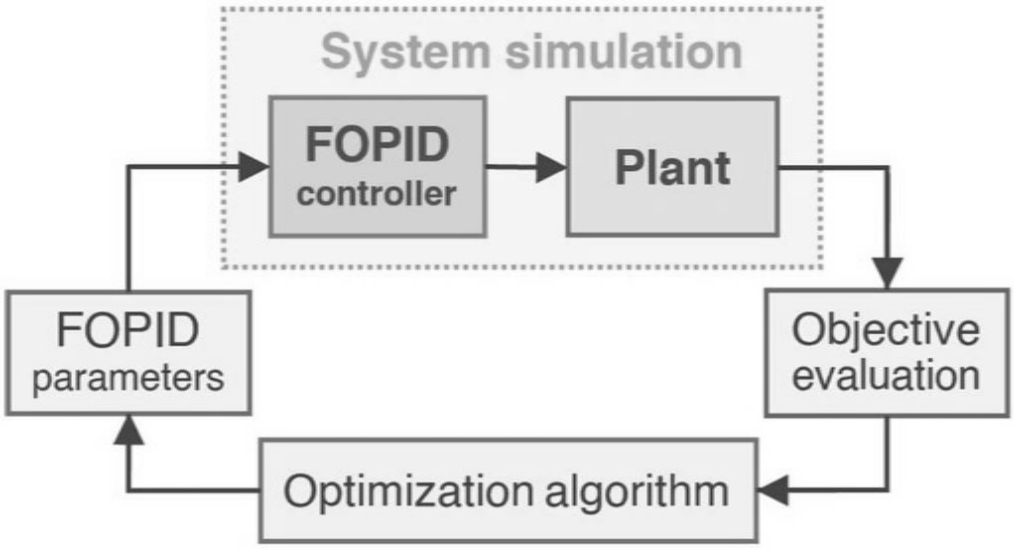


Fig. 4.17 Optimization process

4.6.2 Introduction to PSO

The Particle Swarm Optimization (PSO) is one of the stochastic optimization algorithms that are population based algorithms and is derived from the social behavior of birds flocks and fish schools. It was first introduced by Kennedy and Eberhart in 1995 and has been applied to many engineering problems involving solving nonlinear optimization problems in multiple dimensions and complex problems.

PSO is an algorithm that searches for the best solution by moving a swarm of candidate solutions (particles) through the search space. All particles have a set of controller parameters and continuously adjust their position based on their own experience and the experience of nearby particles. Personal best and global best solutions are used in the movement of particles during the optimization.

The parameters of the Fractional-Order PID (FOPID) controller for the coupled quarter-car and biodynamic human model are optimized using PSO algorithm in the present study. The optimization goal is to reduce vibration transmission and enhance ride comfort, for different road excitations.

4.6.3 Mathematical Formulation of PSO

In Particle Swarm Optimization, each particle represents a potential solution vector:

$[x(i)] = [K_p, K_I, K_D, \lambda, \mu]$

where;
K_p = Proportion gain with range [0-1500]; K_I = Integral gain [0-1500];
K_D = Derivative gain [0-1500]; λ = Fractional integral order [0-1];
μ= Fractional derivative order [0-1]

Each particle has a velocity vector and position vector that are updated iteratively according to the Eq (4.8)-(4.9).

Velocity Update Equation

$$v_i^{k+1} = wv_i^k + c_1 r_1 \left(p_{best,i} - x_i^k\right) + c_2 r_2 \left(g_{best,i} - x_i^k\right) \quad (4.8)$$

Position Update Equation

$$x_i^{k+1} = x_i^k + v_i^{k+1} \quad (4.9)$$

where;

v_i^k : velocity of ith particle in kth iteration

x_i^k : Position of ith particle in kth iteration

$p_{best,i}$: Personal best position

$g_{best,i}$: Global best position

r_1, r_2 : Random numbers in [0,1]

w : Inertia weight

c_1, c_2 : Acceleration coefficient [0,2]

The inertia weight determines the exploration capability of the particles, and the acceleration coefficients direct the particles to better solutions. The optimization process is repeated until the termination criterion is reached (e.g., the number of iterations reaches a maximum of 10 or the error becomes below a certain threshold).

4.6.4 Steps Involved in PSO Optimization

The Particle Swarm Optimization (PSO) technique is used to optimize the parameters of the Fractional-Order PID (FOPID) controller in a systematic manner as depicted in Fig 4.19. The coupled quarter-car and biodynamic human model was first created to describe the dynamic relationship between the vehicle suspension system and human body. After that, the configuration of the FOPID controller is designed and investigated using five controller parameters, including proportional gain (K_p), integral gain (K_I), derivative gain (K_D), fractional integral order (λ) and fractional derivative order (μ). The

PSO algorithm was then initialized with random particle position and the optimization parameters (particle size, inertia weight and acceleration coefficients).

The suspension model was simulated by applying the controller parameters generated by the particles and the system response under road excitation was obtained. Objective functions like Integral Time Square Error (ITSE) and RMS acceleration were used to assess the performance of each particle, directly related to ride comfort and vibration suppression.

The fitness value of the solutions was calculated in each iteration and then the personal best (P_{best}) and global best (G_{best}) solutions were updated. Then, the velocity and position of the particles were adjusted by using the PSO update equations so that the search direction would be towards the optimal solution. The process was repeated until the convergence criterion was met (either the minimum error value or the maximum number of iterations). Finally, optimal FOPID controller parameters were derived and applied to further enhance the vibration isolation and ride comfort properties of the coupled vehicle–human suspension system.

4.6.5 Objective Function

In the present study, Integral Time Square Error (ITSE) is selected as the objective function for optimization.

$$ITSE = \int_0^T t.e(t)^2 \tag{4.10}$$

where:

- t = Time
- $e(t)$ = Error signal
- T = Total simulation or observation time
- $e(t)^2$ = Squared error (prevent negative and positive error to cancel each other)

The objective of optimization is to minimize ITSE, thereby reducing vibration transmission and improving ride comfort performance.

Table 4.3 Employed parameter in PSO algorithm

Parameter	Value
C_1 coefficient	1.5
C_2 coefficient	2
Inertia coefficient (w)	1
Population size	40
Lower bound	-5
Upper bound	+5
Number of iteration	50

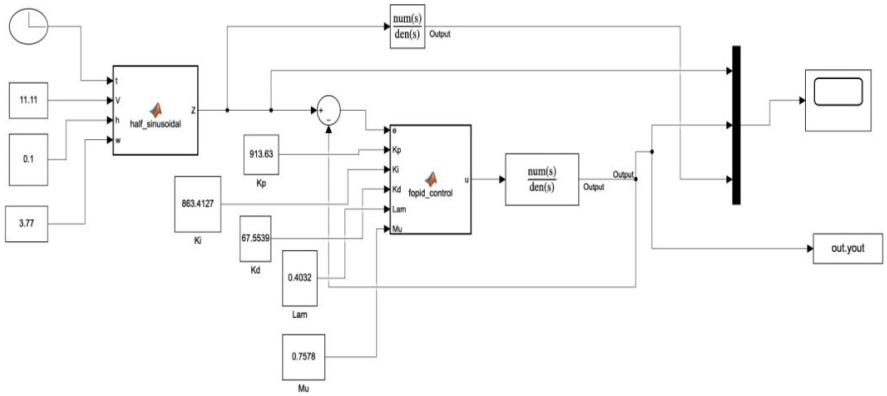


Fig. 4.18 FOPID controller Simulink model

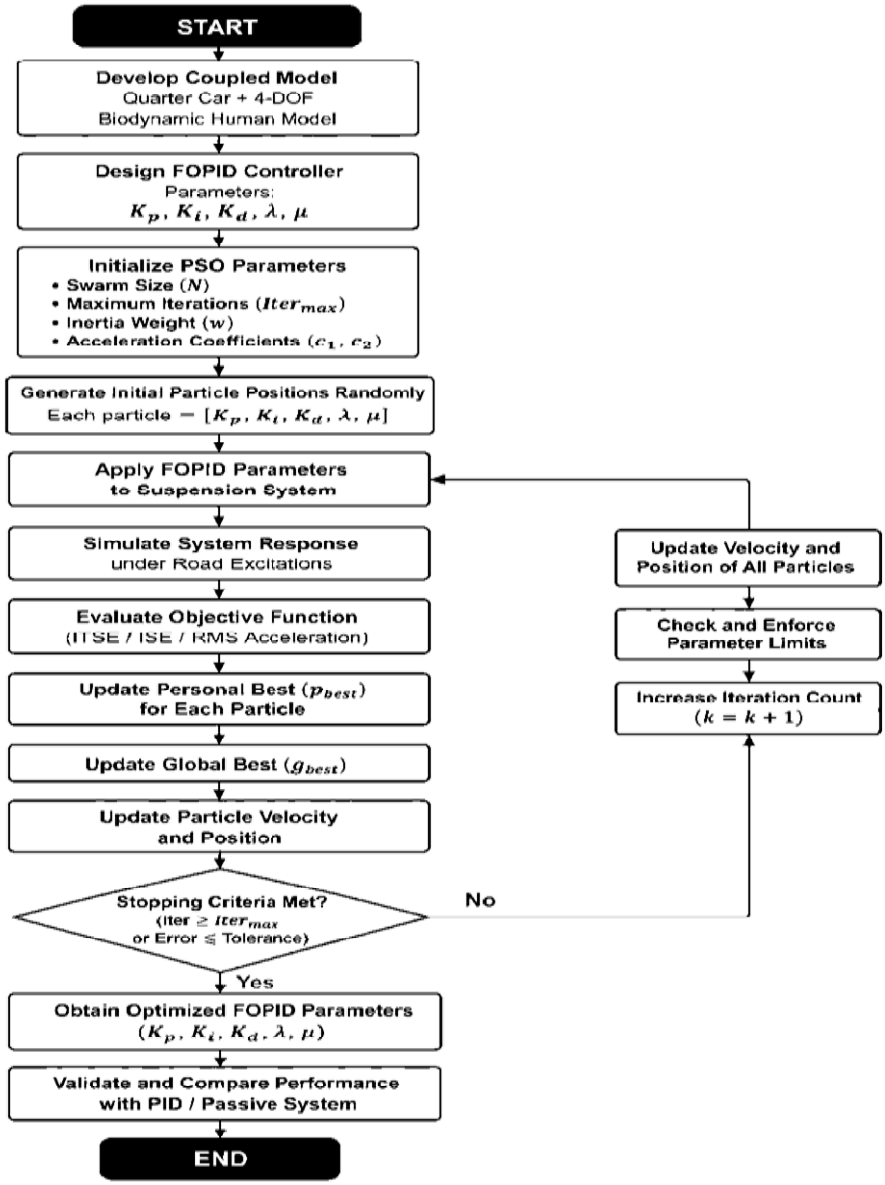


Fig. 4.19 PSO algorithm flow chart

4.6.6 Results and Discussion

Optimization of the FOPID controller parameters of the coupled suspension system using the PSO algorithm was successfully performed. The optimization procedure was

able to obtain stable convergence properties, with the value of the objective function gradually decreasing at each iteration.

At first, the value of the errors were large because the particles were randomly initialized. Fig 4.20 shoes the particles gradually moved towards the best answer as the iterations went on and on the ITSE values were significantly reduced as The first few iterations exhibited fast convergence rates due to the large number of search space explorations all over the globe, and the later, exhibited gradual convergence towards the optimal solution.

The final optimized controller parameters obtained using PSO are summarized in Table 4.4 The results demonstrate that the PSO method for tuning the FOPID controller has better performance in suppressing vibration and improving ride comfort performance for the coupled vehicle–human suspension system.

The optimized FOPID controller showed enhanced ride comfort compared to a conventional PID controller and passive suspension system as represented in Fig 4.21. Also, the controller enhanced the system stability and vibration isolation performance in the frequency range most susceptible to the human body.

Table 4.4 Optimized parameter using PSO algorithm

Parameter	Optimized Value
K_p (Proportion gain)	913.63
K_I (Integral gain)	863.41
K_D (Derivative gain)	67.55
λ (Fractional integral order)	0.4032
μ (Fractional derivative order)	0.7578

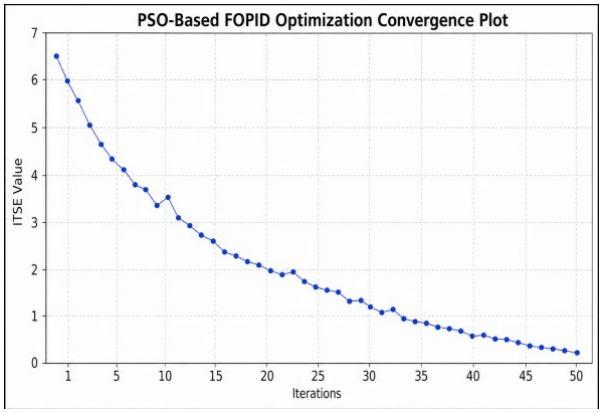


Figure 4.20: Convergence plot showing reduction in ITSE during PSO-based optimization of FOPID controller parameters.

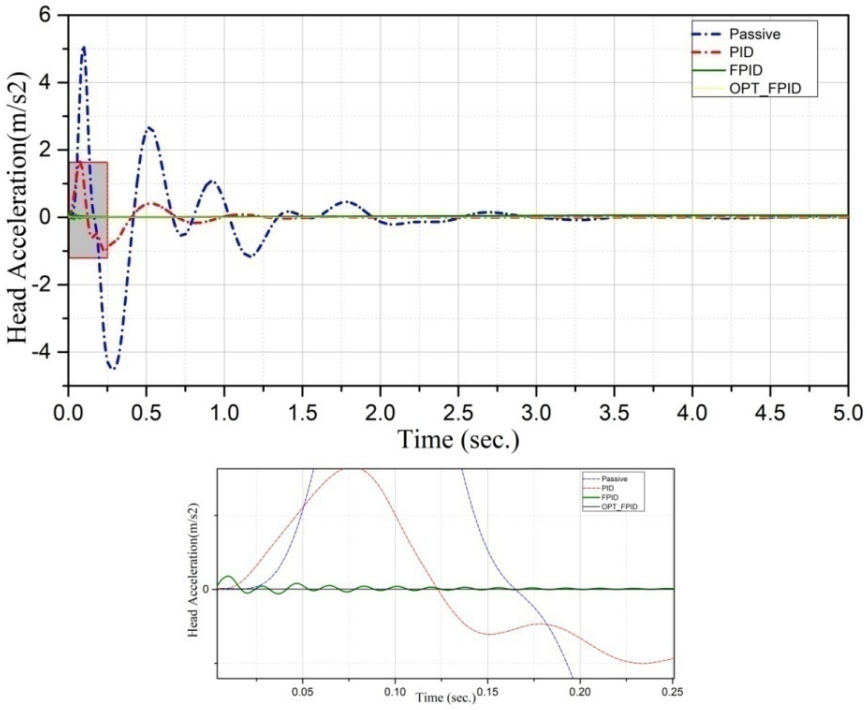


Fig. 4.21 Head Acceleration response using PSO optimized FOPID controller Parameter

This figure shows the comparative head acceleration response of passive, PID, FPID and optimized FPID controlled suspension system to the road excitation. Passive suspension system exhibits the highest oscillatory response, the maximum acceleration of the system is nearly ±5 m/s², and the settling time is longer, which means that it has poor vibration isolation and reduced ride comfort. The amplitude of acceleration is greatly reduced, and the vibrations are suppressed better than they are in the passive system, but very noticeable oscillations can be seen during the transient response of the PID controller.

The FOPID controller also exhibits the better damping effect due to the introduction of the fractional order control action, which results in smoother and faster damping effect. The FOPID controller is the optimized configuration of all suspension configurations with minimum peak acceleration, negligible oscillations and shortest settling time. It quickly approaches zero, thus showing good vibration suppression performance and stability of the system. The enlarged inset figure shows the transient response during the first time interval, in which the optimized FOPID controller keeps head acceleration very close to zero when compared with the passive, PID and conventional FOPID controllers. Thus, the optimized FOPID controller offers better ride comfort and increased vibration isolation performance of the proposed suspension system.

4.7 Conclusion

The bond graph approach was used in this study to explain the dynamic behavior of a 7 DOF passive vehicle suspension system based on a quarter automobile model linked with a lumped human biomechanical model in the temporal domain when subjected to sinusoidal input. Further effect of bump was reduced using novel Bond Graph modeled PID controller which shows satisfactory results. RMS responses (ride comfort and head displacement) compared for both passive and active vehicle system for velocities ranging from 10 to 100 Km/h. After analysing the results, it was discovered that employing a PID controller with a bond graph successfully improving ride comfort and also reduced vibration communicated to human body parts.

The optimized FPID controller had minimum head acceleration, negligible oscillations and had good settling time among all the tested configurations. The optimized controller successfully reduced vibration amplitude during the transient phase and kept the vibration amplitude stable throughout the response duration. The results show that the parameters of FPID can be optimized to achieve better results in the suspension performance and ride comfort of the passengers. Thus, the optimized FPID controlled suspension system can be regarded as an efficient and reliable solution in advanced vehicle suspension applications for improved vibration isolation and better comfort for occupants.

CHAPTER 5

FULL-CAR MODEL ANALYSIS UNDER TRANSIENT BUMP USING BOND GRAPH

In this chapter, an integrated computer model is developed through the bond graph methodology to analyse the dynamic behaviour of a large road vehicle. The initial stage is to create the 3D models of each vehicle base, suspension unit, tyre, seat, and joint as bond graph elements with power ports for physical connections. This work demonstrates the dynamic behaviour of the 4 DOF lumped human biomechanical model coupled with an 11 DOF full-car vehicle model using the bond graph simulation technique. Ride comfort conditions as per ISO 2631:1997 standards are used to validate the dynamic response of the bio-dynamic human coupled with a full car. Various other dynamic responses in the time domain have been captured in simulation for the conditions where the vehicle passes over different bumps of the same height and width of 1 m, 2 m and 3.7 m with a 40 km/h speed. Additionally, RMS responses have been studied for

different vehicle velocities. The results presented in the chapter show the fascinating behaviour of full-car vehicles.

5.1 Introduction

Road irregularities are a significant source of discomfort for the driver as well as the passengers. Therefore, road safety is one of the prime objectives nowadays and various organisations are working to decrease road fatalities and accidents. The design of a vehicle is also an important criterion for reducing the vibration that occurs during movement on road irregularities. The function of suspension system in vehicles is to act as a mechanical filter that isolates the passengers by absorbing vibrations caused by road bumps and irregularities, thus providing better ride comfort. When a tyre hits a bump, the sudden vibration transmitted to the vehicle not only cause long term damages to the vehicle suspension, but also might affect human health in many ways, such as causing back pain, slipping of the disc, and spinal injury depending upon the strength of the shock.

An enormous amount of research has been conducted for ride comfort analysis, and various human models coupled with quarter and half car models have been developed to examine the complex characteristics of human motion from single to multi-degrees of freedom. *Mohite et al. (2018)* used a 2-DOF quarter car linear and non linear model and found that the RMS acceleration of a non-linear suspension system is greater than that of the linear system. *Mitra et al.(2013)* developed a 4 DOF quarter-car model to investigate

ride comfort and vehicle handling. *Server et al. (2017)* designed an 'L2 gain state derivative feedback controller' and analysed the ride comfort of a 5 DOF quarter car model with a seated human model. *Zhilin et al. (2022)* suggested an anti-roll control method to stop rollover-related deadly road accidents for sport utility vehicles through proper driving action. *Mitra et al. (2018)* developed the ADAMS model of a quarter car for simulation. *Jasiūnienė et al. (2018)* explored the effects of trapezoidal speed bumps, a type of traffic-calming device, on the drivers and passengers in cars. *Farid et al. (2011)* carried out an optimisation using the GA algorithm to achieve a better ride comfort and determined optimised vehicle suspension parameters while three human biomechanical models (two 4 DOF and one 7 DOF) coupled with the quarter car in a sitting posture without a backrest were presented by *Abbas et al. (2010)* to study dynamic response in the vertical vibration direction. *Desai et al. (2018)* optimised the model parameters of a 20 DOF human model using the genetic algorithm for a seated human considering vertical or fore-and-aft vibrations. *Bae et al. (2018)* introduced the biodynamic reactions on a sitting human model with five degrees of freedom and recorded jump phenomena. Based on data reported by other authors, *Rakheja et al. (2010)* reviewed various bio-dynamic responses of standing and seated human body when exposed to whole body vibration.

Talukdar et al. (2012) used various models like the quarter-car, half-car (2 DOF), and half-car (4 DOF) model for a ride comfort analysis by incorporating a flexible tyre model. *Singh et al. (2015)* considered human body segments as an ellipsoidal shape in free undamped conditions and studied a lumped parameter model without backrest

support. *Ahmed et al. (2013)* proposed a preview controller in a half car model for semi-active suspension. *Xiaoming et al. (2023)* developed a yaw dynamic model taking into account road curvature, to guarantee handling stability and driving safety; a stability control technique based on a 'linear time-varying model predictive control' (LTV-MPC) is suggested for high-speed autonomous vehicles. *Tuakhia et al. (2016)* developed a 4 DOF half car mathematical model and simulated it utilising MATLAB/SIMULINK. *Abbas et al. (2011)* designed a passive seat suspension system using a 4 DOF human biodynamic model coupled with the half car model. *Rakheja et al. (2012)* indicated that the dynamic responses relating to drivers, concerning the health and safety of the occupants, are significantly influenced by the forward speed, vehicle load, tyre inflation pressure, and road roughness. *Mahala et al. (2004)* studied a full-car 7 DOF model for pitching and rolling motion using MATLAB/SIMULINK and obtained various response parameters. *Jin et al. (2016)* developed an 11 DOF full-car mathematical model and analysed poor ride comfort due to increased un-sprung mass. *Qinghua et al. (2023)* suggested a unique extended high-gain observer (EHGO) based nonlinear vehicle active suspension control method to improve ride comfort and handling stability. Ikenaga et al. (2000) demonstrated the performance of active suspension control in a full-car vehicle model without seats. *Bouazara et al. (2001)* improved the ride comfort and road holding in a 3D vehicle through optimisation.

Jiangyiet al. (2023) revealed that the vehicle's rollover index is greatly influenced by the speed and height of the barrier. *Jamali et al. (2018)* assessed the biodynamic responses of a 6 DOF biomechanical model in sitting posture without a backrest

support coupled with quarter-car vehicle model using polyline and roughness profiles. *Shirahatt et al. (2008)* applied an optimisation technique to optimise the passive and active suspension parameters of passenger car, satisfying the performance as per ISO 2631 standards *(Standard, 1997)*.

Models reviewed in the literature are relatively simple in comparison with full-car models. However, there remains ample scope to study the effects of various road profile bumps on the human body, so a full car model with a seated human biomechanical model and an attached passenger seat would be more realistic. The effects of roll and pitch motion can be included for a dynamic simulation of such complex models, and other computer-based modelling techniques may be considered.

In this chapter, a full-car model is built using bond graph modelling. This modelling technique is used by various researchers, as it facilitates the integration of various energy domain models into a single energy domain, which makes it more efficient and convenient in dynamic simulation *(Borutzky, 2009)*. *Margolis et al. (2001)* studied a nonlinear vehicle dynamics model by developing a full-car model with controllers and electric brakes for vehicle safety using bond graph modelling. Silva et al. (2008) developed an electric (hybrid) vehicle through multi-bond graph modelling. *Filippini et al. (2014)* studied the nonlinear effect of a 3D vehicle by including transmission and engine modelling using a bond graph. *Adibi-asl et al. (2009)* developed a full-car bond graph model with an active suspension for simulation, whereas *Banerjee et al. (2009)* developed an integrated bond graph model of a railway truck to capture the dynamic

responses and found its dynamical behaviour differs dramatically from that documented in the literature.

5.2 Modeling of 4 DOF lumped human biomechanical model coupled with an 11 DOF full-car vehicle

5.2.1 Physical Model

The integrated full car model is connected to a 4 DOF biodynamic driver body model, as shown in Fig 5.1. Considering a local coordinate reference frame (x, y, z), the vehicle chassis is represented and coupled to the centre of mass and positioned with the primary inertia axes. It has mass 'm' and the major inertia moments: roll (I_r) about y-axis and pitch (I_p) about x-axis. Considering the human body as a combination of several lumped masses connected through springs, m_h, m_{ut}, m_{lt}, and m_p are the lumped masses of 'head', 'upper torso', 'lower torso' and 'pelvis', respectively, which receive the direct excitation from the seat. C_{ij} and K_{ij} are damping and stiffness between the two body sections (the subscripts i and j signify the first alphabet of the connected body parts).

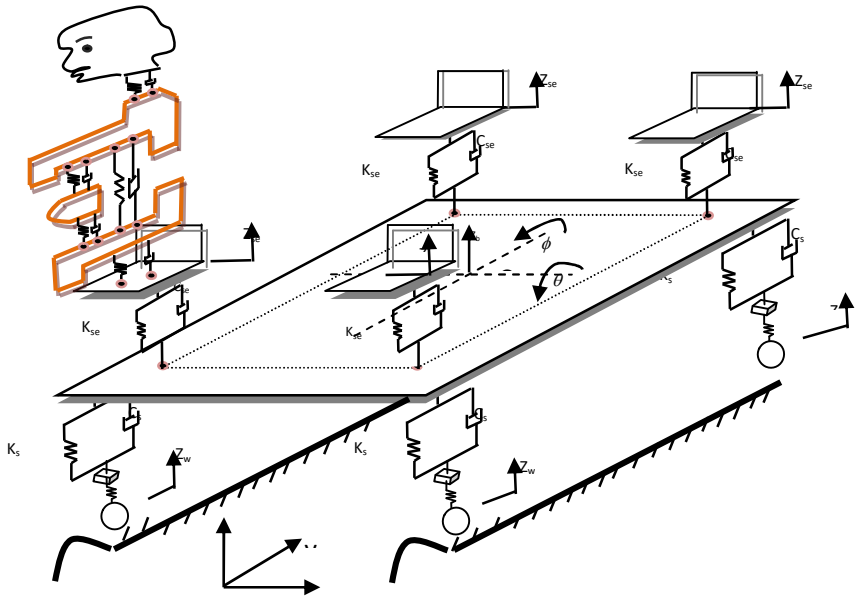


Figure 5.1: Schematic diagram of 4 DOF biodynamic lumped human model coupled with full car 11 DOF model

K_{se} and C_{se} represent the stiffness and damping coefficients of seat suspension; Z_{se} is the excitation from the seat; Z_h, Z_{ut}, $Z_{lt,}$ and Z_p indicate various mass displacements on 'head', 'upper torso', 'lower torso' and 'pelvis', respectively. *Z* represents the road input in the form of a sinusoidal profile bump. *Cs* and *Ks* represents the damping and stiffness coefficients of the car suspension. K_t represents the compressibility of the pneumatic tyre. The front and rear suspensions are positioned at a distance of 'L_f' and 'L_r', while the seats are located at distances 'a' and 'b' from the car body's C.G along the roll axis (y-axis), respectively. On the other hand, the distances of the right and left suspensions are represented as 'T_r' and 'T_l', while for the seats, the distances are given as 'c' and 'd' along the pitch axis (x-axis), respectively.

Fig 5.1 illustrates a full-car (11 DOF) model with four passenger seats. The sprung mass alludes to the car body that is supported by springs, whereas the un-sprung mass corresponds to wheel assembly. The tire is modeled considering stiffness with negligible damping. Tires, passenger seats, and suspension are modeled using springs that are positioned parallel to the dampers. In the model, the sprung mass is assumed having motion with 3 DOF ('bounce', 'pitch', and 'roll'), while the four seats and four un-sprung masses are modeled with 1 DOF each.

5.2.2 Mathematical Model

A full car model (11 DOF) is considered for analysis. Fig 5.1 illustrates a full car (11 DOF) model consisting of four passenger seats, a sprung mass, and un-sprung mass. The tyre, with its neglected damping, is replaced by its equivalent stiffness. Linear springs arranged parallel with dampers are used to model the suspension, tyres, and passenger seats.

Z_{bfr}, Z_{bfl}, Z_{brr}, and Z_{brl} symbolize vertical displacements of the vehicle body and suspension at 'front-right', 'front-left', 'rear-right', and 'rear-left' connection points. Similarly, Z_{sefr}, Z_{sefl}, Z_{serr}, and Z_{serl} indicate the vertical displacements of the seat and car body at the 'front-right', 'front-left', 'rear-right', and 'rear-left' connection points.

Using Newton's second law of motion, the dynamic motion equations are obtained for the full car suspension, seats, and driver's body.

Human Model Equation

$$m_h\ddot{Z}_h = -C_{hu}(\dot{Z}_h - \dot{Z}_{ut}) - K_{hu}(Z_h - Z_{ut}) \tag{5.1}$$

$$m_{ut}\ddot{Z}_{ut} = C_{hu}(\dot{Z}_h - \dot{Z}_{ut}) + K_{hu}(Z_h - Z_{ut}) - C_{ul}(\dot{Z}_{ut} - \dot{Z}_{lt}) - K_{ul}(Z_{ut} - Z_{lt}) - C_{up}(\dot{Z}_{ut} - \dot{Z}_p) - K_{up}(Z_{ut} - Z_p) \tag{5.2}$$

$$m_{lt}\ddot{Z}_{lt} = C_{ul}(\dot{Z}_{ut} - \dot{Z}_{lt}) + K_{ul}(Z_{ut} - Z_{lt}) - C_{lp}(\dot{Z}_{lt} - \dot{Z}_p) - K_{lp}(Z_{lt} - Z_p) \tag{5.3}$$

$$m_p\ddot{Z}_p = C_{lp}(\dot{Z}_{lt} - \dot{Z}_p) + K_{lp}(Z_{lt} - Z_p) + C_{up}(\dot{Z}_{ut} - \dot{Z}_p) + K_{up}(Z_{ut} - Z_p) - C_{pse}(\dot{Z}_p - \dot{Z}_{sefr}) + K_{pse}(Z_p - Z_{sefr}) \tag{5.4}$$

Four Seat Equations

$$m_{sefr}\ddot{Z}_{sefr} = +C_{pse}(\dot{Z}_p - \dot{Z}_{sefr}) + K_{pse}(Z_p - Z_{sefr}) - C_{sefr}(\dot{Z}_{sefr} - \dot{x}_{sefr}) - K_{sefr}(Z_{sefr} - x_{sefr}) \tag{5.5}$$

$$m_{sefl}\ddot{Z}_{sefl} = -C_{sefl}(\dot{Z}_{sefl} - \dot{x}_{sefl}) - K_{sefl}(Z_{sefl} - x_{sefl}) \tag{5.6}$$

$$m_{serr}\ddot{Z}_{serr} = -C_{serr}(\dot{Z}_{serr} - \dot{x}_{serr}) - K_{serr}(Z_{serr} - x_{serr}) \tag{5.7}$$

$$m_{serl}\ddot{Z}_{serl} = -C_{serl}(\dot{Z}_{serl} - \dot{x}_{serl}) - K_{serl}(Z_{serl} - x_{serl}) \tag{5.8}$$

Four Wheel Equations

$$m_{wfr}\ddot{Z}_{wfr} = C_{sfr}(\dot{Z}_{bfr} - \dot{Z}_{wfr}) + K_{sfr}(Z_{bfr} - Z_{wfr}) - K_{wfr}(Z_{wfr} - Z) \tag{5.9}$$

$$m_{wfl}\ddot{Z}_{wfl} = C_{sfl}(\dot{Z}_{bfl} - \dot{Z}_{wfl}) + K_{sfl}(Z_{bfl} - Z_{wfl}) - K_{wfl}(Z_{wfl} - Z) \tag{5.10}$$

$$m_{wrr}\ddot{Z}_{wrr} = C_{srr}(\dot{Z}_{brr} - \dot{Z}_{wrr}) + K_{srr}(Z_{rrb} - Z_{wrr}) - K_{wrr}(Z_{wrr} - Z) \tag{5.11}$$

$$m_{wrl}\ddot{Z}_{wrl} = C_{srl}(\dot{Z}_{brl} - \dot{Z}_{wrl}) + K_{srl}(Z_{brl} - Z_{wrl}) - K_{wrl}(Z_{wrl} - Z) \tag{5.12}$$

Vertical Motion of Car Body

$$\begin{aligned} m_b\ddot{Z}_b = & -C_{sfr}(\dot{Z}_{bfr}-\dot{Z}_{wfr})-K_{sfr}(Z_{bfr}-Z_{wfr})-C_{sfl}(\dot{Z}_{bfl}-\dot{Z}_{wfl}) \\ & -K_{sfl}(Z_{bfl}-Z_{wfl})-C_{srr}(\dot{Z}_{brr}-\dot{Z}_{wrr})-K_{srr}(Z_{brr}-Z_{wrr}) \\ & -C_{srl}(\dot{Z}_{brl}-\dot{Z}_{wrl})-K_{srl}(Z_{brl}-Z_{wrl})+C_{sefr}(\dot{Z}_{sefr}-\dot{x}_{sefr}) \\ & +K_{sefr}(Z_{sefr}-x_{sefr})+C_{sefl}(\dot{Z}_{sefl}-\dot{x}_{sefl})+K_{sefl}(Z_{sefl}-x_{sefl}) \\ & +C_{serr}(\dot{Z}_{serr}-\dot{x}_{serr})+K_{serr}(Z_{serr}-x_{serr})+C_{serl}(\dot{Z}_{serl}-\dot{x}_{serl}) \\ & +K_{serl}(Z_{serl}-x_{serl}) \end{aligned} \tag{5.13}$$

Pitch Motion of Car Body

$$\begin{aligned} I_p\times\ddot{\theta} = & L_f\times\left[C_{sfr}(\dot{Z}_{bfr}-\dot{Z}_{wfr})+K_{sfr}(Z_{bfr}-Z_{wfr})\right] \\ & +L_f\times\left[C_{sfl}(\dot{Z}_{bfl}-\dot{Z}_{wfl})+K_{sfl}(Z_{bfl}-Z_{wfl})\right] \\ & -L_r\times\left[C_{srr}(\dot{Z}_{brr}-\dot{Z}_{wrr})+K_{srr}(Z_{brr}-Z_{wrr})\right] \\ & -L_r\times\left[C_{srl}(\dot{Z}_{brl}-\dot{Z}_{wrl})+K_{srl}(Z_{brl}-Z_{wrl})\right] \\ & -a\times\left[C_{sefr}(\dot{Z}_{sefr}-\dot{x}_{sefr})+K_{sefr}(Z_{sefr}-x_{sefr})\right] \\ & -a\times\left[C_{sefl}(\dot{Z}_{sefl}-\dot{x}_{sefl})+K_{sefl}(Z_{sefl}-x_{sefl})\right] \\ & +b\times\left[C_{serr}(\dot{Z}_{serr}-\dot{x}_{serr})+K_{serr}(Z_{serr}-x_{serr})\right] \\ & +b\times\left[C_{serl}(\dot{Z}_{serl}-\dot{x}_{serl})+K_{serl}(Z_{serl}-x_{serl})\right] \end{aligned} \tag{5.14}$$

Roll Motion of Car Body

$$\begin{aligned} I_r\times\ddot{\varphi} = & T_r\times\left[C_{sfr}(\dot{Z}_{bfr}-\dot{Z}_{wfr})+K_{sfr}(Z_{bfr}-Z_{wfr})\right] \\ & -T_l\times\left[C_{sfl}(\dot{Z}_{bfl}-\dot{Z}_{wfl})+K_{sfl}(Z_{bfl}-Z_{wfl})\right] \\ & +T_r\times\left[C_{srr}(\dot{Z}_{brr}-\dot{Z}_{wrr})+K_{srr}(Z_{brr}-Z_{wrr})\right] \\ & -T_l\times\left[C_{srl}(\dot{Z}_{brl}-\dot{Z}_{wrl})+K_{srl}(Z_{brl}-Z_{wrl})\right] \\ & -c\times\left[C_{sefr}(\dot{Z}_{sefr}-\dot{x}_{sefr})+K_{sefr}(Z_{sefr}-x_{sefr})\right] \\ & +d\times\left[C_{sefl}(\dot{Z}_{sefl}-\dot{x}_{sefl})+K_{sefl}(Z_{sefl}-x_{sefl})\right] \\ & -c\times\left[C_{serr}(\dot{Z}_{serr}-\dot{x}_{serr})+K_{serr}(Z_{serr}-x_{serr})\right] \\ & +d\times\left[C_{serl}(\dot{Z}_{serl}-\dot{x}_{serl})+K_{serl}(Z_{serl}-x_{serl})\right] \end{aligned} \tag{5.15}$$

Displacement at car frame and suspension interface

$$Z_{bfr} = Z_b - L_f\times\theta - T_r\times\varphi \tag{5.16}$$

$$Z_{bfl} = Z_b - L_f\times\theta + T_l\times\varphi \tag{5.17}$$

$$Z_{brr} = Z_b + L_r \times \theta - T_r \times \varphi \tag{5.18}$$

$$Z_{brl} = Z_b + L_r \times \theta + T_l \times \varphi \tag{5.19}$$

Displacement at car frame and seat interface

$$x_{sefr} = Z_b - a \times \theta - c \times \varphi \tag{5.20}$$

$$x_{sefl} = Z_b - a \times \theta + d \times \varphi \tag{5.21}$$

$$x_{serr} = Z_b + b \times \theta - c \times \varphi \tag{5.22}$$

$$x_{serl} = Z_b + b \times \theta + d \times \varphi \tag{5.23}$$

Velocity at car frame and suspension interface

$$\boldsymbol{V_{bfr}} = \dot{\boldsymbol{Z}}_{\boldsymbol{bfr}} = \dot{\boldsymbol{Z}}_{\boldsymbol{b}} - \boldsymbol{L}_{\boldsymbol{f}} \times \boldsymbol{\omega}_{\boldsymbol{p}} - \boldsymbol{T}_{\boldsymbol{r}} \times \boldsymbol{\omega}_{\boldsymbol{r}} \tag{5.24}$$

$$\boldsymbol{V_{bfl}} = \dot{\boldsymbol{Z}}_{\boldsymbol{bfl}} = \dot{\boldsymbol{Z}}_{\boldsymbol{b}} - \boldsymbol{L}_{\boldsymbol{f}} \times \boldsymbol{\omega}_{\boldsymbol{p}} + \boldsymbol{T}_{\boldsymbol{l}} \times \boldsymbol{\omega}_{\boldsymbol{r}} \tag{5.25}$$

$$V_{brr} = \dot{Z}_{brr} = \dot{Z}_b + L_r \times \omega_p - T_r \times \omega_r \tag{5.26}$$

$$V_{brl} = \dot{Z}_{brl} = \dot{Z}_b + L_r \times \omega_p + T_l \times \omega_r \tag{5.27}$$

Velocity at at car frame and seat interface

$$v_{sefr} = \dot{x}_{sefr} = \dot{Z}_b - a \times \omega_p - c \times \omega_r \tag{5.28}$$

$$v_{sefl} = \dot{x}_{sefl} = \dot{Z}_b - a \times \omega_p + d \times \omega_r \tag{5.29}$$

$$v_{serr} = \dot{x}_{serr} = \dot{Z}_b + b \times \omega_p - c \times \omega_r \tag{5.30}$$

$$v_{serl} = \dot{x}_{serl} = \dot{Z}_b + b \times \omega_p + d \times \omega_r \tag{5.31}$$

5.2.3 Bond graph modeling

The car model has three interfaces. The first interface is defined between the car body and four wheels motion; the second interface is between the car body and four seats motion; and the third interface is between the seat and driver model. Fig 5.5 illustrates a 15 DOF full-car Bond Graph model comprising an integrated 11 DOF full-car system coupled with a 4 DOF biodynamic human model. For modeling and simulation, the software SYMBOLS 2000 (Samantaray, 2015) used in this work facilitates the creation of complete Bond Graph models.

The Bond Graph utilizes two junction elements: *1*-(common flow) and *0*-(common effort); three basic elements: *I*-(inertial), *C*-(compliant), and *R*-(resistive); two source elements: efforts *SE* (effort source) and *SF* (flow source); and two 2-port elements: *TF* (transformer) and *GY* (gyrator). All these elements are connected through lines called bonds, where energy exchange between elements in the Bond Graph occurs via these bonds in the form of power, i.e., effort and flow.

Starting with the human Bond Graph model, as illustrated in Fig 5.2, four I-elements are utilized at each 1-junction to represent the mass of different human body parts. A flow-activated (C-element) is attached to each 1-junction to capture the displacement and velocity of the human body parts. Stiffness and damping between each body part are introduced by attaching C and R elements between the 1-junctions. The acceleration of

various body parts is captured by the I-elements. The Bond Graph model of the human body parts is further integrated with the seat Bond Graph model.

The 1-junction with subscripts θ, G, and φ represents the pitch, bounce, and roll velocities of the vehicle. I-elements are utilised at the 1-junction for the car body mass m_b, and for the moment of inertia I_p and I_r at 1_G, 1_θ, and 1_φ junctions, respectively. Transformers (TF) with respective moduli, as obtained from Eqs. (5.24)-(5.27) are then utilised to convert the pitch and roll velocities into linear velocity components. All linear velocities are subsequently summed at the 0-junctions, which serve as the interface junctions between the car body and the wheels. A flow-activated C-element at 1_G records the vertical motion at the C.G. of the car body, while a flow-activated C-element at 1_θ and 1_φ records the pitch and roll motions of the vehicle, respectively.

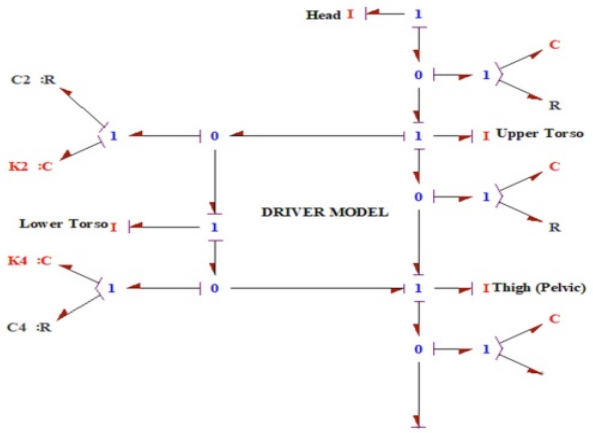


Figure 5.2: Bond Graph model of 4DOF bio-dynamics human

Furthermore, the interface between the car body (sprung-mass) and the wheels (un-sprung masses) is established by connecting the BG models of car and wheels at 0-

junctions, with the introduction of C and R elements representing stiffness (K_s) and damping (C_s) of the wheel suspension. Tyre stiffness (K_t) is incorporated using a C-element, while the damping of the tyre neglected. However, it is represented in the wheel Bond Graph (BG) graph model illustrated in Fig 5.4.

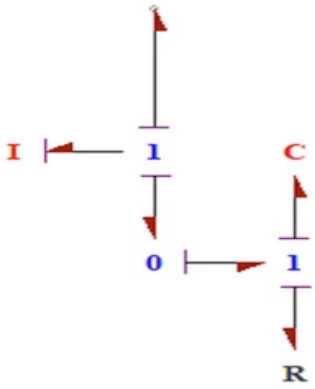


Figure 5.3 Seat BG model

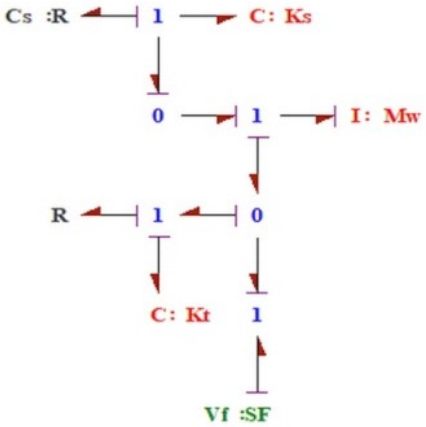


Figure 5.4 Wheel BG model

The four seats are coupled with the three motions of the car body using appropriate transformers with their respective moduli, as obtained from Eqs. (5.28)-(5.31). An interface between the car body and the seats is formed using C and R elements, which represent the stiffness and damping coefficients of the seat suspension system. Fig 5.3 illustrates a Bond Graph (BG) model of a seat. Each activated C-element on the four seats records the seat displacement. Finally, the BG model of the human is connected to the seat through C and R elements, representing the stiffness and damping parameters of the pelvis (thigh). Fig 5.5 presents the complete bond graph of the Bio-Dynamic Human Model coupled with the Full Car Model for simulation.

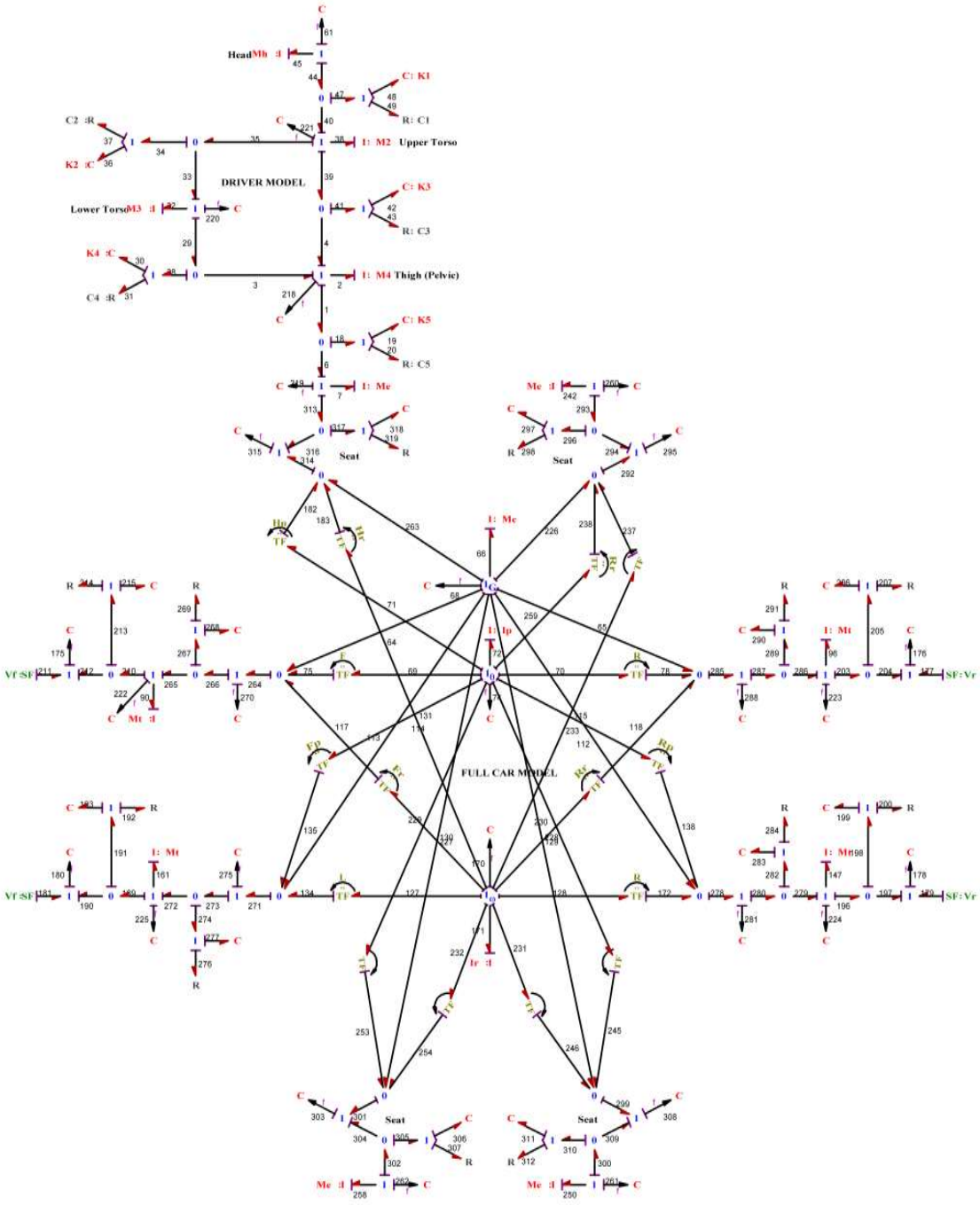


Figure 5.5 Integrated Bond Graph model of 11DOF Full car coupled with 4DOF bio-dynamic human

5.3 Road Excitation

A sinusoidal road profile bump of the same height (0.1 m) but varying widths (1 m, 2 m and 3.7 m) was used for analysis, as illustrated in Fig. 5.67. The right and left side wheels encounter the same amplitude road profile. Additionally, the trajectory of the rear wheel and the front wheels is identical, with a delay time of (F+R)/v. The road conditions, as a function of time, are expressed as follows

5.3.1 Sinusoidal road input

For front wheel

$$\begin{cases} Z = \mathrm{h} * \sin\left(\dfrac{\pi.\mathrm{v}}{\mathrm{w}} * t\right) & for\ t < \dfrac{w}{v} \\ = 0 & for\ t > \dfrac{L}{v} \end{cases} \tag{5.32}$$

and for rear wheel

$$\begin{cases} Z = \mathrm{h} * \sin\left[\dfrac{\pi.\mathrm{v}}{\mathrm{w}} * \left(\mathrm{t} - \left(\mathrm{F} + \mathrm{R}\right)/\mathrm{v}\right)\right] & for\ \dfrac{F+R}{v} < t < \dfrac{F+R+w}{v} \\ = 0 & for\ t > \dfrac{F+R+w}{v} \end{cases} \tag{5.33}$$

In the Bond Graph (BG), road input modeling is performed using the SF (source of flow) element. Thus, the flow to the wheel is determined by differentiating Z with respect to time.

SF to front wheel is

$$\begin{cases} \dot{Z} = \dfrac{\mathrm{h}.\pi.\mathrm{v}}{\mathrm{w}} * \cos\left(\dfrac{\pi.\mathrm{v}}{\mathrm{w}} * t\right) & for\ t < \dfrac{w}{v} \\ = 0 & for\ t > \dfrac{w}{v} \end{cases} \tag{5.34}$$

and SF to rear wheel is

$$\begin{cases} \dot{Z} = \dfrac{\mathrm{h}.\pi.\mathrm{v}}{\mathrm{w}} * \cos\left[\dfrac{\pi.\mathrm{v}}{\mathrm{w}} * \left(\mathrm{t} - \left(\mathrm{F} + \mathrm{R}\right)/\mathrm{v}\right)\right] & for\ \dfrac{F + R}{v} < t < \dfrac{F + R + w}{v} \\ = 0 & for\ t > \dfrac{F + R + w}{v} \end{cases} \tag{5.35}$$

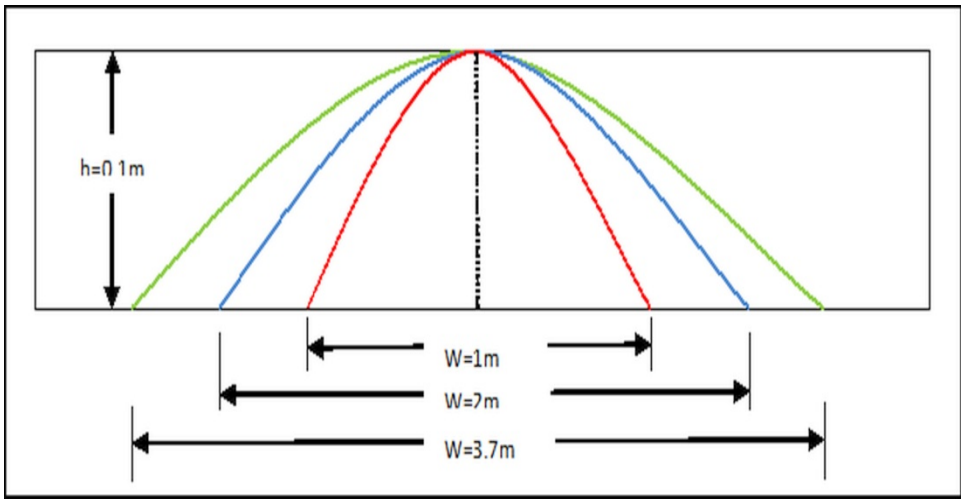


Figure 5.6 Various bump profiles used for simulations

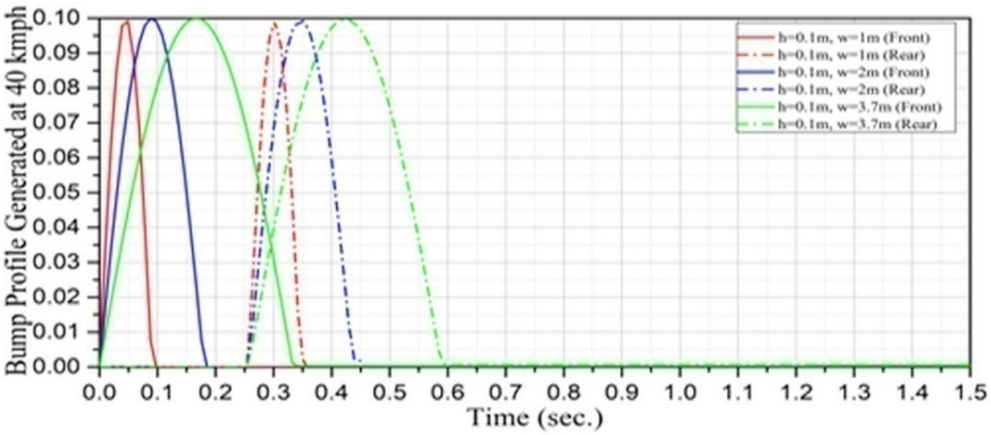


Figure 5.7 BG generated Various bump profiles used for simulations

5.4 Simulation studies

The differential equations produced the Bond Graph are solved using fifth-order Runge-Kutta method. The simulation is carried out for 5 seconds to obtain various dynamic responses. Simulation records are utilized, with errors in the order of 5.0 x 10^{-4}. The parameters used for the simulation are provided in Table 1.(Margolis and Shim, 2000; Abba *et al.*, 2011)

Table 5.1 Human and car model parameters for simulation

Vehicle parameter			
Symbol	Parameters	Value	Units
	Human model parameter by abbas		
m_h	Mass of head	4.17	kg
m_{ut}	Mass of upper torso	15	kg
M_{lt}	Mass of lower torso	5.5	kg
M_p	Mass of pelvis (thigh)	36	kg
C_{hu}	Damping between head & upper torso	310	N-s/m
K_{hu}	Stiffness between head & upper torso	166990	N/m
C_{ul}	Damping between upper torso & lower torso	200	N-s/m

K_{ul}	Stiffness between upper torso & lower torso	10000	N/m
C_{up}	Damping between upper torso & pelvis	909.1	N-s/m
K_{up}	Stiffness between upper torso & pelvis	144000	N/m
C_{lp}	Damping between lower torso & pelvis	330	N-s/m
K_{lp}	Stiffness between lower torso & pelvis	20000	N/m
	Seat parameter		
$C_{sefl}/C_{sefr}/C_{serl}/C_{serr}$	Damping coefficient of four passenger seat	150	N-s/m
$K_{sefl}/K_{sefr}/K_{serl}/K_{serr}$	Stiffness coefficient of four passenger seat	15000	N/m
$m_{sefl}/m_{sefr}/m_{serl}/m_{serr}$	Mass of four passenger seat	35	kg
	Wheel and suspension parameter		
m_{wfl}/m_{wfr}	Mass of front wheel	21.46	kg
m_{wrl}/m_{wrr}	Mass of rear wheel	21.46	kg
C_{sfl}/C_{sfr}	Damping coefficient of front left and right suspension	1385.4	N-s/m
C_{srl}/C_{srr}	Damping coefficient of rear left and right suspension	1385.4	N-s/m
K_{sfl}/K_{sfr}	Stiffness coefficient of front left and right suspension	12394	N/m
K_{srl}/K_{srr}	Stiffness coefficient of rear left and right suspension	12394	N/m
$K_{wfl}/K_{wfr}/K_{wrl}/K_{wrr}$	Stiffness coefficient of four tyres	123940	N/m
	Car body frame parameter		
m_b	Mass of vehicle body	858.6	kg
L_f , L_r	Perpendicular distance between front and rear axle from C.G	1.17, 1.68	m
a,b	Perpendicular distance between front and rear seats from C.G	1, 1.25	m
d,c	Perpendicular distance of left and right seats from C.G	0.5	m
T_l , T_r	Perpendicular distance of left and right wheel from C.G	0.77	m
I_p , I_r	Pitch and roll moment of inertia of vehicle body	2443.26, 637.26	kg-m^2

5.5 Results and discussion

Various dynamic responses in the time domain have been captured in simulations for conditions where the vehicle was moving at 40 km/h over three different geometric obstacles (bumps). Additionally, RMS responses were analysed for different vehicle velocities ranging from 10 to 100 km/h. The results presented in this paper show the intriguing behaviour of the full-car vehicle while traversing various bumps. The time-domain responses examined in this research include the acceleration and displacement of body parts, the four occupant seats, bounce, pitch and roll acceleration and displacements, as well as the front and rear suspension strokes.

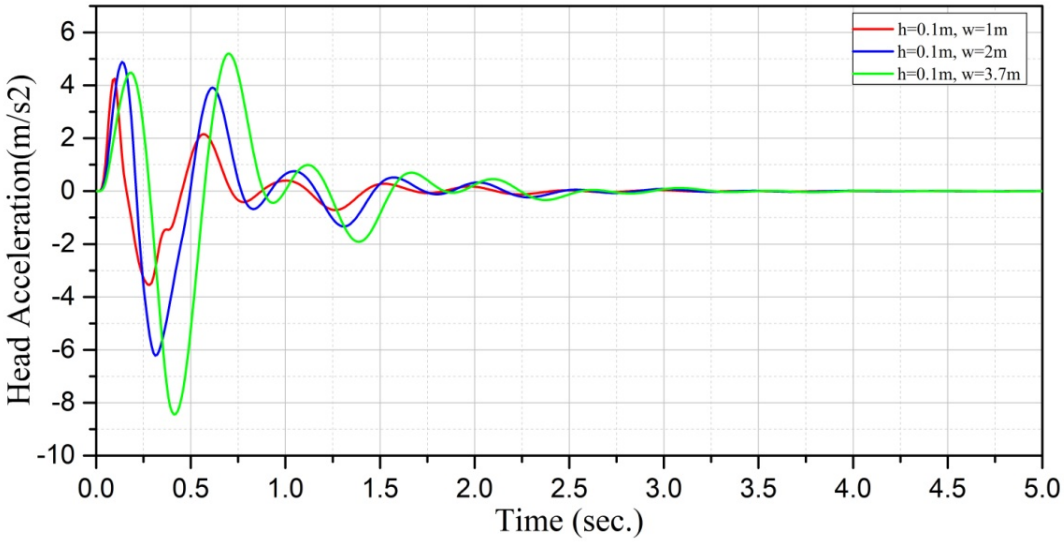


Figure 5.8(a) Bump responses on Vertical Acceleration of Head at 40 km/h

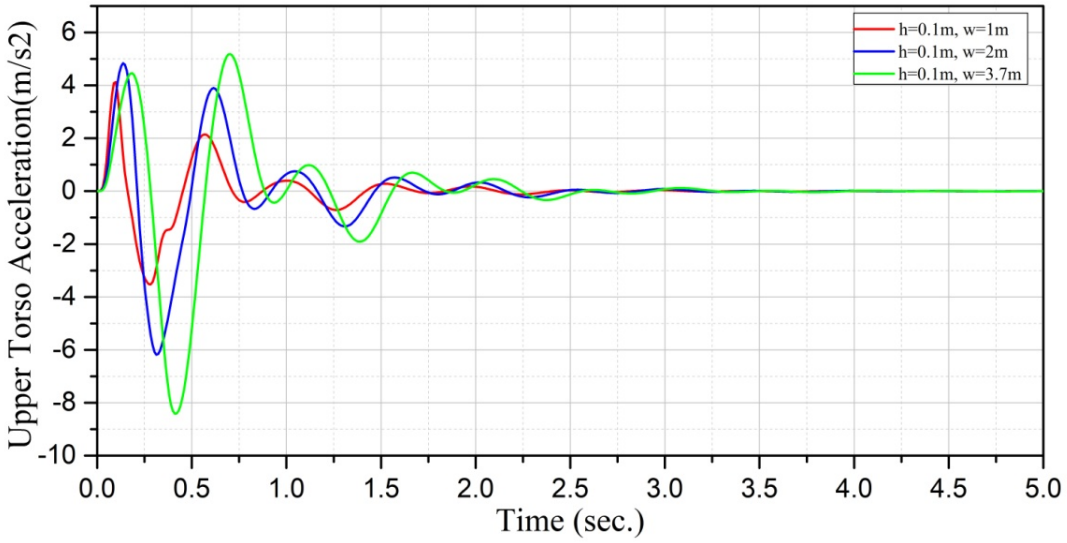


Figure 5.8(b) Bump responses on Vertical Acceleration of Upper Torso at 40 km/h

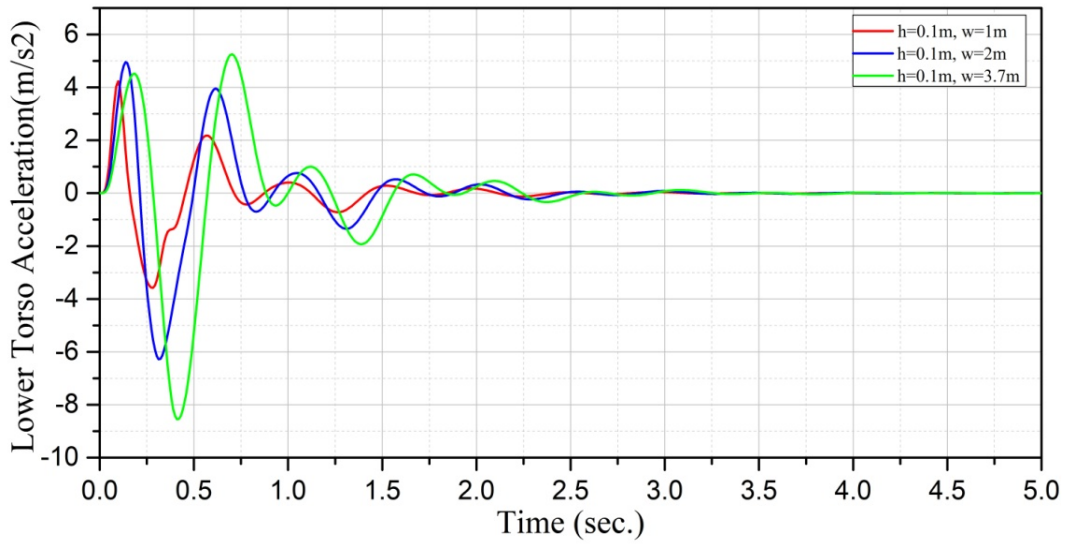


Figure 5.8(c) Bump responses on Vertical Acceleration of Lower Torso at 40 km/h

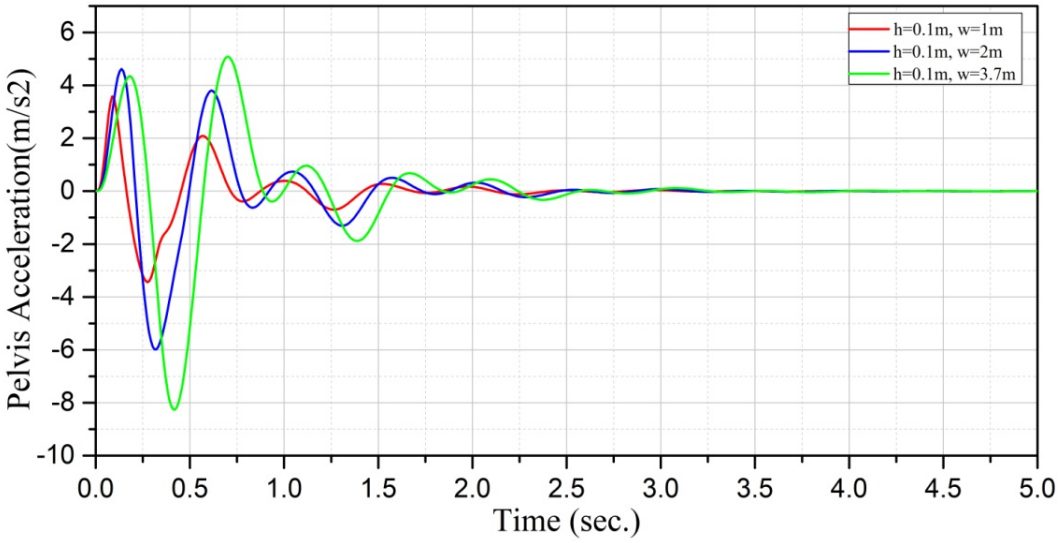


Figure 5.8(d) Bump responses on Vertical Acceleration of Pelvis (Thigh) at 40 km/h

Fig (5.8)-(5.9) illustrate the vertical acceleration and displacement of body parts ('head', 'upper torso', 'lower torso', and 'pelvis'). The acceleration of body parts is an indicator of comfort level. The peak accelerations and displacements of all body parts are observed to be nearly identical for the corresponding bump. Fig (5.10)-(5.11) present RMS acceleration and displacement response comparisons for the scenario where the vehicle traverses three different bumps at varying speeds.

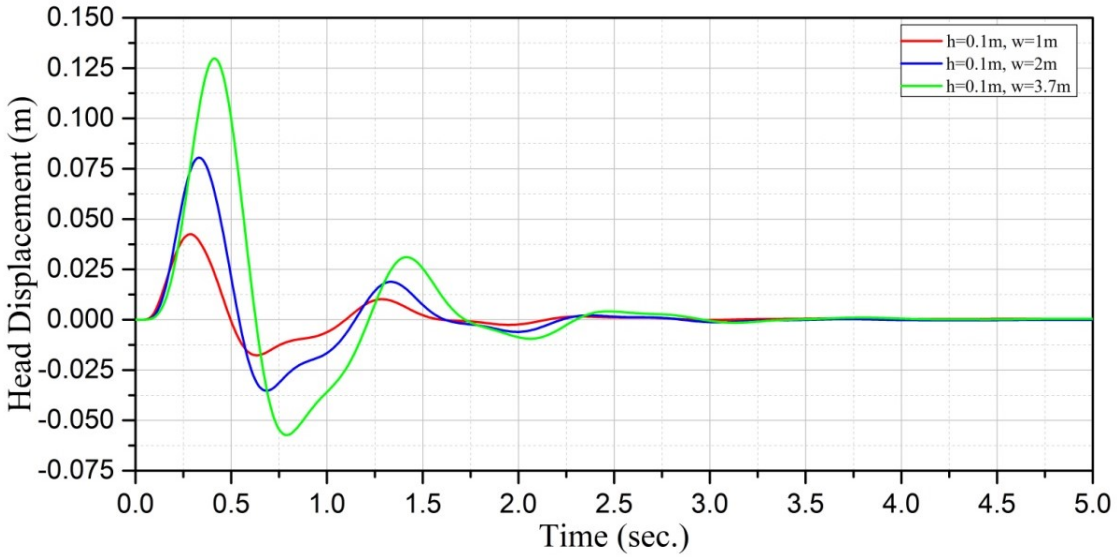


Figure 5.9(a) Bump responses on Vertical Displacement of Head at 40 km/h

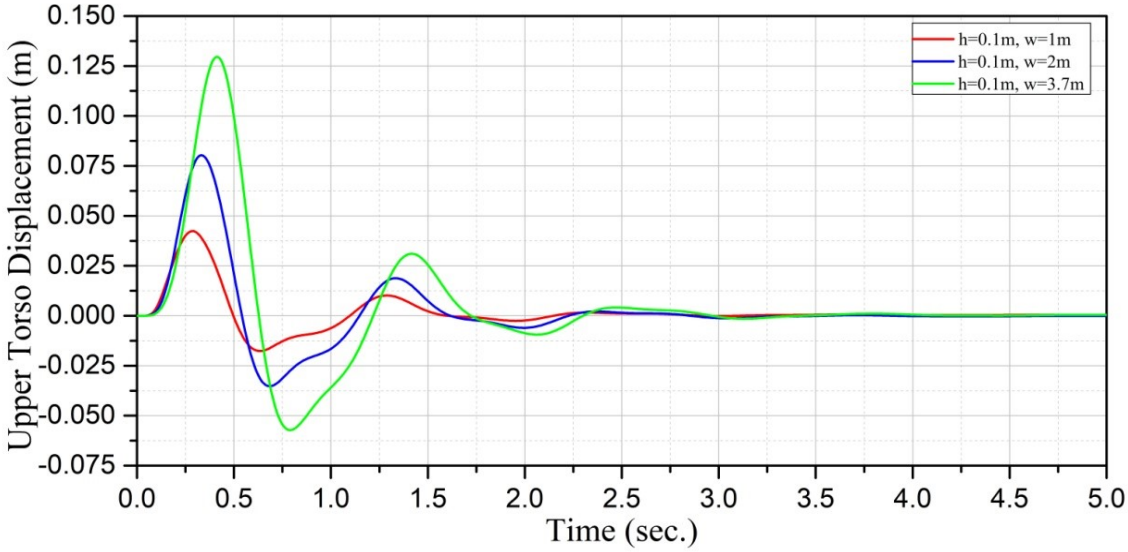


Figure 5.9(b) Bump responses on Vertical Displacement of Upper Torso at 40 km/h

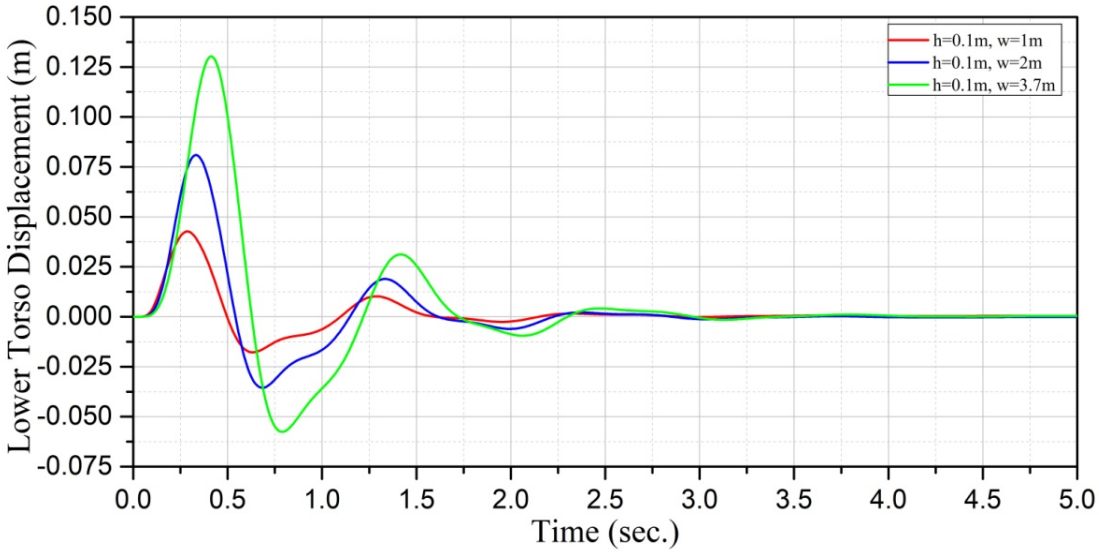


Figure 5.9(c) Bump responses on Vertical Displacement of Lower Torso at 40 km/h

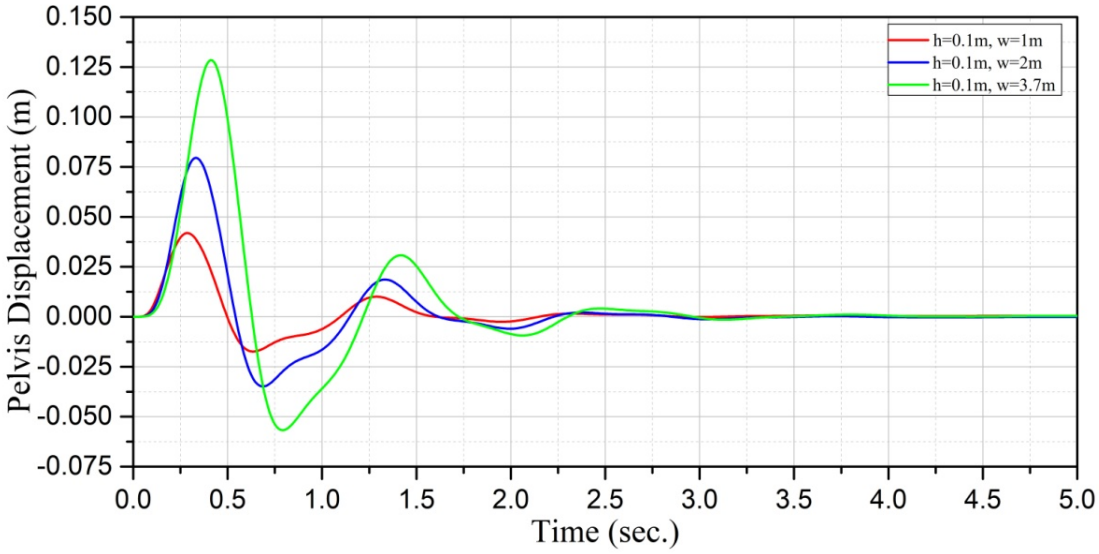


Figure 5.9(d) Bump responses on Vertical Displacement of Pelvis (Thigh) at 40 km/h

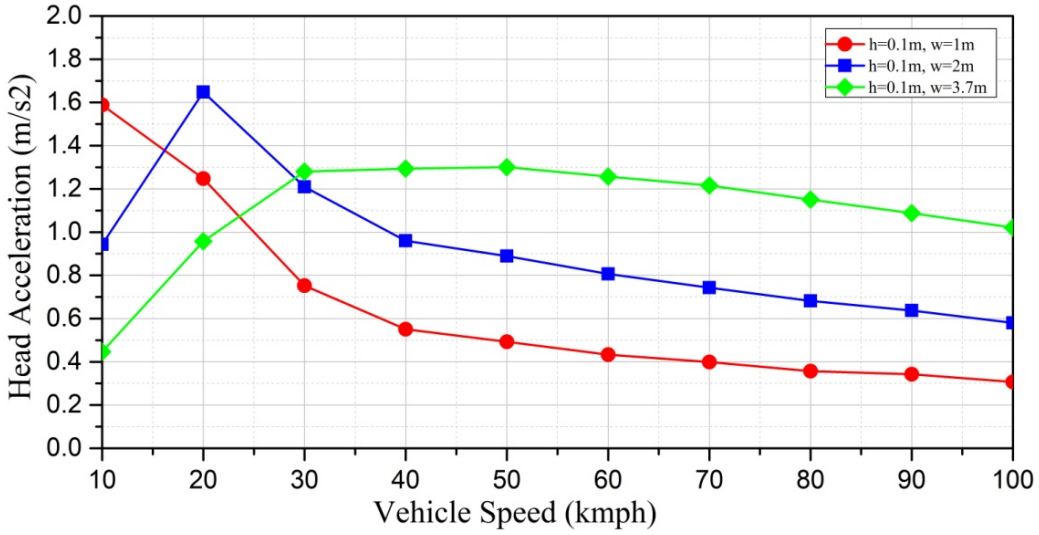


Figure 5.10(a) RMS Acceleration response comparison of Head under various Bump with different vehicle speeds

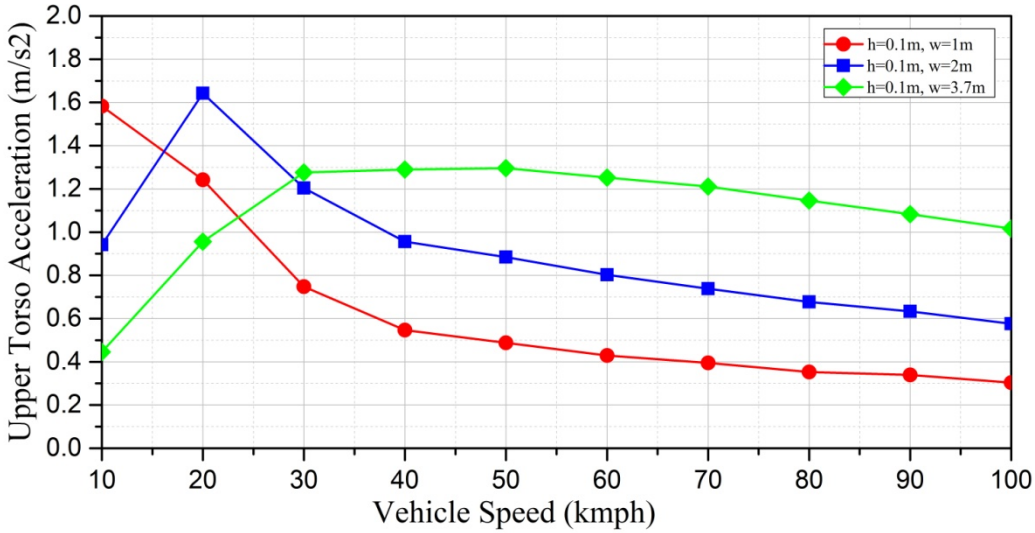


Figure 5.10(b) RMS Acceleration response comparison of Upper Torso under various Bump with different vehicle speeds

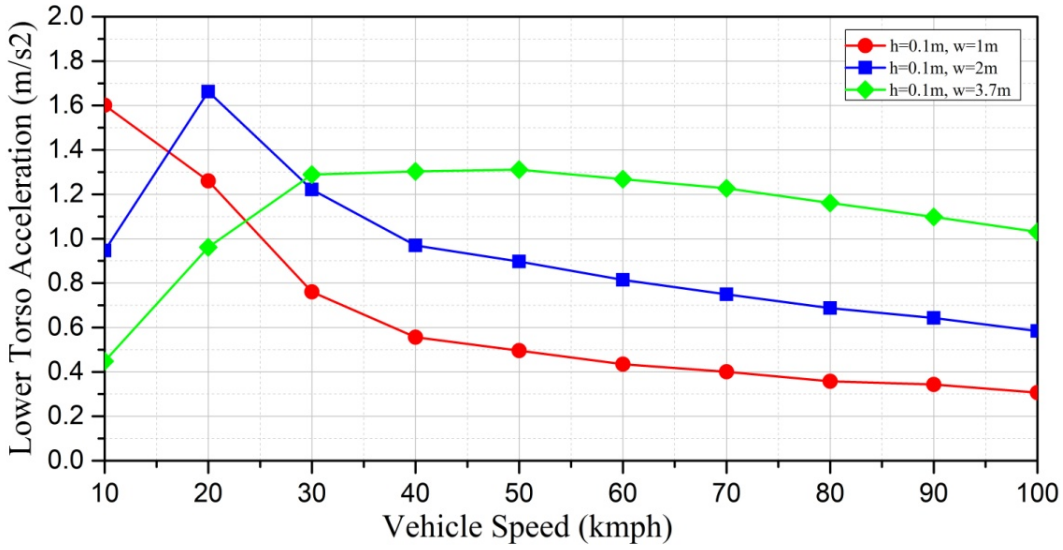


Figure 5.10(c) RMS Acceleration response comparison of Lower Torso under various Bump with different vehicle speeds

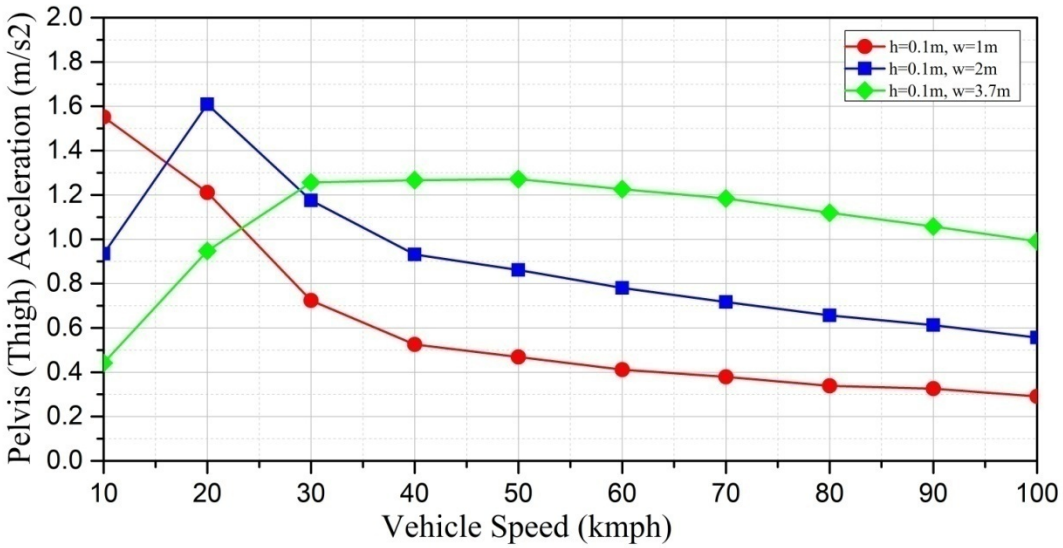


Figure 5.10(d) RMS Acceleration response comparison of Pelvis (Thigh) under various Bump with different vehicle speeds

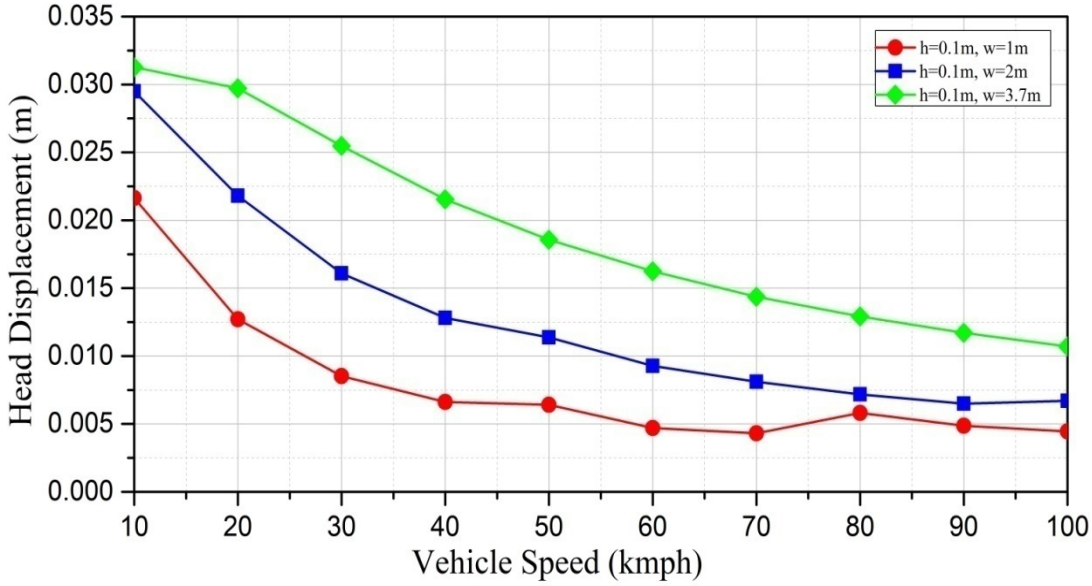


Figure 5.11(a) RMS Displacement response comparison of Head under various Bump with different vehicle speeds

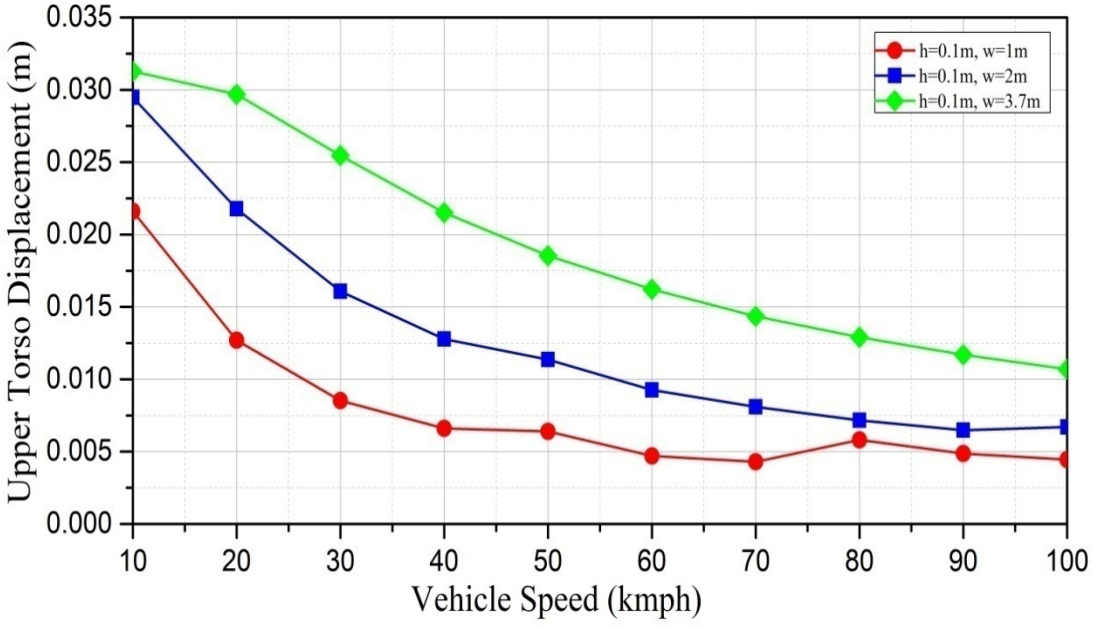


Figure 5.11(b) RMS Displacement response comparison of Upper Torso under various Bump with different vehicle speeds

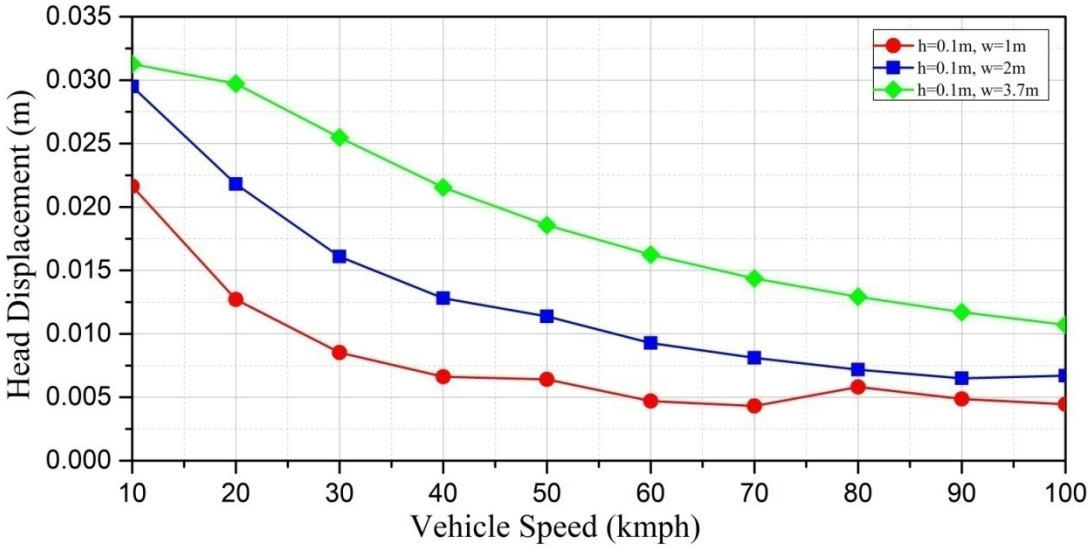


Figure 5.11(c) RMS Displacement response comparison of Lower Torso under various Bump with different vehicle speeds

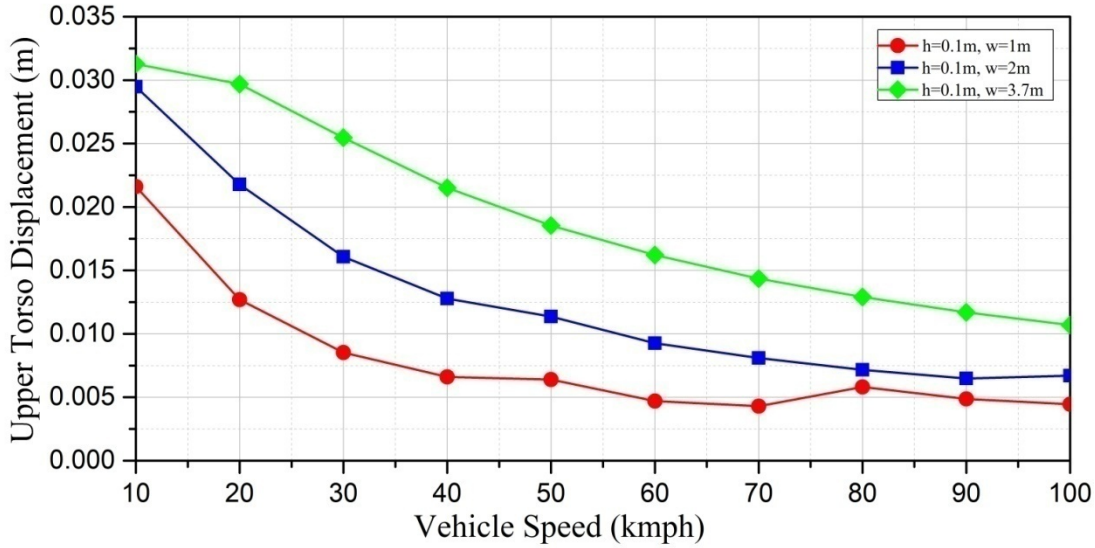


Figure 5.11(d) RMS Displacement response comparison of Pelvis (Thigh) under various Bump with different vehicle speeds

Fig 5.10(a)-(d) shows that body parts' acceleration decreases with increasing vehicle speed for a bump width of 1 m, then remains nearly the same at higher speeds. Furthermore, ride comfort is observed better for a bump of width 3.7 m (highway bump

as per IRC 99 standard) at speeds as low as 10 to 25 km/h. However, at these speeds, acceleration deteriorates for smaller bumps with widths of 1m and 2m, which are typically used as city bumps.

For the occupant's health and safety, the displacement of body parts, particularly the head, is also a significant concern (BS 6841-1987), as it is a result of force transmitted to the human body through seat interaction in response to disturbances originating from the road via bumps.

The relative displacement of body parts remains the same across all vehicle speeds. However, Fig 5.11 demonstrates a decrease in vertical displacement with increasing vehicle speed, which stabilizes higher speed ranges. Additionally, the difference in body parts' displacements appears much smaller across various bumps.

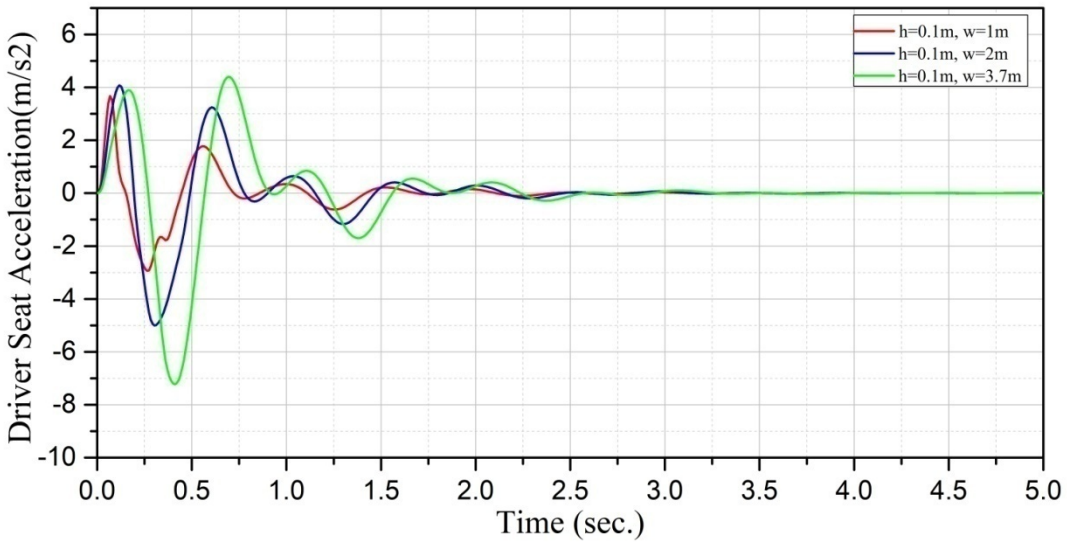


Figure 5.12(a) Bump responses on Vertical Acceleration of Front Right seat at 40 km/h

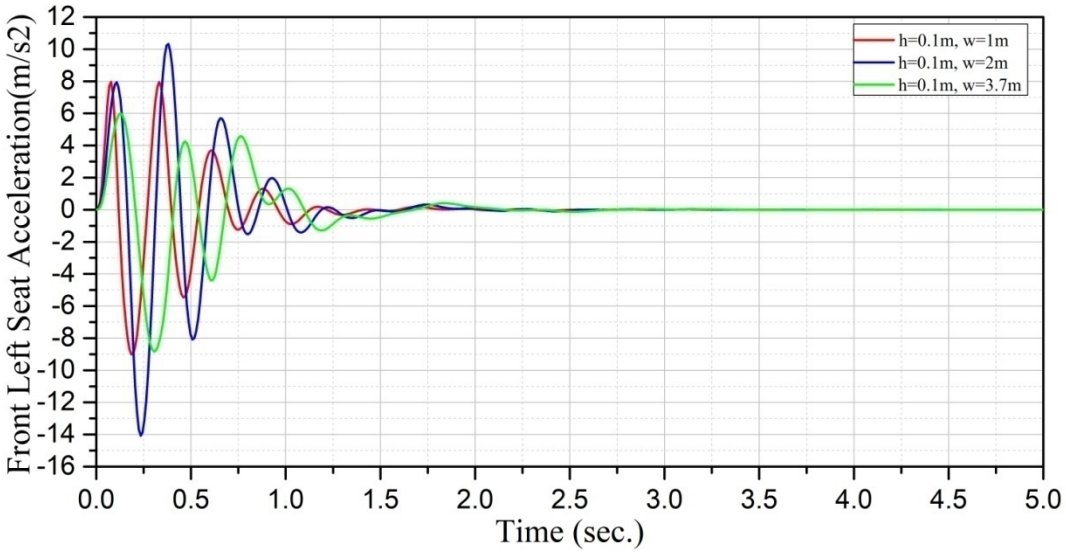


Figure 5.12(b) Bump responses on Vertical Acceleration of Front left seat at 40 km/h

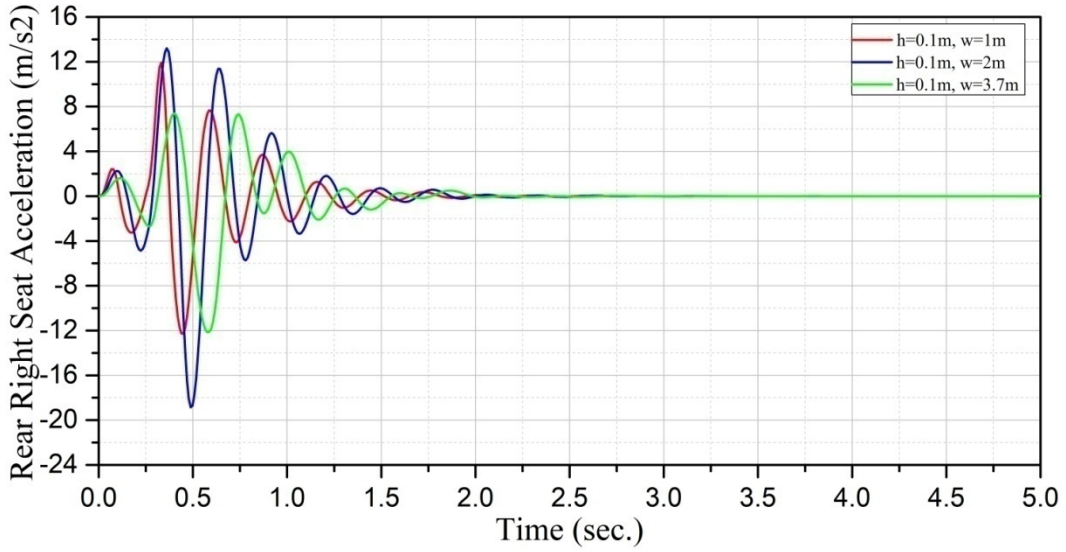


Figure 5.12(c) Bump responses on Vertical Acceleration of Rear Right seat at 40 km/h

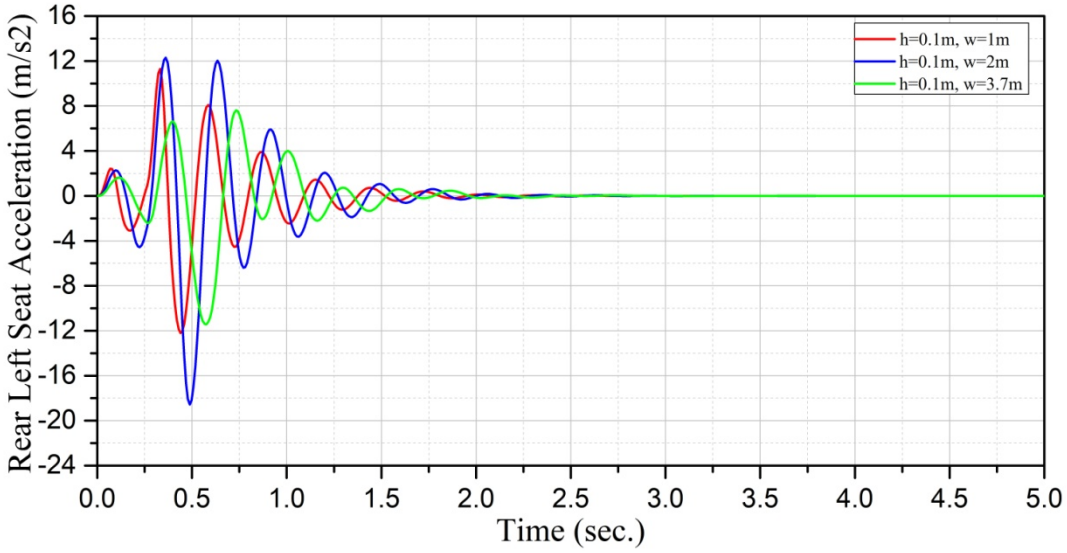


Figure 5.12(d) Bump responses on Vertical Acceleration of Rear Left seat at 40 km/h

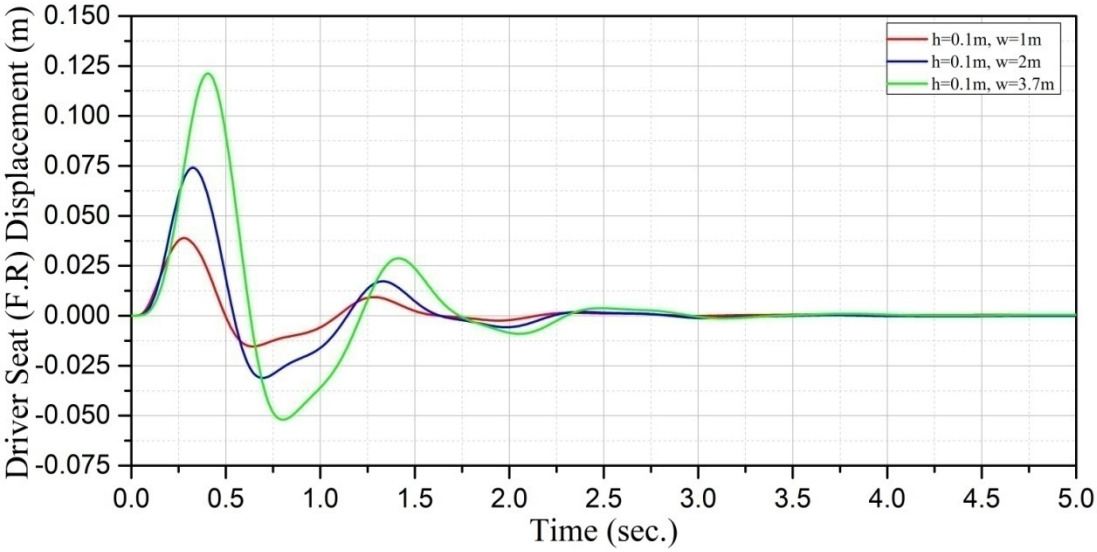


Figure 5.13(a) Bump responses on Vertical Displacement of Front Right seat at 40 km/h

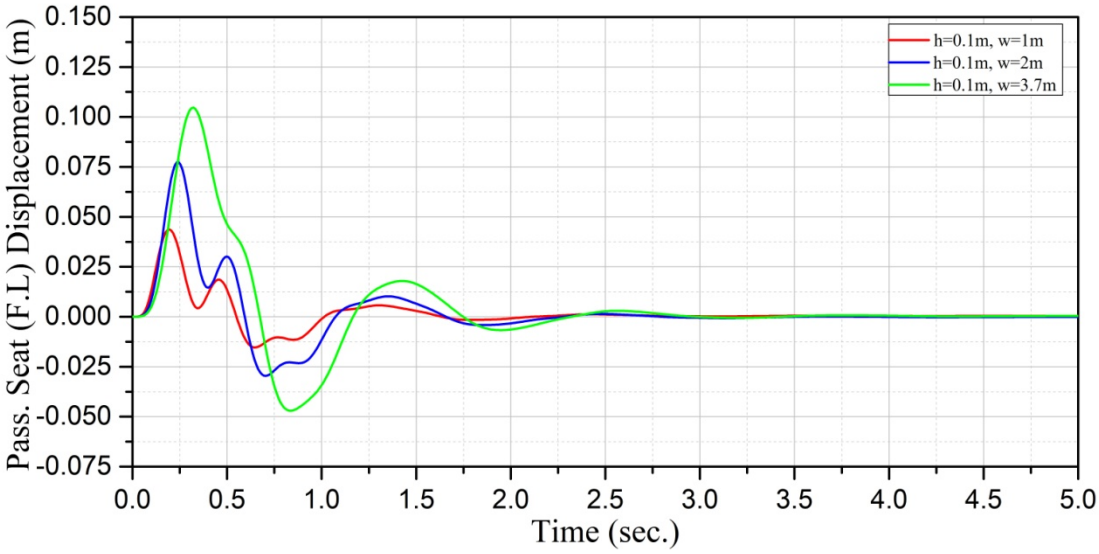


Figure 5.13(b) Bump responses on Vertical Displacement of Front left seat at 40 km/h

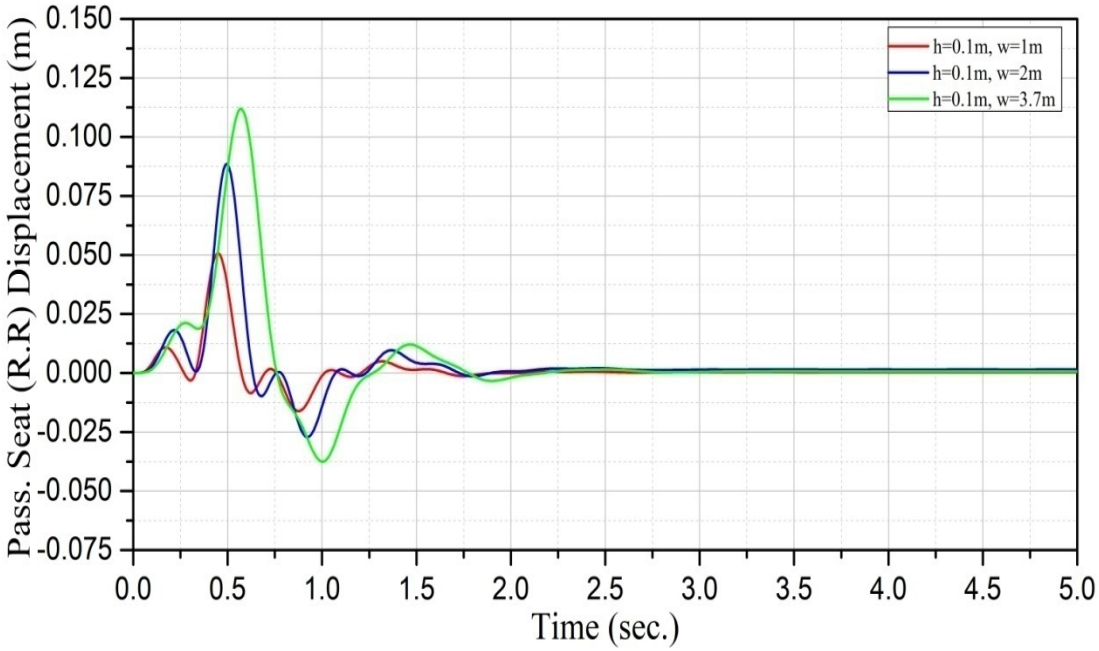


Figure 5.13(c) Bump responses on Vertical Displacement of Rear Right seat at 40 km/h

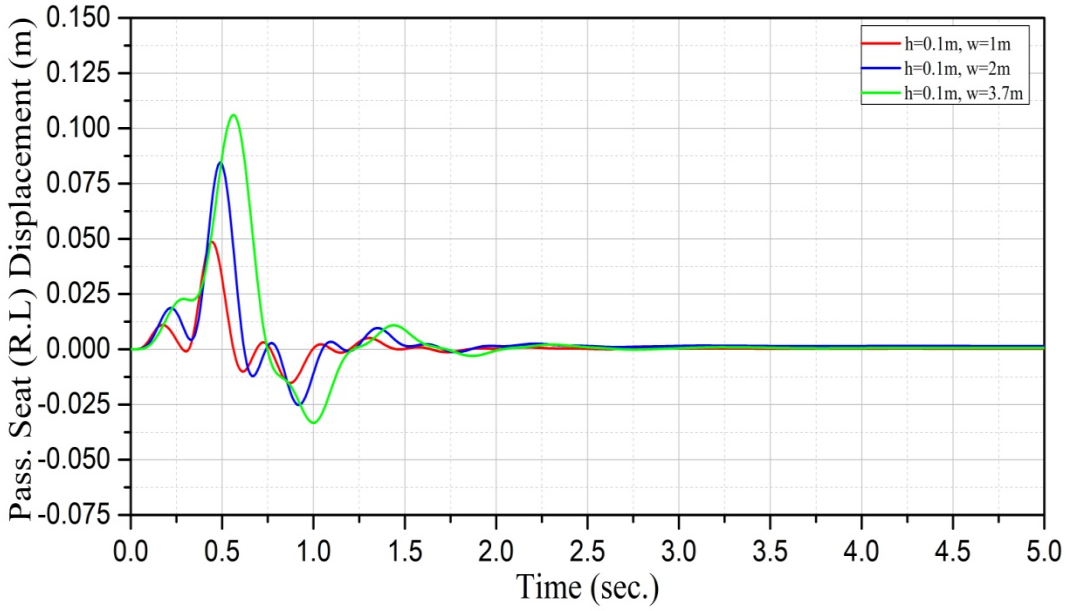


Figure 5.13(d) Bump responses on Vertical Displacement of Rear Left seat at 40 km/h

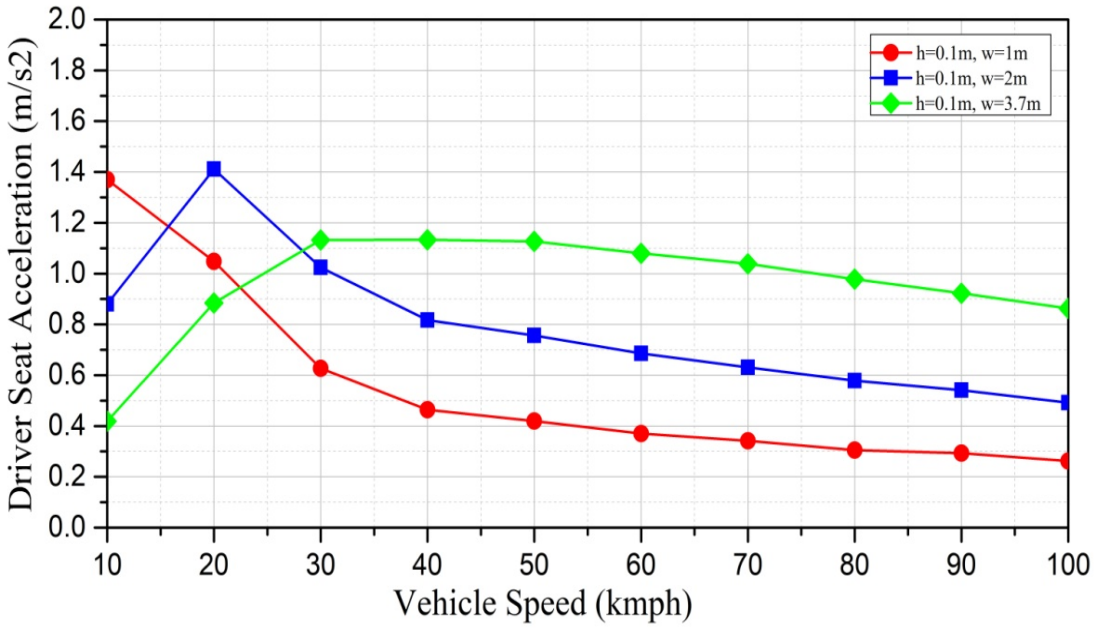


Figure 5.14(a) RMS Acceleration response comparison of Front Right (Driver) seat under various Bump with different vehicle speeds

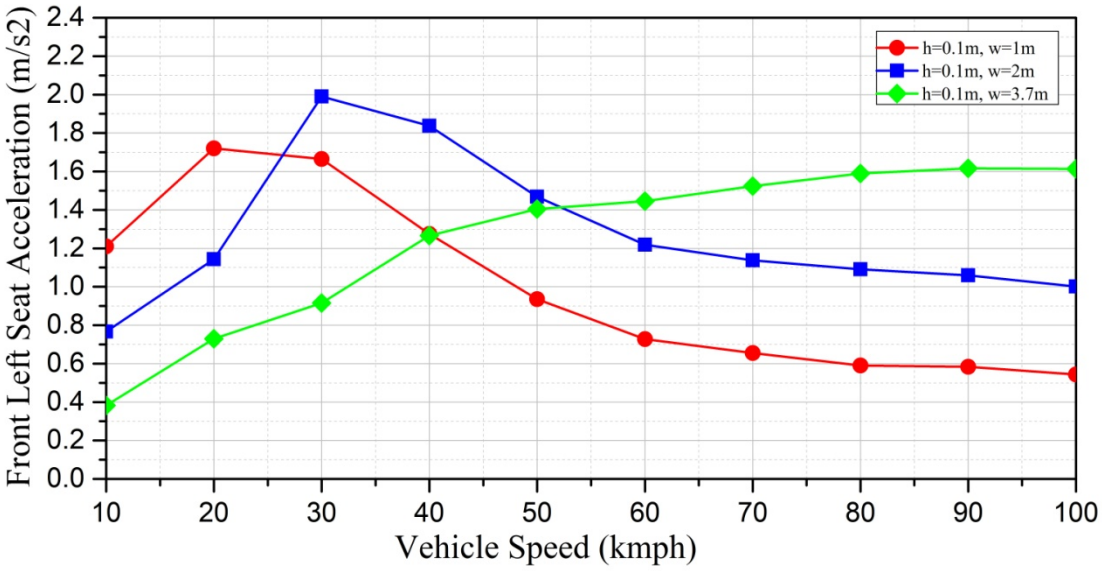


Figure 5.14(b) RMS Acceleration response comparison of Front left seat under various Bump with different vehicle speeds

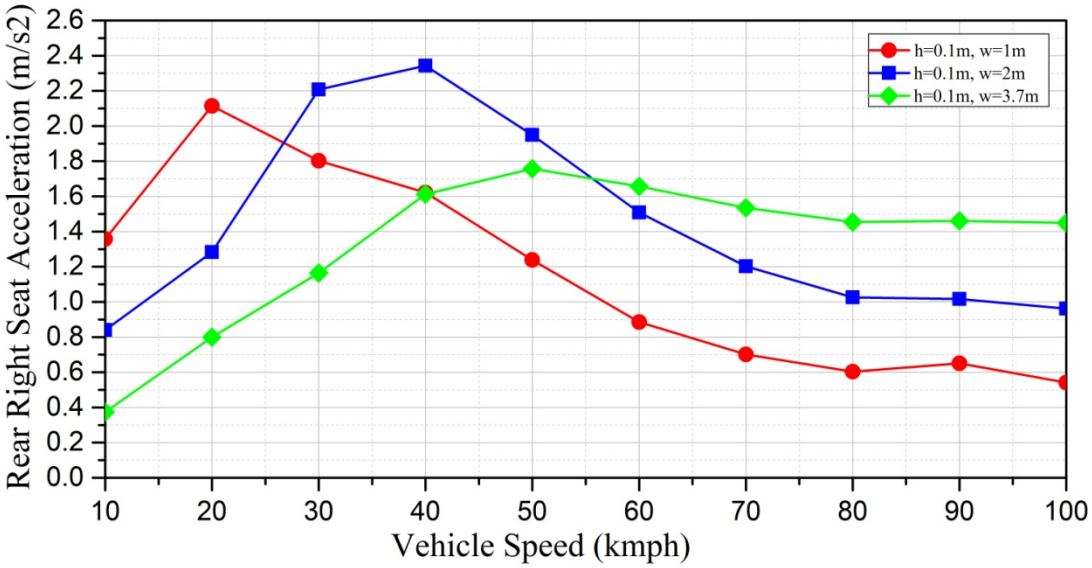


Figure 5.14(c) RMS Acceleration response comparison of Rear right seat under various Bump with different vehicle speeds

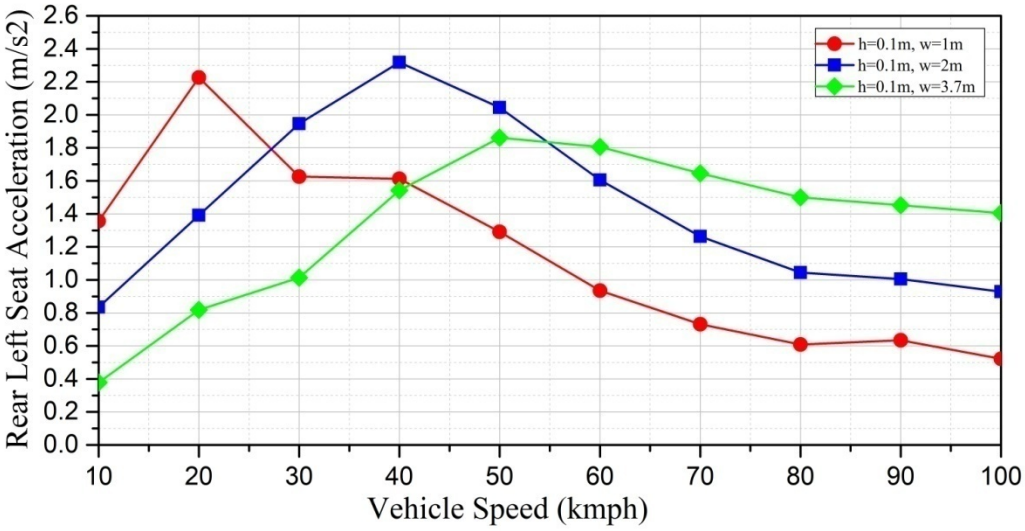


Figure 5.14(d) RMS Acceleration response comparison of Rear left seat under various Bump with different vehicle speeds

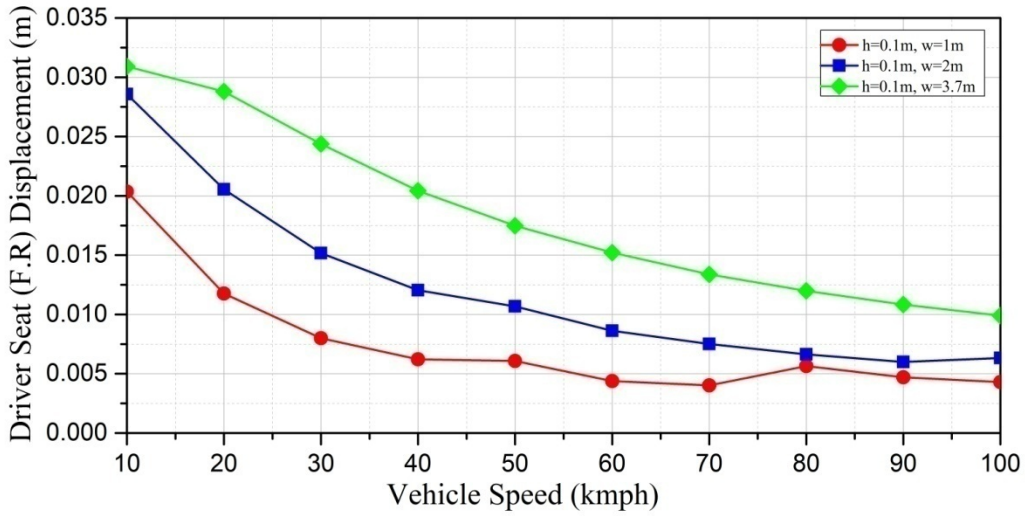


Figure 5.15(a) RMS Displacement response comparison of Front Right (Driver) seat under various Bump with different vehicle speeds

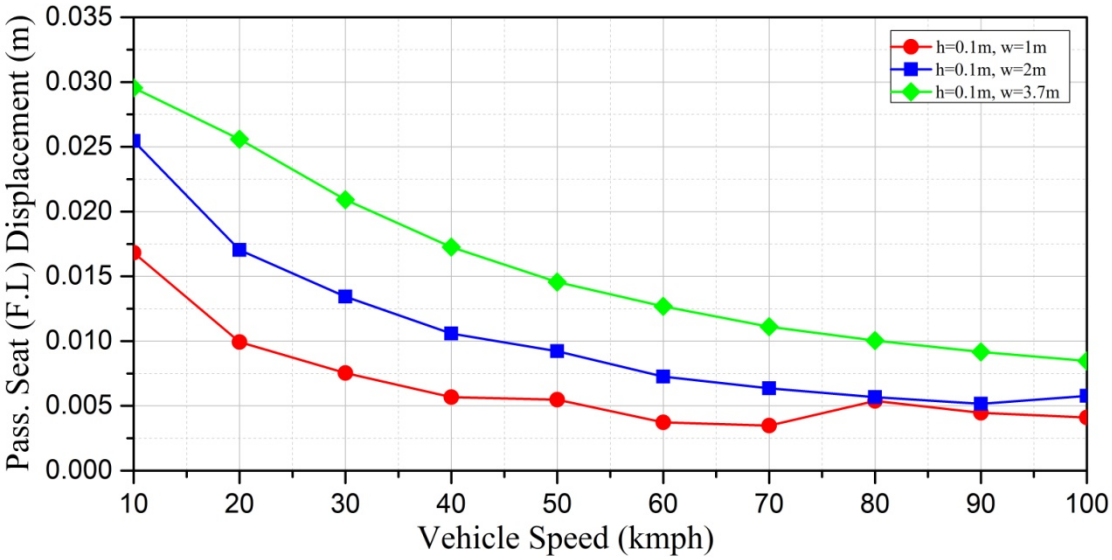


Figure 5.15(b) RMS Displacement response comparison of Front left seat under various Bump with different vehicle speeds

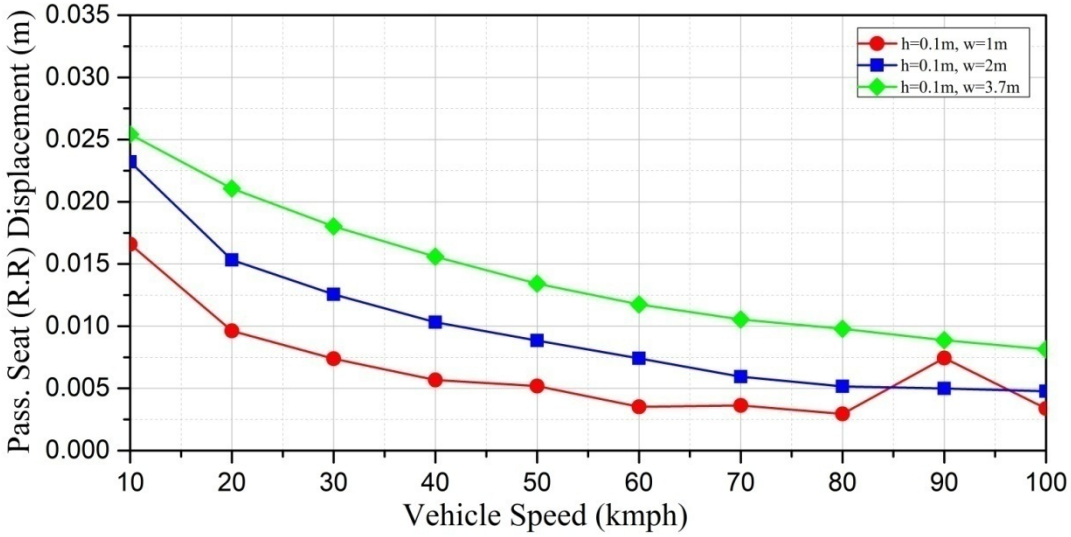


Figure 5.15(c) RMS Displacement response comparison of Rear Right seat under various Bump with different vehicle speeds

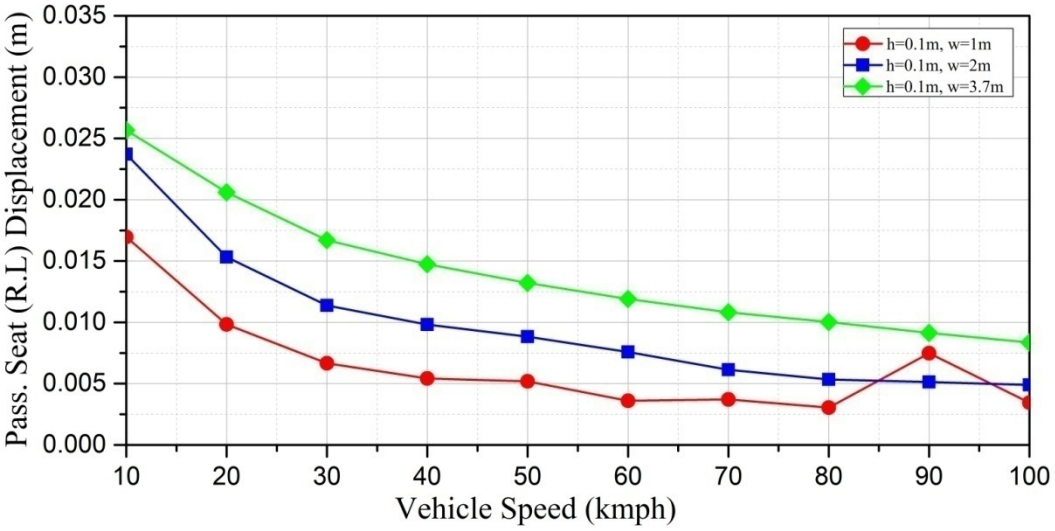


Figure 5.15(d) RMS Displacement response comparison of Rear left seat under various Bump with different vehicle speeds

Fig. 5.12-5.13 illustrate the bump responses of all four seats in terms of vertical acceleration and displacement. As observed from Fig 5.12**,** the peak acceleration of the driver's seat (front right) is 50-60% lower than that of the other three passenger seats for all three bumps, attributed to the occupant's mass. Furthermore, the rear left and right seats exhibit similar behavior in both acceleration and displacement.

Fig 5.14 indicates that the RMS acceleration of the front seat is lower than that of the rear seats at speeds below 60 km/h for all bumps and remains nearly unchanged with a further increase in speed, and this could be because, at higher speeds, the suspensions do not have sufficient time to respond effectively. Furthermore, the RMS acceleration of all seats is better for the third bump (w=3.7 m) in the low-speed range. Fig 5.15 shows that the RMS displacement decreases as vehicle speed increases, with the displacement of

the front seats being relatively larger than that of the rear seats for all three bump widths at speeds below 60 km/h. At higher speeds, however, the difference in displacement is minimal.

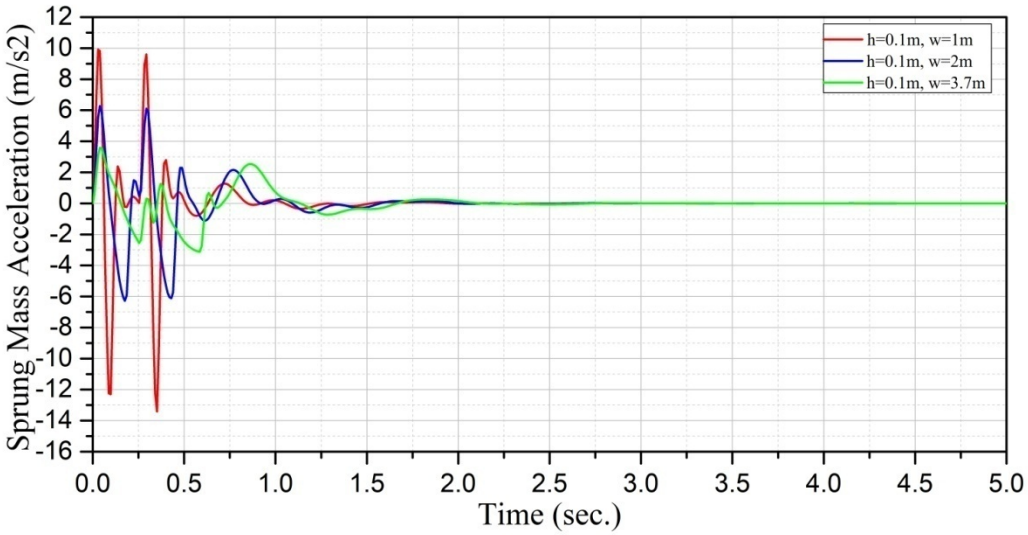


Figure 5.16(a) Various bump responses on Car body Acceleration (bounce) at 40 km/h

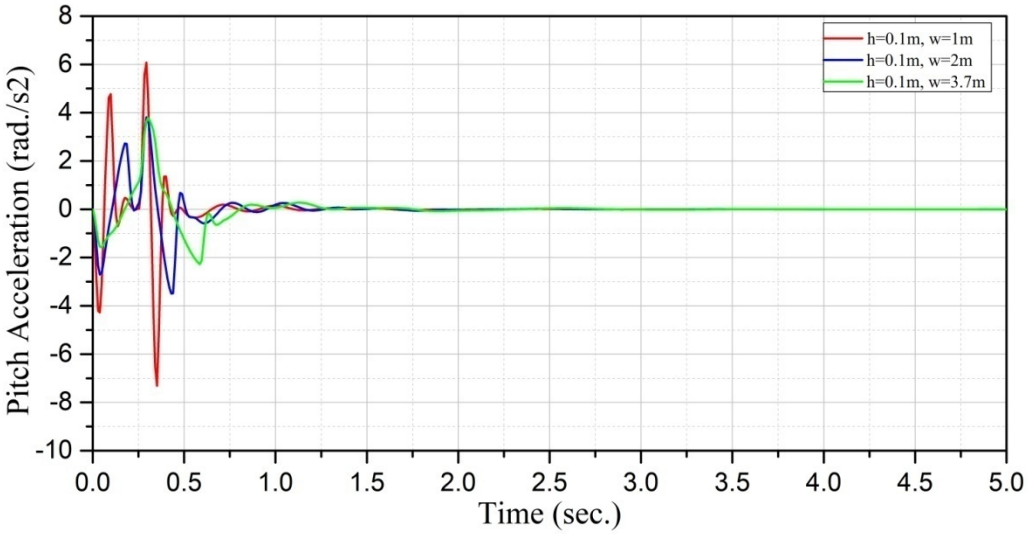


Figure 5.16(b) Various bump responses on Car body Acceleration (Pitch) at 40 km/h

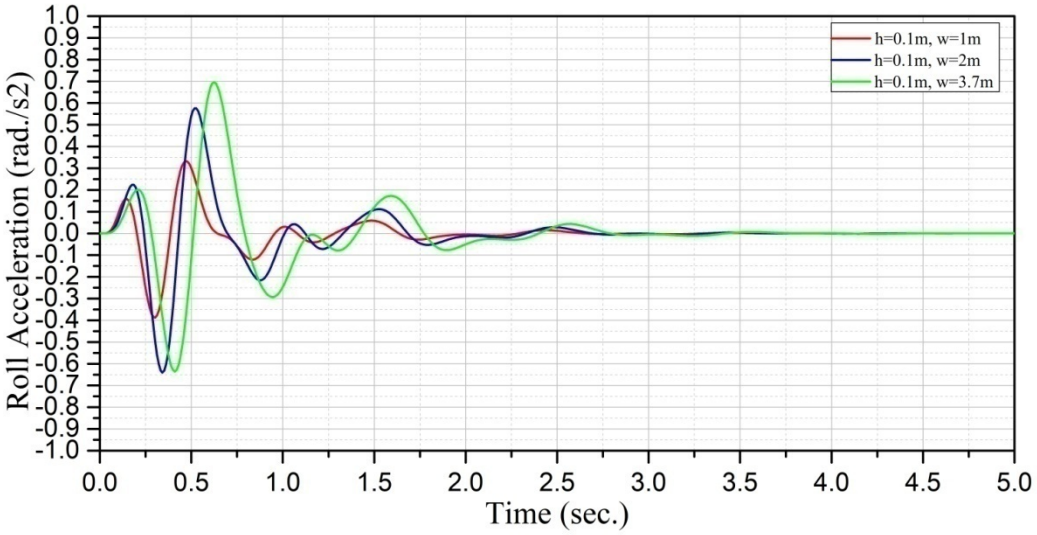


Figure 5.16(c) Various bump responses on Car body Acceleration (Roll) at 40 km/h

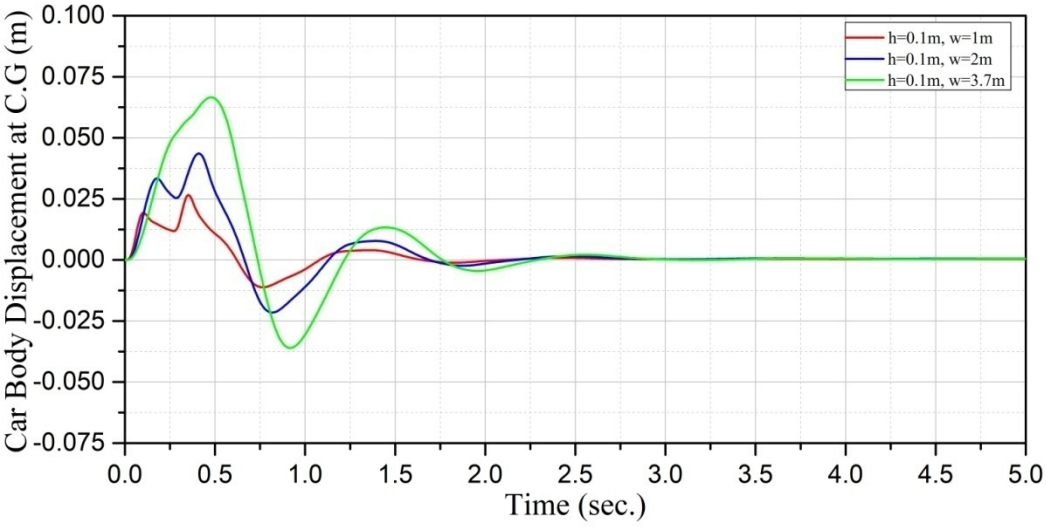


Figure 5.17(a) Various bump responses on Car body displacement (bounce) at 40 km/h

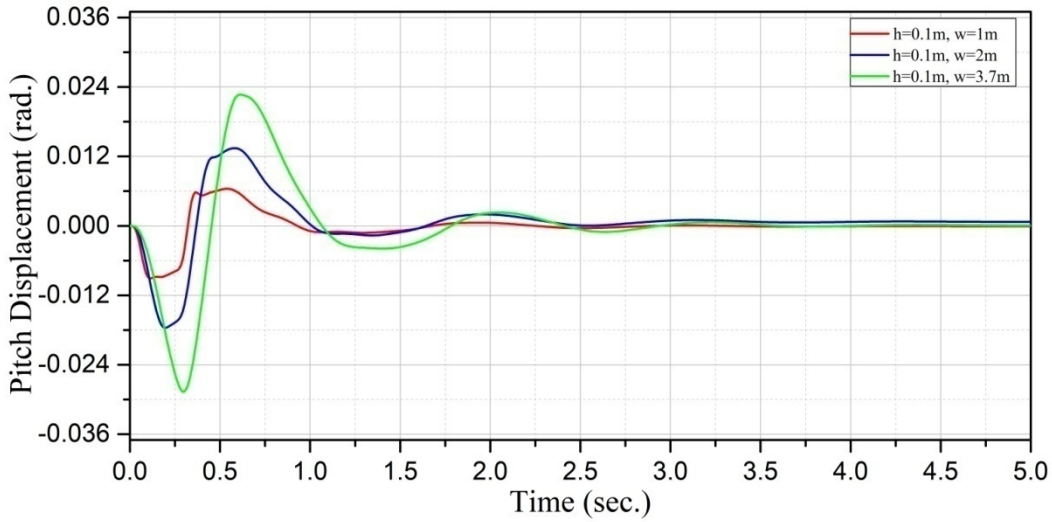


Figure 5.17(b) Various bump responses on Car body displacement (Pitch) at 40 km/h

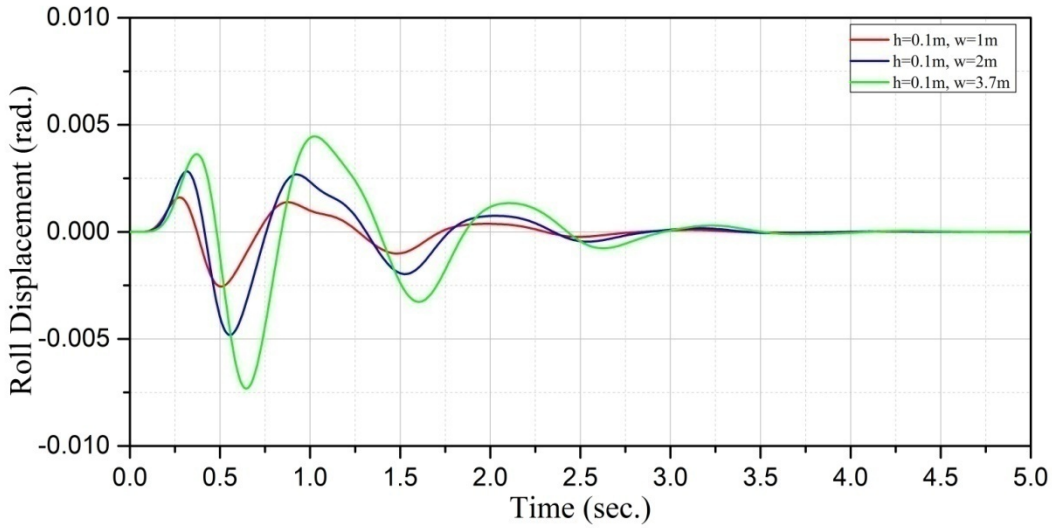


Figure 5.17(c) Various bump responses on Car body displacement (Roll) at 40 km/h

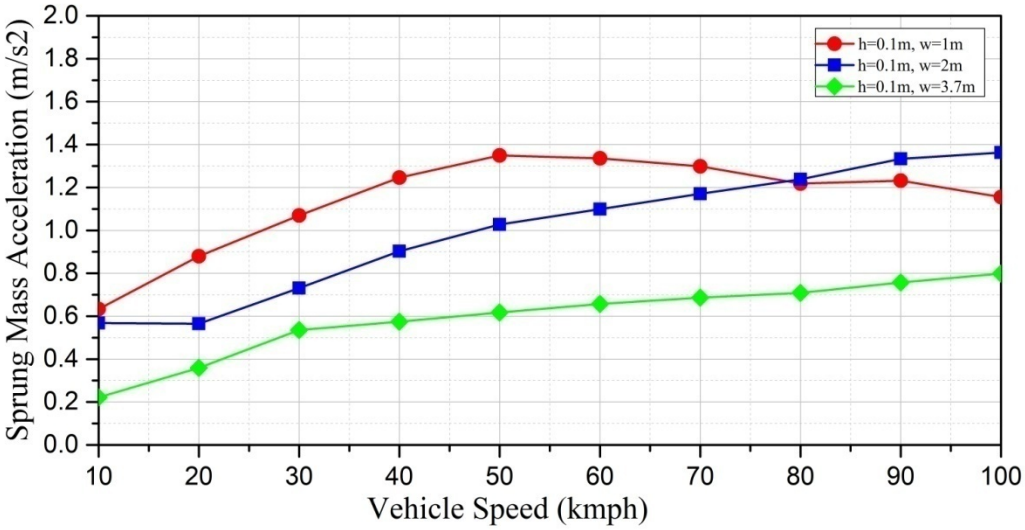


Figure 5.18(a) RMS acceleration (Bounce) response comparison of car body motion at C.G under various bumps with different vehicle speeds

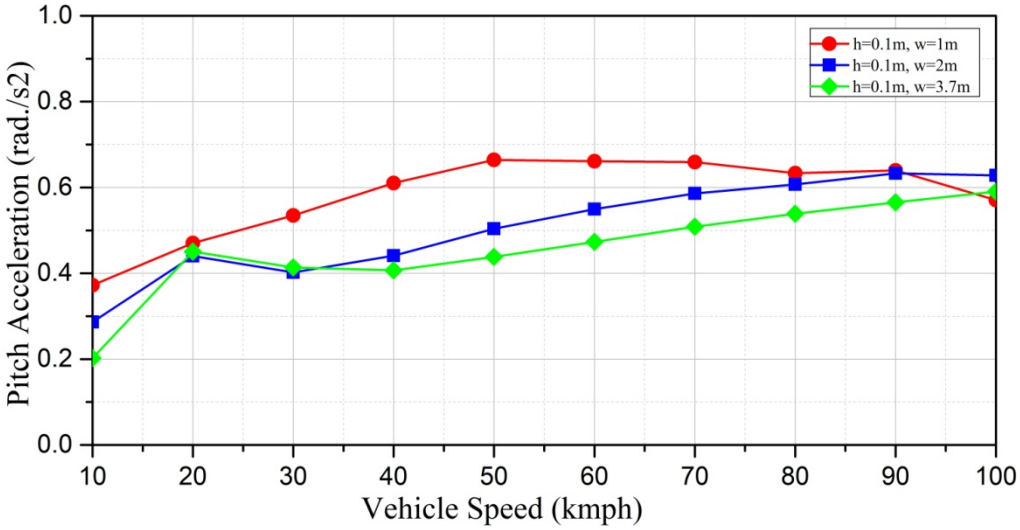


Figure 5.18(b) RMS acceleration (Pitch) response comparison of car body motion at C.G under various bumps with different vehicle speeds

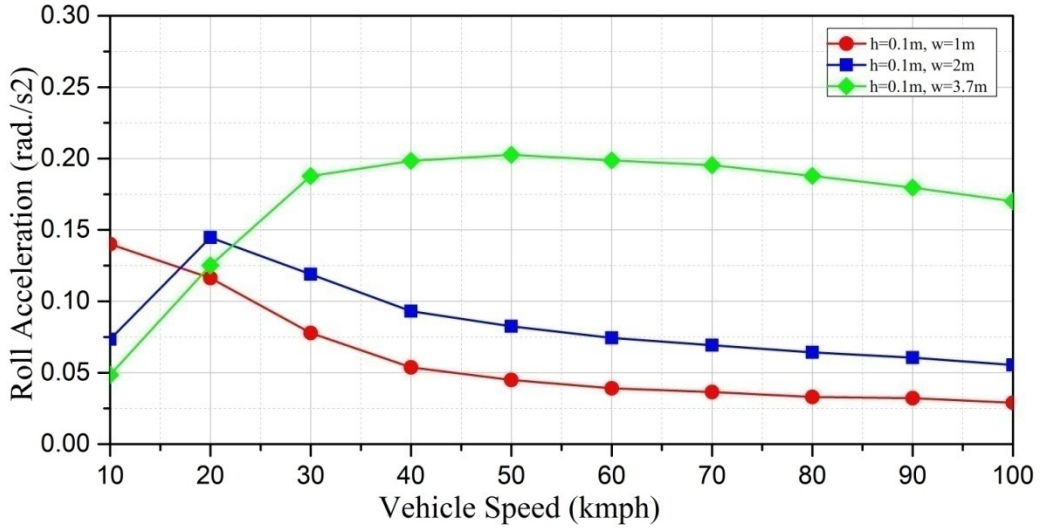


Figure 5.18(c) RMS acceleration (Roll) response comparison of car body motion at C.G under various bumps with different vehicle speeds

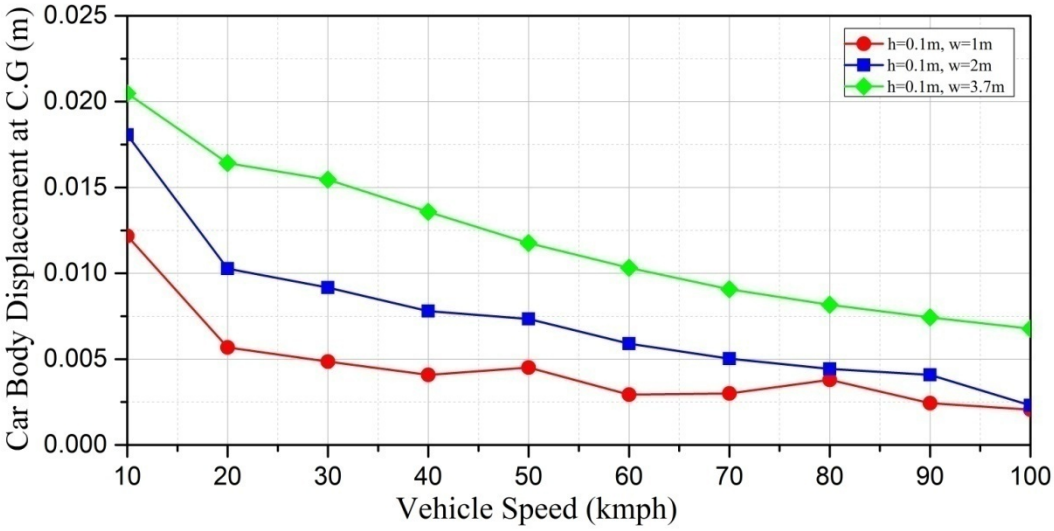


Figure 5.19(a) RMS Displacement (Bounce) response comparison of car body motion at C.G under various bumps with different vehicle speeds

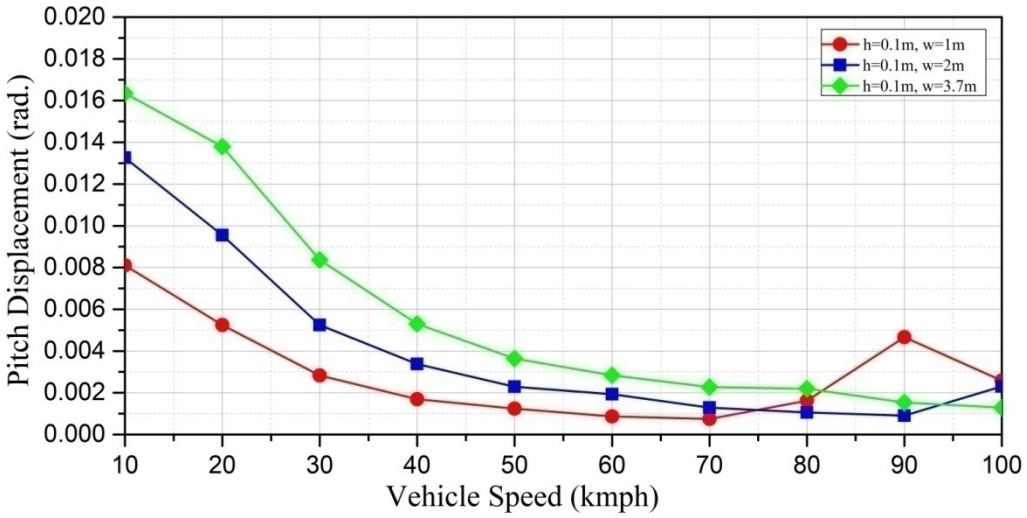


Figure 5.19(b) RMS Displacement (Pitch) response comparison of car body motion at C.G under various bumps with different vehicle speeds

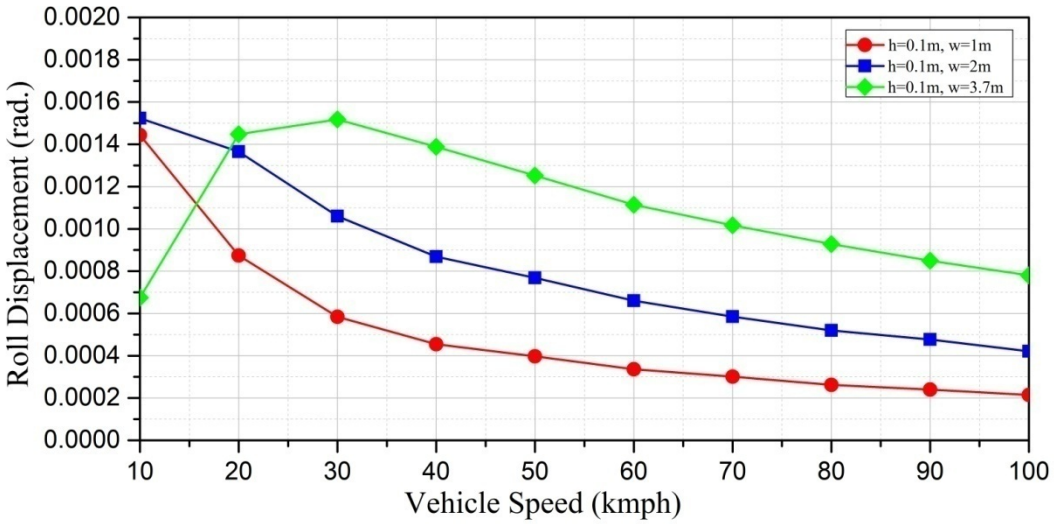


Figure 5.19(c) RMS Displacement (Roll) response comparison of car body motion at C.G under various bumps with different vehicle speeds

The car body's dynamic behaviour (bounce, pitch, and roll) at the C.G. for a vehicle of speed 40 km/h is shown in Figures 5.16-5.17. From Figure 5.18 (a)-(b), it is observed that the third bump condition (width=3.7 m) produces the minimum vertical and pitch acceleration compared to the first (width=1 m) and second (width=2 m) road conditions

across all speeds. The roll acceleration in Fig 5.16(c) appears to be significantly lower, as the height of both the left and right bumps was the same, validating the results with practical on-road behaviour. It is further observed that roll acceleration increases with vehicle speed up to 30 km/h for a bump width of 3.7 m and then decreases or remains unaffected with further increases in vehicle speed.

Fig. 5.17(d)-(f) shows that the RMS bounce, pitch, and roll displacements for a bump width of 3.7 m are slightly larger than those for a 1 m and 2 m bump width. The RMS bounce and pitch displacement decrease as vehicle speed increases, while roll displacement increases up to 30 km/h and then decreases with higher vehicle speeds. Roll acceleration and displacement are observed to be minimal at a speed of 10 km/h.

To further analyze the effect of geometric obstacles on various performance aspects, the car suspension stroke while passing over different bump road inputs at a speed of 40 Km/h is shown in Fig 5.19. According to the mechanic's principle, suspension stroke is calculated as the difference in displacement at the car frame suspension interface and the wheel displacement, i.e., $(Z_{bij}-Z_{wij})$, where i refers to the front or rear, and j refers to the right or left. Displacement at the respective location is measured by applying an activated compliance element in the bond graph model. The formula for the front right suspension, can be written as $(Z_{bfr}-Z_{wfr})$. To prevent the wheel from hitting the car frame and to ensure better ride comfort, the actual suspension stroke and the maximum allowable suspension stroke must be properly matched, as ride comfort becomes poor with an increase in suspension stroke.

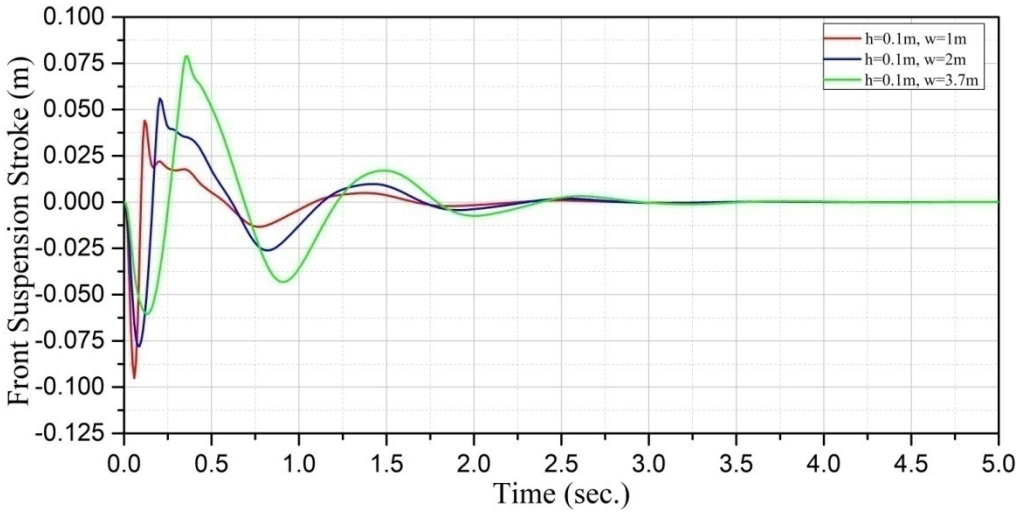


Figure 5.20(a) Various bump responses on suspension stroke (Front) at 40 km/h

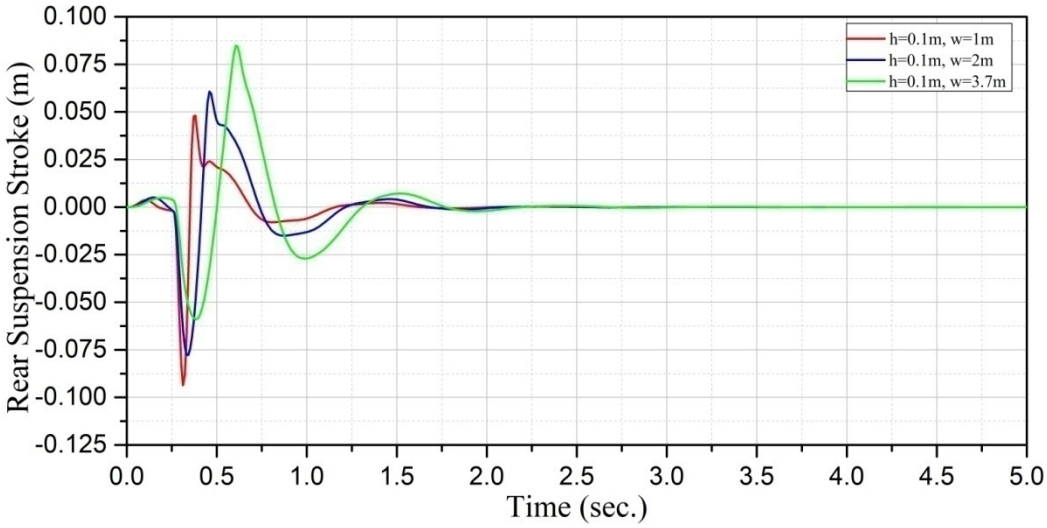


Figure 5.20(b) Various bump responses on suspension stroke (Rear) at 40 km/h

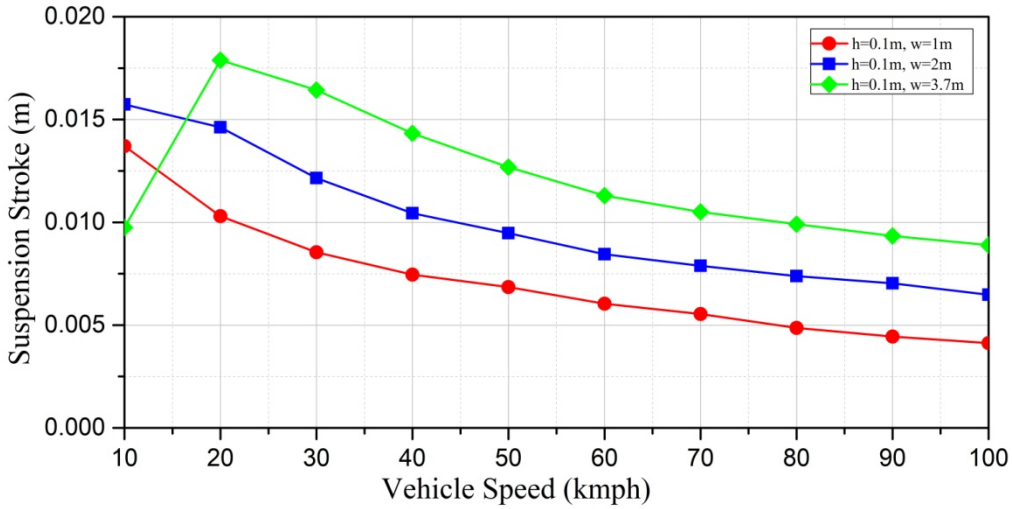


Figure 5.21(a) RMS Suspension Stroke (Front) response comparison under various bump under various bumps with different vehicle speeds

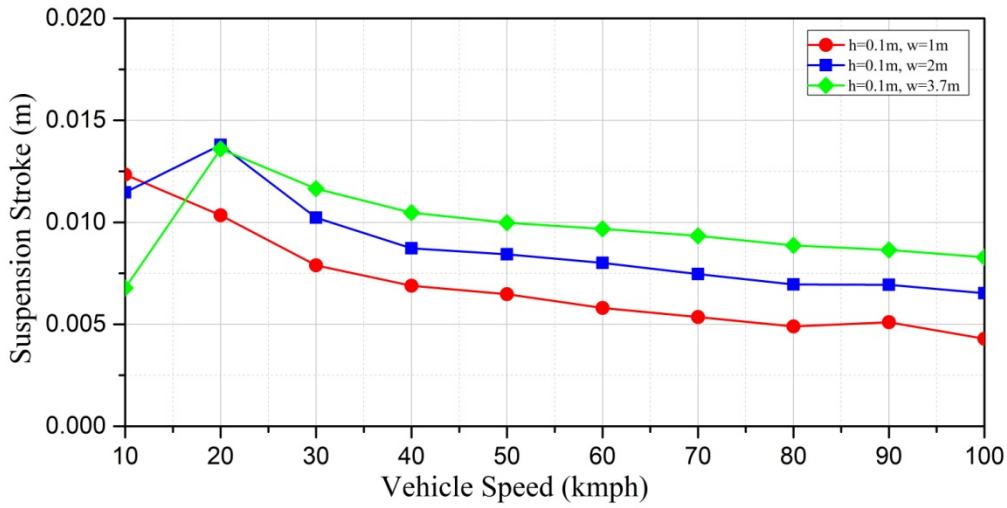


Figure 5.21(b) RMS Suspension Stroke (Rear) response comparison under various bump under various bumps with different vehicle speeds

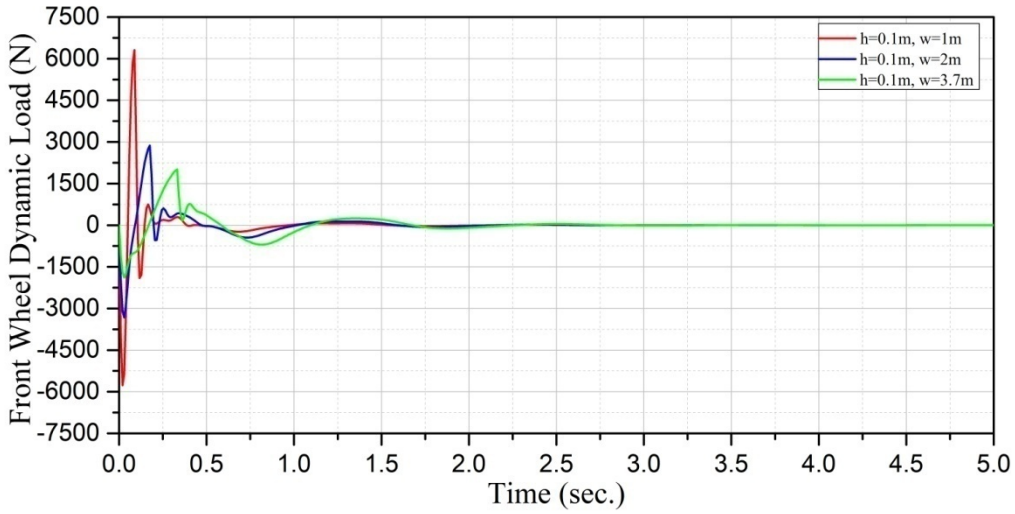


Figure 5.22(a) Various bump responses on wheel (Front) dynamic load at 40 km/h

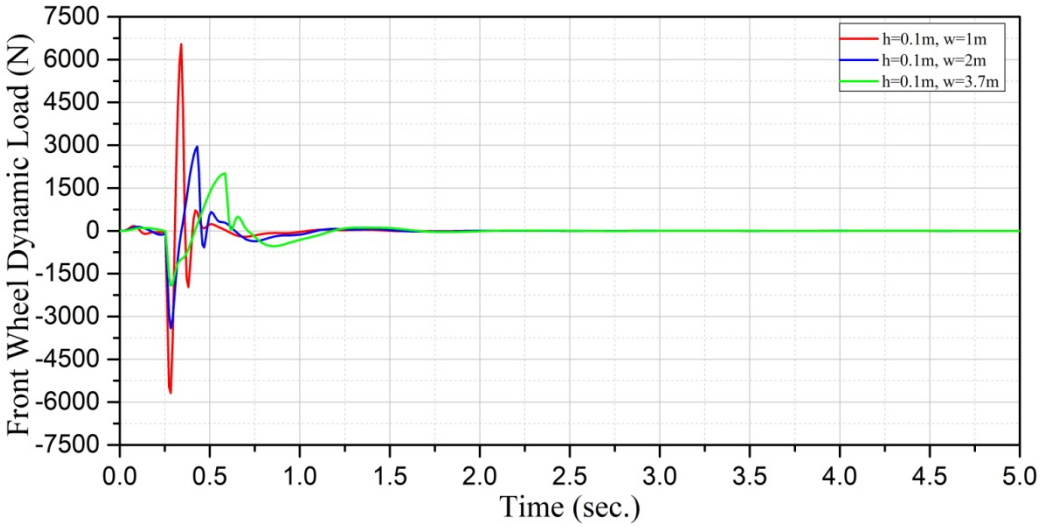


Figure 5.22(b) Various bump responses on wheel (Rear) dynamic load at 40 km/h

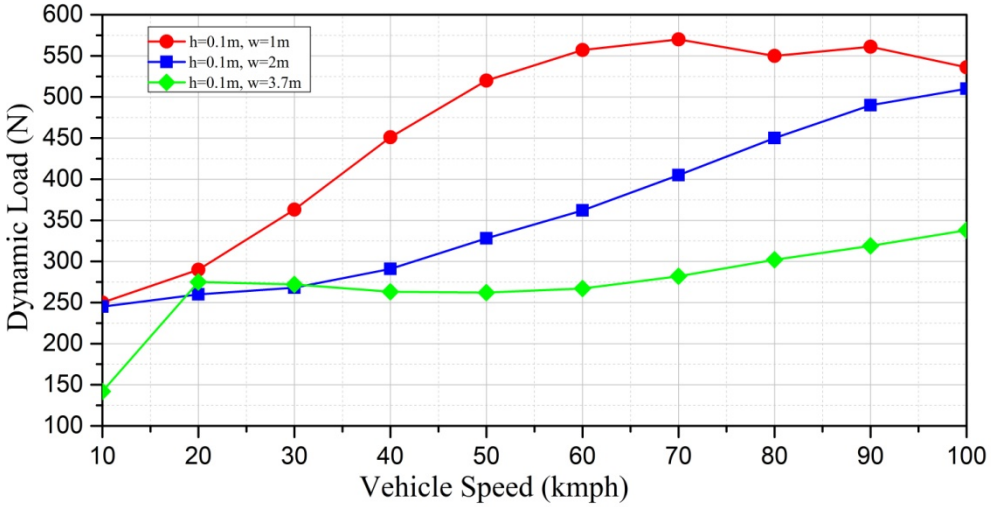


Figure 5.23(a) RMS wheel dynamic load (Front) response comparison under various bump under various bumps with different vehicle speeds

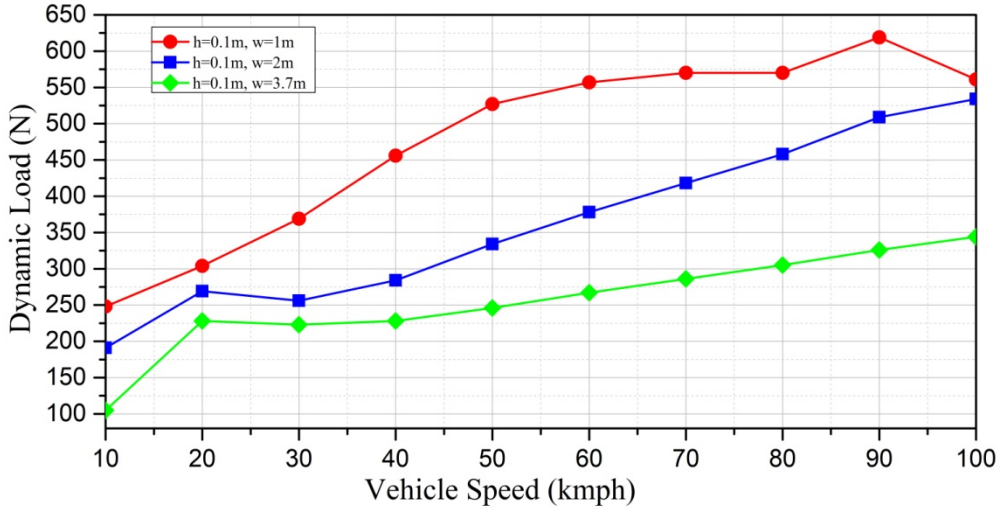


Figure 5.23(b) RMS wheel dynamic load (Rear) response comparison under various bump under various bumps with different vehicle speeds

Fig 5.20 illustrates the front and rear suspension stroke behavior in the time domain. It is observed that the suspension stroke for the front suspension is slightly larger than that of

the rear suspension stroke across all speed ranges, and a bump with a width of 1 m generates less suspension stroke compared to a bump with a width of 2 m and 3.7 m. However, a bump with a width of 3.7 m provides better ride comfort in terms of head and other body parts' acceleration at a lower speed range, as demonstrated in Fig 5.10. Similarly, according to the principle of mechanics, the formula for calculating the dynamic load on each wheel (Jin, Yu and Fu, 2016) is given as

$$Fd_{ij} = m_{wij}\ddot{Z}_{wij} - C_{sfr}(\dot{Z}_{bij} - \dot{Z}_{wij}) - K_{sij}(Z_{bij} - Z_{wij}) \quad (5.36)$$

Dynamic load behaviors on the left and right wheels for both front and rear axles are identical. Fig 5.22 illustrates the dynamic load on the front and rear wheels at a 40 Km/h vehicle speed. From the simulation curve shown in Fig 5.22**,** it can be observed that a bump with a width of 3.7 m produces significantly less dynamic load on both the front and the rear wheels. Furthermore, Fig 5.23, shows that RMS dynamic load is lower when the vehicle passes over a bump profile with a width of 3.7 m, compared to bump widths of 1 m and 2 m, for all vehicle speed ranges.

5.6 Conclusion

From an engineering perspective, it is crucial and significant to create easy and efficient biodynamic models of seated individuals. This work conducted a thorough and methodical investigation of a 4 DOF lumped-parameter biodynamic model subjected to vertical vibration to comprehend dynamic behavior. The dynamic behavior of a human

driver and a passenger car under different road input conditions is examined. The current work leads to the following conclusions.

1. The Bond Graph model was built in a modular fashion with the help of mathematical models and equations incorporated into the Symbol Shakti environment. With a better knowledge of the mechanical system interaction, the design, simulation and implementation of the previously discussed models will be more efficient.

2. This study presented the Bond Graph methodology to understand the dynamic behavior of a 15 DOF passive vehicle suspension system based on a full-car model coupled with the lumped human biomechanical model.

3. The study reveals the effect of various bump widths on human body parts as well as on the vehicle in the time domain, and the result shows that a bump with a width (3.7 m) and height (0.1 m) transmits the least vibration to the human body under 30 km/h speed. Furthermore, it causes the least bounce, pitch, and roll acceleration to the vehicle.

4. Ride comfort is observed to be better for a 3.7 m bump width (highway bump as per IRC 99 standard) at speeds as low as 10 to 25 km/h. However, acceleration becomes poor in this speed range for smaller bumps with widths of 1 m and 2 m, which are typically used as city bumps.

5. Additionally, it is observed that a bump with a width (3.7 m) and height (0.1 m) produces the least dynamic load on both the front and rear wheel compared to bumps with widths of 1 m and 2 m across all speed ranges, varying from 10 km/h to 100 km/h.

6. This study provides an in-depth investigation of the lumped parameter human models and a comprehensive understanding of the bio-dynamic responses of a driver (seated) subjected to vertical vibration. Future research could focus on the following areas:

(a) Developing the lumped parameter models with the required complexity to meet specific analytical requirements and designing novel Bond Graph controller modeling techniques.

(b) Conducting a more thorough evaluation of seat design to mitigate human vibration resulting from the interaction among the vehicle and the road profile.

The foundation for further in-depth studies and technical applications of seated human bio-dynamics is established by a 15 DOF biodynamic human and vehicle Bond Graph model. The future scope involves utilizing the developed models to enhance the comfort of the vehicles used for transportation and to achieve the objectives of a healthy and comfortable ride.

turnitin Page 206 of 269 - Integrity Submission Submission ID trn:oid:::29034:141996562

CHAPTER 6

Suspension Parameter Optimization Using Response Surface Optimization (RSM)

The previous chapter presented the analysis of an 11-DOF full car model coupled with a 4-DOF biodynamic human model under IRC: 99–1988 bump excitations to study the vibration response and ride comfort characteristics of different human body parts. The present chapter focuses on optimization of suspension parameters for the quarter car coupled biodynamic human model using Response Surface Methodology (RSM) to achieve improved ride comfort and road holding.

6.1 Introduction

In the past, the design of vehicle suspension systems has been done by trial and error, involving the designers to adjust the suspension design variables and reanalyze the system until the desired performance is obtained. This is not only time consuming, but also labor intensive. The development of computational power and analytical tools have changed the way suspension design is considered from the traditional numerical analysis

approach, to systematic design synthesis using optimization techniques. Since then, a number of optimization methods have been used to find optimal suspension properties.

In the early days work on suspension design was mainly aimed at optimizing single components, rather than a comprehensive approach to the overall performance of the system. In recent years, however, more advanced techniques have been used to optimize a number of objectives, many of which are conflicting, such as ride comfort and handling stability *(Nagarkar et al.,, 2019).* Passive suspension systems consisting of a fixed spring constant and damper have been widely studied, with factors such as optimal spring and damper device parameters to improve ride comfort being the focus of optimization efforts *(Samaroo et al., 2025)* These systems, however, have a trade-off between ride comfort and handling, so researchers are investigating adaptive and active suspension technologies *(Llopis-Albert et al., 2023)*. These are more complex systems that provide increased flexibility for adapting to different road environments and driving conditions, but also add complexity in controlling and optimizing them *(Ryazantsev & Li, 2020)*. Thus, the use of Response Surface Methodology has become a valuable method to deal with this complexity, which reduces the computational effort needed to analyze and optimize multi-variable systems (Llopis-Albert et al., 2023). This method can be used to explore large design spaces efficiently and to find the best set of parameters for the best suspension performance.

It should be noted that many of these studies are aimed at optimizing individual suspension components, rather than a complete suspension system, or at a simplified

human body response to vibration of the vehicle *(Fernandes, 2017)*. This restriction typically does not acknowledge the bio-dynamic interactions between the human occupant and the vehicle, which are important for an overall evaluation of ride comfort and possible health effects. To fill this gap, more detailed human bio-dynamic models must be incorporated into multi-objective optimization algorithms to more realistically evaluate the ride quality. This requires the creation of complex multi-physics models combining detailed biomechanical models of human occupants with vehicle dynamics. Moreover, if such detailed human models are incorporated into the optimization process, a more comprehensive assessment of the effects of vibration exposure can be performed, which results in optimized designs that not only improve ride comfort, but also improve the health and safety of the occupants *(Rezanoori et al., 2019)*

The current paper describes an extensive multi-response optimization technique on suspension parameters in a quarter-car model combined with a 4 DOF Human Biodynamic Model through Response Surface Methodology in order to improve both ride comfort and handling stability. Specifically, this research aims at identifying optimal values of spring stiffness and damper parameters which would minimize acceleration and motion sickness incidence without compromising road holding properties through comprehensive simulations in order to solve essential design issues in modern vehicles. Multi-objective optimization in the context of the problem above through RSM is extremely important as it will allow for an effective balance between ride comfort and handling stability – two factors which often conflict with each other in vehicles. The design expert software was used to perform regression and graphics for the

output response. Contour plot analysis was performed to determine the effects of input parameters on the output responses. Validity of the proposed model was checked and significant factors were identified through ANOVA.

6.2 Response Surface Methodology (RSM)

Response surface methodology (RSM) is a collection of statistical and mathematical techniques used in the development, improvement, and optimization of a process. In addition, it is also having considerable applications in the development of new product ideas, formulating new products and creating new products.

RSM is most commonly used in the industrial sector, particularly when there are more than one input that can affect the outcome of process or product attributes or performance measurements. These quality attributes or performance metrics are referred to in the response. Responses to attributes, ranks, sensory reactions are not rare, but are typically recorded on a scale along the continuum. In the real world, most applications will need a number of responses from RSM. At least, for the purpose of a test or experiment, the engineer or scientist is able to control the input variables – often called the independent variables.

In RSM, a set of mathematical and statistical tools used to create models and analyze processes that have multiple input factors that affect the response. The fundamental principle is to systematically investigate the relationship(s) among the independent variables (factors) and the dependent variable (response), so as to optimize the response. It is especially beneficial in engineering, chemical and biological studies

when experiments are time consuming and expensive, and can decrease the number of experiments needed while giving accurate predictions. It is an important subject in the design of statistical experiments. Independent components can be quantitatively expressed (Eq 6.1) in a variety of experimental situations.

$$y = f(x_1, x_2, x_3 \ldots\ldots x_k) + \varepsilon \tag{6.1}$$

Where, Y is the response; x_1, x_2, x_3, x_k are quantitative factor; '*f' is* the response function and ε is the experimental error. The response behavior can be linear, quadric or cubic. The first order linear model equation can be represented as (Eq. 6.2)

$$y = \beta_o + \sum_{i=1}^{k} \beta_i x_i + \varepsilon \tag{6.2}$$

If there is curvature in the relationship between the response and input variables, then the model must be of a higher order polynomial, specifically the second order model (Eq. 6.3), defined by, must be used.

$$y = \beta_o + \sum_{i=1}^{k} \beta_i x_i + \sum_{i=1}^{k} \beta_{ii} x_i^2 + \sum \sum_{i<j=2}^{k} \beta_{ij} x_i x_j + \varepsilon \tag{6.3}$$

where ϵ is the response error and β_i is the second order regression coefficients. The second term represents the linear effect, the third term represents the higher order quadric effect, and the interactive effects (quadric) of the input parameters are represented by the fourth terms. The use of one or both of these models is almost universal in all RSM problems. A polynomial model can be a reasonable model for the

underlying functional relationship for the entire space of the independent variables, albeit it can be a valid model for a relatively small region.

In the present study, RSM is employed to develop a mathematical model for the ride comfort through multiple regression equation. Second order models have been constructed with linear, squared and cross product terms of the independent variables. To optimize the reaction or the region of interest where the answer is found near the optimum value, the use of RSM is to perform analysis of the reaction throughout the factor space.

6.3 Central Composite Design (CCD)

In the RSM, the central composite design (CCD) is one of the most widely used designs due to its flexibility and efficiency. But CCD is not a complete 3-level factorial experiment and we can use it to make a 2nd order (quadratic) model of the response variable. It is a combination of factorial or fractional factorial runs with extra “star points” (axial points) and centre points, which enables curvature effects in the response surface to be estimated..

6.3.1 CCD Design Matrix Structure

A Central Composite Design is composed of three types of points:

- **Factorial points**: These are located at the corners of a cube, representing all possible combinations of the three factors at their high (+1) and low (−1) levels. For three factors, this corresponds to 2^3=8 factorial runs.
- **Axial (star) points**: These lie along the coordinate axes at a distance of $\pm\alpha$ from the center, while the other two factors are kept at their central level (0). For three factors, a total of six axial points (2*k)* are required. The choice of α depends on the design criterion: for rotatable CCD,
- **Center points**: This is located at the origin (0,0,0), where all factors are set at their mid-levels. Multiple center runs are usually included to provide an estimate of pure experimental error and to improve model precision. Thus, the total number of experiments in CCD is

$$N = 2^k + 2k + n_c \qquad (6.4)$$

Where, N is total no. of runs; *k* is no. of factor; n_c is number of center points. This design enables the estimation of the linear, quadratic and interaction effects of the factors. The main structure is provided by the factorial points, the curvature in the response surface is represented by the axial points, and the replicated center points are used for robustness against the experimental noise. Hence, CCD provides a more efficient design than a complete three-level factorial design to construct a complete second-order polynomial model.

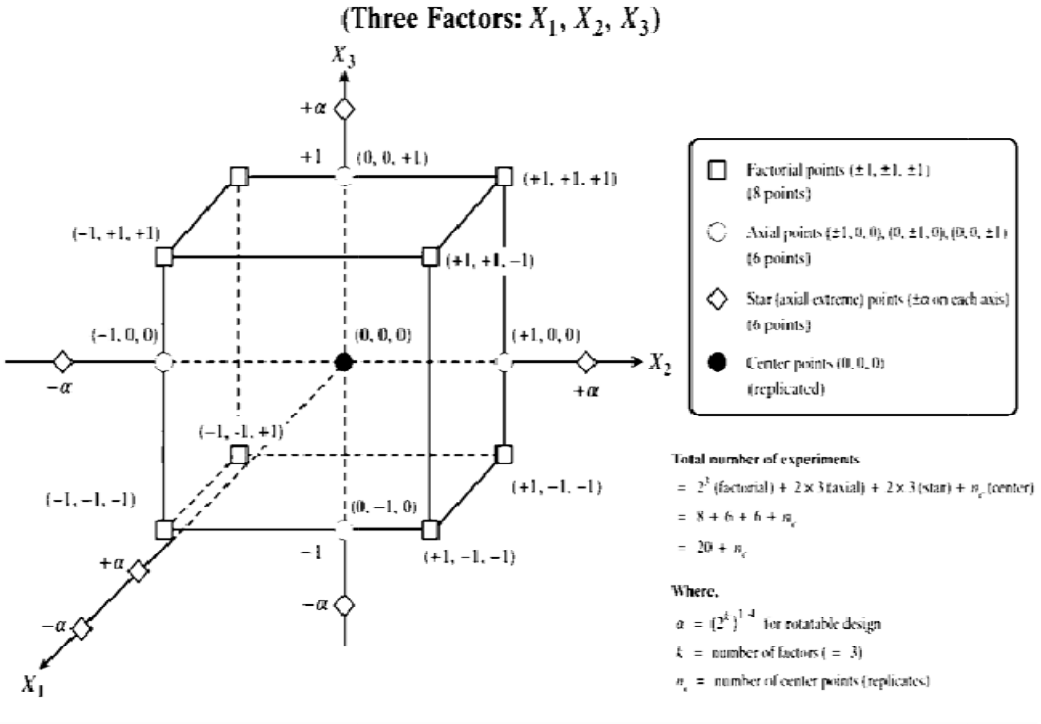


Figure 6.1 3D Central Composite Design (CCD) Layout

6.3.2 Rotatability and its Importance

The rotatable CCD is essential to RSM, from the operational and historical point of view. The analyst has to be aware that a second-order design need not be precisely rotatable. If one chooses the appropriate axial distance, α, for the CCD, rotatability can be achieved. The most successful CCD, from a variance point of view is to use $\alpha=\sqrt{k}$ and have three to five center runs, if the region of the design is intended to be spherical. This design is almost a rotational, but is not necessarily rotational. The stability and size in the spherical design zone serve as the basis for the advice.

For example, for k=3, $\alpha=\sqrt{k}$ does not provides a rotatable design. However, the loss in rotatability is actually trivial, and the larger value of results in a design which is slightly preferable based on improved stability and minimizing the average and worst-case prediction variance. Even if the requirements for rotatability were not precisely met, achieving near rotatability for a design can have the intended impact of creating strong stability of prediction variance throughout the design domain.

6.3.3 Choice of α (Alpha)

Table 6.1 Value of α for second order rotatable Central Composite Design

Variables (k)	**Factorial Points (2^k)**	**Star Points ($2k$)**	**Total Runs (N)**	**Value (α)**
2	4	4	$8 + n_c$	1.414
3	8	6	$14 + n_c$	1.682
4	16	8	$24 + n_c$	2.000
5($\frac{1}{2}$rep)	16	10	$26 + n_c$	2.000
5	32	10	$42 + n_c$	2.378
6 ($\frac{1}{2}$rep)	32	12	$44 + n_c$	2.378
6	64	12	$76 + n_c$	2.828
7 ($\frac{1}{2}$rep)	128	14	$142 + n_c$	3.364
7	64	14	$78 + n_c$	2.828

In the case of the CCD, rotatability is achieved by making a proper choice of α, the axial distance. Condition 1 above will hold as long as the factorial portion is a full $2k$ or a

fraction with resolution V or higher. The factor α denotes the radius of circle or sphere on which star points are located and its value depends upon design requirement. Generally it varies between 1 to $\sqrt{k}$. For face centered CCD (CCF) the value of α is 1 and for inscribed CCD (CCI), the value of α is less than 1 (inside factorial cube) and for rotatable CCD the value of α is given by

$$\propto = (2^k)^{1/4} \quad (6.5)$$

It is important to note that rotatability is achieved by using α as in Eq 6.5 *regardless of the number of center runs*. The value of α *in a* rotatable design is presented in Table 6.1 *(Montgomery, 2007)* for various number of design variables.

6.3.4 Benefits of Central Composite Design (CCD) over Box–Behnken Design (BBD)

Although CCD and BBD are both used second order experimental designs under RSM, CCD has several distinct advantages in most practical situations:

- The factor levels can be further extended from the factorial cube in CCD with the inclusion of axial points (α and -α) to improve detection of curvature. BBD, meanwhile, does not make experiments in a spherical or cubic area, or in the extreme corners of the design space.
- Appropriate choice of the axial distance (α) can make CCD rotatable. This will keep the variance of predictions the same at all points the same distance from the

center and make the predictions more reliable. The larger the variance in the predicted results across the experimental area the less uniform BBD is, generally not being rotatable.

- For accurate modelling when there is curvature, the inclusion of axial (star) points in CCD affords greater capability to estimate quadratic effects. BBD is not sensitive to axial points and in certain instances may not be as good as in capturing strong curvature.
- The number of factors ($k \geq 2$) can be any number, but the fewer the number of runs the better. BBD is not defined for less than three factors and will not be efficient for very high numbers of factors.
- An important part of CCD is that it contains several center points, so pure error can be directly estimated and model adequacy can be tested. BBD generally has fewer center runs, so the error estimation might not be as accurate without being replicated.
- CCD not only covers the factorial region, but also points outside the region, providing broader coverage of the experimental domain. Whereas, BBD does not involve extreme combinations of levels of the factors (no corner points), and this can be a problem if responses at the boundaries is of concern.

In summary, CCD is more flexible, more easily rotated and more sensitive to curvature than BBD. Therefore it is often desirable when a correct model for the entire design space is desired. In circumscribed designs, in particular, BBD may be more economical than CCD, but may require greater runs if the CCD is used.

6.4 CCD design and methodology

The experimental design used in the present study was the Central Composite Design (CCD), that is efficient enough to explore the design space and model quadratic relationships between the variables. The design is especially useful for multi-objective optimization problem, since it provides construction of a complete response surface with reduced number of experimental runs. In particular, running the CCD can help narrow down the variable ranges of the spring stiffness and damping coefficient to identify the optimal range of parameters for the best ride comfort results, and the results from CCD can be analyzed in a robust statistical manner. Moreover, the CCD method plays an important role in obtaining a quadratic model that helps to explain the interactions between the parameters of the suspension and the multiple responses and to gain a deeper insight into it than that offered by simpler linear models. It enables the exact determination of optimum setting that reduces undesirable vertical acceleration, incident of motion sickness and the loss of the tire/road contact at the same time.

With this experimental design, predictive models is developed which can accurately describe the complicated relationship between the main suspension design parameters and the main indicators of ride comfort. This systematic approach is essential for maximizing the performance of a vehicle's suspension system, where competing goals like handling stability, road-holding and ride comfort must be balanced. The optimization process is comprehensive to guarantee that the parameters optimized are a

true balance across the multiple performance criteria, and that the complex relationship among them is not lost.

This study considered three factors (A, B, C), which were derived from the literature and correspond to Cs, Ks and Kt respectively. All the factors were given three levels: high (+1), intermediate (0), and low (–1). The actual test variables were coded according to coding equation (Eq 6.7-6.9) where x_i represents the coded value of an independent variable, A_i is the actual value of the independent variable, X_0 is the value of the independent variable when the independent variable is at the center point, and ΔX is the step change of the independent variable. The simulations were performed with a Bond Graph model (Fig. 3.2), following the Central Composite Design (CCD) and the data obtained from the simulations are summarized in Table 6.1

Table 6.2 Levels and parameters range for CCD design

Parameters	Range	Levels		
		-1	0	1
A-Cs (N/m)	12000-20000	12000	16000	20000
B-Ks (N.s/m))	480-1480	480	980	1480
C-Kt (N/m)	120000-200000	120000	160000	200000

6.4.1 Development of mathematical model

Response Surface Methodology (RSM) is a set of mathematical and statistical methods used to maximize processes and improve product quality. Designing experiments to study the interaction of several process variables and a response of interest in a

systematic way. The result of experiments is then statistically modeled to determine the optimum parameters for desired performance. The developed regression models by RSM can also be used to predict responses for new combinations of parameters, which will save time and cost since the number of experiments will be reduced. In addition, response surface and contour plots are useful for visualizing the interaction between the input factors and output responses, which can be used to rapidly and efficiently identify the optimal process conditions. The general form of the 2nd order response surface regression model is written as below:

$$y = \beta_o + \sum_{i=1}^{k} \beta_i x_i + \sum_{i=1}^{k} \beta_{ii} x_i^2 + \sum \sum_{i<j=2}^{k} \beta_{ij} x_i x_j + \varepsilon \qquad (6.6)$$

Table 6.3 Process parameters and Output response

		Factor 1	Factor 2	Factor 3	Factor 1	Factor 2	Factor 3	Response 1	Response 2
		Actual Units			Coded Units				
Std	Run	A:Ks	B:Cs	C:Kt				RC	RH
		N/m	N-s/m	N/m	x1	x2	x3	m/s2	m
4	1	20000	1480	120000	1	1	-1	0.7788	0.00177
11	2	16000	139.104	160000	0	-1.6818	0	0.7252	0.00165
8	3	20000	1480	200000	1	1	1	0.8428	0.00192
16	4	16000	980	160000	0	0	0	0.7098	0.00162
6	5	20000	480	200000	1	-1	1	0.6438	0.00146
3	6	12000	1480	120000	-1	1	-1	0.7194	0.00164
5	7	12000	480	200000	-1	-1	1	0.4294	0.00098
2	8	20000	480	120000	1	-1	-1	0.7436	0.00169
15	9	16000	980	160000	0	0	0	0.7096	0.00162
10	10	22727.2	980	160000	1.6818	0	0	0.6842	0.00156
9	11	9272.83	980	160000	-1.6818	0	0	0.507	0.00115

14	12	16000	980	227272	0	0	1.6818	0.5748	0.00131
18	13	16000	980	160000	0	0	0	0.6418	0.00153
1	14	12000	480	120000	-1	-1	-1	0.6422	0.00146
17	15	16000	980	160000	0	0	0	0.673	0.00153
20	16	16000	980	160000	0	0	0	0.6642	0.00151
12	17	16000	1820.9	160000	0	+1.6818	0	0.9428	0.00215
19	18	16000	980	160000	0	0	0	0.6806	0.00153
7	19	12000	1480	200000	-1	1	1	0.7002	0.00159
13	20	16000	980	92728.3	0	0	-1.6818	0.6834	0.00156

Here the variables x_1, x_2, and x_k are in centered and scaled design units; the term ε is the usual random error component and y either of RC or RH, and x1, x2, and x3 are Cs, Ks, and Kt

The column 3,4 and 5 are actual units value of A, B and C, while the column 6,7 and 8 are the corresponding coded variables x_1, x_2 and x_3 where

$$x_{i1} = \frac{A_{i1}-[max(A)+min(A)]/2}{[max(A)-min(A)]/2} = \frac{A_{i1}-[20{,}000+12{,}000]/2}{[20{,}000-12{,}000]/2} = \frac{A_{i1}-16{,}000}{4000} \quad (6.7)$$

$$x_{i2} = \frac{B_{i2}-[max(B)+mi\ \ (B)]/2}{[max(B)-min(B)]/2} = \frac{B_{i1}-[1480+480]/2}{[1480-480]/2} = \frac{B_{i1}-980}{500} \quad (6.8)$$

$$x_{i3} = \frac{C_{i3}-[max(C)+min(C)]/2}{[max(C)-mi\ \ (C)]/2} = \frac{B_{i1}-[200000+120000]/2}{[200000-120000]/2} = \frac{B_{i1}-160000}{40000} \quad (6.9)$$

The α =√3 CCD is nearly rotatable. This is not surprising because α =1.682 results in exact rotatability. The slight deviation from rotatability occurs close to the design perimeter.

6.4.2 Adequacy of the developed model

The ANOVA results also demonstrate that the model developed is statistically significant ($p < 0.05$), thus confirms the suitability of the regression equation to predict Ride Comfort (RC). The main factors with the highest percentage contribution to RC are the tire stiffness (Kt) and the damping coefficient (Cs), with values of almost 70% of the total variation. This illustrates that tire compliance and damping characteristics are most important for ride comfort. The contribution of stiffness in the spring is still important but less so, ranging from 15-20% stiffness (Ks). In addition, the cross effects ($C_s \times K_s$, $C_s \times K_t$, $K_s \times K_t$) are also significant, suggesting that it is not possible to optimize one parameter at a time. The quadratic terms in the model also reveal the non-linear relationship between RC and the suspension and tire parameters. The ANOVA analysis confirms that K_t and C_s are the major factors affecting comfort and K_s is a secondary but important factor.

The developed models for RC and RH are found to be satisfactory based on the results of the ANOVA analysis within the 95 % confidence interval (CI). This is corroborated by the fact that the calculated F-ratio values for the models are lower than the standard F-ratio at 95% CI. Further, the prob > F values for three models were < 0.05 showing that the models were statistically significant and the lack-of-fit was found to be non-significant. The normal probability and residual plots also suggest that the residuals are normally distributed and this is desirable. Likewise, the model results compare well with experimental results and demonstrate a high level of correlation between the two,

confirming the model's prediction. The significance of all the coefficients were tested using F-test at 95% CI and the final predictive models for RC and RH of vehicle motion were obtained. The design of experiments, collection of data, model fitting and optimization were carefully carried out for developing these mathematical models using Response Surface Methodology (RSM). The use of appropriate statistical techniques made sure that the data was accurate and reliable. The developed equations are then correlated with the input parameters into usable empirical correlations, which provide a good relationship between the output responses and the input parameters.

RC=+0.520577 + 0.000057***Ks -** 0.000534***Cs**-1.91689E-06***Kt**-7.11250E-09***(Ks * Cs)**+1.53281E-10***(Ks * Kt)**+2.23375E-09***(Cs * Kt)**-1.84940E-09***Ks**^{2}+2.18787E-07***Cs**^{2}-1.10914E-11***Kt**^{2} (6.2)

RH= +0.001088 + 1.35698E-07 ***Ks** -1.19377E-06 ***Cs** -3.86996E-09 ***Kt** -1.56250E-11 ***(Ks * Cs)** +3.51562E-13 ***(Ks * Kt)** +5.06250E-12 ***(Cs * Kt)** -4.45608E-12 ***Ks**^{2} +4.85557E-10 ***Cs**^{2} -2.68832E-14 ***Kt**^{2} (6.3)

6.5 Optimizing the vehicle suspension parameters

Contour plots are good for parameter optimization and visually show the relationship between the process parameters and the output responses. These plots can show interaction between factors by changing any two significant factors of the model, maintaining the others constant, and determining the optimal combination of factors that result in the maximum response. After the stationary point is defined on the contour plot,

the response surface around the stationary point should be checked to determine if it is a maximum, minimum or saddle point. In this way contour plots will help not only to help predict responses, but to also identify the optimum factor regions for better responses. The developed model was tested for its adequacy through ANOVA which showed that the developed model is statistically significant at 95% confidence interval (CI) as shown in table 6.3-6.5.

Table 6.4 ANOVA results for Ride Comfort (RC)

Source	Sum of Squares	df	Mean Square	F-value	p-value	
Model	0.2187	9	0.0243	56.01	< 0.0001	significant
A-Ks	0.0487	1	0.0487	112.35	< 0.0001	
B-Cs	0.0658	1	0.0658	151.76	< 0.0001	
C-Kt	0.0149	1	0.0149	34.25	0.0002	
AB	0.0016	1	0.0016	3.73	0.0822	
AC	0.0048	1	0.0048	11.09	0.0076	
BC	0.0160	1	0.0160	36.81	0.0001	
A^2	0.0126	1	0.0126	29.09	0.0003	
B^2	0.0431	1	0.0431	99.40	< 0.0001	
C^2	0.0045	1	0.0045	10.46	0.0089	
Residual	0.0043	10	0.0004			
Lack of Fit	0.0008	5	0.0002	0.2315	0.9329	not significant
Pure Error	0.0035	5	0.0007			
Cor Total	0.2230	19				

Table 6.5 ANOVA results for Road Holding (RH)

Source	Sum of Squares	df	Mean Square	F-value	p-value	
Model	1.138E-06	9	1.264E-07	80.78	< 0.0001	significant
A-Ks	2.532E-07	1	2.532E-07	161.78	< 0.0001	
B-Cs	3.451E-07	1	3.451E-07	220.50	< 0.0001	
C-Kt	7.775E-08	1	7.775E-08	49.68	< 0.0001	
AB	7.812E-09	1	7.812E-09	4.99	0.0495	
AC	2.531E-08	1	2.531E-08	16.17	0.0024	
BC	8.201E-08	1	8.201E-08	52.40	< 0.0001	
A^2	7.326E-08	1	7.326E-08	46.81	< 0.0001	
B^2	2.124E-07	1	2.124E-07	135.69	< 0.0001	
C^2	2.666E-08	1	2.666E-08	17.04	0.0021	
Residual	1.565E-08	10	1.565E-09			
Lack of Fit	3.317E-09	5	6.634E-10	0.2689	0.9121	not significant
Pure Error	1.233E-08	5	2.467E-09			
Cor Total	1.153E-06	19				

The results of the ANOVA test for the output solutions are shown in Table 6.4 and Table 6.5. The model is adequate with all models having a huge Fisher's F value. An extended RC model has a Fisher's F value of 56.01, meaning there is a significant improvement. An F-value of the proposed model could occur due to noise with a 0.01% error chance. The Fisher's F value for LOF: 0.9329 means that the LOF is minor. The value of F should be insignificant in terms of the established model's appropriateness. Table 6.4 shows that the residual error value 0.0043, which has to be the total of significance of pure error (0.0035) and the value of LOF (0.0008). The developed model of RH was considered significant as it had a Fisher's F value of 80.78. A Fisher's value for the proposed model would occur due to noise with a 0.01% error chance. The fisher's F value for LOF was 0.9121, indicating that the LOF is minor. The value of F should be very small, compared with the suitability of the established model.

The Fisher's F value is a statistical test to ascertain if there is a significant difference in the variances of the means from different groups. The Fisher's F value for both the statistical model for predicting RC and RH are significant and reliable. The adequacy of the model was evaluated by the coefficient of determination (R^2) which values near to unity are ideal values. The R^2 values for RC and RH were 0.9805 and 0.9864 respectively, which means there is a high level of adequacy as presented in Table 6.6. The study provides valuable insights into the relationship between the response variables and the factors affecting them in vehicle behaviour.

Table 6.6 Fit statistic data for RC and RH

Parameters	Std. Dev.	Mean	C.V%	R^2	Adjusted R^2	Predicted R^2	Adeq Precision
RC	0.0208	0.6848	3.04	0.9805	0.9630	0.9487	34.6088
RH	0.0000	0.0016	2.53	0.9864	0.9742	0.9623	41.5725

6.6 Consequence of processing parameters on RC and RH

The RSM optimization technique is used for optimizing both input and output responses. Three dimensional surface and contour plots were created for the developed model with optimal parameters. These plots show the road holding and ride comfort response dependence on the input parameters: blue regions have lower responses while reddish yellow regions have high peak responses.

6.6.1 Ride Comfort Analysis

6.6.1.1 Ride Comfort (RC) variation with C_s and K_s

The response surface of damping coefficient (C_s) and spring stiffness (K_s) results (Fig 6.2) show that the damping coefficient has more effect on RC than the spring stiffness. The influence of C_s on RC is seen to be very significant when reducing C_s from it's upper range to it's lower range, which causes RC to drop by almost 25–30%. On the other hand, the variation in K_s over the range is smaller but significant (15-20%) This indicates that both parameters influence the ride comfort, but the parameter C_s is more

dominant and optimum ride comfort is obtained at low value of C_s and moderate value of K_s.

6.6.1.2 Ride Comfort (RC) variation with K_t and K_s

When tire stiffness (K_t) and spring stiffness (K_s) are varied simultaneously, K_t exerts a stronger influence on RC. The reduction of K_t stiffness from stiff to soft results in an RC reduction of around 30-35%, and shows the importance of the compliance of the tire in filtering road excitations. As described earlier, however, a variation in K_s over its range of operation varies RC by a similar 15-20%. The best comfort can be achieved if the stiffness of the tire is low (soft tires) and the stiffness of the spring is also moderate (in between), hence the RC values in the response contour are lowest as presented in Fig 6.3.

6.6.1.3 Ride Comfort (RC) variation with K_t and C_s

In Fig 6.4, the cross correlation of K_t and C_s again highlights their strong influence. The greatest noticeable difference occurs in the stiffness of the tire, which is expressed by the RC value: a change from a stiff to a soft tire results in an improvement of 30–35% in RC value. Another important factor is the damping coefficient (C_s) - a lower Cs from higher to lower, brings down RC by about 20 – 25%. It is now established that both are important in determining ride comfort. The best condition is when K_t is minimized and C_s is kept in the lower to moderate range, in which the RC values are lowest.

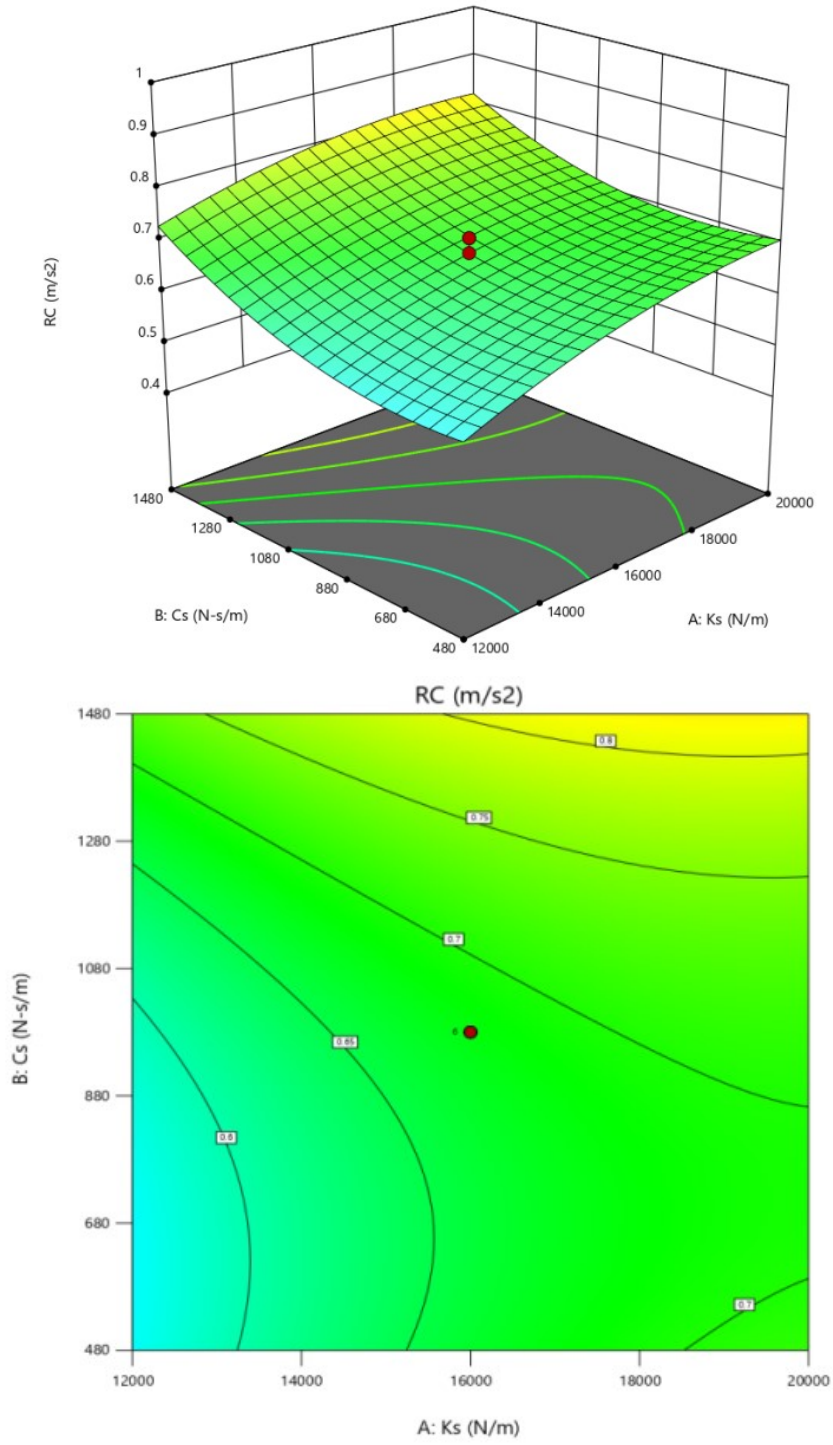


Figure 6.2 3D response contour and surface plot of Ride Comfort (RC) variation with C_s and K_s

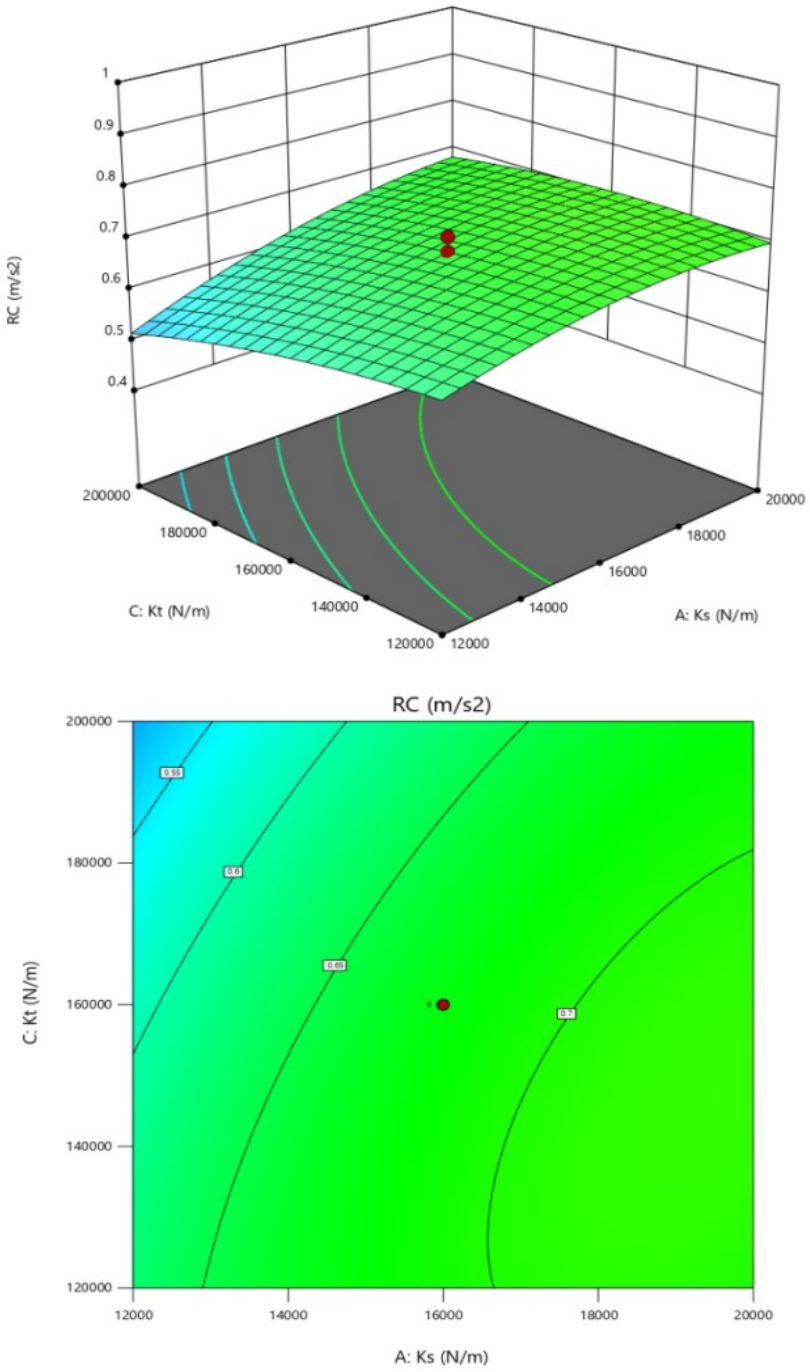


Figure 6.3 3D response contour and surface plot of Ride Comfort (RC) variation with K_t and K_s

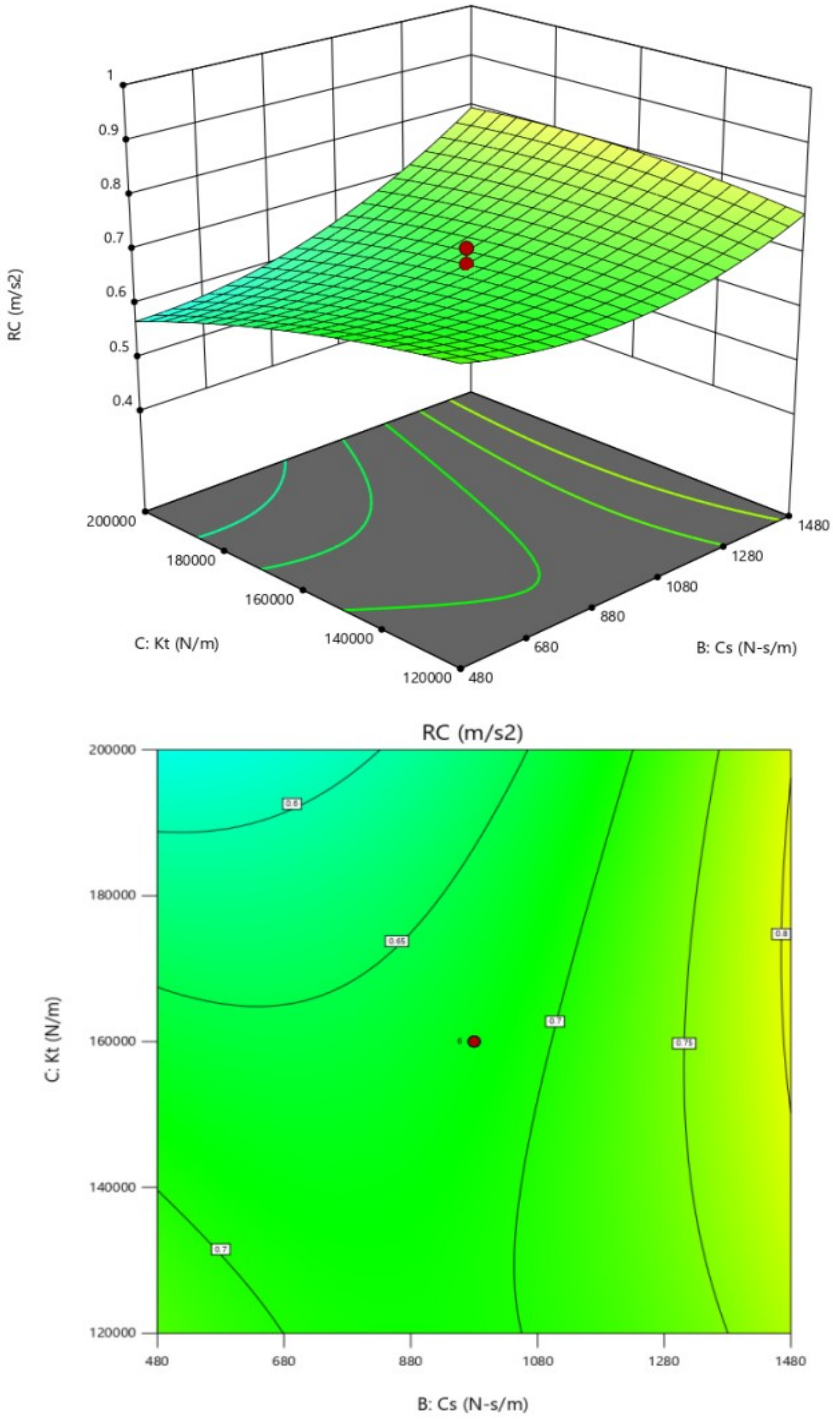


Figure 6.4 3D response contour and surface plot of Ride Comfort (RC) variation with K_t and C_s

6.6.2 Road holding Analysis

6.6.2.1 Road holding (RH) variation with C_s and K_s

The surface and contour plots (Fig 6.5) show a non-linear and smooth relationship between the surface parameters of the road holding (RH) and the damping coefficient (C_s) and the stiffness of the suspension (K_s). In general, the stiffer the suspension, the more positive the RH, suggesting that the stiffer the suspension, the less deflection of the tires and, thus, the better the tires hold the road and the greater the RH. This improvement, however, is not very large: as the stiffness increases, the improvement is diminishing. Meanwhile, the influence of the damping coefficient (C_s) on RH is more noticeable. At lower values of C_s, RH is relatively lower, that is, less good contact with the road as there is insufficient energy dissipation. As Cs increases, RH will improve up to an optimal region in which damping will be able to suppress oscillations. In this area, the further increase of C_s does not significantly increase the value, while the value shows a slight decrease, suggesting the over-damping feature. This is supported by the contour plot that indicates a gradual gradient; the optimal RH is around moderate values of K_s and C_s. In general, the optimum range of RH is set in the middle to provide an optimum level of vibration control and tire road contact.

6.6.2.2 Road holding (RH) variation with K_t and K_s

Both the 3D surface and contour plots (Fig 6.6) shows that the variation of road holding (RH) with respect to suspension stiffness (K_s) and tire stiffness (K_t) has a smooth and nonlinear relationship. It can be seen that RH improves as the suspension stiffness (K_s)

is raised. This is because the stiffer the suspension the less it will move the body and the more likely it is to keep the tyre in contact with the road surface. However, for moderate values of Ks, the rate of improvement diminishes, which is a signal of effects of increased system rigidity, or diminishing returns.

Likewise, the stiffness of the tire or wheel (K_t) significantly affects the value of RH. An increase in K_t will also result in an increase in RH, indicative of better road contact as tire deformation is reduced. A firmer tire is better at reacting to the road's irregularities and is better able to maintain grip. However, when K_t is too large, a flatter response surface results, suggesting that the increases are relatively small.

This behavior is further emphasized by the contour plot, which indicates a smoother variation in the RH values and the optimal range is at moderate values of both K_s and K_t. In summary, the optimal road holding occurs when the suspension stiffness and tire stiffness are both high, but not too high or too low, so that the stability is improved but not so great as to make the vehicle harsh, or too compliant as to cause poor road holding.

6.6.2.3 Road holding (RH) variation with K_t and C_s

The surface and contour plots (Fig 6.7) demonstrate the coupled and nonlinear nature of the variation of RH with respect to C_s and K_t. The stiffness of the tire (K_t) has a significant effect on the RH; as K_t goes up, RH goes up, meaning the tire–road contact is better because the tire is less deformable. A harder tire will have a better ability to transfer road inputs which will increase the level of road holding. Once a certain level is

exceeded, however, the benefit of increased stiffness is diminished, indicating that too high a stiffness may result in decreased benefit.

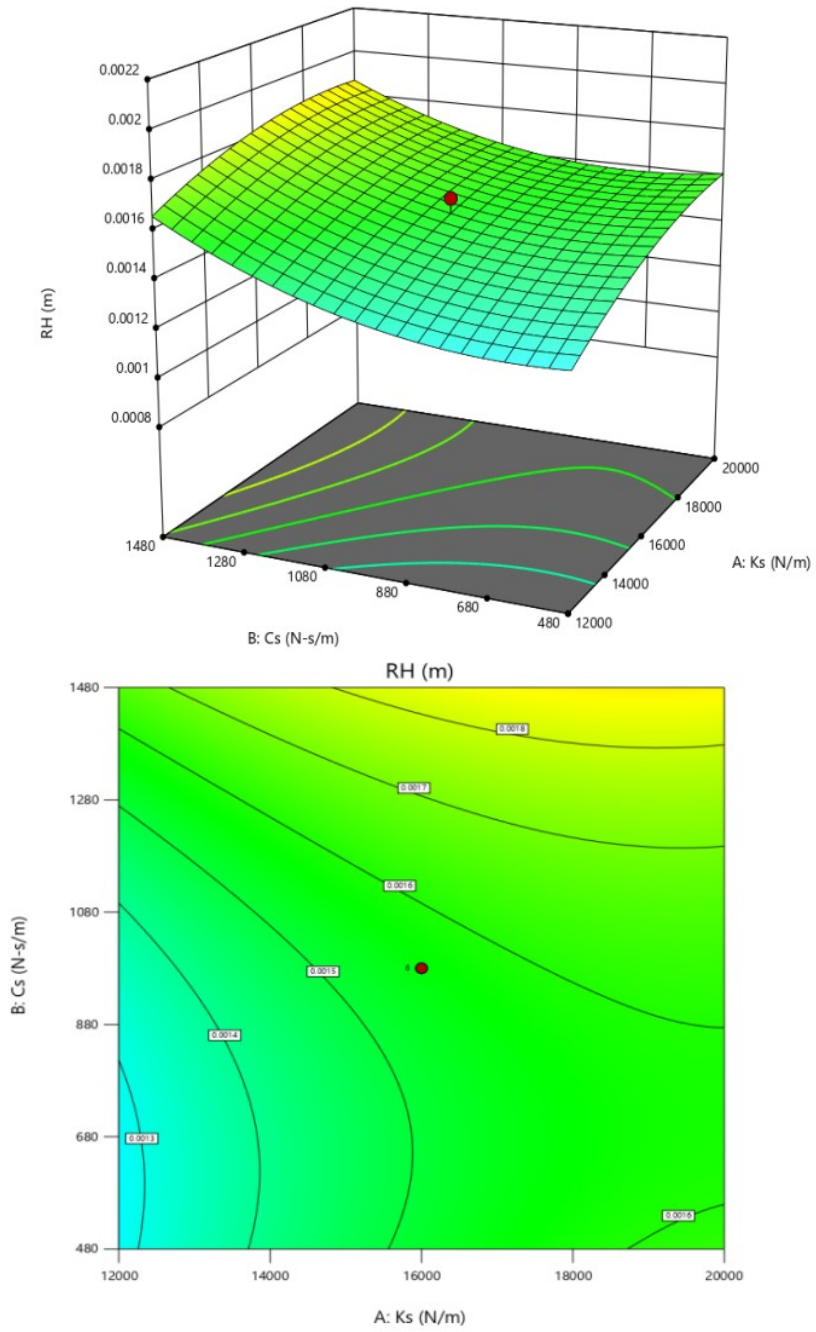


Figure 6.5 3D response contour and surface plot of Road Holding (RH) variation with C_s and K_s

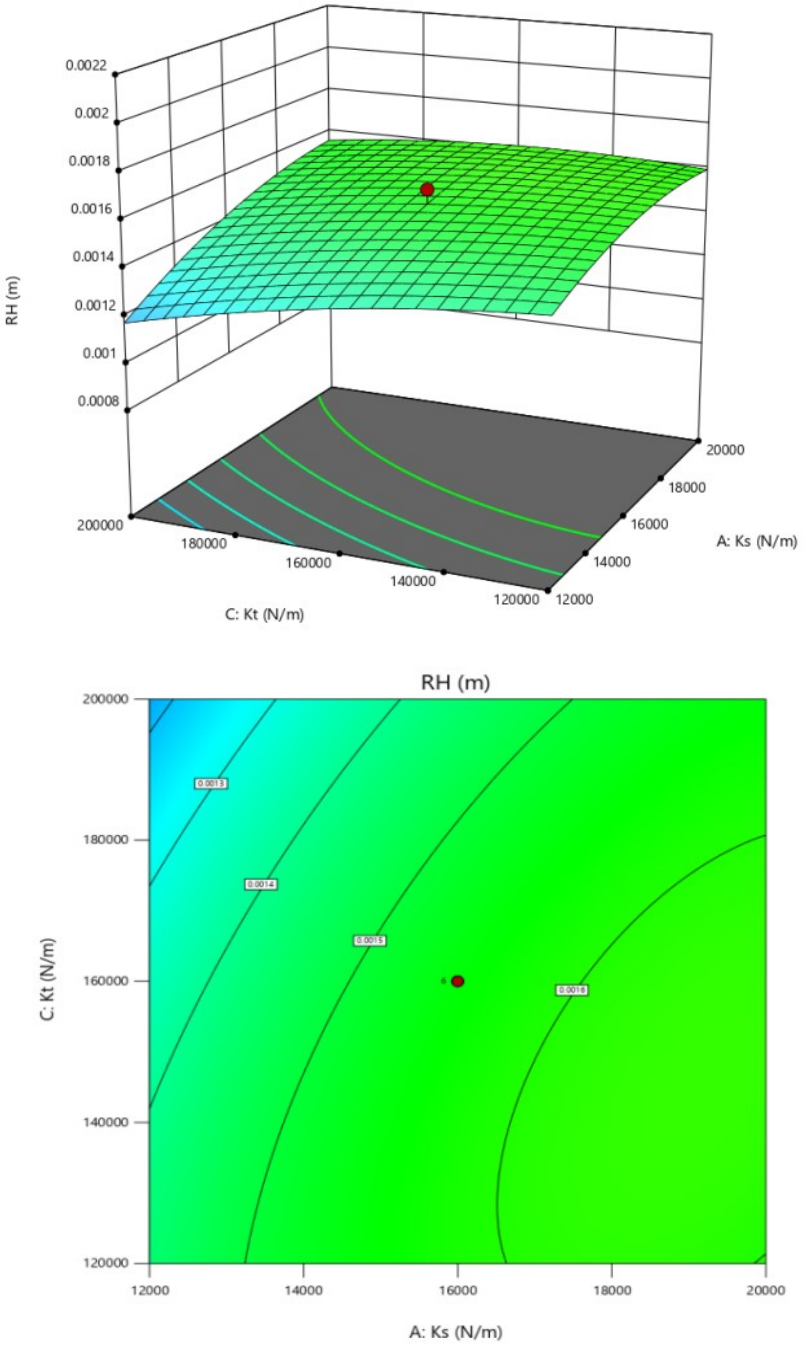


Figure 6.6 3D response contour and surface plot of Road Holding (RH) variation with K_t and K_s

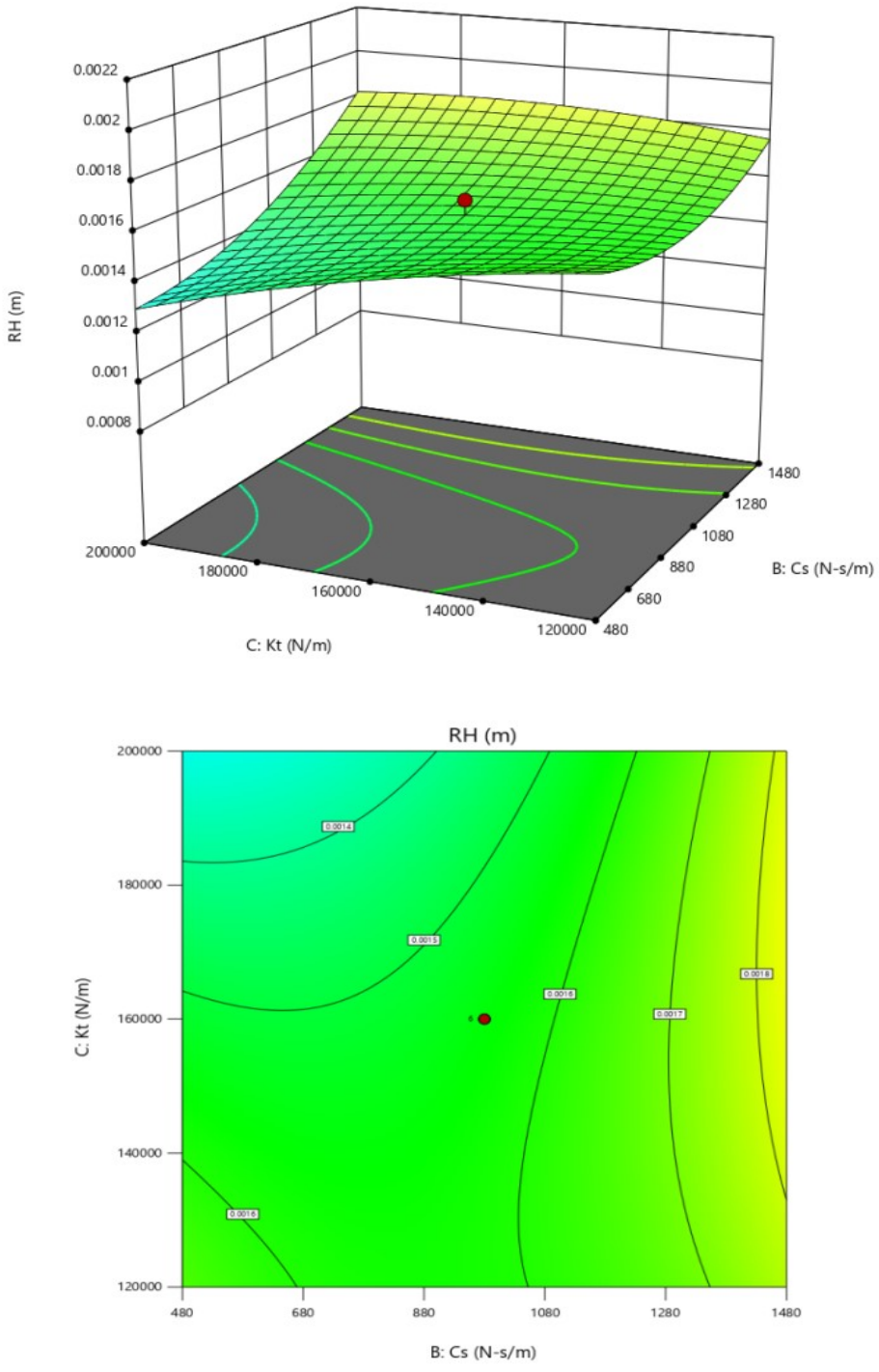


Figure 6.7 3D response contour and surface plot of Road Holding (RH) variation with K_t and C_s

The effect of the damping coefficient (C_s) on RH is more subtle. At lower values of Cs, the RH is relatively poor, since the suspension does not have enough ability to control the oscillations. The increase in RH is attributed to increase in the energy dissipation and decrease in amplitude of the vibrations as C_s increases. More C_s, however, after a maximum damping effect, does not significantly improve RH, and may even slightly dampen performance, causing the suspension to "over-damp" because it responds too slowly.

This is confirmed by the contour plot where gradients are smoother and optimal values are found around moderate C_s values and relatively high k_t values. In general, if the stiffness of the tires is high enough and they are damped at an optimal middle ground, then they will exhibit good road holding without sacrificing response.

The developed model has shown good predictive accuracy for the responses of the output, as shown in Fig 6.8. The agreement between the predicted and experimental values in the scatter plot, along the 45° line, suggests that the model is a good representation of the behaviour of the underlying system. The standard deviation of the deviations from the predicted values is also approximately the same throughout the period confirming that the residuals are random and unbiased. The high correlation between the predicted and observed data is good, indicating the reliability of the model and its ability to accurately represent the patterns and dependencies in the data. It can therefore be safely used to make predictions for new or untried conditions.

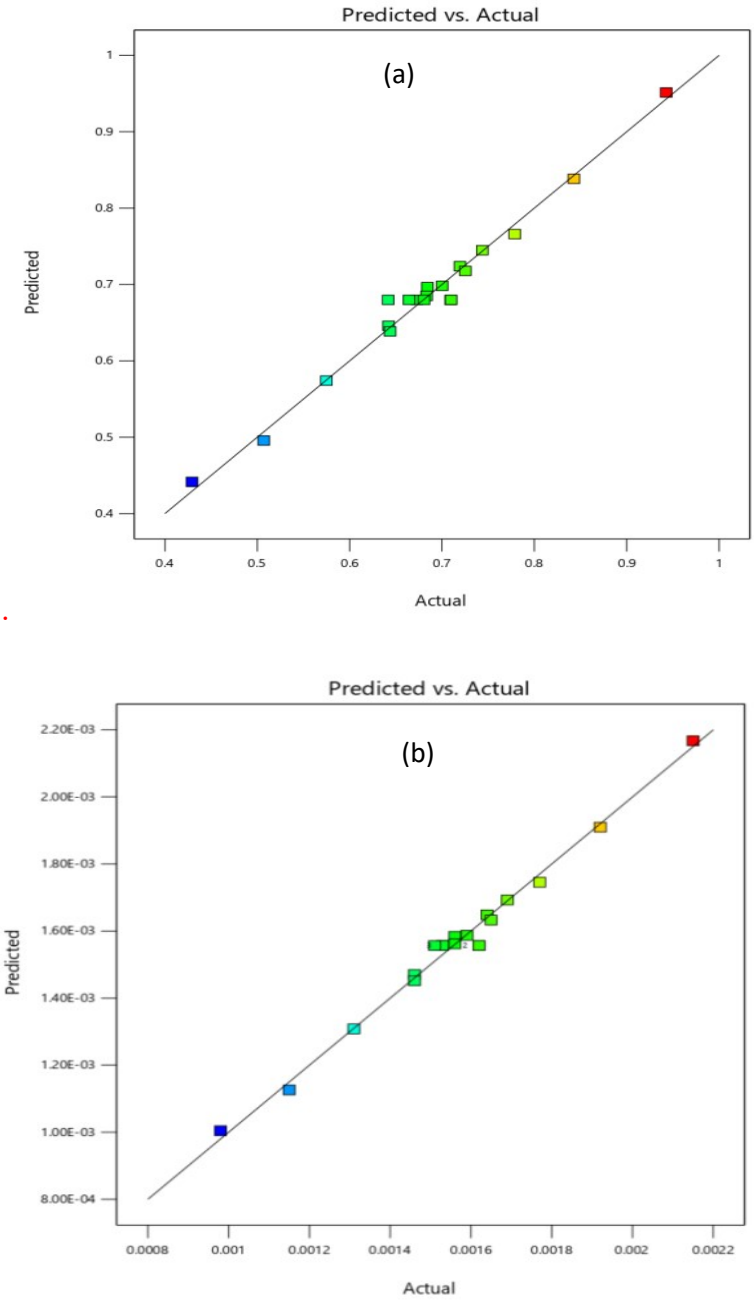


Figure 6.8 Predicted vs. actual scatter plot (a) RC (b) RH

A graphical display of the sensitivity of suspension parameters (Ks, Cs and Kt) with regard to vehicle ride comfort is achieved using the perturbation curveas shown in Fig 6.9. It shows how the performance of each parameter changes when the parameter value

is slightly altered around a chosen value in the design space and how this affects both ride comfort and road holding. The sensitivity (steepness) of the curve corresponds to the influence of the corresponding parameter on the ride comfort.

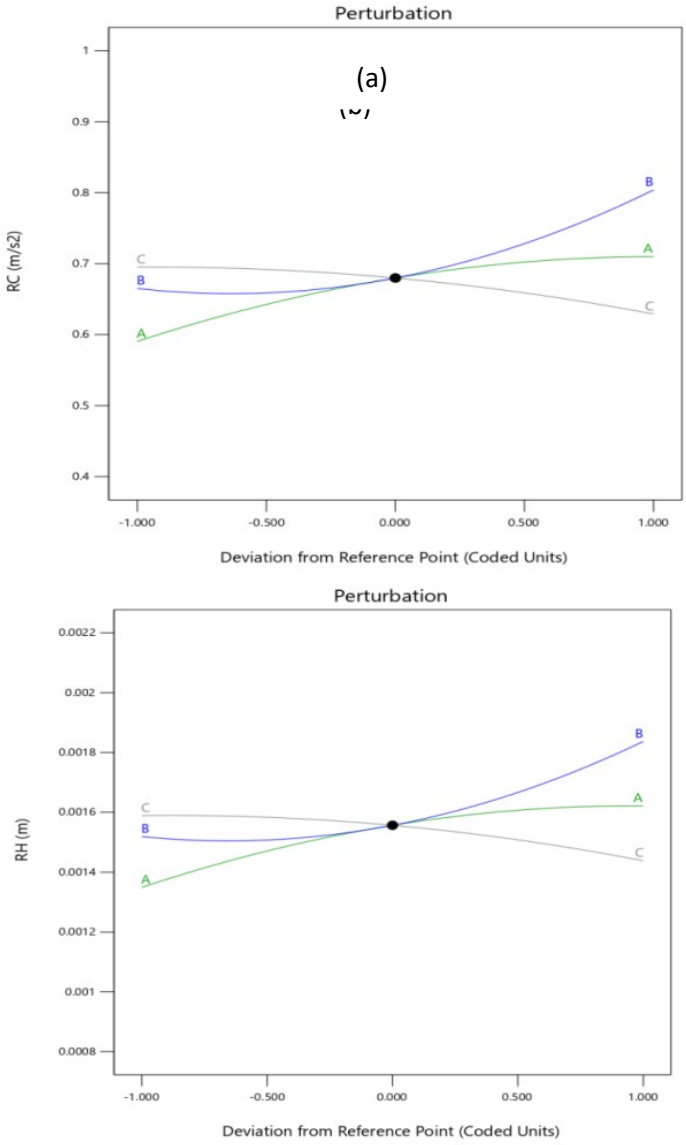


Fig 6.9 Perturbation curve (a) RC (b) RH

6.7 Suspension parameters Optimization for ride comfort and road holding with desirability

In designing a vehicle's suspension system, performance characteristics such as ride comfort, suspension travel, vehicle durability, and stability play a critical role. Among these, **ride comfort and vehicle stability** are the most significant attributes. In the present thesis, ride comfort has been selected as the **primary criterion** for identifying the optimal suspension configuration, while ensuring that the stability requirement (road holding) is simultaneously satisfied. Accordingly, the range of suspension parameters has been defined to maintain vehicle stability across all selected values. Based on these considerations, the optimization problem can be formulated as follows:

RC min and RH=0

Subjected to

$$12000 \text{ N/m} \leq Ks \geq 20000 \text{ N/m}$$

$$480 \text{ N.s/m} \leq Cs \geq 1480 \text{ N.s/m}$$

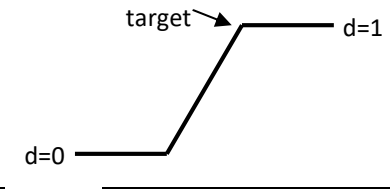
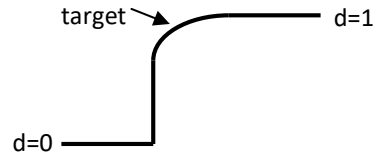
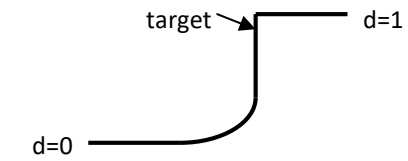
$$160000 \text{ N/m} \leq Kt \geq 200000 \text{ N/m}$$

The response optimizer determines a response's desirability using a transfer function. *Derringer and Suich (1980)* introduced the desirability function approach as a method for multi-response optimization. A function's desirability is determined by the response's value, which is translated on a scale from 0 to 1 and indicates the degree to which the response's defined goal has been met. Depending on the optimization goal, as indicated in Table 6.7, the form of the desirability function is determined by specifying "Weight," which shows its distribution on the interval between the minimum (or maximum) value and the target. By appropriately assigning weights, the relative importance of each

response can be adjusted according to the design objectives. The method is fundamentally based on the reduced gradient algorithm, which iteratively searches for the optimal parameter combination. After evaluating several potential solutions, the algorithm determines the configuration that yields the highest composite desirability. The underlying concept of this approach is that a process or product is considered unsatisfactory if any of its quality characteristics lie outside the specified "desirable" range *(Candioti et al., 2014)*. To have a high desirability, the response should be closer to the goal value when the weight is higher.

Individual desirability and composite desirability are the two categories of desirabilities. Individual desirability is computed for each response independently and evaluates the optimization quality of a single response. Table. 6.7 illustrates how individual desirability depends on the optimization's goal.

Table 6.7 Weight and their effect on desirability function

For weight = 1 As the response gets closer to the target, desirability rises linearly. Target and bound are given equal weight.	
For weight < 1 Desirability increases even if response is within the specified limit even if it is away from its target.	
For weight > 1 Higher desirability can be attained by having a response that is as close to the aim as possible.	

Desirability is only 1 when the response reaches the target value for the targeted goal, is greater than the target for the maximization goal, or is less than the target for the minimization goal. It is zero if the response is outside the bounds for the targeted goal, less than the lower bound for the maximization goal, or higher than the upper bound for the minimization goal. The estimated individual desirabilities are 1.000 and the optimal settings of all the elements have been acquired at their highest desirabilities because both the RC and RH have achieved values that are much below the stipulated aim in a minimization goal.

In the case of a mult-response system, composite desirability is the weighted geometric mean of all the individual desirabilities and indicates how well the setings optimize a set of responses. The composite desirability should be at its highest level for an ideal solution. In this case, the maximum Composite desirability of 1.000 is attained with the equal weight and importance of I for both responses, thereby confirming the attainment of an optimal and "close to target" solution. To increase the effect of more important response in composite desirability, importance value is specified, which shows the relative significance of a response as compared to the other.

The two objective functions – Ride Comfort (RC) and Ride Holding (RH) – were optimized together by the multi-response optimization approach in the vehicle dynamic simulation. The optimum results found were minimum values of RC as 0.492147 m/s2 and RH as 0.00124243 m. As a result, the optimal parameters of the suspension have

been optimized to be Ks = 13,883.6 N/m, Cs = 588.166 N•s/m, and Kt = 1,89,460 N/m respectively shown in Fig 6.10. The optimized values suggest that the suspension system is finely tuned to provide the desired ride and handling characteristics. In addition, the optimized set of parameters is the best combination of spring stiffness, damping coefficient and tire stiffness required to improve the ride comfort and ride holding of the vehicle.

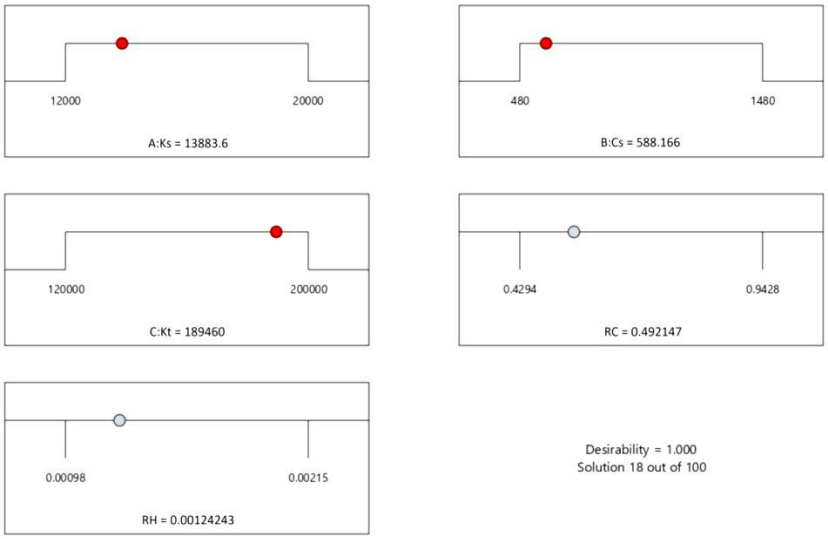


Fig 6.10 Ramp chart with optimized parameters for output response RC and RH with desirability

6.8 Result Comparison (Passive vs. Optimized)

The results of Fig.6.11 and Table 6.12 show that there is decay in corresponding amplitudes after optimization thus indicating improvement in ride comfort. This implies that for the same road input, the disturbance experienced by the body and sprung mass settled faster for the optimized setting. Upon calculating RMS responses, the optimized

suspension parameter reduces the driver's vertical acceleration by 23.32% when compared to passive suspension for sinusoidal motion. Further there was reduction of 23.71%, 16.69%, 11.14% in acceleration in other body parts (Upper torso, Lower torso, Pelvis) and seat respectively.

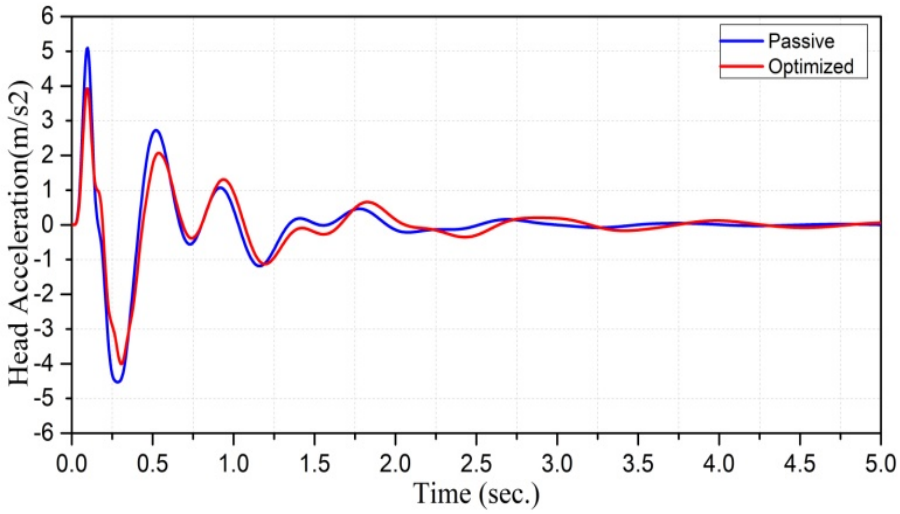


Fig 6.11 Head acceleration comparison for passive vs optimized suspension parameter

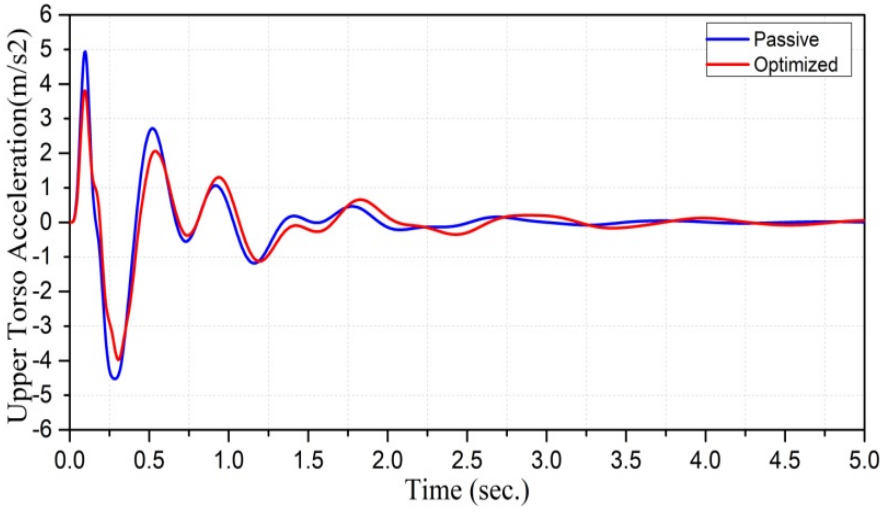


Fig 6.12 Upper Torso acceleration comparison for passive vs optimized suspension parameter

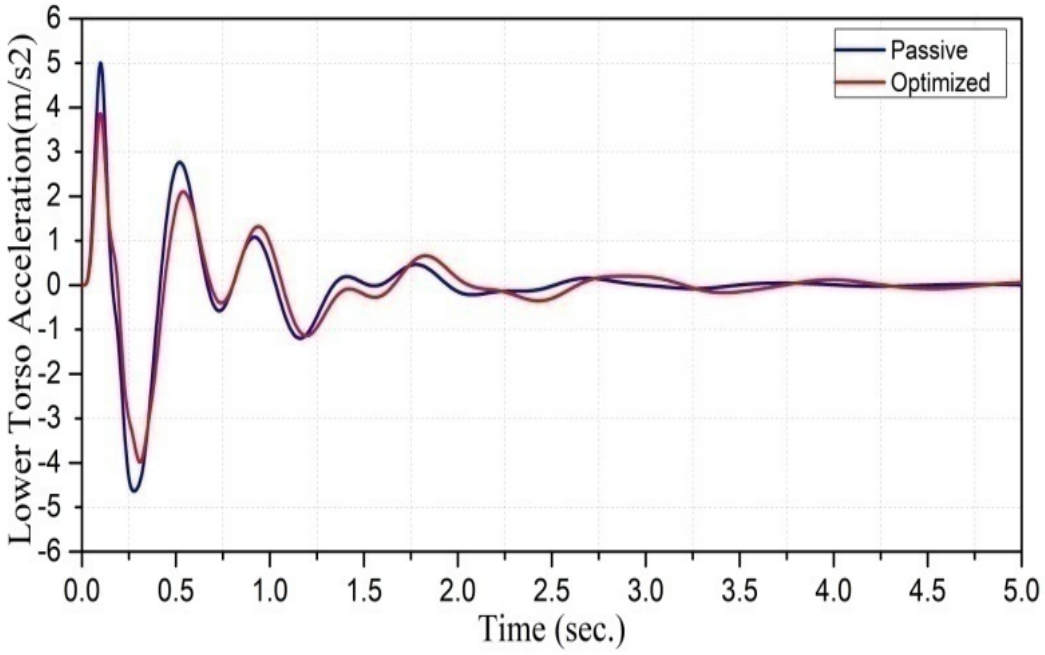


Fig 6.13 Lower Torso acceleration comparison for passive vs optimized suspension parameter

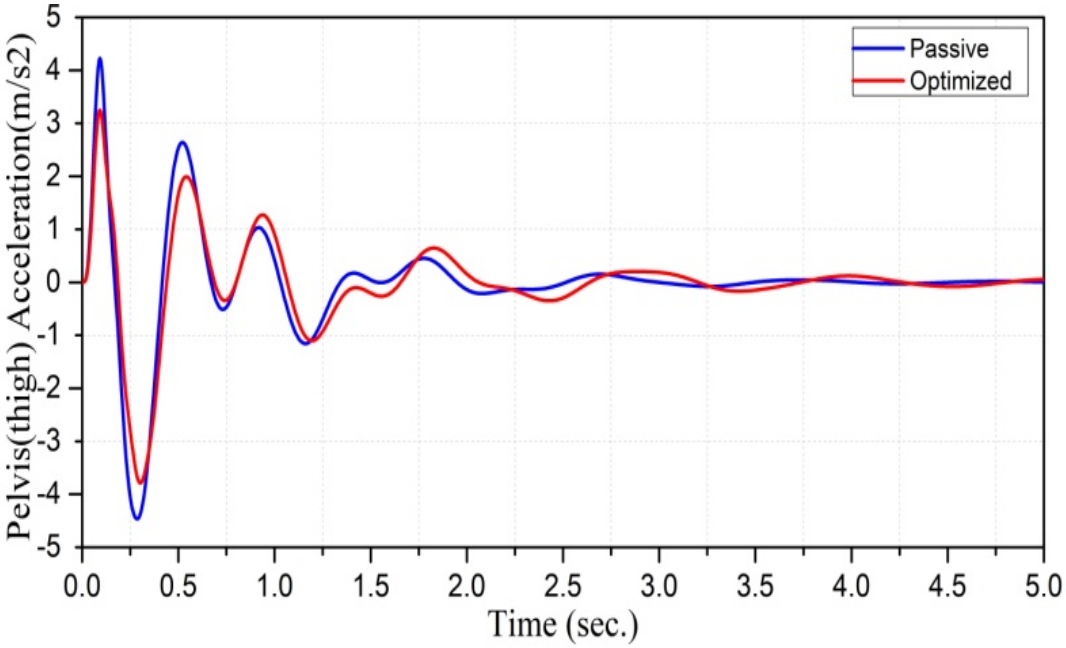


Fig 6.14 Pelvis (Thigh) acceleration comparison for passive vs optimized suspension parameter

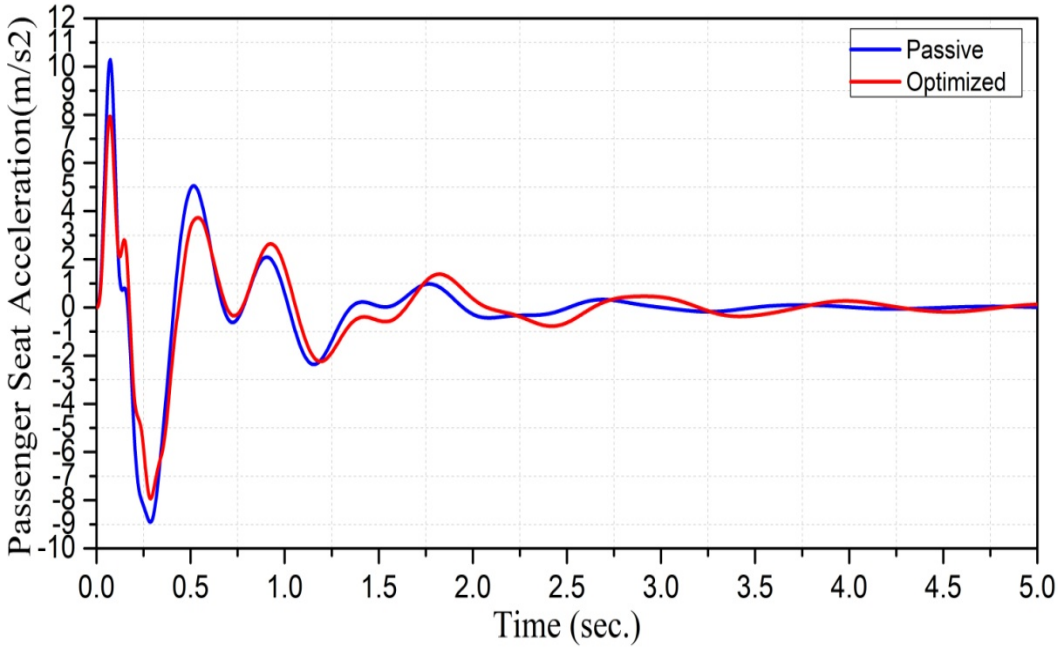


Fig 6.15 Seat acceleration comparison for passive vs optimized suspension parameter

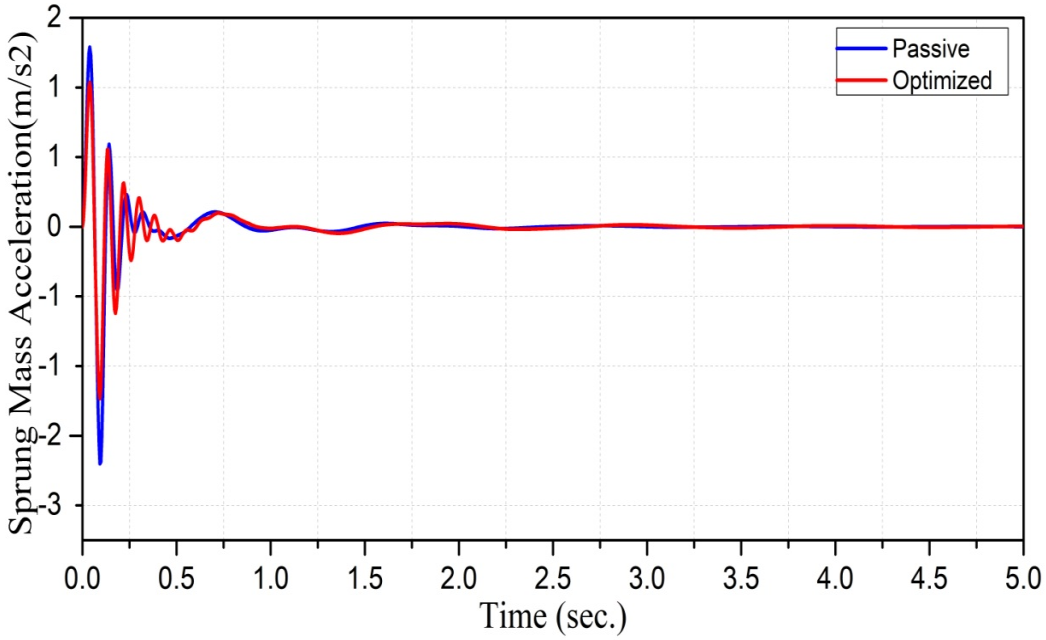


Fig 6.16 Sprung Mass acceleration comparison for passive vs optimized suspension parameter

Table.6.8 RMS Acceleration Improvement (r

	Head	Upper Torso	Lower Torso	Pelvis	Seat	Sprung Mass
Passive	0.6418	0.6324	0.5883	0.5624	1.13475	0.24674
Optimized	0.4921	0.4824	0.4901	0.4997	0.98563	0.19863
Percentage Improvement	**23.32%**	**23.71%**	**16.69%**	**11.14%**	**13.14%**	**19.49%**

6.9 Conclusion

This work investigated the optimized parameter for vehicle comfort in terms of ride comfort and road holding using RSM technique and observes following conclusions. Validated computation model using bond graph was used to perform 20 experiments for various vehicle parameter combination as per CCD model to implement RSM methodology for the purpose of obtaining optimal parameters.

The present study was successfully able to optimize the parameters of suspension system for the coupled quarter-car and 4-DOF biodynamic human model using Response Surface Methodology (RSM). The derived optimization framework was able to correctly identify the contributions of the important suspension parameters – suspension stiffness, damping coefficient, and tyre stiffness - to ride comfort characteristics. The statistical modelling and optimization method allowed the systematic investigation of the interactions and contribution of the parameters to the vibration transmission.

An optimized suspension configuration led to a marked decrease of the acceleration of the sprung mass, of the acceleration of the seat and of vibration transmission to various parts of the human body. The optimized parameters led to reduced vibration response, as verified, which showed a significant improvement of the ride comfort of the vehicle and reduced exposure of the human body to whole-body vibration. The findings also suggested that the selection of the suspension parameters is of vital importance to regulate resonance behavior and to improve the overall dynamic stability of the vehicle–human system.

The response surface plots and optimization results showed that damping and suspension stiffness are the most important parameters that influence the ride comfort performance. The optimized model had better vibration isolation performance than the original suspension model for various road excitations. Moreover, the optimization results also matched well with simulation results and this ensured the applicability of RSM as an efficient statistical optimization technique for suspension design problems.

In general, the study confirmed that Response Surface Methodology is a reliable and computationally efficient method for optimization of suspension parameters of coupled vehicle–human systems. The optimized suspension system resulted in improved ride comfort, vibration transmissibility reduction and enhanced passenger safety, proving the feasibility of the proposed methodology for advanced suspension systems design.

turnitin Page 248 of 269 - Integrity Submission Submission ID trn:oid:::29034:141996562

CHAPTER 7

CONCLUSION, FUTURE SCOPE AND SOCIAL IMPACT

7.1 Conclusions

1. This work has resulted in two models for a coupled vehicle–human system that can effectively describe the dynamic interaction in the system under a broad range of road excitations.

2. It was determined that the human exposure to vibration is highly dependent on the frequency of the excitation and the degree of roughness of the road profile, and that the roughness of the road classes caused higher peaks in the acceleration when analysed according to ISO 8608.These roads were analysed in terms of sinusoidal, trapezoidal, square and ISO 8608 road characteristics, and the results indicated that human vibration exposures were strongly correlated with the degree of road

roughness and the frequency of the vibration exciting factors, with higher acceleration peaks experienced on the rougher road classes.

3. The biodynamic human model showed that the lumbar and upper torso regions are most susceptible to transmitted vibrations, aligning with ISO 2631 comfort criteria and validating the modelling approach.

4. The Bond Graph–based modelling framework offered a physically consistent and modular way to simulate the suspension–human system yielding accurate energy domain representation of the systems behaviour.

5. The integration of the PID controller system into the Bond Graph model system led to significant reduction of vertical acceleration and vertical displacement at the seat and important body segments which contributed to the overall improvement of the ride comfort.

6. Through the comparison between the fractional-order PID (FOPID) controller and classical PID, the ability of fractional-order PID to control vibration is obviously better than classical PID, which illustrates the advantage of the application of fractional calculus in vibration control.

7. Through full-car simulation with a 11-DOF model, a strong influence of pitch, roll and multi-axle interaction on passenger comfort has been demonstrated, particularly under transient disturbances such as the IRC:99:1988 bump.

8. The full car results verified the importance of the location of passengers and the seat–vehicle coupling for its vibration transmissibility and demonstrated the failure of the simplified models for the assessment of real-life comfort.

9. Response Surface Methodology provided a systematic approach to optimise the parameters of the suspension, determining the most significant ones, and provided an optimised suspension configuration that enhanced the ride comfort.

10. The optimum parameters resulted in a significant reduction of the human body acceleration and the level of vibrations, hence the use of RSM as a powerful optimization tool for suspension design was justified.

11. Correlation between simulation results and experimental values obtained from the test rig showed excellent results, which further substantiated the validity of the Bond Graph model.

As a whole, the present research work presents a complete approach involving modeling, control, full vehicle simulation, and optimization, which will aid in increasing ride comfort in future suspensions.

7.2 Future Scope

1. The present work could be extended to develop and analyze of semi-active and full-active suspension systems with advanced actuators like magneto rheological (MR) dampers, hydraulic actuators, and electromagnetic suspension system, which would provide a better vehicle stability and ride comfort.
2. The current 4-DOF biodynamic human model can be expanded to a higher degree-of-freedom biomechanical human model with detailed spinal dynamics, neck motion and nonlinear properties of the body segments to obtain more realistic human vibration analysis.

3. Future research could consist of the inclusion of nonlinear suspension characteristics, including nonlinear springs, nonlinear tyres and hysteresis damping for the purpose of enhancing the model's accuracy in severe road excitations and high speed driving conditions.

4. The proposed control strategies can be validated through real-time implementation of the developed controllers on the Hardware-in-the-Loop (HIL) or embedded control platforms to validate the effectiveness and practical feasibility of the proposed control strategies.

5. The proposed Bond Graph framework can be combined with Artificial Intelligence (AI) and Machine Learning (ML) tools to enhance the suspension control system and predict intelligent rides under different road and load conditions.

6. Advanced optimization techniques such as: Genetic Algorithm (GA), Particle Swarm Optimization (PSO), Differential Evolution (DE) and Reinforcement Learning may be explored in order to fine-tune suspension and controller parameters for more efficient tuning.
7. Future work could examine the relationship between driver posture, seat ergonomics, age, BMI, and anthropometric differences with ride comfort, as a way to create individualized vibration mitigation techniques.

8. The full car model can be expanded to incorporate steering dynamics, braking effects and lateral vehicle dynamics, allowing for the analysis of ride comfort, road handling and stability to be evaluated together.

9. On-road vehicle testing can be further validated experimentally using vehicles under real traffic conditions and various environments with varying vehicle speeds, payload conditions, road surface irregularities.

10. The developed methodologies can be easily adapted for the application of Electric and Autonomous Vehicles (EVs/ AVs): Engine noise is decreasing, and cabin configuration is changing, so passenger comfort is becoming more important.

11. Future work should also consider the long-term health effects from exposure to WBV, particularly commercial vehicle operators who are exposed to rough road surfaces for extended periods.

12. The integration of the developed ride comfort models with the digital twin technology and smart vehicle monitoring systems could enable real-time prediction of the passenger comfort and suspension condition.

These future directions offer ample potential to further develop vehicle suspension research and design of intelligent, adaptive, and human-centric ride comfort systems for future transportation technologies.

7.3 Social Impact of the Research

7.3.1 Improvement in Passenger Ride Comfort

The present research is an important contribution to enhance the passenger ride comfort by reducing the transfer of harmful vibrations from the vehicle suspension system to the human body. In modern vehicles, road conditions can change constantly, leading to discomfort and fatigue for passengers due to continuous vibrations. The optimized suspension parameters and the developed coupled vehicle–human models aid in the decrease of vertical acceleration experienced by the occupants. This enhancement will make the travel experience better for passengers in long-haul or regular travel trips. The suggested methodologies can then contribute to the design of comfort oriented vehicles in the future.

7.3.2 Enhancement of Human Health and Well-Being

Exposure to whole body vibration can trigger negative health impacts like lower back pain, spinal stress, muscle fatigue, and neck and upper torso discomfort. In the present study, the vibration response of the sensitive human body segments was specifically studied by using a biodynamic human model. The study to pinpoint affected body regions and the mitigation of transmitted vibration, using advanced control and optimization, is an important step towards healthier transportation environments. Minimizing vibration exposure can enhance physical health, mitigate occupational health hazards for drivers, and contribute to safer work practices.

7.3.3 Reduction in Driver Fatigue and Physical Stress

One of the primary reasons for poor driving efficiency and road crashes is driver fatigue, particularly on rough roads over extended distances. Over-exposure to vibration causes discomfort, stress, decreased concentration and slower reaction times. The benefits of PID, fractional PID control and optimized suspension parameters make a significant contribution to alleviating physical stress on drivers. Improved ride quality ensures driver alertness and minimizes driver mental and physical fatigue, leading to safer and more efficient driving conditions. Commercial vehicle operators, public transport driver and applications for heavy vehicles are especially affected

7.3.4 Contribution toward Road Safety

Low ride quality, and high vibration levels in the vehicle can adversely affect steering control, braking and driving comfort, particularly on rough roads and speed bumps. The proposed research aims to contribute indirectly to the issue of road safety by studying the performance of vibration isolation and vehicle stability under various road excitations. The addition of transient bump analysis based on IRC:99:1988 profiles further enhances the relevance of the work to actual road conditions. Better suspension performance can help prevent driver discomfort related errors and enhance the control of the vehicle, which can help to contribute to safer transportation systems and minimise accident risk.

7.3.5 Advancement in Intelligent Suspension Technology

The research presents the modern modeling and control techniques, such as the Bond Graph model and fractional-order PID control, of vehicle suspension systems. The methodologies are the basis for the development of intelligent and adaptive suspension technologies that can adapt themselves based on varying road conditions automatically. These intelligent suspensions can contribute in many ways to the development of future automotive engineering, improving the overall comfort, vehicle stability and transportation safety. The study also aims to promote the incorporation of modern control methods into real-time automotive applications.

7.3.6 Promotion of Human-Centric Vehicle Design

In traditional automotive suspension system designs, emphasis has been more on performance and stability of the vehicle rather than on the vibration behavior of humans. Through the research carried out, it becomes possible to adopt a human-centered approach whereby biodynamic models of human beings are incorporated in the analysis of the automobile suspension system. In this way, issues related to the health and comfort of the passengers are given equal importance while designing new automobiles.

7.3.7 Industrial Relevance and Automotive Applications

The optimization of suspension systems and control algorithms achieved in this study has high practical value to the industry. Car companies always look for new suspension solutions that allow greater ride comfort without losing vehicle dynamics. These models and optimization algorithm will help automotive engineers in the designing and testing processes of various cars and buses. The findings of the study will also help in reducing development time and increasing customer satisfaction.

7.3.8 Relevance for Developing Road Infrastructure Conditions

Most emerging economies have highly varying road profiles, characterized by potholes, rough road surfaces, and poorly designed speed breakers. In these types of road profiles, vehicle occupants usually have to bear high levels of vibrations. The current study investigates the effects of various road profiles, including the ISO and IRC road profiles

on the response of a passenger vehicle. These results may help design more suitable vehicles for such road surfaces.

7.3.9 Applicability to Multiple Transportation Sectors

Not only the methodologies used in this study restricted to passenger cars, but the results obtained can even extend to other means of transport such as public transport, ambulances, military transport, agricultural tractors, construction machinery, and electric automobiles. In such cases, factors like vibrations and isolation are important due to which there is an increasing importance of this work in various industrial settings.

7.3.10 Support for Sustainable and Efficient Mobility

Suspension systems that are more efficient will lead to better dynamic performance and less mechanical stress on various parts of the vehicle; therefore, they may have a positive effect on both the durability and energy efficiency of the automobile. Through the optimization of suspension system settings and avoiding unnecessary vibrations, the research presented here promotes efficient and sustainable transportation.

7.3.11 Practical Reliability Through Experimental Validation

The use of physical test rig for the validation of the developed Bond Graph models makes the research more practically reliable and technically meaningful. Validation through experimental values helps in making sure that the theoretical models simulate

the vibrations realistically. This makes it easy to implement the proposed methodologies for practical industrial application. The practical nature of the experiment gives it greater chances of technological realization in the future.

7.3.12 Overall Societal Contribution

On the whole, the research makes an effort to contribute to the development of safer and more comfortable transport systems using aspects of vehicle dynamics, human biodynamics, modern control algorithms, and optimization methods. The results of this research could benefit car design, increase the comfort of public transportation, eliminate health threats caused by vibrations, and increase road safety. Therefore, the research has a significant social value because it is directed at human prosperity, sustainable development, and technological progress.

turnitin Page 260 of 269 - Integrity Submission Submission ID trn:oid:::29034:141996562

REFERENCE

Abba, W. *et al.* (2011) 'Optimal Seat Suspension Design Using Genetic Algorithms', *Journal of Mechanics Engineering and Automation*, 1, pp. 44–52.

Abbas, W. *et al.* (2010) 'Optimization of Biodynamic Seated Human Models Using Genetic Algorithms', *Engineering*, 02(09), pp. 710–719. doi: 10.4236/eng.2010.29092.

Abdelati, M. H., Mahmoud, K. R., Mokbel, E. F., Elnasr, G. S., & Youssef, I. M. (2026) 'Coefficient diagram method-based control of semi-active vehicle suspensions with performance evaluation over circular and trapezoidal speed humps at multiple speeds', *Journal of Engineering and Applied Science*, 73(1), p. 7.

Adibi-asl, H. and Rideout, G. (2009) 'B OND GRAPH M ODELING AND SIMULATION OF A FULL CAR MODEL WITH ACTIVE SUSPENSION N', pp. 1–6.

Agrawal, S. K. and Das, S. (2013) 'A modified adaptive control method for synchronization of some fractional chaotic systems with unknown parameters', *Nonlinear Dynamics*, 73(1–2), pp. 907–919. doi: 10.1007/s11071-013-0842-7.

Agrawal, S. K., Srivastava, M. and Das, S. (2012) 'Synchronization of fractional order chaotic systems using active control method', *Chaos, Solitons and Fractals*, 45(6), pp. 737–752. doi: 10.1016/j.chaos.2012.02.004.

Agrawal, S. K. and Vishal, K. (2017) 'Existence of Chaos, dynamical behaviour with fractional order derivatives and modified adaptive function projective synchronization with uncertain parameters of a chaotic system', *Optik*, 131, pp. 89–103. doi: 10.1016/j.ijleo.2016.11.070.

Ahmed, M. and Svaricek, F. (2013) 'Preview control of semi-active suspension based on a half-car model using Fast Fourier Transform', in *2013 10th International Multi-Conference on Systems, Signals and Devices, SSD 2013*, pp. 1–6. doi: 10.1109/SSD.2013.6564120.

Ajayi, A. B., Ojogho, E., Adewusi, S. A., Ojolo, S. J., Campos, J. C. C., & de Oliveira Siqueira, A. M. (2023) 'Parametric study of rider's comfort in a vehicle with semi-active suspension system under transient road conditions', *The Journal of Engineering and Exact Sciences*, 9(5), pp. 15287–01e.

Allen, G. (1978) 'A critical look at biomechanical modeling in relation to specifications for human tolerance of vibration and shock', in *AGARD Conference Proceedings No. 253, Paper A25-5, Paris,* pp. 6–10.

Ashish, G. and Vikas, R. (2012) 'Dynamic modeling and control of off-road truck using bondgraphs', in *Advances in Intelligent and Soft Computing*. doi: 10.1007/978-81-322-0491-6_41.

Bae, J. J. and Kang, N. (2018) 'Development of a Five-Degree-of-Freedom Seated Human Model and Parametric Studies for Its Vibrational Characteristics', *Shock and Vibration*, 2018. doi: 10.1155/2018/1649180.

Banerjee, N. *et al.* (2009) 'Bond graph modeling of a railway truck on curved track', *Simulation Modelling Practice and Theory*, 17(1), pp. 22–34. doi: 10.1016/j.simpat.2008.02.001.

Banerjee, S., Balamurugan, V. and Krishnakumar, R. (2016) 'Ride Comfort Analysis of Math Ride Dynamics Model of Full Tracked Vehicle with Trailing Arm Suspension', in *Procedia Engineering*. doi: 10.1016/j.proeng.2016.05.074.

Boileau, P.E., Rakheja, S. (1998) 'Whole body vertical biodynamic response characteristics of the seated vehicle driver – Measurement and model development', *International Journal of Industrial Ergonomics*, 22, pp. 449–472.

Borutzky, W. (2006) 'Bond Graph Modelling and Simulation of Mechatronic Systems An Introduction into the Methodology'.

Bouazara, M. and Richard, M. J. (2001) 'An optimization method designed to improve 3-D vehicle comfort and road holding capability through the use of active and semi-active suspensions', *European Journal of Mechanics, A/Solids*, 20(3), pp. 509–520. doi: 10.1016/S0997-7538(01)01138-X.

Chi, Z., He, Y. and Naterer, G. F. (2008) 'DESIGN OPTIMIZATION OF VEHICLE SUSPENSIONS WITH A QUARTER-VEHICLE MODEL', in *Transactions ofthe CSME Ide fa SCGM*, pp. 297–312.

Coermann, R. R. (1962) 'The mechanical impedance of the human body in sitting and standing position at low frequencies', *Human Factors*, 4(5), pp. 227–253.

Cokmez, E. *et al.* (2018) 'Fractional-order PI Controller Design for Integrating Processes Based on Gain and Phase Margin Specifications', *IFAC-PapersOnLine*. doi: 10.1016/j.ifacol.2018.06.206.

Dabiri, A., Moghaddam, B. P. and Machado, J. A. T. (2018) 'Optimal variable-order

fractional PID controllers for dynamical systems', *Journal of Computational and Applied Mathematics*. doi: 10.1016/j.cam.2018.02.029.

Desai, R., Guha, A. and Seshu, P. (2018) 'Multibody Biomechanical Modelling of Human Body Response to Direct and Cross Axis Vibration', *Procedia Computer Science*, 133, pp. 494–501. doi: 10.1016/j.procs.2018.07.062.

Dogruer, T. and Tan, N. (2018) 'Design of PI Controller using Optimization Method in Fractional Order Control Systems', *IFAC-PapersOnLine*. doi: 10.1016/j.ifacol.2018.06.124.

Dupuis, H., & Zerlett, G. (2012) *The effects of whole-body vibration.* Springer Science & Business Media.

Farid, T. M., Salah, A. and Abbas, W. (2011) 'Design of optimal linear suspension for quarter car with human model using genetic algorithms', *Journal of Applied Sciences Research*, 7(11), pp. 1709–1720.

Fernandes, E. S. (2017) 'Optimization of Vehicle Suspension System to Improve Comfort', *IOSR Journal of Mechanical and Civil Engineering*, 17(1), pp. 33–40. doi: 10.9790/1684-17010013340.

Filippini, G., Nigro, N. and Junco, S. (2014) 'Vehicle dynamics simulation using bond graphs', (June).

Freddi, M., Pagliari, C., & Frizziero, L. (2025) 'Parametric Sensitivity Analysis of Suspension Design Using Response Surface Techniques', *Applied Sciences*, 15(22), p. 11887.

Frih, A., Chalh, Z. and Mrabti, M. (2017) 'Modeling of a vehicle vertical dynamic model using Bond graph', *2017 14th International Multi-Conference on Systems, Signals and Devices, SSD 2017*, 2017-Janua(figure 1), pp. 827–832. doi: 10.1109/SSD.2017.8166919.

Gandhi, P., Adarsh, S. and Ramachandran, K. I. (2017) 'Performance Analysis of Half Car Suspension Model with 4 DOF using PID, LQR, FUZZY and ANFIS Controllers', in *Procedia Computer Science*. doi: 10.1016/j.procs.2017.09.070.

Gawthrop, P. J. (1995) 'Physical Model-based Control " A Bond Graph Approach', *Journal of the Franklin Institute*, 332(3), pp. 285–305.

Gupta, A. and Rastogi, V. (2016) 'Effects of Various Road Conditions on Dynamic Behaviour of Heavy Road Vehicle', in *Procedia Engineering*. doi: 10.1016/j.proeng.2016.05.078.

Guruguntla, V., & Lal, M. (2023) 'Multi-body modelling and ride comfort analysis of a seated occupant under whole-body vibration', *Journal of Vibration and Control*, 29(13–14), pp. 3078–3095.

Hamilton, A. (1918) 'Reports of physicians for the bureau of labor statistics- a study of spastic anemia in the hands of stone cutters', *Industrial Accidents and Hygiene National Technical Information Service, Bulletin*, (236), pp. 53–66.

Heidari, M. and Homaei, H. (2013) 'Design a PID controller for suspension system by back propagation neural network', *Journal of Engineering (United States)*. doi: 10.1155/2013/421543.

Hrovat, D. (1990) 'Optimal active suspension structures for quarter-car vehicle models', *Automatica*. doi: 10.1016/0005-1098(90)90002-Y.

Ikenaga, S. *et al.* (2000) *Active Suspension Control of Ground Vehicle based on a Full-Vehicle Model**.

Iskandarani, M. Z. (2022) 'MATLAB Simulation and Analysis of Effect of Stiffness to Damping Ratio and Variable Road Elevations on Vehicular Driving Comfort and Safety', *The Open Transportation Journal*, 16(1).

Jamali Shakhlavi, S., Marzbanrad, J. and Tavoosi, V. (2018) 'Various vehicle speeds and road profiles effects on transmitted accelerations analysis to human body segments using vehicle and biomechanical models', *Cogent Engineering*, 5(1), pp. 1–17. doi: 10.1080/23311916.2018.1461529.

Jasiūnienė, V. *et al.* (2018) 'Analysis and evaluation of trapezoidal speed humps and their impact on the driver', *Baltic Journal of Road and Bridge Engineering*, 13(2), pp. 104–109. doi: 10.7250/bjrbe.2018-13.404.

Jiangyi Han, Y. W. and C. S. (2023) 'A method for analysing the lateral stability of wheeled farm tractors by obstacles on slopes', *International journal of vehicle design*, 91(4), p. pp 289-302. doi: https://doi.org/10.1504/IJVD.2023.131209.

Jin, L., Yu, Y. and Fu, Y. (2016) 'Study on the ride comfort of vehicles driven by in-wheel motors', *Advances in Mechanical Engineering*. doi: 10.1177/1687814016633622.

K. Samaroo, A. W. Awan, S. Marimuthu, M. N. Iqbal, K. Daniel, and N. S. (2025) 'Performance Investigation of Active, Semi-Active and Passive Suspension Using Quarter Car Model', *Algorithms*, 18(2), p. 100. doi: 10.3390/a18020100.

Kuang, H., Qiu, Y., Liu, C., & Zheng, X. (2023) 'A nonlinear biodynamic model of

seated human body exposed to vertical vibration with sensitivity analysis', *Mechanical Systems and Signal Processing*, 204, p. 110758.

Kumar, J., & Bhushan, G. (2023) 'Dynamic analysis of quarter car model with semi-active suspension based on combination of magneto-rheological materials', *International Journal of Dynamics and Control*, 11(2), pp. 482–490.

Kumbhar, P.B., Xu, P. and Yang, J. (2012) 'A literature survey of biodynamic models for whole body vibration and vehicle ride comfort.', in *International Design Engineering Technical Conferences and Computers and Information in Engineering Conference*. American Society of Mechanical Engineers, pp. 671–687.

Lewis, C.H., Griffin, M.J. (2002) 'Evaluating the vibration isolation of soft seat cushions using an active anthropodynamic dummy', *Journal of Sound and Vibration*, 253(1), pp. 295–311.

Li, X. and Wei, D. (2009) 'Feedback control optimization of vehicle suspension system on uneven road', in *2009 International Conference on Intelligent Human-Machine Systems and Cybernetics, IHMSC 2009*. doi: 10.1109/IHMSC.2009.245.

Liu, X.X., Shri, J., Li, G.H. (1998) 'Biodynamic response and injury estimation of ship shock motion induced by underwater explosion', in *Proceeding of 69th Shock and Vibration Symposium, Vol. 18, St. Paul,* pp. 1–18.

Lixia, J. and Wanxiang, L. (2008) 'Chaotic vibration of a nonlinear quarter-vehicle model', in *2008 IEEE Vehicle Power and Propulsion Conference, VPPC 2008*. doi: 10.1109/VPPC.2008.4677697.

Llopis-Albert, C., Rubio, F., Devece, C., & Zeng, S. (2023) 'Multiobjective optimization framework for designing a steering system considering structural features and full vehicle dynamics', *Scientific Reports*, 13(1), p. 19537.

M. Nagarkar, M. El-Gohary, Y. Bhalerao, G. J. V. Patil, and R. N. Z. P. (2019) 'Artificial neural network predication and validation of optimum suspension parameters of a passive suspension system', *SN Applied Sciences*, 1(6), p. 569. doi: 10.1007/s42452-019-0550-0.

Magid, E. B., & Coermann, R. R. (1960) 'he reaction of the human body to extreme vibrations', in *Proceedings of the Institute of Environmental Science*, p. 135.
Mahala, M. K., Gadkari, P. and Deb, A. (2009) 'MATHEMATICAL MODELS FOR DESIGNING VEHICLES FOR RIDE COMFORT', in *2nd International Conference on Research into Design, Bangalore, India*, pp. 168–175.

Mahmoodi-Kaleibar, M. *et al.* (2013) 'Optimization of suspension system of off-road

vehicle for vehicle performance improvement', *Journal of Central South University*, (4), pp. 902–910. doi: 10.1007/s11771-013-1564-1.

Margolis, D. and Shim, T. (2000) 'A Bond Graph Model Incorporating Sensors, Actuators and Vehicle Dynamics for Developing Controllers for Vehicle Safety', *IFAC Proceedings Volumes*, 33(26), pp. 675–680. doi: 10.1016/s1474-6670(17)39223-6.

Margolis, D. and Shim, T. (2001) 'A bond graph model incorporating sensors , actuators , and vehicle dynamics for developing controllers for vehicle safety', 338, pp. 21–34.

Mehta, V. *et al.* (2016) 'A Novel Approach in Designing PID Controller for Semi-active Quarter Car Model', in *MATEC Web of Conferences*, p. 04001. doi: 10.1051/04001.

Ministry of Road and Highway Transport Rsearch Wing (2023) *ROAD ACCIDENTS IN INDIA 2023*.

Mitra, A. C., & Benerjee, N. (2013) 'Ride comfort and Vehicle handling of Quarter Car Model Using SIMULINK and Bond Graph', in *Proceedings of the 1st International and 16th National Conference on Machines and Mechanisms (iNaCoMM2013)*, pp. 18–20.

Mitra, A. C. *et al.* (2018) 'Development and Validation of a Simulation Model of Automotive Suspension System using MSC-ADAMS', in *Materials Today: Proceedings*. doi: 10.1016/j.matpr.2017.11.698.

Mitra, A. C., Patil, M. V. and Banerjee, N. (2015) 'Optimization of Vehicle Suspension Parameters for Ride Comfort Based on RSM', *Journal of The Institution of Engineers (India): Series C*, 96(2), pp. 165–173. doi: 10.1007/s40032-014-0156-7.

Mitra, A. C., Soni, T. and Kiranchand, G. R. (2016) 'Optimization of Automotive Suspension System by Design of Experiments: A Nonderivative Method', *Advances in Acoustics and Vibration*, 2016. doi: 10.1155/2016/3259026.

Modi, Mahendra J, Turakhia, T. P. and Modi, M J (2016) *Mathematical Modeling and Simulation of a Simple Quarter Car Vibration Model SEE PROFILE Mathematical Modeling and Simulation of a Simple Quarter Car Vibration Model*, *IJSRD-International Journal for Scientific Research & Development|*. Available at: https://www.researchgate.net/publication/311302749.

Modibbo, M. A., Babangida, A. and Szemes, P. T. (2025) 'Robust and Optimal Control Design for Vehicle Suspension System', *Óbudai Egyetem*, 22(5), pp. 109–126.
Mohite, A. G. and Mitra, A. C. (2018) 'Development of Linear and Non-linear Vehicle Suspension Model', in *Materials Today: Proceedings*. doi: 10.1016/j.matpr.2017.11.697.

Mouleeswaran, S. (no date) *4 Design and Development of PID Controller-Based Active Suspension System for Automobiles*. Available at: www.intechopen.com.

Muksian, R., Nash, C.D. (1974) 'model for the response of seated human to sinusoidal displacement of seat', *Journal of Biomechanics*, 7, pp. 209–215.

Muksian, R., Nash, C. . (1976) 'On frequency dependent damping coefficients in lumped parameter models of human beings', *Journal of Biomechanics*, 9, pp. 339–342.
Nigam, S.P., Malik, M. (1987) 'A study on a vibratory model of a human body', *Journal of Biomechanical Engineering*, 109(2), pp. 148–153.

Paynter, H. M. (1961) 'Analysis and design of engineering systems'.
Qinghua Meng; Bingji Li; Chuan Hu (2023) 'Nonlinear vehicle active suspension system control method based on the extended high gain observer', *International journal of vehicle design*, 91(4), p. pp.303-321. doi: 10.1504/IJVD.2023.131154.

R., L. *et al.* (2014) 'Optimal Design and Analysis of Vehicle Suspension System', pp. 87–108. doi: 10.2507/daaam.scibook.2014.07.

Rakheja, S. *et al.* (2010) 'Biodynamics of the human body under whole-body vibration: Synthesis of the reported data', *International Journal of Industrial Ergonomics*, 40(6), pp. 710–732. doi: 10.1016/j.ergon.2010.06.005.

Rao, K. D. (2014) 'Modeling, simulation and control of semi active suspension system for automobiles under MATLAB Simulink using PID controller', in *IFAC Proceedings Volumes (IFAC-PapersOnline)*. doi: 10.3182/20140313-3-IN-3024.00094.

Rezanoori, A., Ariffin, M. K. A. M., Delgoshaei, A., Jalil, N. A. A., & Zulkefli, Z. A. b. (2019) 'A new method to improve passenger vehicle safety using intelligent functions in active suspension system', *Engineering Solid Mechanics*, 7(4), pp. 313–330.

Ryazantsev, V. I., & Li, H. (2020) 'Structures active suspension for stabilizing vertical reactions of the road to the car wheels when driving over irregularities', *IOP Conference Series Materials Science and Engineering*, 971(5), p. 52096.

S. Lee and N. Kang (2024) 'Vehicle suspension recommendation system: multi-fidelity neural network-based mechanism design optimization', *Structural and Multidisciplinary Optimization*, 68(3), p. 44. doi: 10.1007/s00158-024-03957-x.

Sam, Y. M., Osman, J. H. S. and Ghani, M. R. A. (2004) 'A class of proportional-integral sliding mode control with application to active suspension system', *Systems and Control Letters*, 51(3–4), pp. 217–223. doi: 10.1016/j.sysconle.2003.08.007.

Samantaray, A. K. (2015) 'Users Manual of SYMBOLS Shakti', (January 2006).

Sathishkumar, P. *et al.* (2007) *Mathematical modelling and simulation quarter car vehicle suspension*, *International Journal of Innovative Research in Science, Engineering and Technology An ISO*. Available at: www.ijirset.com.
Schiehlen, W. and Iroz, I. (2015) 'Uncertainties in road vehicle suspensions', in *Procedia IUTAM*, pp. 151–159. doi: 10.1016/j.piutam.2015.01.016.

Sever, M. and Yazici, H. (2017) 'Active control of vehicle suspension system having driver model via L2gain state derivative feedback controller', in *2017 4th International Conference on Electrical and Electronics Engineering, ICEEE 2017*. doi: 10.1109/ICEEE2.2017.7935822.

Shah, P. and Agashe, S. (2016) 'Review of fractional PID controller', *Mechatronics*. doi: 10.1016/j.mechatronics.2016.06.005.

Shirahatt, A. *et al.* (2008) 'Optimal design of passenger car suspension for ride and road holding', *Journal of the Brazilian Society of Mechanical Sciences and Engineering*, 30(1), pp. 66–76. doi: 10.1590/s1678-58782008000100010.

Silva, L. I. *et al.* (2008) 'Vehicle dynamics using Multi-Bond Graphs: Four Wheel electric vehicle modeling', *IECON Proceedings (Industrial Electronics Conference)*, (December), pp. 2846–2851. doi: 10.1109/IECON.2008.4758410.

Singh, D. and Aggarwal, M. L. (2017) 'Passenger seat vibration control of a semi-active quarter car system with hybrid Fuzzy–PID approach', *International Journal of Dynamics and Control*. doi: 10.1007/s40435-015-0175-0.

Singh, I., Nigam, S. P. and Saran, V. H. (2015) 'Modal analysis of human body vibration model for Indian subjects under sitting posture', *Ergonomics*, 58(7), pp. 1117–1132. doi: 10.1080/00140139.2014.961567.

Sinha, G. K. and Prasad, U. (2017) 'VIBRATION CONTROL OF CAR SUSPENSION SYSTEM USING DIFFERENT CONTROLLERS', in *ICETETSM-17*, pp. 20–30.

Standard, I. (1997) 'Mechanical vibration and shock-Evaluation of human exposure to whole-body vibration-Part 1: General requirements Vibrations et chocs mkaniques-ivaluation de /' exposition des individus A des vibrations globaies du corps-Partie 7: Exigences g&Wales', 1997.

Subhash Rakheja, D. C. and Z. W. (2012) 'Urban bus driver ride and road–friendliness. Part I: Model development and role of operating parameters', *International journal of vehicle design*, 57(4), p. pp 305-332. doi: https://doi.org/10.1504/IJVD.2011.045769.

Suggs, C.W., Abrams, C.F., Stikeleather, L.F. (1969) 'Application of a damped spring-mass human vibration simulator in vibration testing of vehicle seats', *Applied*

Ergonomics, 12, pp. 79–90.

Talukdar, S. *et al.* (2012) 'Mathematical Modeling in Vehicle Ride Dynamics', in. doi: 10.4271/2012-01-0056.

Technical, I. M. vibration-road surface profiles-reporting of measured data. and Report 8608, International Organization for Standardization, 1995 (1995) म □ नक .

Tiwari, P. and Mishra, D. G. R. (2014) 'Simulation OF Quarter Car Model', *IOSR Journal of Mechanical and Civil Engineering*. doi: 10.9790/1684-11238588.

Tran, K. T., Jin, S., Deng, L., Du, H., Nguyen, H. Q., & Li, W. (2024) 'Semi-active inerters: a review of the literature', *Frontiers in Materials*, 11, p. 1347060.

Turakhia, T. P. and Modi, M. J. (2016) *Mathematical Modelling and Simulation of a Simple Half-Car Vibration Model*, *IJSRD-International Journal for Scientific Research & Development*|. Available at: www.ijsrd.com.

Wan, Y., Schimmels, J. (1995) 'A simple model that captures the essential dynamics of a seated human exposed to whole body vibration', *Advances in Bioengineering, ASME, BED,* 31, pp. 333–334.

Wei, L., Griffin, J. (1998) 'Mathematical models for the Apparent Mass of the seated Human body exposed to vertical vibration', *Journal of Sound and Vibration*, 212(5), pp. 855–74.

Xiaoming Liu, F. L. and J. G. (2023) 'Research on stability of high-speed autonomous vehicles based on linear time-varying model predictive control', *International journal of vehicle design*, 91(4), p. pp 360-383. doi: https://doi.org/10.1504/IJVD.2023.131177.

Yang, S., Lu, Y., & Li, S. (2013) 'An overview on vehicle dynamics', *International Journal of Dynamics and Control*, 1(4), pp. 385–395.

Zheng, W. *et al.* (2018) 'An Improved Frequency-domain Method for the Fractional Order PIλDμController Optimal Design', *IFAC-PapersOnLine*. doi: 10.1016/j.ifacol.2018.06.180.

Zhilin Jin; Zhenghua Yan; Wanzhong Zhao (2022) 'Rollover stability and anti-roll control of sport utility vehicle with driver in the loop', *International journal of vehicle design*, 90(1/2/3/4), p. pp.19-41. doi: 10.1504/IJVD.2022.129162.